Université Pierre et Marie Curie

Ecole doctorale des Sciences de l'Environnement

Station Biologique de Roscoff

UMR7144 AD2M

Equipe Chimie Marine

Dynamics of the carbonate system and air-sea CO_2 fluxes in western European shelf waters:

A multi-scale approach

Par Pierre Marrec

Thèse de doctorat d'Océanographie Chimique

Dirigée par Yann Bozec et Pascal Morin (HDR)

Présentée et soutenue publiquement le 8/12/2014

Devant un jury composé de :

Mr. Stéphane Blain, Professeur, Observatoire Océanologique de Banuyls, Examinateur

Mme. Jacqueline Boutin, Directrice de Recherche, LOCEAN (UPMC), Examinatrice

Mme. Aïda F. Rios, Professeure, Instituto de Investigaciones Marinas de Vigo (CSIC, Espagne), Rapporteuse

Mr. Helmuth Thomas, Professeur, Dalhousie University (Canada), Rapporteur

Mr. Pascal Morin, Directeur de Recherche, IPEV, Directeur de Thèse

Mr. Yann Bozec, Chargé de Recherche, Station Biologique de Roscoff, Directeur de Thèse

Except where otherwise noted, this work is licensed under
http://creativecommons.org/licenses/by-nc-nd/3.0/

Dedicace

Contents

Chapter 1: Introduction ..... - 1 -

1. Climate change ..... - 3 -
2. The global and the oceanic carbon cycle ..... - 6 -
   2.1 The global carbon cycle ..... - 6 -
   2.2 The oceanic carbon cycle ..... - 8 -
3. Dissolved inorganic carbon in seawater ..... - 10 -
   3.1 The carbonate system ..... - 10 -
   3.2 Inorganic carbon dynamics ..... - 14 -
   3.3 Air-sea CO_2 fluxes ..... - 15 -
4. Continental shelves ..... - 16 -
5. Thesis objectives ..... - 17 -
6. Thesis outlines ..... - 18 -

References ..... - 20 -

Chapter 2: Seasonal and latitudinal variability of the CO_2 system in the western English Channel based on Voluntary Observing Ship (VOS) discrete measurements over three contrasted years. ..... - 27 -

Abstract ..... - 29 -
1. Introduction ..... - 30 -
2. Material and Methods ..... - 32 -
   2.1 Surface measurements on the VOS line ..... - 32 -
   2.2 Water column measurements at fixed stations ..... - 34 -
   2.3 Calculation of the partial pressure of CO_2 and air-sea CO_2 fluxes ..... - 35 -
   2.4 Calculation of the Net Ecosystem Production ..... - 36 -
3. Results ..... - 37 -
   3.1 Hydrographical setting ..... - 37 -
   3.2 Surface distributions of DO%, Chl-*a* and nutrients ..... - 44 -
   3.3 Surface distributions of CO_2 system parameters ..... - 47 -
4. Discussion ..... - 51 -
   4.1 Latitudinal dynamics of the carbonate system in the WEC ..... - 51 -
   4.2 Processes controlling the seasonal pCO_2 variability ..... - 53 -
   4.3 Air-Sea CO_2 exchange ..... - 57 -
   4.4 Estimation of Net Ecosystem Production at the fixed stations ..... - 60 -
5. Concluding remarks ..... - 64 -

References ..... - 65 -

Chapter 3: Spatio-temporal dynamics of biogeochemical processes and air-sea CO_2 fluxes in the Western English Channel based on two years of FerryBox deployment. ... - 71 -

Abstract ... - 73 -
1. Introduction ... - 74 -
2. Material and Methods ... - 76 -
2.1 The VOS line and the FerryBox system ... - 76 -
2.2 Bimonthly discrete sampling ... - 77 -
2.3 CO_2 system and air-sea CO_2 fluxes calculation ... - 79 -
3. Results and discussion ... - 80 -
3.1 Reliability of the FerryBox system ... - 80 -
3.2 Observation of the physical structure of the WEC ... - 84 -
3.3 Inter-annual dynamics of phytoplankton blooms ... - 87 -
3.4 Short time-scale dynamics of pCO_2 and air-sea CO_2 fluxes ... - 90 -
4. Concluding remarks and perspectives ... - 96 -
References ... - 98 -

Chapter 4: Dynamics of air-sea CO_2 fluxes in the north-west European shelf based on Voluntary Observing Ship (VOS) and satellite observations. ... - 103 -

Abstract ... - 105 -
1. Introduction ... - 106 -
2. Study area ... - 107 -
3. Material and Methods ... - 110 -
3.1 FerryBox datasets ... - 110 -
3.2 Satellite and other environmental data ... - 111 -
3.3 Development of pCO_2 algorithms ... - 114 -
3.4 SOCAT data ... - 117 -
3.5 Calculation of air-sea CO_2 fluxes ... - 118 -
4. Results and discussion ... - 120 -
4.1 Performance of MLR ... - 120 -
4.2 Spatial and temporal extrapolation of the algorithms ... - 125 -
4.3 Seasonal variability of biogeochemical properties in stratified vs. permanently well-mixed systems ... - 128 -
4.4 Inter and multi-annual variability of pCO_2 and air-sea CO_2 fluxes ... - 135 -
5. Concluding remarks and perspectives ... - 139 -
References ... - 141 -

Chapter 5: Summary, concluding remarks and perspectives ..... - 153 -

1. Summary ..... - 155 -
   1.1 Three years of bimonthly measurements ..... - 155 -
   1.2 High frequency measurements ..... - 157 -
   1.3 Development of pCO_2 algorithms and air-sea CO_2 flux in WEC, CS and IS over a decade ..... - 159 -
   1.4 Conclusion ..... - 161 -
2. Concluding Remarks and Perspectives ..... - 162 -
   2.1 Time-scale discrepancies and other uncertainties of the CO_2 system in coastal seas ..... - 162 -
   2.2 Towards global coastal carbon observatories ..... - 168 -
   2.3 Long-term time series and climate change ..... - 171 -

References ..... - 173 -

Remerciements ..... - 180 -

CV and bibliography of author ..... - 182 -

Liste of figures ..... - 185 -

List of Tables ..... - 192 -

Chapter 1: Introduction

1. Climate change

The reconstruction of the atmospheric carbon dioxide (CO_2) concentrations over the last 800,000 years from ancient air trapped in bubbles from Antarctic ice cores (Figure 1, Petit et al., 1999; Siegenthaler et al., 2005; Lütthi et al., 2008) revealed strong correlations between temperatures and atmospheric CO_2 concentrations throughout 8 glacial cycles. The glacial inter-glacial atmospheric CO_2 cycles varied by ~100 ppm and remained between ~180 ppm at the glacial maxima and ~280 ppm during the warm interglacial phases. However, the mechanisms and the causes of the glacial-interglacial variations in atmospheric CO_2 remain poorly understood, and Earth system models have been unable to reproduce the full magnitude of these variations. From April to June 2014, monthly atmospheric CO_2 concentrations overpassed for the first time the symbolic threshold of 400 ppm at Mauna Loa Observatory (see the Keeling Curve, https://scripps.ucsd.edu/programs/keelingcurve/), a level never reached for at least 2.1 million years (CO_2 estimates based on the boron isotopic composition of planktic foraminifer shells, Hönisch et al., 2009). The excess CO_2 can definitively be attributed to human activities based on carbon isotopes and ice-core CO_2 measurements (IPCC, 2013).

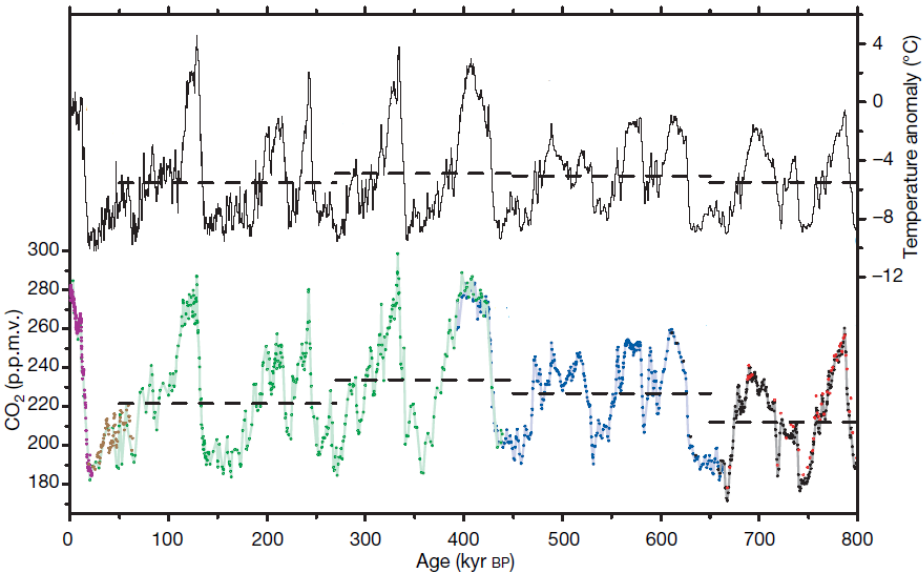


Figure 1: Compilation of CO_2 records in air trapped in sea ice cores from Antarctica and temperature anomaly over the past 800 kyr adapted from Lüthi et al. (2008).

Since the pre-industrial times, the atmospheric concentration of CO_2 have increased by 40%, from 280 ppm in 1750 to 400 ppm in 2014 (Figure 2, MacFarling Meure et al., 2006). As mentioned above, this increase is due to human activity, primarily from fossil fuel emissions and secondarily from net land use change emissions (IPCC, 2013). The CO_2 is the second most effective greenhouse gas (GHG) in the atmosphere, after water vapour. GHGs are atmospheric gaseous constituents that absorb and emit radiations at specific wavelengths, as infrared radiations, emitted by the Earth's surface, the atmosphere itself, and by clouds, thus trapping heat in the atmosphere and keeping the Earth's surface warmer than it would be if they were not present.

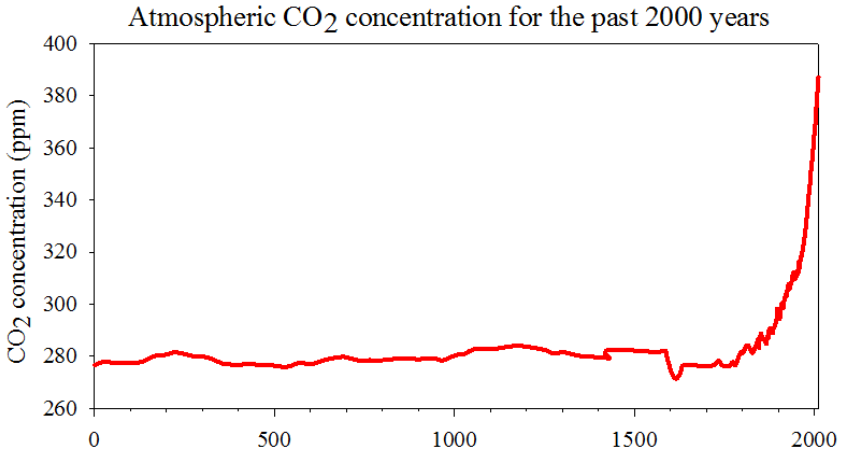


Figure 2: Evolution of the atmospheric CO_2 during the last 2000 years in ppm from the Law Dome (Antarctica) ice core and firn air records adapted from MacFarling Meure et al. (2006).

The increase of atmospheric concentration of GHG as CO_2, as well as methane (CH_4) and nitrous oxide (N_2O), by anthropogenic activities is "extremely likely" (95-100% probability) the main driver of climate change (IPCC, 2013). The climate change are and will be characterized by a global warming of the atmosphere and the ocean, changes in the global water cycle, reduction in snow and ice cover, global mean sea level rise, changes in some climate extremes and will affect carbon and other biogeochemical cycles. These changes also affect, e.g. concerning the ocean, global marine-species distribution and marine biodiversity in sensitive regions (Drinkwater et al., 2010; Ottersen et al., 2010). Shifts in geographic ranges, seasonal activities, migration patterns, abundances, species interactions of marine species or the progressive expansion of oxygen minimum zones and anoxic "dead zones" are and will be consequences of ongoing climate change (IPCC, 2014) in the ocean. In addition, as a consequence of increasing atmospheric CO_2 concentration, and its absorption by the

ocean (see section 2.2), the surface ocean pH has decreased by 0.1 unit and is expected to further decrease by as much as 0.4 by the end of the century (Orr et al., 2005; Bopp et al., 2013). Ocean acidification, "the other CO_2 problem" (Doney et al., 2009), causes wholesale shifts in seawater carbonate chemistry (see section 3) and impacts carbonate shell-forming marine organisms from plankton to benthic molluscs, echinoderms and corals (Gattuso and Hansson, 2011).

The increase of anthropogenic CO_2 emissions will surely continue over the next decades without substantial and sustained reductions of fossil fuel consumption (IPCC, 2013). Depending of the scenario (the Representative Concentration Patways, RCPs, defined by the IPCC), atmospheric CO_2 levels will likely range between 420 ppm by the end of the century, (if CO_2 emissions are drastically reduced from 2020) and 940 ppm (in a very high CO_2 scenario) (Figure 3). Most aspects of climate change will persist and even amplify for many centuries even if emissions of CO_2 are stopped (IPCC, 2013).

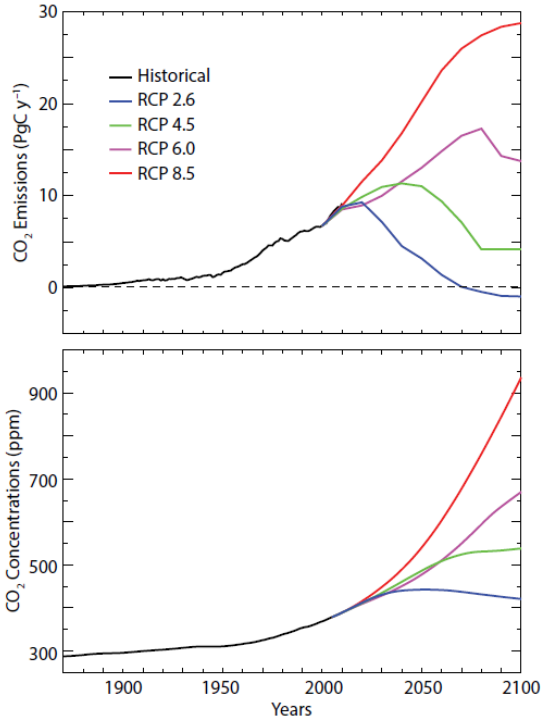


Figure 3: CO_2 emissions trajectories and atmospheric CO_2 concentrations from historical data (black lines) and four of the RCPs for the 21st century (colored lines), adapted from Doney et al. (2014).

In addition to climate change issues and anthropogenic perturbation such as ocean acidification, the accumulation of anthropogenic CO_2 in the atmosphere has a strong impact on the global carbon cycle and on the fluxes of carbon between the natural carbon cycle reservoirs and particularly the ocean.

2. The global and the oceanic carbon cycle

2.1 The global carbon cycle

Carbon forms the key component for supporting life; it is a major constituent of many minerals and the fourth most abundant element in the universe. The global carbon cycle can be viewed as a series of reservoirs of carbon in the Earth System, which are connected by exchange fluxes of carbon. Toward assessing the impact of climate change and anthropogenic forcings on the earth system, it is essential to better understand the global carbon cycle and to better quantify the carbon fluxes between its reservoirs.

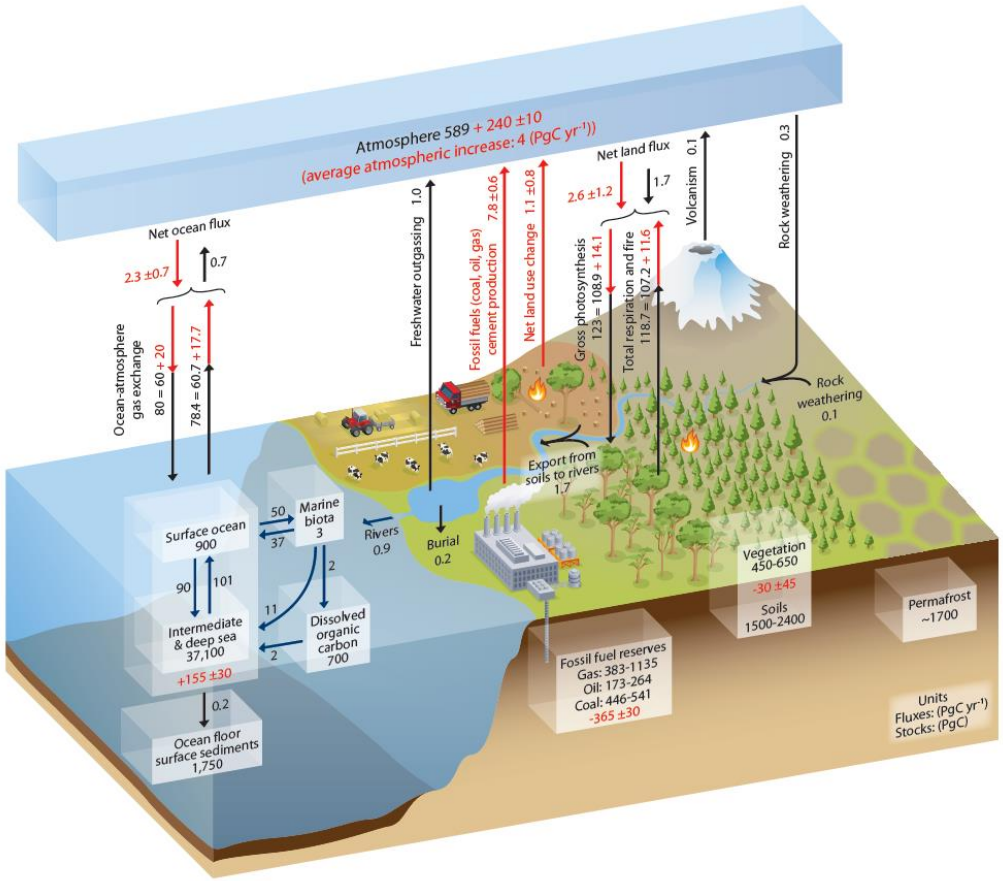


Figure 4: Simplified schematic of the global carbon cycle (IPCC, 2013). Numbers represent carbon stocks in Pg C and annual carbon exchange fluxes in Pg C yr^{-1}. Black numbers and arrows indicate carbon stocks and exchange fluxes estimated for the time prior to the Industrial Era. Red arrows and numbers indicate annual "anthropogenic" fluxes averaged over the 2000-2009 time period.

The global carbon cycle can be dissociated in two distinct domains related to the time-scales of the exchange fluxes. The "slow domain" is characterized by the geological carbon storage in rocks and sediment (fossil organic carbon and rock carbonates) reservoirs with slow and small natural exchanges of carbon with the other reservoirs (ocean, terrestrial biosphere and atmosphere) over long time-scales (> 10,000 years). The "slow domain" is thus weakly impacted by the recent anthropogenic emissions of CO_2 to the atmosphere. The "fast domain" consists of large exchange fluxes of carbon over relatively shorter time-scales (from a few years for the atmosphere to thousands years in the ocean) between the atmosphere, the ocean, surface ocean sediments, terrestrial biosphere, including the soils, and freshwaters. Figure 4 shows a schematic of the global carbon cycle with focus on the "fast domain".

Most of the carbon on Earth is stored in the lithosphere in sedimentary rocks, in both limestone and kerogen (organic matter in sedimentary rocks), carbon reservoirs of $60x10^6$ and $15x10^6$ Pg C (1 Pg C=1 Gt C=10^{15} g C) with small and slow exchanges with active carbon reservoirs. The atmosphere is the smallest carbon reservoir with CO_2 as dominant source (more than 99%). Since the pre-industrial time, the amount of carbon in the atmosphere has increased by 40%, from 590 to 830 Pg C (Figure 4). Terrestrial biosphere hosts around 4,000-5,500 Pg C in vegetation living biomass, dead organic matter in litter and soil, wetland soils and permafrost. The ocean carbon pool is the largest non-geological reservoir, with ~38,000 Pg C. In the ocean, carbon is available predominantly as Dissolved Inorganic Carbon (DIC), but also as Dissolved Organic Carbon (DOC, ~700 Pg C) and in the marine biota (phytoplankton and other organisms, ~3 Pg C). Most of the carbon in the ocean is stored in deep and intermediate waters. Inorganic carbon in the ocean originates mainly from the long time river inputs due to weathering of limestone and land.

Over the Anthropocene (from 1750 to 2011), humankind has released about 555 Pg C to the atmosphere (Table 1) due to combustion of fossil fuels and cement production (375 Pg C) and land use change (180 Pg C), and less than half have accumulated in the atmosphere (240 Pg C). The anthropogenic CO_2 that did not accumulate in the atmosphere (315 Pg C) is either taken up by the ocean or by the land biosphere; the ocean and the terrestrial biosphere have thus acted as anthropogenic carbon sink. Since 1750, the higher CO_2 levels (via the "CO_2 fertilisation effect", Sitch et al., 2008), changes in climate favoring terrestrial carbon sink and nitrogen deposition, have been likely responsible of a sink of 160 Pg C of anthropogenic carbon by terrestrial ecosystems not affected by land use change. Thus, terrestrial ecosystems have a net carbon balance close to neutral. The amount of

anthropogenic carbon accumulated in the ocean can be estimated based on inorganic carbon measurements and tracer-based separation techniques (Vazquez-Rodriguez et al., 2009, for a comparison of techniques). The most recent ocean sink reported in the last IPCC report, based on the most relevant carbon budget studies, is 155 Pg C of anthropogenic carbon stored since 1750 , thus closing the global carbon budget.

	1750-2011 Cumulative Pg C
Atmospheric increase	240 ± 10
Fossil fuel and cement production	375 ± 30
Ocean-to-atmospher flux	-155 ± 30
Land-to-atmosphere flux	30 ± 45
Net land use change	180 ± 80
Residual land sink	-160 ± 90

Table 1: Global anthropogenic CO_2 budget accumulated since the Industrial Revolution (from IPCC, 2013). Negative flux is equivalent to a gain of carbon by the corresponding reservoirs.

2.2 The oceanic carbon cycle

On an annual scale, the ocean naturally exchanges about 80 Pg C yr^{-1}, essentially CO_2, with the atmosphere, in each direction (Figure 4). The mean CO_2 net uptake by the global ocean is about 1.6 ± 0.9 Pg C yr^{-1}, estimated from surface ocean partial pressure of CO_2 (pCO_2) measurements obtained between 1970 and 2007 (Takahashi et al., 2009). Physical and biological processes control the ocean carbon cycle with the solubility pump and the biological pump, respectively (Figure 5).

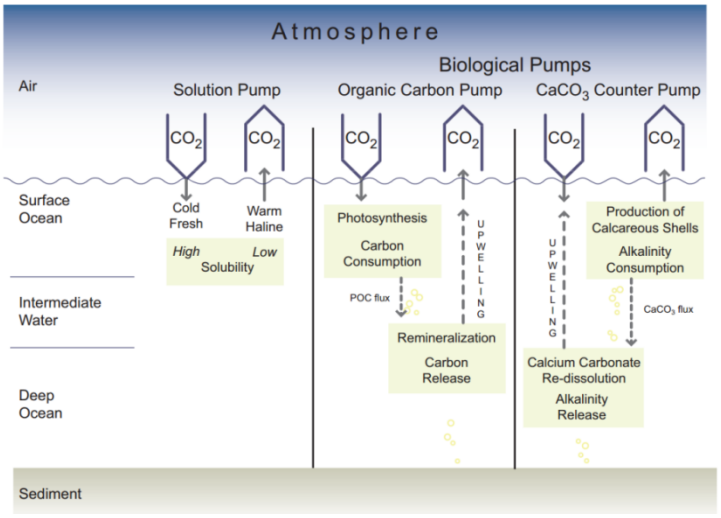


Figure 5: Regulation of natural atmospheric CO_2 changes by the ocean by the solubility pumps, the organic carbon pump and the $CaCO_3$ counter pump (from IPCC, 2007).

2.2.1 The solubility pump

The solubility of CO_2 is higher in cooler waters, and the ocean circulation is driven by the formation of deep waters at high latitudes (mainly in the North Atlantic by the Norwegian and the Labrador Seas and in the Weddell Sea), where seawater is cooler and denser. Surface waters at high latitudes with higher CO_2 solubility sinks to greater depth, transferring carbon to deep waters. Solubility and circulation processes act together to pump carbon from the atmosphere to the ocean interior. The opposite process can occur at equatorial and tropical latitudes where upwelled waters outgas CO_2 to the atmosphere due to CO_2 supersaturated waters being brought to the surface.

Climate warming is projected to reduce CO_2 solubility, to increase vertical stratification, to slow ocean circulation and to reduce deep water formation, which will reduce ocean uptake of anthropogenic CO_2 (Doney et al., 2014). On the other hand, the projected strengthening of westerly winds in the Southern Ocean may enhance ocean uptake of CO_2, acting as a negative feedback. Earth system models predict a decrease of carbon uptake by the solubility pump under a warming climate and there are some evidences that changing climate is already slowing ocean CO_2 uptake (Le Quéré et al., 2010).

2.2.2 The biological pump

The biological pump corresponds to the transfer of carbon from the ocean's surface layers to the deep ocean by the primary production of marine phytoplankton. Phytoplankton converts dissolved inorganic carbon into organic matter through photosynthesis depending on light and nutrient availability (De La Rocha and Passow, 2007). Most of the particulate organic matter formed by phytoplankton in the euphotic zone sinks in the deeper layer of the ocean where it is oxidized through heterotrophic processes in dissolved inorganic carbon. An additional part is exported in the deep ocean as particulate organic carbon (phytoplankton cells, plankton detritus, zooplankton fecal pellets …). Photosynthesis lowers the pCO_2 in the upper ocean and thereby promotes the absorption of CO_2 from the atmosphere. Despite representing only 0.2% of the photosynthetically active carbon biomass on Earth, phytoplankton account for about the half of global primary productivity on Earth (Field et al.,

1998; Falkowski et al., 1998). In an ocean with the biological pump turned off (the so-called "Strangelove Ocean"), atmospheric CO_2 concentration would increase by around 200 ppm (Parekh et al., 2006; Sarmiento and Toggweiler, 1984; Boyd and Hurd, 2009). The efficiency of the biological pump is relative to the fraction of primary production exported from the euphotic zone to the deep sea.

Several phytoplankton and zooplankton organisms develop calciferous shells (coccolithophores, foraminifers, pteropods…) in the upper ocean. The formation of $CaCO_3$ leads to a release of CO_2 (see Section 3.2) in the surface waters, thus the carbonate counter-pump acts as a source of CO_2 to the atmosphere and counters the biological pump. The $CaCO_3$ shells sink into the deep ocean, where some fraction dissolves; deep waters being undersaturated with respect to $CaCO_3$. The remainder of the $CaCO_3$ particles enters in marine sediments. Only a small fraction (0.2 PgC yr^{-1}) of the carbon is exported by biological processes (both organic carbon and carbonate pumps) from the surface to the seafloor, where it is stored in sediments for millennia and longer (IPCC, 2007).

3. Dissolved inorganic carbon in seawater

In this thesis, we mainly focus on the dissolved inorganic carbon system. The following section describes the chemistry and the thermodynamic of the dissolved inorganic carbon system in seawater. For a detailed overview of the CO_2 system in seawater, the reader should refer to Zeebe and Wolf-Gladrow (2001).

3.1 The carbonate system

Dissolved inorganic carbon in seawater exists under four chemical species: CO_2 in its aqueous form ($CO_{2,aq}$), carbonic acid (H_2CO_3), bicarbonate (HCO_3^-) and carbonate (CO_3^{2-}) ions. The relative abundance of each species depends on thermodynamical equilibriums related to salinity, temperature and pressure. The concentration of H_2CO_3 is much smaller than that of $CO_{2,aq}$, and, in seawater, H_2CO_3 and $CO_{2,aq}$ are analytically indistinguishable, therefore we consider:

$$[CO_2] = [H_2CO_3] + [CO_{2,aq}] \qquad (1)$$

At typical seawater conditions, the percentage of the dissolved species is $[CO_2]$: $[HCO_3^-]$: $[CO_3^{2-}]$ ≈ 1% : 90% : 9%. In thermodynamic equilibrium with gaseous CO_2 ($CO_2(g)$):

$$CO_2(g) \overset{K_0}{\Leftrightarrow} CO_2 \qquad (2)$$

the concentration of CO_2 is given by Henry's law with K_0 being the solubility coefficient of CO_2 in seawater, which depends on temperature and salinity (Weiss, 1974).

The thermodynamic equilibrium between the three main carbonate species is given by the following equations:

$$CO_2 + H_2O \overset{K_1}{\Leftrightarrow} HCO_3^- + H^+ \overset{K_2}{\Leftrightarrow} CO_3^{2-} + 2H^+ \qquad (3)$$

where K_1 and K_2 are the first and second dissociation constants of carbonic acid, respectively. To describe the carbonate system in seawater, stoichiometric equilibrium constants, related to concentrations, are used:

$$K_1 = \frac{[HCO_3^-][H^+]}{[CO_2]} \qquad (4)$$

$$K_2 = \frac{[CO_3^{2-}][H^+]}{[HCO_3^-]} \qquad (5)$$

These equilibrium constants, which are functions of temperature, pressure and salinity, have been derived by fitting experimental data. In this manuscript, I choose to use the equilibrium constants proposed by Mehrbach et al. (1973), refitted by Dickson and Millero (1987) on the seawater pH scale, as recommended by Dickson et al. (2007).

In seawater, there are four measurable carbonate parameters: total alkalinity (TA), dissolved inorganic carbon (DIC), pH and pCO_2. The carbonate system can be quantitatively described from any two of these four measurable variables. These variables are defined in the following sections.

3.1.1 Dissolved inorganic carbon

Dissolved inorganic carbon (DIC) is the sum of the concentration of the dissolved CO_2, HCO_3^- and CO_3^{2-}:

$$\mathrm{DIC} = [\mathrm{CO_2}] + [\mathrm{HCO_3^-}] + [\mathrm{CO_3^{2-}}] \quad (6)$$

Analytical techniques and recommendations to determined DIC in seawater samples, as well as the three other measurable variables, are available in the "Guide for best practice for ocean CO_2 measurements" written by Dickson et al. (2007). The methods we used in this study are described in the Material and Method sections of the three following chapters.

3.1.2 Total Alkalinity

The most exact definition of total alkalinity (TA) was given by Dickson (1981): "*The total alkalinity of a natural water is thus defined as the number of moles of hydrogen ion equivalent to the excess of proton acceptors (based formed from weak acids with a dissociation constant $K \leq 10^{-4.5}$, at 25°C and zero ionic strength) over proton donors (acids with $K > 10^{-4.5}$) in one kilogram of sample.*". In seawater TA is given by:

$$\mathrm{TA} = [\mathrm{HCO_3^-}] + 2[\mathrm{CO_3^{2-}}] + [\mathrm{B(OH)_4^-}] + [\mathrm{OH^-}] + [\mathrm{HPO_4^{2-}}] + 2[\mathrm{PO_4^{3-}}] + [\mathrm{SiO(OH)_3^-}] + [\mathrm{NH_3}] + [\mathrm{HS^-}] - [\mathrm{H^+}]_\mathrm{F} - [\mathrm{HSO_4^-}] - [\mathrm{HF}] - [\mathrm{H_3PO_4}] \quad (7)$$

where $[H^+]_F$ is the free proton concentration.

Essentially, TA is a measure of the seawater buffer capacity, which allows keeping track of the charges of the ions of weak acids, while DIC keeps track to the inorganic carbon. HCO_3^- and CO_3^{2-} account for about 98% of the TA, introducing the concept of carbonate alkalinity (CA):

$$\mathrm{CA} = [\mathrm{HCO_3^-}] + 2[\mathrm{CO_3^{2-}}] \quad (8)$$

Borate, sulphate and fluorine can be derived from salinity, while phosphate and silicate can be measured independently. It is then possible to estimate CA from measured TA

and by taking into account the other minor species, to finally totally constrain the carbonate system when DIC concentration is known.

3.1.3 pH

pH reflects the thermodynamic state of the acid-base systems in the seawater. It is not the pH that controls the concentrations of carbonate species in seawater, but the carbonate system that is the natural buffer for seawater pH. The conventional definition of pH is the negative logarithm of the concentration of free protons:

$$\mathrm{pH} = -\log[\mathrm{H}^+] \qquad (10)$$

This equation is not useful because free protons are not present in significant amount in seawater. Furthermore, in seawater protonation of ions such sulfate and fluoride occurs. The total (pH_T) and the seawater (pH_{SWS}) pH scales are used for the determination of pH in seawater:

$$\mathrm{pH_T} \approx -\log([\mathrm{H}^+] + [\mathrm{HSO_4^-}]) \qquad (11)$$

$$\mathrm{pH_{SWS}} \approx -\log([\mathrm{H}^+] + [\mathrm{HSO_4^-}] + [\mathrm{HF}]) \qquad (12)$$

In the present study, we used the total scale, as recommended by Dickson (1993).

3.1.4 Partial pressure and fugacity of CO_2

The fugacity and partial pressure of CO_2 (fCO_2 and pCO_2, respectively) assigned to a seawater sample refers to the fugacity and partial pressure of CO_2 in the gas phase that is in equilibrium with that seawater. The mole fraction of CO_2 (xCO_2 in µmol mol^{-1}) in the gas phase is determined by equilibrating a large volume of seawater with a small and fixed volume of air, from which the partial pressure is calculated:

$$\mathrm{pCO_2} = \mathrm{xCO_2} \times \mathrm{p} \qquad (13)$$

where p is the total pressure of the mixture in atm.

fCO_2 takes into account the non-ideal nature of CO_2 in air and is about 0.3% to 0.4% lower than pCO_2. The fugacity can be calculated from the partial pressure:

$$fCO_2 = pCO_2 \times \exp\left(p\frac{B+2\delta}{RT}\right) \qquad (14)$$

where fCO_2 and pCO_2 are in µatm, the total pressure p is in Pa, the first virial coefficient B (Weiss, 1974) and parameter δ are in $m^3\ mol^{-1}$, R=8.314 J K^{-1} mol^{-1} is the gas constant and the absolute temperature T is in K.

3.2 Inorganic carbon dynamics

The dynamics of the carbonate system in the ocean is controlled by a number of biological (photosynthesis/respiration, calcium carbonate formation/dissolution), physical (mixing) and chemical (CO_2 uptake/release) processes. Figure 6 shows the effects of these processes on DIC and TA (Zeebe and Wolf-Gladrow, 2001).

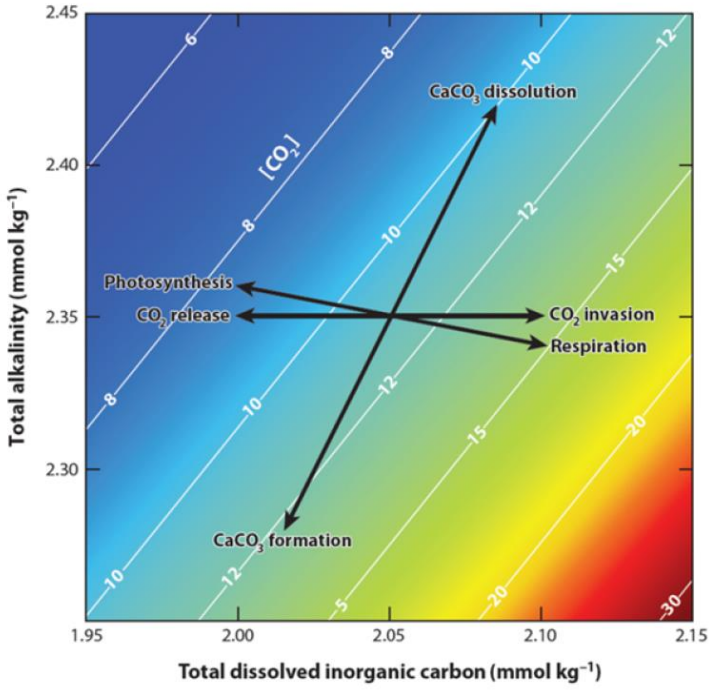


Figure 6: Effect of various processes on the carbonate system parameters (from Zeebe and Wolf-Gladrow, 2001).

Photosynthesis and respiration tend to decrease and increase DIC concentrations repectively. Both processes have a minor effect on TA because in addition to inorganic carbon, nutrients (mainly nitrate) are taken up and released by photosynthesis and respiration, respectively (Brewer and Goldman, 1976; Zeebe and Wolf-Gladrow, 2001). Formation and dissolution of $CaCO_3$ decreases and increases, respectively, both DIC and TA in a ratio of 1:2. Many planktonic (coccolithophores, pteropods, foraminifers…) and benthic (bivalves, corals, marine calcareous algae…) organisms are involved in formation/dissolution of $CaCO_3$. $CaCO_3$ is present in various forms, calcite and aragonite, which differ in their crystallographic structures. As a result of formation of $CaCO_3$, the system shifts to higher CO_2 levels, whereas $CaCO_3$ dissolution process consumes seawater CO_2. The uptake and release of CO_2 by dissolution and formation of $CaCO_3$ processes, respectively, only affect the DIC concentration and do not change TA because the charge balance is not affected. Mixing effects can also affect DIC and TA. In the ocean, DIC and TA are both conservative quantities with respect to mixing and their variations are related to changes of salinity (Millero et al., 1998; Friis et al., 2003; Wolf-Gladrow et al., 2007), including freshwater addition (precipitation, river inputs, sea-ice melting) and removal processes (evaporation or sea-ice formation). However, pCO_2 and pH are not conservative during mixing and do not follow a conservative behaviour.

3.3 Air-sea CO_2 fluxes

As mentioned above, a large amount of CO_2 is exchanged between the ocean and the atmosphere. Air-sea CO_2 fluxes are driven by the CO_2 concentration gradients between these two reservoirs and are computed according to:

$$F = k \times ([CO_2]_{Sea} - [CO_2]_{Air}) = \alpha \times k \times (pCO_{2,Sea} - pCO_{2,Air}) \qquad (15)$$

where F is the air-sea CO_2 flux in mol m^{-2} s^{-1}, k is the gas transfer velocity in m s^{-1}, α is the solubility coefficient of CO_2 in seawater in mol atm^{-1} m^{-3}, $[CO_2]_{Sea}$ is the CO_2 concentration of surface waters and $[CO_2]_{Air}$ is the concentration of CO_2 of the atmosphere in mol m^{-3}, and $pCO_{2,Sea}$ and $pCO_{2,Air}$ are the respective partial pressure in µatm.

In the ocean and the atmosphere, pCO_2 can be precisely and accurately measured and the solubility coefficient of CO_2 α can be calculated according to Weiss (1974) from seawater salinity and temperature. Several gas transfer parametrizations have been developed based on

a wide range of theoretical, laboratory and field studies (Wanninkhof et al., 2009, for a review of the developments in techniques quantifying air-sea gas exchanges and gas transfer velocities). Gas transfer velocity depends on water turbulences mainly generated by wind stress. Most commonly, gas transfer velocity k is only expressed as a k-wind relationship. However, surfactant films, bubble entrainment, breaking waves, rain, boundary layer stability or friction velocity can also affect gas transfer processes. In this thesis, we used the Nightingale et al. (2000) k-wind parametrization established in the Southern Bight of the North Sea (SBNS). In Chapter 5, we discuss the impact of different gas transfer velocity parametrizations on air-sea CO_2 fluxes computation for our study area.

4. Continental shelves

During the past decades, surface pCO_2 measurements have increased considerably in the ocean (Takahashi et al., 2009; Bakker et al., 2014). Based upon about 3 million measurements of surface pCO_2, Takahashi et al. (2009) built a climatological atlas of seawater pCO_2 and air-sea CO_2 fluxes in the global open ocean. The pCO_2 and air-sea CO_2 flux climatology was estimated month-by-month with a spatial resolution of 4° (latitude) x 5° (longitude) for a reference year 2000. The annual mean for the contemporary net CO_2 uptake flux over the global oceans is estimated at -1.6 ± 0.9 Pg C yr^{-1}.

While the atmospheric CO_2 sink is reasonably well-constrained for the open-ocean, CO_2 flux estimates for the coastal ocean are subject to large uncertainties. Continental shelf seas, as an interface between land, ocean and atmosphere, host a multitude of biogeochemical processes (Walsh, 1991; Liu et al., 2010) and play a key role in the global carbon cycle (Walsh et al. 1981; Muller-Karger et al., 2005; Bauer et al., 2013). Although marginal seas occupy only 7% of global oceanic area, they host enhanced biological activity, which accounts for 10-30% of global oceanic primary production, 30-50% of inorganic carbon and around 80% of organic carbon burial in sediments (Gattuso et al., 1998, Mackenzie et al., 2004). These productive regions are characterized by enhanced air-sea CO_2 fluxes compared to open oceans (Tsunogai et al., 1999; Thomas et al., 2004) and are particularly vulnerable to anthropogenic forcings such as eutrophication and ocean acidification (Borges and Gypsen, 2010; Borges et al., 2010; Wallace et al., 2014). In a context of climate change, with rising

anthropogenic CO_2 levels in the atmosphere and the oceans, it is essential to better constrain the carbon cycle dynamics and particularly air-sea CO_2 fluxes. Given the large diversity and heterogeneity of coastal ecosystems, this goal remains challenging. Rapid expansion of partial pressure of CO_2 (pCO_2) observations over the past decade has allowed the first assessments of the contribution of coastal ecosystems in terms of global air-sea CO_2 fluxes (Borges, 2005; Borges et al., 2005; Cai et al., 2006; Chen and Borges, 2009; Laruelle et al., 2010; Cai, 2011). The most recent synthesis from Laruelle et al. (2010) estimates a net sink of atmospheric CO_2 over continental shelf seas of -0.21 ± 0.36 Pg C yr^{-1}, while estuaries accounted for a source of CO_2 to the atmosphere of +0.27 ± 0.23 PgC yr^{-1}. The air-sea CO_2 flux per surface area over continental shelf seas (-0.7 ± 1.2 mol C m^{-2} yr^{-1}) is twice higher than the value in the open ocean. However, extrapolation from local to global estimates still involves large uncertainties due to important spatial heterogeneity of coastal seas, and because many continental shelf seas and estuaries remain under-sampled. Further, the dynamic of the carbonate systems in coastal seas is characterized by high temporal variability, from daily (Dai et al., 2009; Bozec et al., 2011; Thomas et al., 2012) to inter-annual (Friederich et al., 2002; Borges et al., 2008; Bozec et al., 2011) time scales, which need to be investigated.

5. Thesis objectives

In a context of climate change, and regarding the insufficient data coverage both in time and space in coastal ecosystems, this PhD thesis investigated the spatial and temporal variability of the CO_2 system and air-sea CO_2 fluxes in contrasted ecosystems of the North-West European continental shelf. These highly active biogeochemical environments host representative hydrographical systems (permanently well-mixed, seasonally stratified, frontal structures, estuarine) of temperate zones, in which the dynamic of the CO_2 system were poorly documented.

An autonomous ocean observing system equipped with high precision oceanographic sensors (FerryBox system, -4H-Jena inc.) was installed in 2010 on the Voluntary Observing Ship (VOS) *Armorique* operated by Brittany Ferries. This vessel crossed the Western English Channel (WEC) between Roscoff (France) and Plymouth (United Kingdom) up to three times a day from December 2010 to January 2014. Based on three years of bimonthly discrete

samplings onboard the ferry and two years of high-frequency FerryBox records, we built a comprehensive dataset for biogeochemical and CO_2 system parameters in the WEC.

Based on this dataset, the objectives of this study were firstly to assess the biological, chemical and physical processes controlling the CO_2 system in the WEC from daily to inter-annual time-scales. Secondly, to quantify air-sea CO_2 fluxes in the WEC provinces as part of the overall assessment of CO_2 fluxes in coastal seas. Finally, to develop an innovative method based on satellite observations to extend our air-sea CO_2 flux estimates both in time (over a decade) and in space (in the adjacent Celtic and Irish Seas).

6. Thesis outlines

This thesis is based on published (Chapters 2 and 3) and submitted (Chapter 4) articles in peer-reviewed journals. In Chapter 2, the original published article was modified by incorporating two more years of data to the initial one year study with corresponding results and discussions updates. A description of the methods used for the sampling procedure and analytical measurements are available in each "Material and Methods" section of each chapter. The study areas are described in details in the introduction of Chapter 2, 3 and 4.

Chapter 2 is based on three years of bimonthly discrete samplings onboard the VOS *Armorique* between Roscoff and Plymouth. We describe and discuss the seasonal and inter-annual biogeochemical variability of the surface waters of the WEC, with a main focus on the CO_2 system and air-sea CO_2 exchanges. We also estimate net ecosystem production (NEP) based on DIC budgets and relate it to air-sea CO_2 fluxes.

Chapter 3 deals with the short time-scale dynamics of the WEC. In this chapter, we make a detailed assessment of the reliability of our FerryBox system with a particular focus on the first deployment of a next generation pCO_2 sensor (Contros HydroC/CO_2 FT). Based on two years of corrected high-frequency measurements from the FerryBox system we then evaluate the short-time scale processes driving air-sea CO_2 fluxes in the WEC.

In chapter 4, based on three years of pCO_2 data from the VOS (both bimonthly and high-frequency pCO_2 data), we developed algorithms to link our surface pCO_2 to remotely sensed (SST, Chl-*a*, PAR, wind-speed) and modeled (MLD) variables. We established

specific relationships between our pCO_2 dataset and these environmental variables, using multiple linear regressions. We extrapolated the relations obtained in WEC based on the 2011-2013 dataset 1) temporally over a decade; and 2) spatially in the adjacent Celtic and Irish Seas (CS and IS). Based on this reconstructed decadal dataset, we investigate the inter and multi-annual variability of pCO_2 and air-sea CO_2 fluxes over the shelf.

Chapter 6 is a general discussion based on the major results obtained during the three years of investigations. We present these results in a wider context and discuss their implications and possible recommendations for future research.

References

Bakker, D. C. E., Pfeil, B., Smith, K., Hankin, S., Olsen, A., Alin, S. R., Cosca, C., Harasawa, S., Kozyr, A., Nojiri, Y., O'Brien, K. M., Schuster, U., Telszewski, M., Tilbrook, B., Wada, C., Akl, J., Barbero, L., Bates, N. R., Boutin, J., Bozec, Y., Cai, W.-J., Castle, R. D., Chavez, F. P., Chen, L., Chierici, M., Currie, K., De Baar, H. J. W., Evans, W., Feely, R. A., Fransson, A., Gao, Z., Hales, B., Hardman-Mountford, N. J., Hoppema, M., Huang, W.-J., Hunt, C. W., Huss, B., Ichikawa, T., Johannessen, T., Jones, E. M., Jones, S., Jutterstrøm, S., Kitidis, V., Körtzinger, A., Landschützer, P., Lauvset, S. K., Lefèvre, N., Manke, A. B., Mathis, J. T., Merlivat, L., Metzl, N., Murata, A., Newberger, T., Omar, A. M., Ono, T., Park, G.-H., Paterson, K., Pierrot, D., Ríos, A. F., Sabine, C. L., Saito, S., Salisbury, J., Sarma, V. V. S. S., Schlitzer, R., Sieger, R., Skjelvan, I., Steinhoff, T., Sullivan, K. F., Sun, H., Sutton, A. J., Suzuki, T., Sweeney, C., Takahashi, T., Tjiputra, J., Tsurushima, N., Van Heuven, S. M. A. C., Vandemark, D., Vlahos, P., Wallace, D. W. R., Wanninkhof, R. and Watson, A. J., 2014. An update to the Surface Ocean CO_2 Atlas (SOCAT version 2). Earth System Science Data 6, 69-90.

Bauer, J. E., Cai, W.-J., Raymond, P. A., Bianchi, T. S., Hopkinson, C. S., Regnier, P. A. G., 2013. The changing carbon cycle of the coastal ocean. Nature 504, 61–70.

Bopp, L., Resplandy, L., Orr, J. C., Doney, S. C., Dunne, J. P., Gehlen, M., Halloran, P., Heinze, C., Ilyina, T., Séférian, R., Tjiputra, J., Vichi, M., 2013. Multiple stressors of ocean ecosystems in the 21st century: projections with CMIP5 models. Biogeosciences 10, 6225–6245.

Borges, A., 2005. Do we have enough pieces of the jigsaw to integrate CO_2 fluxes in the coastal ocean? Estuaries and Coasts 28(1), 3–27.

Borges, A. V., Alin, S. R., Chavez, F. P., Vlahos, P., Johnson, K. S., Holt, J. T., Balch, W. M., Bates, N., Brainard, R., Cai, W. J., Chen, C. T. A., Currie, K., Dai, M., Degrandpre, M., Delille, B., Dickson, A., Evans, W., Feely, R. A., Friederich, G. E., Gong, G.-C., Hales, B., Hardman-Mountford, N., Hendee, J., Hernandez-Ayon, J. M., Hood, M., Huertas, E., Hydes, D., Ianson, D., Krasakopoulou, E., Litt, E., Luchetta, A., Mathis, J., McGillis, W. R., Murata, A., Newton, J., Ólafsson, J., Omar, A., Perez, F. F., Sabine, C., Salisbury, J. E., Salm, R., Sarma, V. V. S. S., Schneider, B., Sigler, M., Thomas, H., Turk, D., Vandemark, D., Wanninkhof, R., Ward, B., 2010. A global sea surface carbon observing system: inorganic and organic carbon dynamics in coastal oceans. Proceedings of OceanObs'09: Sustained Ocean Observations and Information for Society (Vol. 2),

Venice, Italy, 21-25 September 2009, Hall, J., Harrison, D.E. & Stammer, D., Eds., ESA Publication WPP-306.

Borges, A. V., Gypens, N., 2010. Carbonate chemistry in the coastal zone responds more strongly to eutrophication than to ocean acidification. Limnology & Oceanography 55(2), 1–8.

Borges, A. V., Delille, B., Frankignoulle, M., 2005. Budgeting sinks and sources of CO_2 in the coastal ocean: Diversity of ecosystems counts. Geophysical Research Letters 32, L14601.

Borges, A. V., Tilbrook, B., Metzl, N., Lenton, A., Delille, B., 2008. Inter-annual variability of the carbon dioxide oceanic sink south of Tasmania. Biogeosciences 5, 141–155.

Bozec, Y., Merlivat, L., Baudoux, a-C., Beaumont, L., Blain, S., Bucciarelli, E., Danguy, T., Grossteffan, E., Guillot, A., Guillou, J., Répécaud, M., Tréguer, P., 2011. Diurnal to inter-annual dynamics of pCO_2 recorded by a CARIOCA sensor in a temperate coastal ecosystem (2003–2009). Marine Chemistry 126, 13–26.

Boyd, P. W. and Hurd, C. L., 2009. Ocean Nutrients. In Surface Ocean-Lower Atmosphere Processes, C. Le Quéré and E. S. Saltzman editors, eds., Geophysical Monograph Series 187, 329 pp.

Brewer, P.G. and Goldman, J.C., 1976. Alkalinity changes generated by phytoplankton growth. Limnology and Oceanography 21(1): 108-117.

Cai, W.-J., Dai, M., Wang, Y., 2006. Air-sea exchange of carbon dioxide in ocean margins: A province-based synthesis. Geophysical Research Letters 33, L12603.

Cai, W.-J., 2011. Estuarine and Coastal Ocean Carbon Paradox : CO_2 Sinks or Sites of Terrestrial Carbon Incineration. Annual Review of Marine Science 3, 123–145.

Chen, C.A., Borges, A.V., 2009. Reconciling opposing views on carbon cycling in the coastal ocean : Continental shelves as sinks and near-shore ecosystems as sources of atmospheric CO_2. Deep-Sea Research 56, 578–590.

Dai, M., Lu, Z., Zhai, W., Chen, B., Cao, Z., Zhou, K., Cai, W.J., Chen, C.T.A., 2009. Diurnal variations of surface seawater pCO_2 in contrasting coastal environments. Marine Geology 54, 735–745.

De La Rocha, C.L., Passow, U., 2007. Factors influencing the sinking of POC and the efficiency of the biological carbon pump. Deep Sea Research Part II: Topical Studies in Oceanography 54, 639–658.

Dickson, A.G., 1981. An exact definition of total alkalinity and a procedure for the estimation of alkalinity and total inorganic carbon from titration data. Deep-Sea Research I 28:

609-623.

Dickson, A.G. and Millero, F.J., 1987. A comparison of the equilibrium constants for the dissociation of carbonic acid in seawater media. Deep-Sea Research Part a - Oceanographic Research Papers 34(10): 1733-1743.

Dickson, A. G., 1993. The measurement of sea water pH. Marine Chemistry 44(2-4), 131–142.

Dickson, A. G., Sabine, C. L., and Christian, J. R., 2007. Guide to best practices for ocean CO_2 measurements, PICES Special Publication 3, IOCCP report No. 8, 191 pp.

Doney, S., Bopp, L., Long, M., 2014. Historical and future trends in ocean climate and biogeochemistry. Oceanography 27, 108–119.

Doney, S.C., Fabry, V.J., Feely, R. a., Kleypas, J. a., 2009. Ocean Acidification: The Other CO_2 Problem. Annual Review of Marine Science 1, 169–192.

Drinkwater, K. F., Beaugrand, G., Kaeriyama, M., Kim, S., Ottersen, G., Perry, R. I., Pörtner, H.-O., Polovina, J. J., Takasuka, A., 2010. On the processes linking climate to ecosystem changes. Journal of Marine Systems 79, 374–388.

Falkowski, P., Barber, R., Smetacek, V., 1998. Biogeochemical controls and feedbacks on ocean primary production. Science 281, 200–206.

Field, C. B., Behrenfeld, M. J., Randerson, J. T., Falkowski, P., 1998. Primary Production of the Biosphere: Integrating Terrestrial and Oceanic Components. Science 281, 237–240.

Friederich, G., Walz, P., 2002. Inorganic carbon in the central California upwelling system during the 1997–1999 El Niño–La Niña event. Progress in Oceanography 54, 185–203.

Friis, K., Körtzinger, A., Wallace D. W. R., 2003. The salinity normalization of marine inorganic carbon chemistry data. Geophysical Research Letters 30, 1–4.

Gattuso, J.P., Frankignoulle, M., Wollast, R., 1998. Carbon and carbonate metabolism in coastal aquatic ecosystems. Annual Review of Ecology and Systematics 29, 405–434.

Gattuso, J.P., and L. Hansson, 2011. Ocean Acidification. Oxford University Press, Oxford UK, eds., 326 pp.

Hönisch, B., Hemming, N.G., Archer, D., Siddall, M., McManus, J.F., 2009. Atmospheric carbon dioxide concentration across the mid-Pleistocene transition. Science 324, 1551–4.

IPCC, 2007. Climate Change 2007: The Physical Science Basis. Contribution of Working Group I to the Fourth Assessment Report of the Intergovernmental Panel on Climate Change [Solomon, S., D. Qin, M. Manning, Z. Chen, M. Marquis, K.B. Averyt, M. Tignor and H.L. Miller (eds.)]. Cambridge University Press, Cambridge, United

Kingdom and New York, NY, USA, 996 pp.

IPCC, 2013. Climate Change 2013: The Physical Science Basis. Contribution of Working Group I to the Fifth Assessment Report of the Intergovernmental Panel on Climate Change [Stocker, T.F., D. Qin, G.-K. Plattner, M. Tignor, S.K. Allen, J. Boschung, A. Nauels, Y. Xia, V. Bex and P.M. Midgley (eds.)]. Cambridge University Press, Cambridge, United Kingdom and New York, NY, USA, 1535 pp.

IPCC, 2014. Climate Change 2014: Impacts, Adaptation, and Vulnerability. Part A: Global and Sectoral Aspects. Contribution of Working Group II to the Fifth Assessment Report of the Intergovernmental Panel on Climate Change [Field, C.B., V.R. Barros, D.J. Dokken, K.J. Mach, M.D. Mastrandrea, T.E. Bilir, M. Chatterjee, K.L. Ebi, Y.O. Estrada, R.C. Genova, B. Girma, E.S. Kissel, A.N. Levy, S. MacCracken, P.R. Mastrandrea, and L.L. White (eds.)]. Cambridge University Press, Cambridge, United Kingdom and New York, NY, USA, 1132 pp.

Laruelle, G. G., Dürr, H. H., Slomp, C. P., Borges, A. V., 2010. Evaluation of sinks and sources of CO_2 in the global coastal ocean using a spatially-explicit typology of estuaries and continental shelves. Geophysical Research Letters 37, L15607.

Le Quéré, C., Takahashi, T., Buitenhuis, E. T., Rödenbeck, C., Sutherland, S. C., 2010. Impact of climate change and variability on the global oceanic sink of CO_2. Global Biogeochemical Cycles 24, GB4007.

Liu, K.-K., Atkinson, L., Quinones, R., and Talaue-McManus, L., 2010. Carbon and Nutrient Fluxes in Continental Margins A Global Synthesis. Eds., IGBP Book Series, Springer, Heidelberg, Germany, 744 pp.

Lüthi, D., Le Floch, M., Bereiter, B., Blunier, T., Barnola, J.-M., Siegenthaler, U., Raynaud, D., Jouzel, J., Fischer, H., Kawamura, K., Stocker, T. F., 2008. High-resolution carbon dioxide concentration record 650,000-800,000 years before present. Nature 453, 379–82.

MacFarling Meure, C., Etheridge, D., Trudinger, C., Steele, P., Langenfelds, R., van Ommen, T., Smith, A., Elkins, J., 2006. Law Dome CO_2, CH_4 and N_2O ice core records extended to 2000 years BP. Geophysical Research Letters 33, L14810.

Mackenzie, F.T., Lerman, A., Andersson, A. J., 2004. Past and present of sediment and carbon biogeochemical cycling models. Biogeosciences 1, 11–32.

Mehrbach, C., Culberso, Ch., Hawley, J.E. and Pytkowic, R.M., 1973. Measurement of apparent dissociation constants of carbonic acid in seawater at atmospheric pressure. Limnology and Oceanography, 18(6): 897-907.

Millero, F.J., Lee, K., Roche, M., 1998. Distribution of alkalinity in the surface waters of the major oceans. Marine Chemistry 60, 111–130.

Muller-Karger, F.E., Varela, R., Thunell, R., Luerssen, R., Hu, C., Walsh, J. J., 2005. The importance of continental margins in the global carbon cycle. Geophysical Research Letters 32, L01602.

Nightingale, P.D., Malin, G., Law, C.S., Watson, A.J., Liss, P.S., Liddicoat, M.I., Boutin, J., Upstill-Goddard, R.C., 2000. In situ evaluation of air-sea gas exchange parameterizations using novel conservative and volatile tracers. Global Biogeochemical Cycles 14, 373–387.

Orr, J.C., Fabry, V.J., Aumont, O., Bopp, L., Doney, S.C., Feely, R. a, Gnanadesikan, A., Gruber, N., Ishida, A., Joos, F., Key, R.M., Lindsay, K., Maier-Reimer, E., Matear, R., Monfray, P., Mouchet, A., Najjar, R.G., Plattner, G.-K., Rodgers, K.B., Sabine, C.L., Sarmiento, J.L., Schlitzer, R., Slater, R.D., Totterdell, I.J., Weirig, M.-F., Yamanaka, Y., Yool, A., 2005. Anthropogenic ocean acidification over the twenty-first century and its impact on calcifying organisms. Nature 437, 681–6.

Ottersen, G., Kim, S., Huse, G., Polovina, J.J., Stenseth, N.C., 2010. Major pathways by which climate may force marine fish populations. Journal of Marine Systems 79, 343–360.

Parekh, P., Follows, M. J., Dutkiewicz, S., Ito, T., 2006. Physical and biological regulation of the soft tissue carbon pump. Paleoceanography 21, PA3001.

Petit, J., Jouzel, J., Raynaud, D., Barkov, N., 1999. Climate and atmospheric history of the past 420,000 years from the Vostok ice core, Antarctica. Nature.

Sarmiento, J., Toggweiler, J. R., 1984. A new model for the role of the oceans in determining atmospheric pCO_2. Nature 339, 429-436.

Siegenthaler, U., Stocker, T., Monnin, E., 2005. Stable carbon cycle–climate relationship during the late Pleistocene. Science 310, 1313–1317.

Sitch, S., Huntingford, C., Gedney, N., Levy, P. E., Lomas, M., Piao, S. L., Betts, R., Ciais, P., Cox, P., Friedlingstein, P., Jones, C. D., Prentice, I.C., Woodward, F. I., 2008. Evaluation of the terrestrial carbon cycle, future plant geography and climate-carbon cycle feedbacks using five Dynamic Global Vegetation Models (DGVMs). Global Change Biology 14, 2015–2039.

Takahashi, T., Sutherland, S. C., Wanninkhof, R., Sweeney, C., Feely R. A., Chipman, D. W., Hales, B., Friederich, G., Chavez, F., Sabine, C., Watson, A., Bakker, D. C. E., Schuster, U., Metzl, N., Yoshikawa-Inoue, H., Ishii, M., Midorikawa, T., Nojiri, Y., Körtzinger,

A., Steinhoffm, T., Hoppema, M., Olafsson, J., Arnarson, T. S., Tilbrook, B., Johannessen, T., Olsen, A., Bellerby, R., Wong, C. S., Delille, B., Bates, N. R., de Baar, H. J. W., 2009. Climatological mean and decadal change in surface ocean pCO_2, and net sea–air CO_2 flux over the global oceans. Deep Sea Research Part II: Topical Studies in Oceanography 56, 554–577.

Thomas, H., Bozec, Y., Elkalay, K., de Baar, H. J. W., 2004. Enhanced open ocean storage of CO_2 from shelf sea pumping. Science 304, 1005–8.

Thomas, H., Craig, S.E., Greenan, B.J.W., Burt, W., Herndl, G.J., Higginson, S., Salt, L., Shadwick, E.H., Urrego-Blanco, J., 2012. Direct observations of diel biological CO_2 fixation on the Scotian Shelf, northwestern Atlantic Ocean. Biogeosciences 9, 2301–2309.

Tsunogai, S., Watanabe, S., Sati, T., 1999. Is there a "continental shelf pump" for the absorption of atmospheric CO_2? Tellus B 51, 701–712.

Vazquez-Rodriguez, M., Touratier, F., Lo Monaco, C., Waugh, D. W., Padin, X. A., Bellerby, R. G. J., Goyet, C., Metzl, N., Rios, A. F., and Perez, F. F., 2009. Anthropogenic carbon distributions in the Atlantic Ocean: data-based estimates from the Arctic to the Antarctic. Biogeosciences 6, 439–451.

Wallace, R. B., Baumann, H., Grear, J. S., Aller, R. C., Gobler, C. J., 2014. Coastal ocean acidification: The other eutrophication problem. Estuarine, Coastal and Shelf Science 148, 1–13.

Walsh, J. J., Rowe, G. T., Iverson, R. L., McRoy, C. P., 1981. Biological export of shelf carbon is a sink of the global CO_2 cycle. Nature 291, 196-201.

Walsh, J. J., 1991. Importance of continental margins in the marine biogeochemical cycling of carbon and nitrogen. Nature 350, 53-55.

Wanninkhof, R., Asher, W.E., Ho, D.T., Sweeney, C., McGillis, W.R., 2009. Advances in quantifying air-sea gas exchange and environmental forcing. Annual review of marine science 1, 213–44.

Weiss, R.F., 1974. Carbon dioxide in water and seawater: the solubility of a non-ideal gas. Marine Chemistry 2, 203-215.

Wolf-Gladrow, D., Zeebe, R., Klaas, C., Kortzinger, A, Dickson, A, 2007. Total alkalinity: The explicit conservative expression and its application to biogeochemical processes. Marine Chemistry 106, 287–300.

Zeebe R. E. and Wolf-Gladrow, D. A., 2001. CO_2 in seawater: equilibrium, kinetics, isotopes, Elsevier Oceanography Series, 65, Amsterdam, 346 pp.

Chapter 2: Seasonal and latitudinal variability of the CO_2 system in the western English Channel based on Voluntary Observing Ship (VOS) discrete measurements over three contrasted years.

This chapter is adapted from an article published in 2013 in Marine Chemistry 155 (29-41): "Seasonal and latitudinal variability of the CO2 system in the western English Channel based on Voluntary Observing Ship (VOS) measurements."

P. Marrec, T. Cariou, E. Colin, A. Durand, M. Latimier, E. Macé, P. Morin, S. Raimund, M. Vernet and Y. Bozec.

Abstract

We investigated the dynamics of the CO_2 system across the Western English Channel (WEC) between Roscoff (France) and Plymouth (UK) using a Voluntary Observing Ship (VOS). From December 2010 to December 2013, 57 return crossings were carried out to collect a comprehensive dataset of CO_2 system parameters and ancillary data. The hydrographical structure of the water column across the latitudinal transect was investigated at 3 fixed stations: ASTAN (southern WEC, sWEC, offshore Roscoff), E1 and L4 (northern WEC, nWEC, offshore Plymouth). Based on these profiles and sea surface temperature (SST) anomalies from the ferry transects, we defined two provinces, the stratified nWEC (49.40°N-50.20°N) and the well-mixed sWEC (48.80°N-49.40°N), which were periodically separated by a thermal front. These contrasted hydrographical properties strongly influenced the ecosystem dynamics. Biological production/respiration processes were the main driver of pCO_2 variability from spring to fall and thermodynamical processes control the pCO_2 variability during winter. The nWEC showed enhanced biological activities characterized by an extensive autotrophic phase, which maintained the pCO_2 below the atmospheric equilibrium until early fall and acted as sink for atmospheric CO_2 at a rate of -0.4 ± 0.1 mol C m^{-2} y^{-1}. The sWEC was characterized by a shorter autotrophic phase and a longer heterotrophic phase compared to nWEC and acted as source of CO_2 to the atmosphere at a rate of +0.5 ± 0.2 mol C m^{-2} y^{-1}. On annual scale, calculation of Net Ecosystem Production (NEP) revealed that surface waters at E1 and ASTAN were both autotrophic at rates of 2.4 ± 1.0 mol C m^{-2} y^{-1} and 0.7 ± 0.5 mol C m^{-2} y^{-1}, respectively. Our latitudinal approach resolved the discrepancy between the directions of the fluxes in the WEC observed in previous studies by differentiating between the hydrological regions. The combined approach of using data from VOS tracks and fixed coastal observatories stations provided new insights into the control of air-sea CO_2 fluxes in the different provinces of the WEC. This combined approach could be applied in other continental shelf systems where data on the CO_2 system are sparse.

1. Introduction

Despite the relatively moderate size of continental shelves (7%) compared to the global ocean, these ecosystems play a significant role in the biogeochemical cycle of carbon and in oceanic uptake of atmospheric CO_2 (Walsh et al., 1981; Walsh, 1991). The high biological activity occurring in the marginal seas, ranging from 15% to 30% of oceanic primary production (Gattuso et al., 1998), causes enhanced air-sea CO_2 fluxes (Thomas et al., 2004; Borges et al., 2005). These marginal seas act as sinks for atmospheric CO_2 whereas near-shore ecosystems act as sources of CO_2 for the atmosphere (Chen & Borges, 2009). Because of the large diversity and heterogeneity of coastal ecosystems, a robust estimation of air-sea CO_2 fluxes in the coastal ocean at the global scale remains a challenge. Recently, Borges et al. (2010) pointed out the need for a global sea surface carbon observing system to unravel inorganic carbon dynamics in coastal ecosystems. Such an observing system would rely on Voluntary Observing Ship (VOS) and time-series measurements of the different parameters of the CO_2 system in seawater for various coastal ecosystems. In this respect, the global estimate of air-sea CO_2 fluxes in costal ecosystems would be improved by a better coverage of these fluxes in different hydrographical regimes.

The Western English Channel (WEC) is part of one of the world's most expended margins, the north-west European continental shelf. This area is characterized by relatively shallow depth and by intense tidal streams with maximum speeds ranging from 0.5 to 2.0 $m.s^{-1}$ (maxima for the entire English Channel (EC)) (Reid et al., 1993). The WEC hosts three different hydrographical structures: all year well-mixed, seasonally stratified and thermal front structures. Along the French coast (southern WEC, sWEC), where the tidal currents are the strongest, the water column remains vertically mixed whereas near the English coast (northern WEC, nWEC), where tidal streams are less intense, seasonal stratification occurs. Between these two distinct structures, a frontal zone oscillates, separating well-mixed and stratified waters (Pingree & Griffiths, 1978). Such water column characteristics are also observed in adjacent seas of the North-West European continental shelf, i.e. in the Irish Sea and in the North Sea (Hill et al., 2008). In this complex hydrographical context, important spatial and temporal variability occur in the dynamics of the CO_2 system (Borges and Frankignoulle, 2003; Padin et al., 2007; Dumousseaud et al., 2010; Kitidis et al., 2012) necessitating high frequency sampling strategy throughout the year for accurate assessment. Previous studies of the CO_2 system in the WEC were either based on longitudinal transects (Borges & Frankignoule, 2003; Padin et al. 2007; Dumousseaud et al., 2010) or a fixed station approach (Kitidis et al., 2012). However, these authors pointed out the need for a latitudinal approach, which

would cover each of the hydrographical structures of the WEC and thus better constrain the main drivers of CO_2 system dynamics in the WEC.

In the present study, as part of the European cross-border INTERREG IV project MARINEXUS (Our shared seas: Mechanisms of ecosystem change in the Western Channel) we exploited a VOS route between the French and English coasts (Figure 7), which crosses the different hydrographical structures of the WEC described above. Bi-monthly sampling on the *Armorique* ferry (Brittany Ferries) over three contrasted years provided a comprehensive new dataset of the CO_2 system and ancillary data in the WEC. Furthermore, data were also collected as part of the Western Channel Observatory of Plymouth (NERC National Capability of the Plymouth Marine Laboratory and Marine Biological Association) and the French network for observation of the coastal ocean (SOMLIT) at three fixed stations, one off the French coast (ASTAN, all year well-mixed) and two off the English coast (E1, L4, seasonally stratified), to determine the physical structure of the water column in these contrasting systems.

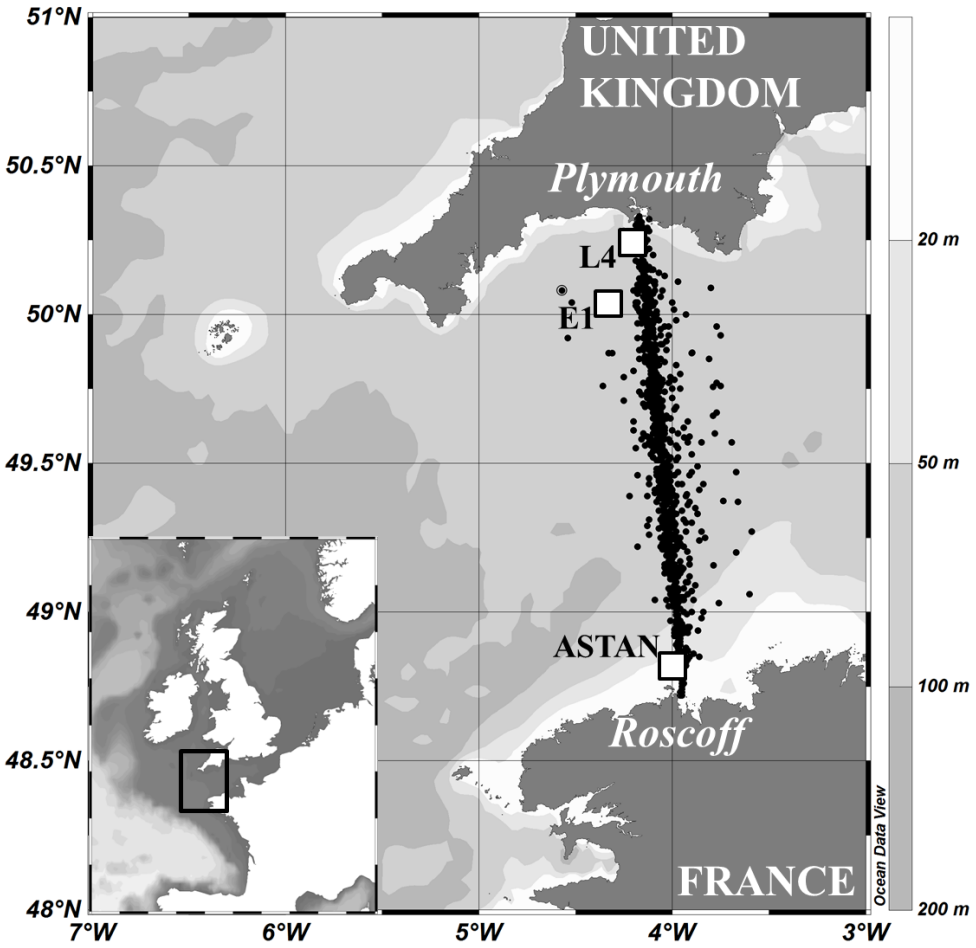


Figure 7: Map and bathymetry of the study area with the locations of the 1019 stations sampled along the 57 Ferry transects from January 2011 to December 2013 and location of the fixed stations ASTAN, E1 and L4.

Based on this dataset, we investigated the carbonate system dynamics along a latitudinal gradient for the first time in the WEC. In the present chapter, we firstly present the physical characteristics of the different WEC provinces and the spatio-temporal distribution of the carbonate system and ancillary data in these provinces. We then discuss the processes controlling the spatial distribution and the temporal variability of surface water partial pressure of CO_2 (pCO_2) and air-sea CO_2 fluxes across the WEC. Based on the dissolved inorganic carbon (DIC) data and air-sea CO_2 flux calculations, we estimate the net ecosystem production (NEP) in the well-mixed and seasonally stratified systems and relate it to the trophic status of each system.

2. Material and Methods

2.1 Surface measurements on the VOS line

Data were collected from the 22nd of December 2010 to the 13th of December 2013 across the Western English Channel between Roscoff (France, 48°43'38N 3°59'03E) and Plymouth (United Kingdom, 50°22'12N 4°08'31E) (Figure 7). Transects were performed on a bimonthly basis on board the *Armorique* ferry (Brittany Ferries) (Table 2). A -4H- JENA engineering FerryBox system was installed at the engine room level on the ferry in 2010. The FerryBox pumped seawater at 4 meters depth with a high flow rate to avoid warming of seawater in the water column circuit. The pump was operational only when the ferry was sufficiently far from the harbours to avoid introducing particle-rich waters into the system. A Sea Bird SBE 38 temperature sensor recorded the *in-situ* seawater temperature with a precision of 0.01°C whereas a Sea Bird SBE 45 thermosalinograph recorded the temperature and salinity inside the seawater circuit of the Ferry Box with precisions of 0.01°C and 0.001, respectively.

During the three years of study, we undertook 57 return crossings between Roscoff and Plymouth and sampled a total of 1019 surface stations in the WEC (Table 2). During each cruise, 18 water samples were sampled from the Ferry Box seawater circuit for the determination of dissolved oxygen (DO), dissolved inorganic carbon (DIC), total alkalinity (TA), nutrients, chlorophyll-*a* (Chl-*a*) and salinity. Discrete salinity samples were collected to calibrate the autonomous SBE 45 sensor. Discrete samples were measured on a portasal salinometer at the SHOM (Service Hydrographique et Oceanographique de la Marine) with a precision of 0.002 and were in good agreement with the SBE 45 measurements ($Salinity_{SBE45}=Salinity_{SHOM}$ x 0.99, n=270, $r^2=0.96$). DO samples (280 mL

brown glass bottles) were poisoned with 1.7 mL of manganese chlorate (600 g L^{-1}) immediately after sampling; samples were kept into the dark in a water bath and analyzed within a week of sampling. DO concentrations were determined by the Winkler method using a potentiometric end-point determination with an estimated accuracy of 0.5 µmol L^{-1}. The oxygen saturation level (DO%) was then calculated according to Weiss (1974) from the observed DO and the DO at saturation using the *in-situ* temperature and salinity. The first year, DIC and TA were collected in 100 mL and 250 mL borosilicate glass bottles, respectively, poisoned with 100 µL of $HgCl_2$, and analyzed within a week of sampling. DIC was determined with an AIRICA system (Marianda Inc.) after acidification of a 2.3 mL aliquot with phosphoric acid, extraction by a carrier gas (N_2) and detection with an IR detector LICOR-7000. TA was measured with a TA-ALK 2 system (Appolo SciTech.) by the Gran electrotitration method on 25 mL aliquots. The accuracies of DIC and TA measurements were determined with Certified Reference Materials (CRM) provided by A. G. Dickson, Scripps Institution of Oceanography (Batch 92). CRM standards were measured at the start and at the end of each day of analysis and every 10 samples during the runs. Accuracies of the DIC and TA measurements were 2 µmol kg^{-1} and 3 µmol kg^{-1}, respectively. In 2012 and 2013, because of the large amount of samples collected, we chose to analyse DIC and TA at the national facility for analysis of carbonate system parameters (SNAPO-CO_2, LOCEAN, Paris), which allows simultaneous measurements of DIC/TA by potentiometric titration. DIC and TA were collected in 500 mL borosilicate glass bottles, poisoned with 300 µL of $HgCl_2$, stored at 4°C and analyzed simultaneously by potentiometric titration derived from the method developed by Edmond (1970) using a closed cell. The calculation of equivalence points was done using a non-linear regression (D.O.E. 1994). These simultaneous DIC and TA analysis were performed at the SNAPO-CO_2 with an accuracy of ±2 µmol kg^{-1} for DIC and TA. Inter-calibration between the two DIC methods and two TA methods confirmed the accuracies of TA and DIC of ±2 µmol kg^{-1} and ±3 µmol kg^{-1}, respectively. To determine chlorophyll-*a* concentrations (Chl-*a*), 0.5 L of seawater were filtered through glass-fibre filters (Whatman GF/F) and immediately frozen. Samples were extracted in 5 mL of acetone, acidified with an HCl solution and Chl-*a* concentrations were measured using a fluorometer (model 10 analog fluorometer Turner Designs) according to EPA (1997), with an estimated accuracy of 0.05 µg L^{-1}. Nutrient concentrations (NO_3^-, NO_2^-, PO_4^{3-} and SiO_4^-) were determined using an AA3 auto-analyser (AXFLOW) following the method of Aminot and Kérouel (2007) with accuracies of 0.02 µg L^{-1}, 1 ng L^{-1}, 1ng L^{-1} and 0.01 µg L^{-1} for NO_3^-, NO_2^-, PO_4^{3-} and SiO_4^-, respectively.

#	2011	#	2012	#	2013	Month	Number of crossings
1	22 Dec 2010	*21*	21 Feb	*40*	3 Jan	Jan	1
2	17 Feb	*22*	6 Mar	*41*	22 Feb	Feb	3
3	3 Mar	*23*	20 Mar	*42*	8 Mar	Mar	7
4	15 Mar	*24*	4 Apr	*43*	26 Mar	Apr	6
5	29 Mar	*25*	22 Apr	*44*	9 Apr	May	6
6	13 Apr	*26*	6 May	*45*	22 Apr	Jun	6
7	30 Apr	*27*	24 May	*46*	6 May	Jul	6
8	14 May	*28*	7 Jun	*47*	21 May	Aug	5
9	30 May	*29*	21 Jun	*48*	4 Jun	Sep	4
10	15 Jun	*30*	5 Jul	*49*	18 Jun	Oct	6
11	29 Jun	*31*	17 Jul	*50*	9 Jul	Nov	3
12	11 Jul	*32*	2 Aug	*51*	29 Jul	Dec	4
13	27 Jul	*33*	21 Aug	*52*	19 Aug		
14	17 Aug	*34*	6 Sep	*53*	10 Sep		
15	31 Aug	*35*	7 Oct	*54*	23 Sep		
16	14 Sep	*36*	21 Oct	*55*	10 Oct		
17	8 Oct	*37*	4 Nov	*56*	30 Oct		
18	22 Oct	*38*	22 Nov	*57*	13 Dec		
19	8 Nov	*39*	11 Dec				
20	19 Dec						

Table 2: Dates of transects Roscoff-Plymouth-Roscoff between the 22nd of December 2010 and the 13th December 2013 and number of samples for each month.

2.2 Water column measurements at fixed stations

During the same period, we acquired water column profiles of temperature and salinity from three fixed stations representative of the physical structure of the WEC (homogenous vs. stratified). The ASTAN station (48°46'40N 3°56'15W, bottom depth of 60 m), situated 3.5 km north of Roscoff (Figure 7), is representative of a well mixed water column system as described by Wafar et al. (1983) and was visited every two weeks as part of the Roscoff Coastal Observatory (SOMLIT). At ASTAN, CTD profiles were obtained with a Seabird SBE 19+, with precisions for temperature and computed salinity of 0.005°C and 0.002, respectively. Station E1 (50.03°N 4.37°W; depth 75m) and L4 (50.25°N 4.22°W; depth 50m), located approximately 38 km and 12 km off Plymouth (Figure 7), were representative of seasonally stratified open shelf seas and coastal waters of the WEC, respectively (Smyth et al., 2010). Measurements were undertaken by the Western Channel

Observatory (NERC National Capability of the Plymouth Marine Laboratory and Marine Biological Association), weekly at coastal station L4 and fortnightly at open shelf station E1. CTD profiles were obtained with a Seabird SBE 19+ and provided the same precisions as given above for temperature and salinity. DIC and TA were not directly sampled at the fixed stations ASTAN and E1. In the following discussion, for these two parameters we refer to data sampled from the VOS line in the vicinity of fixed stations ASTAN end E1.

2.3 Calculation of the partial pressure of CO_2 and air-sea CO_2 fluxes

The seawater partial pressure of CO_2 (pCO_2) were calculated from TA, DIC, temperature, salinity and nutrients concentrations with the CO2SYS program (Pierrot et al., 2006) using the equilibrium constants of CO_2 proposed by Mehrbach et al. (1973), refitted by Dickson and Millero (1987) on the seawater pH scale, as recommended by Dickson et al. (2007). The computed values of pCO_2 from DIC and TA have uncertainty of ± 6 µatm (Zeebe and Wolf-Galdrow, 2001) which does not include uncertainties in the dissociation constants and ignores the contribution of organic compounds to alkalinity (Koeve et al., 2011, Hope et al., 2012). The WEC waters are open continental shelf waters, which are weakly influenced by estuarine plumes. Organic matter levels are thus low, except in the vicinity of Plymouth. Organic compounds therefore do not significantly influence alkalinity in most of the WEC. Atmospheric pCO_2 ($pCO_{2\ air}$) was calculated from the CO_2 molar fraction (xCO_2) at the Mace Head site (53°33'N 9°00'W, southern Ireland) of the RAMCES network (Observatory Network for Greenhouse gases) and from the water vapor pressure (pH_2O) using the Weiss and Price (1980) equation. Atmospheric pressure (Patm) in the middle of the WEC (49°50'N, 4°00'W) was obtained from the NCEP/NCAR re-analysis project.

The fluxes of CO_2 across the air-sea interface (F) were computed from the pCO_2 air-sea gradient ($\Delta pCO_2 = pCO_{2\ water} - pCO_{2\ air}$, µatm) according to:

$$F = k * \alpha * \Delta pCO_2 \qquad (16)$$

where k is the gas transfer velocity (m s^{-1}) and α is the solubility coefficient of CO_2 (mol atm^{-1} m^{-3}) calculated after Weiss (1974). The exchange coefficient k was computed as a function of wind speed with the algorithm given by Nightingale et al. (2000) established in the Southern Bight of the

North Sea (SBNS). The SBNS and the WEC present similar environmental characteristics: these two shallow continental shelves are both close to land with high tidal currents controlling the physical structure of the water column. Wind speed data corrected to 10 m height were obtained from the NCEP/NCAR re-analysis project (Kalnay et al., 1996) provided by the NOAA-ESRL Physical Sciences Division, (Boulder, CO, USA, http://wwww.esrl.noaa.gov/psd/). Daily wind speed were extracted on the north (>49.5°) and South (<49.5°) parts of the transect. We interpolated the bimonthly pCO_2 estimates in each zone at a daily scale to compute mean seasonal and annual fluxes.

2.4 Calculation of the Net Ecosystem Production

The Net Ecosystem Production (NEP) quantifies the metabolic status of an ecosystem and corresponds to the difference between organic matter production and mineralization. In other terms, it is the difference between gross primary production (GPP) and ecosystem respiration (R). An ecosystem is deemed net autotrophic when production of organic matter is larger than its consumption (NEP > 0). In heterotrophic systems, respiration processes predominate (NEP < 0) and such systems require external organic carbon inputs (Odum, 1956). Gazeau et al. (2005) described and compared several methods to assess NEP for European coastal zones and argued that such assessment can be performed from the DIC budget. Here, NEP was computed from the temporal DIC variations between two cruises using the method employed by Bozec et al., (2006), Schiettecatte et al. (2007) and Borges et al. (2008) according to the following equation:

$$NEP = (DIC_1 - DIC_2) * d / \Delta t - F \qquad (17)$$

where DIC_1 and DIC_2 are the mean values in mmol m^{-3} during two consecutive cruises, d is the Mixed Layer Depth (MLD) in m, Δt is the time interval in days between the two cruises and *F* is the mean air-sea CO_2 flux for the two cruises. This calculation was performed on data from the vicinity of ASTAN station (48.90°N-49.10°N) for the entire water column and on data from the vicinity of E1 (49.80°N-50.00°N) station for the MLD determined from the CTD profiles (Table 3). MLD was defined as the shallowest depth corresponding to a temperature or density difference with the surface water higher than δT=0.5°C or $\delta Dens$=0.125 (Monterey and Levitus, 1997)

NEP assessments were not performed at L4 due to freshwater inputs, which strongly influenced the carbonate system properties on time scales less than 2 weeks. For the other stations, the computations were carried out considering that the relatively low Δt used (two weeks) does not exceed the flushing time in the area, which ranges from 30 to 90 days in the English Channel (Dehlez et al, 2004). Such an approach implies the assumption that air-sea CO_2 exchanges, GPP and R are the main drivers of the CO_2 dynamics. According to Southward et al. (2005) (and references therein), diatoms are the main phytoplankton group during the spring and late summer-early fall blooms (influencing the GPP), whereas dinoflagellates dominate during summer in the WEC. Calcifying species such as coccolithophores can be present in the WEC (Southward et al., 2005; Widdicombe et al., 2010). Satellite images from MODIS-Aqua Particulate Inorganic Carbon (PIC) algorithms (http://oceancolor.gsfc.nasa.gov) revealed that during our three years of study coccolithophores blooms were present in the surface waters at E1 in early June 2011 and between 49.6°N and 49.9°N during one week at the end of July 2011. These observations were supported by phytoplankton class time-series data at station L4 (Western Channel Observatory), which confirmed the presence of coccolithophore bloom at this station. The impacts of these blooms and of benthic calcification on the seasonal and annual NEP computation are discussed below. For this NEP computation, the net advective input/output of DIC between two cruises must be assumed to be constant. The relatively short time intervals of the computation (two weeks) allow make this assumption reasonable to accept. However, short-scale eddies might induce gradients of the carbonate system in the area, which are difficult to quantify in this study but add to the uncertainty of our NEP computations.

3. Results

3.1 Hydrographical setting

3.1.1 Surface waters

In the following sections, we define winter from the 1st of January to the 31st of March, spring from the 1st of April to the 30th of June, summer from the 1st of July to the 30th of September and fall from the 1st of October to the 31st of December. SST in the WEC followed classical dynamics with a warming of surface waters from spring to the end of summer and a cooling from

early fall to winter (Figure 8a). The annual SST amplitudes in the WEC were 8.8°C, 8.9°C and 11.6°C, in 2011, 2012 and 2013, respectively. The coolest and warmest SST were recorded in 2013, with a minimum of 7.2°C in April and a maximum of 18.8°C in August (Table 3). Winter surface waters were cooler in nWEC compared to sWEC. During winter and spring, minimum SST was recorded near the coast at a latitude north of 50°N due to the discharge of freshwater from the Plymouth rivers.

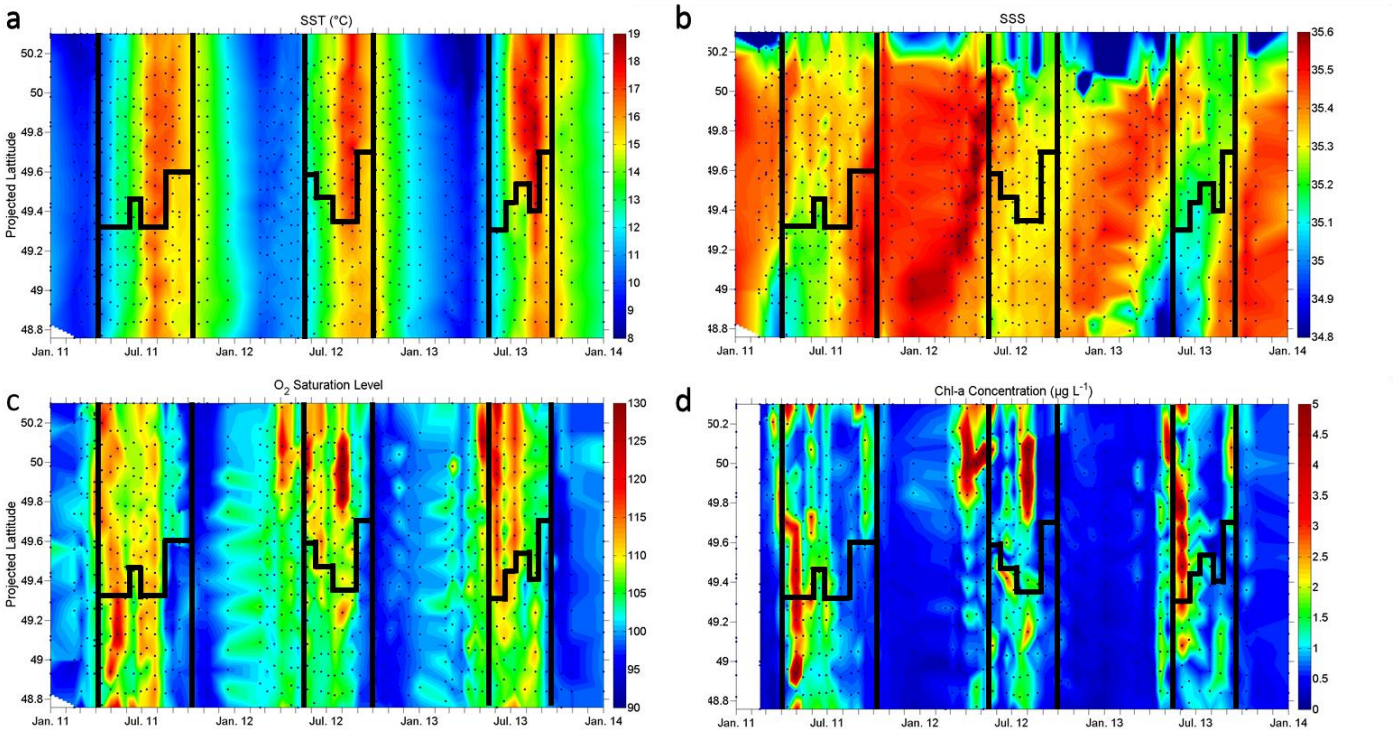


Figure 8: Surface distribution from January 2011 to December 2013 of (A) temperature (°C), (B) salinity, (C) DO% and (D) Chl-*a* (µg L^{-1}) in the WEC between Roscoff and Plymouth. Vertical black lines indicate the onset of the breakdown of thermal stratification at fixed station E1 and horizontal black lines represent an estimate of the location of the thermal front (Figure 4).

These freshwater inputs lowered the salinity (<35.20) of surface waters in the area throughout almost all of the year (Figure 8b). In the sWEC, freshwater inputs also occurred from February to June 2011 and 2013. Sea surface salinity (SSS) remained mainly lower than in the middle of the WEC (<35.30) with minimal values below 35.00 (Figure 8b). According to Kelly-Gerreyn et al. (2006), low saline waters from the Loire plume can reach the sWEC and these coastal waters are also influenced by freshwater discharges from local Britanny rivers. These hypotheses might explain the decrease of salinity observed in the sWEC during spring in 2011 and 2013. In the middle of the WEC, the highest values of SSS were recorded during fall and winter and decreased below 35.20 during spring and early summer.

	Year	Season	SST	SSS	DO%	Chl-*a*	NO_3^-	NO_2^-	PO_4^{3-}	SiO_4^-	DIC	TA	pH	pCO_2
nWEC [49.40°N-50.30°N]	2011	Winter	9,6(8,3- 11,0)	35,17(31,35- 35,52)	102(96- 114)	1,0(0,3- 3,3)	6,4(1,3- 24,9)	0,2(0,1- 0,4)	0,4(0,2- 0,8)	3,2(0,8- 12,3)	2132(2025- 2147)	2331(2169- 2343)	8,08(8,04- 8,14)	369(317- 393)
		Spring	12,7(10,3- 14,7)	35,28(34,51- 35,43)	110(104- 119)	1,5(0,6- 4,6)	0,5(0,0- 5,3)	0,0(0,0- 0,2)	0,1(0,0- 0,3)	1,1(0,0- 3,3)	2094(2072- 2135)	2343(2326- 2351)	8,13(8,08- 8,19)	324(272- 371)
		Summer	16,2(14,8- 17,1)	35,29(34,68- 35,46)	105(94- 114)	0,9(0,4- 3,7)	0,4(0,0- 3,2)	0,1(0,0- 0,5)	0,1(0,0- 0,6)	1,9(0,0- 5,5)	2082(2059- 2121)	2340(2327- 2347)	8,09(8,01- 8,14)	357(311- 449)
		Fall	14,0(11,6- 15,1)	35,40(34,35- 35,51)	98(93- 105)	0,6(0,4- 1,0)	4,1(2,3- 9,3)	0,4(0,1- 1,1)	0,3(0,2- 1,0)	3,5(2,5- 6,2)	2129(2115- 2138)	2338(2312- 2345)	8,03(7,99- 8,06)	422(392- 464)
	2012	Winter	10,1(9,1- 10,6)	35,40(34,41- 35,53)	103(100- 107)	0,9(0,2- 2,7)	6,8(5,1- 10,7)	0,3(0,1- 0,4)	0,4(0,3- 0,5)	2,9(1,2- 5,4)	2139(2127- 2155)	2339(2319- 2356)	8,07(8,06- 8,09)	378(356- 390)
		Spring	12,0(10,2- 14,2)	35,43(35,07- 35,63)	109(100- 124)	1,6(0,3- 7,2)	2,0(0,0- 7,4)	0,1(0,0- 0,3)	0,2(0,0- 0,5)	1,2(0,0- 3,7)	2108(2049- 2140)	2345(2322- 2357)	8,11(8,06- 8,20)	339(264- 393)
		Summer	15,9(14,2- 18,0)	35,26(34,81- 35,39)	108(98- 141)	1,4(0,2- 6,7)	0,2(0,0- 1,9)	0,1(0,0- 0,8)	0,1(0,0- 0,3)	1,0(0,0- 4,1)	2064(1908- 2111)	2334(2300- 2348)	8,12(8,03- 8,35)	336(168- 419)
		Fall	13,7(11,4- 15,1)	35,31(34,33- 35,49)	98(94- 103)	0,6(0,2- 1,2)	4,2(2,0- 9,9)	0,4(0,0- 0,9)	0,4(0,3- 0,5)	3,0(2,0- 5,0)	2127(2107- 2140)	2328(2310- 2340)	8,02(8,00- 8,04)	432(407- 452)
	2013	Winter	9,9(7,4- 11,6)	35,26(33,45- 35,50)	101(99- 113)	0,5(0,2- 1,1)	6,5(5,4- 9,2)	0,2(0,1- 0,3)	0,5(0,3- 0,6)	3,2(2,5- 6,3)	2134(2070- 2148)	2332(2242- 2349)	8,07(8,03- 8,10)	376(353- 405)
		Spring	10,9(7,2- 13,5)	35,23(34,31- 35,49)	110(100- 129)	1,7(0,3- 6,2)	3,4(0,0- 10,7)	0,1(0,0- 0,3)	0,2(0,0- 0,6)	2,3(0,0- 5,2)	2106(2028- 2146)	2338(2316- 2352)	8,13(8,08- 8,23)	327(243- 371)
		Summer	16,3(14,4- 18,8)	35,23(34,94- 35,41)	105(94- 118)	0,9(0,1- 2,9)	1,0(0,0- 3,9)	0,2(0,0- 0,9)	0,1(0,0- 0,3)	1,5(0,2- 3,6)	2085(2047- 2125)	2334(2318- 2348)	8,08(8,01- 8,15)	376(307- 443)
		Fall	13,7(11,5- 15,6)	35,24(32,09- 35,49)	98(92- 102)	0,7(0,5- 1,2)	4,8(2,2- 8,8)	0,4(0,0- 0,9)	0,3(0,1- 0,6)	2,5(1,0- 6,5)	2126(2058- 2142)	2325(2240- 2334)	8,02(7,98- 8,04)	436(416- 482)
sWEC [48.75°N - 49.40°N]	2011	Winter	10,1(9,3- 11,3)	35,27(35,03- 35,49)	100(92- 105)	0,4(0,1- 1,1)	8,0(5,3- 10,3)	0,2(0,1- 0,2)	0,3(0,3- 0,4)	4,2(3,3- 5,0)	2143(2132- 2155)	2338(2326- 2346)	8,06(8,05- 8,07)	387(374- 401)
		Spring	12,7(10,4- 14,9)	35,20(34,99- 35,31)	110(102- 130)	1,8(0,6- 7,1)	2,3(0,0- 8,9)	0,1(0,0- 0,3)	0,2(0,0- 0,3)	2,0(0,2- 5,5)	2100(2040- 2139)	2342(2330- 2351)	8,12(8,05- 8,24)	337(241- 399)
		Summer	15,6(14,5- 17,1)	35,37(35,16- 35,50)	104(95- 114)	0,9(0,5- 1,9)	1,6(0,0- 5,1)	0,3(0,0- 0,7)	0,2(0,0- 0,4)	2,2(0,2- 6,2)	2098(2058- 2131)	2338(2324- 2348)	8,07(8,00- 8,15)	385(303- 453)
		Fall	14,1(12,2- 15,2)	35,48(35,34- 35,58)	98(95- 104)	0,4(0,2- 0,7)	5,0(3,5- 6,5)	0,6(0,0- 1,1)	0,4(0,3- 0,5)	3,6(2,7- 6,6)	2136(2123- 2149)	2336(2331- 2345)	8,01(7,97- 8,04)	449(410- 499)
	2012	Winter	10,6(10,0- 11,1)	35,51(35,38- 35,62)	103(101- 107)	0,5(0,1- 0,8)	6,0(4,5- 8,2)	0,2(0,1- 0,3)	0,3(0,3- 0,6)	2,6(1,9- 4,8)	2143(2140- 2149)	2346(2335- 2354)	8,07(8,05- 8,08)	382(372- 397)
		Spring	11,8(10,7- 13,6)	35,39(35,27- 35,61)	105(101- 111)	0,9(0,3- 2,3)	3,2(0,5- 5,4)	0,2(0,1- 0,5)	0,3(0,0- 0,4)	1,7(0,4- 3,0)	2129(2108- 2144)	2340(2329- 2352)	8,07(8,05- 8,10)	381(347- 403)
		Summer	15,2(13,6- 17,3)	35,34(35,29- 35,41)	104(97- 116)	1,1(0,1- 2,9)	1,3(0,0- 2,8)	0,3(0,0- 1,0)	0,2(0,1- 0,4)	1,8(0,3- 3,1)	2101(2074- 2119)	2331(2320- 2344)	8,06(8,02- 8,11)	395(346- 439)
		Fall	13,7(11,6- 15,6)	35,45(35,35- 35,53)	97(95- 100)	0,4(0,2- 0,9)	5,2(3,1- 7,2)	0,3(0,1- 0,8)	0,4(0,3- 0,5)	3,0(2,1- 5,5)	2129(2113- 2144)	2329(2322- 2343)	8,01(7,99- 8,04)	438(411- 473)
	2013	Winter	10,5(9,1- 11,8)	35,31(34,97- 35,51)	101(98- 105)	0,4(0,2- 0,5)	8,3(5,7- 13,6)	0,1(0,0- 0,2)	0,5(0,3- 0,7)	4,0(2,7- 7,5)	2139(2127- 2148)	2338(2329- 2345)	8,06(8,04- 8,09)	384(360- 411)
		Spring	11,0(8,8- 13,4)	35,04(34,68- 35,28)	106(100- 113)	1,2(0,2- 3,4)	5,7(0,8- 8,7)	0,2(0,0- 0,3)	0,2(0,0- 0,4)	2,6(1,9- 3,7)	2118(2087- 2141)	2339(2328- 2356)	8,10(8,07- 8,17)	346(292- 374)
		Summer	15,2(13,4- 17,2)	35,32(35,04- 35,47)	104(97- 116)	0,9(0,4- 1,9)	2,2(0,1- 3,5)	0,4(0,0- 0,9)	0,2(0,0- 0,3)	2,2(0,7- 4,2)	2105(2073- 2122)	2333(2322- 2345)	8,05(7,99- 8,11)	401(344- 464)
		Fall	14,0(12,4- 15,3)	35,46(35,39- 35,48)	98(95- 99)	0,6(0,4- 1,1)	5,6(3,5- 6,8)	0,5(0,0- 0,9)	0,4(0,2- 0,8)	2,8(1,8- 3,6)	2131(2121- 2149)	2328(2307- 2336)	8,00(7,97- 8,03)	451(422- 497)

Table 3: Seasonal means of SST (°C), SSS, DO%, Chl-*a* (µg L^{-1}), NO_3^- (µmol L^{-1}), NO_2^- (µmol L^{-1}), PO_4^{3-} (µmol L^{-1}), SiO_4^- (µmol L^{-1}), DIC (µmol kg^{-1}), TA (µmol kg^{-1}), pH and pCO2 (µatm) in the nWEC and the sWEC from 2011 to 2013 based on the VOS line measurements. The range of values measured each season is given by the numbers in brackets. Each season is defined as follows: winter (from the 1st of January to the 31st of March), spring (from the 1st of April to the 30th of June), summer (from the 1st of July to the 30th of September) and fall (from the 1st of October to the 31st of December).

3.1.2 Water column properties

Figure 9 shows the annual variations of temperature and salinity in the water column at stations L4, E1 (nWEC, offshore Plymouth) and ASTAN (sWEC, offshore Roscoff). These profiles show that thermal stratification occurred during spring and summer in the northern part of the WEC at station E1 and L4. The MLD (mixed layer depth) at E1 ranged between 5 m and 30 m depth, with an average depth of 18 m (Table 4) and were all computed from a temperature difference with the surface water higher than $\delta T=0.5°C$ as explained in Section 2.4 (Figure 10a). In 2011, thermal stratification started in April, whereas it started in June in 2012 and 2013 (Table 4 and Figure 10a). The breakdown of the water column stratification occurred in early October in 2011 and in September in 2012 and 2013 (Table 4 and Figure 10a). Salinity at this open shelf station ranged between 35.10 and 35.50. Freshwater inputs often decreased salinity at the same latitude and in the vicinity of station E1 compared to the rest of the northern WEC (Figure 8b).

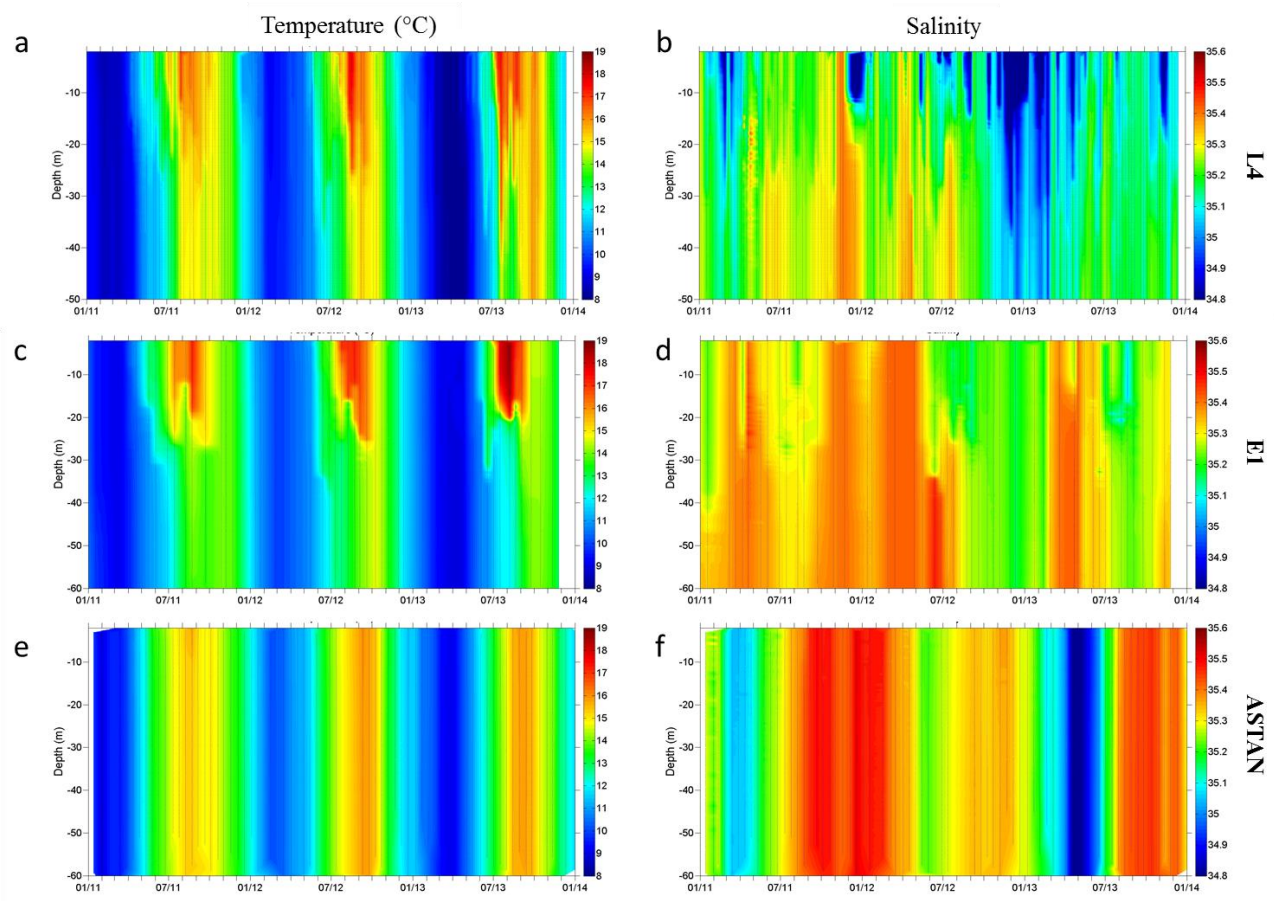


Figure 9: Profiles of temperature (left) and salinity (right) from January 2011 to December 2013 at fixed stations ASTAN, E1 and L4.

The L4 station was even more influenced by river inputs than at the latitude of E1. From the salinity and temperature profiles, we found that the MLD at L4 ranged between 3 m and 40 m, with an average value of 18 m (data not shown). The MLD were all computed from density difference with the surface water higher than δDens=0.125. Stratification occurred almost all year round at station L4 mostly due to the continuous freshwater inputs, but also to warming occurring from April to October.

At ASTAN, hydrographical profiles showed that the water column was well mixed throughout the year. Temperatures ranged between 8.8°C and 16.0°C, with the coolest temperatures observed in January 2011 and March 2013 and the warmest in September 2012 and 2013 (Figure 9). Salinity decreased during spring and increased from summer to reach maxima in fall. The lowest salinity values were recorded during spring 2013 (<34.90), whereas salinity values higher than 35.50 were recorded during winter 2011.

2011	MLD (m)	2012	MLD (m)	2013	MLD (m)
18 Jan	-	13 Jan	-	23 Jan	-
08 Mar	-	23 Jan	-	12 Feb	-
21 Mar	-	28 Feb	-	27 Feb	-
07 Apr	24	14 Mar	-	20 Mar	-
19 Apr	20	27 Apr	-	23 Apr	-
17 May	17	16 May	-	01 May	-
02 Jun	17	12 Jun	12	16 May	-
28 Jun	22	26 Jun	27	04 Jun	16
14 Jul	16	10 Jul	15	18 Jun	32
26 Jul	18	24 Jul	5	02 Jul	16
09 Aug	12	08 Aug	16	16 Jul	12
23 Aug	18	23 Aug	13	07 Aug	17
22 Sep	27	04 Sep	24	20 Aug	15
04 Oct	21	19 Sep	26	03 Sep	18
28 Oct	-	09 Oct	-	24 Sep	-
07 Nov	-	23 Oct	-	15 Oct	-
22 Nov	-	06 Nov	-	12 Nov	-
		29 Nov	-	26 Nov	-
		11 Dec	-		

Table 3: Mixed layer depth (in m) at fixed station E1 (Western Channel Observatory) computed from CTD profiles between 2011 and 2013.

3.1.3 Definition of permanently well-mixed sWEC and seasonally stratified nWEC

Figure 10a shows the difference between the surface temperature and the temperatures recorded along the CTD profiles (dTMP) at the fixed station E1 from January 2011 to December 2013. The dTMP revealed the thermal stratification periods of the water column and width of the MLD at E1. On figure 10b, we computed SST anomalies (dSST) from the difference between SST and mean SST for each Roscoff-Plymouth bimonthly transects. During spring, the transition between negative and positive dSST in the nWEC corresponded to the onset of stratification at E1, whereas, during fall, the reverse transition fitted with the breakdown of water column stratification (Vertical black lines on Figure 10). From spring to fall, negative dSST corresponded to the coolest waters of the sWEC compared to the nWEC and positive dSST corresponded to the nWEC waters. The highest positive and negative dSST values were observed during summer when the SST differences between nWEC and sWEC were the most marked.

Based on these temperature anomalies, we distinguished two main hydrographical provinces in the WEC: the seasonally stratified waters of the nWEC (49.40°N-50.20°N) and the permanently well-mixed waters of the sWEC (48.80°N-49.40°N). These two provinces were seasonally separated by a thermal front (horizontal black lines on Figure 10b), which oscillated around the latitude of 49.40°N as previously described by Pingree and Griffiths (1978). In the following sections, references to nWEC and sWEC will be based on the SST anomaly distinguished on Figure 10b.

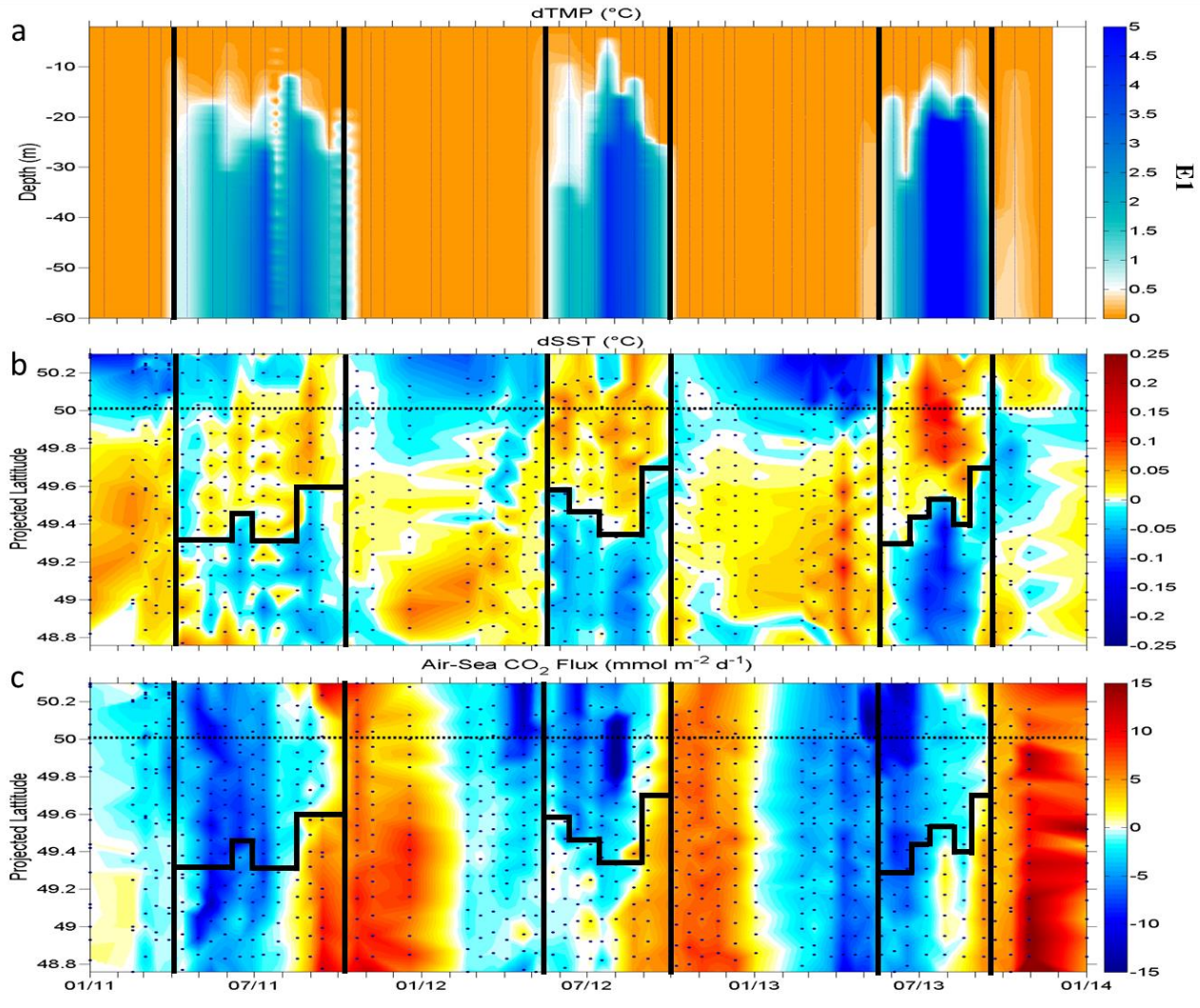


Figure 10: (A) Difference between the surface temperature and the temperatures recorded along the CTD profiles (dTMP, in °C) at the fixed station E1 from January 2011 to December 2013. (B) SST anomalies (dSST, in °C) from the difference between SST and mean SST for each Roscoff-Plymouth bimonthly transect. (C) Surface distribution from January 2011 to December 2013 of air-sea CO_2 fluxes (in mmol C m^{-2} d^{-1}) computed with the Nightingale et al. (2000) k-wind parametrization. Vertical black lines indicate the onset of the breakdown of thermal stratification at fixed station E1 and horizontal black lines represent an estimate of the location of the thermal front. The horizontal dotted line indicates the latitudinal location of fixed station E1.

3.2 Surface distributions of DO%, Chl-*a* and nutrients

In nWEC, winter values of DO% were close to atmospheric equilibrium in a homogeneous water column (Figure 8c and 9c and Table 3). Hydrographical conditions and the low winter irradiance did not allow phytoplankton development and Chl-*a* values remained low (< 1 µg L^{-1}) during winter (Figure 8d and Table 3). Nutrients concentrations reached their maxima during winter thus constituting the winter nutrients stocks. Winter nutrients concentrations ranged from 5 to 10 µmol L^{-1}, 3 to 6 µmol L^{-1} and 0.3 to 0.6 µmol L^{-1} for NO_3^-, PO_4^{3-} and SiO_4^-, respectively (Figure 11 and Table 3). Chl-*a* started to increase during March 2011 and 2012 in nWEC to reach values higher than 3 µg L^{-1} associated to DO oversaturation around 120% during spring. In 2011 and 2013 the first spring phytoplankton blooms, characterized by these higher Chl-*a* values, were concomitant with the start of stratification, whereas in 2012 the spring bloom started one and a half month before the start of stratification observed at the fixed station E1 (Figure 10a). NO_3^-, PO_4^{3-} and SiO_4^- concentrations decreased drastically at the start of phytoplankton blooms and the winter stocks were totally (NO_3^-) or partially (PO_4^{3-}, SiO_4^-) depleted one to two month after. In 2011, the productive period was characterized by an important spring bloom (Chl-*a* > 3µg L^{-1}), which occurred firstly in the northern part of the nWEC in April and one month later in the southern part of the nWEC, with associated surface DO% values around 115%. In the following months, surface water Chl-*a* decreased down to 1 µg L^{-1}, whereas DO% remained above atmospheric equilibrium. Around mid-September 2011, a late phytoplankton bloom occurred between 49.7°N and 50.2°N with Chl-*a* reaching 2 µg L^{-1}. The DO% started to decrease towards atmospheric equilibrium before this phytoplankton bloom, but increased back up to 105% during the bloom. During October and early November, after the breakdown of the stratification, Chl-*a* fell below 1 µg L^{-1} and DO% reached minimum values (between 90% and 100%), before increasing back up to atmospheric equilibrium with re-homogenization of the water column during winter. At the same time we observed the maximum of NO_2^-, while the other nutrients started to increase (Figure 11) before reaching their annual winter maxima, thus closing the annual cycle. In 2012, we observed a spring phytoplankton bloom from April to June with Chl-*a* values higher than 3 µg L^{-1} and associated surface DO% of 115% to 120%, followed by low surface values of Chl-*a* and DO% values down to 105%. In August 2012 an intense summer phytoplankton bloom occurred with Chl-*a* values up to 5µg L^{-1} and associated DO% over 130%. The mechanisms

of this bloom development at short time-scale will be discussed in details in Chapter 3. In 2013, the spring phytoplankton bloom started in May in the northern part of the nWEC and in June in the meridional part of the nWEC with associated maximal values of Chl-*a* and DO% of 4 µg L^{-1} and 120%, respectively. During summer 2013, Chl-*a* values remained low (< 1 µg L^{-1}) and DO% remained above the atmospheric equilibrium (around 105%). A late summer phytoplankton bloom marked by Chl-*a* values of 2 µg L^{-1} occurred prior to the breakdown of stratification, surface DO% remained relatively low with average values of 105%. The dynamics of nutrients during the productive period were similar as in 2011, and NO_2^- maximal values were observed just after the re-homogenization of the water column in early fall.

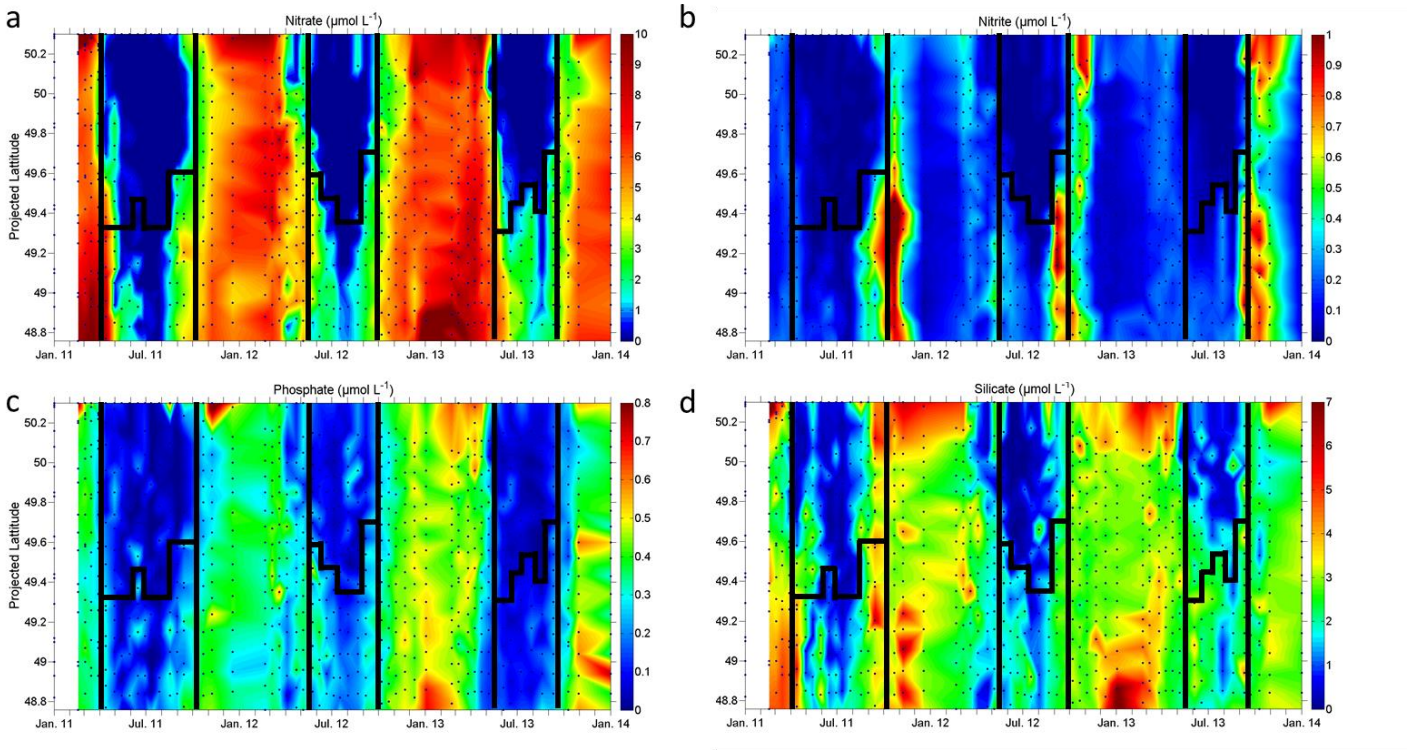


Figure 11: Surface distribution from January 2011 to December 2013 of (A) NO_3^-, (B) NO_2^-, (C) PO_4^{3-} and (D) SiO_4^- concentration (µmol L^{-1}) in the WEC between Roscoff and Plymouth. Vertical black lines indicate the onset of the breakdown of thermal stratification at fixed station E1 and horizontal black lines represent an estimate of the location of the thermal front (Figure 4).

In sWEC, winter values of DO% were close to atmospheric equilibrium and Chl-*a* remained low (Figures 8c and 8d and Table 3), as in nWEC. Compared to the nWEC, Chl-*a* started increasing approximately one month later during spring (Figure 8c and 8d). In late April 2011, an important phytoplankton bloom occurred. During this event, Chl-*a* values increased above 2.5 µg L^{-1} with maximal concentrations over 4 µg L^{-1}. Surface waters DO% increased significantly above atmospheric equilibrium inside the bloom with values reaching 120% in late April 2011 transect, remaining very high during the next crossing two weeks later. The 2011 spring bloom was the most intense in term of Chl-*a* values observed over the three years. In sWEC surface waters, Chl-*a* remained relatively high (> 1µg L^{-1}) with several peaks of Chl-*a* until early July and sWEC surface waters were still oversaturated in DO in August 2011. The productive period, in terms of biological activity, was characterized by high Chl-*a* (> 1 µg L^{-1}) and DO% (> 105%) values, and lasted four months, whereas in nWEC the duration of this period was around 6 months. During the productive period in 2011, NO_3^- and PO_4^{3-} winter nutrient stock were totally depleted and SiO_4^- stock was partially depleted (Figure 11). Surface water DO% decreased and fell below atmospheric equilibrium at the end of August, nearly 1 month earlier than in the northern WEC, and surface waters remained undersaturated in DO during fall before reaching equilibrium during winter. At the same time we observed an increase of NO_2^-, concomitant with NO_3^-, SiO_4^- and PO_4^{3-} increases, with the highest values (1 µmol L^{-1}) recorded in October. DO% decreased at the end of fall, ranging from 90% to 100% with average values around 97%. In 2012, the sWEC was characterized by low biological activity during the productive period, with no phytoplankton bloom during spring and most of biological productivity occurring during summer. Chl-*a* values did not exceed 2 µg L^{-1} and DO% did not overpass 110%. Nutrients were consumed but not totally depleted, except in northern part of the sWEC during summer. In 2013 we observed higher DO% than in 2012 but the biological activity (Chl-*a*) during the productive period was much lower than in 2011. As in 2012, NO_3^- concentration remained higher than 0.5µg L^{-1}. The SiO_4^- decrease was the weakest we recorded, whereas we observed the lowest values of PO_4^{3-}.

In nWEC, the dynamics of surface waters Chl-*a*, DO% and nutrients were highly linked to the start and breakdown of the seasonal stratification. The productive period was in general two months longer than in the sWEC and we recorded more intense biological activity in nWEC surface waters than in sWEC waters.

3.3 Surface distributions of CO_2 system parameters

3.3.1 Total Alkalinity

TA values across the WEC ranged from 2169 µmol kg^{-1} to 2357 µmol kg^{-1} (Figure 12b and Table 3). The lowest TA values were observed near the English coast associated with freshwater inputs (SSS below 35.00). During winter, the mean TA along the transect was 2339 µg kg^{-1}. North of 49.6°N, a linear relationship between TA and SSS was derived (n=465, r^2=0.78, RMSE=6.5 µmol kg^{-1}), suggesting a strong control of SSS on TA, whereas no relationship was found for these parameters in the sWEC. In 2011, we obtained a significant linear relationship between SSS and TA over the whole WEC (n=355, r^2=0.64, RMSE=6.5 µmol kg^{-1}) and we observed the highest mean TA values in the entire WEC from April to August. In 2012 the highest TA values were found across the WEC from January to July and corresponded to the highest SSS (Figure 8b and 12b), but no significant linear relationship was found between SSS and TA. Inversely, in 2013 we observed high TA and low SSS values during spring in the sWEC. Figure 12d shows the distribution of normalized TA (nTA) to a constant salinity of 35. The nTA variability presents roughly the same pattern as TA over the three years of our study with lower concentrations. Interestingly in 2011, high Chl-*a* values during the productive period were always followed by an increase of nTA. From the end of July to fall 2011, TA and nTA decreased to TA values ranging from 2330 to 2340 µmol kg^{-1} and to nTA values ranging from 2315 to 2330 µmol kg^{-1}, except during two weeks after the late summer bloom in the northern WEC. The control of freshwater inputs vs phytoplankton blooms and biogeochemical processes on the spatio-temporal variability of TA is discussed in detailed in section 4.1.

3.3.2 Dissolved Inorganic Carbon

DIC distribution in the WEC (Figure 12a) followed a clear temporal dynamics. During winter, DIC concentrations were high with an average value of 2137 µmol kg^{-1}, with lower DIC concentrations recorded near the English coasts associated to freshwater inputs. Maximum values of DIC (> 2140 µmol kg^{-1}) were measured during winter (Table 3). During

spring and summer, much lower DIC concentrations (< 2100 µmol kg^{-1}) were recorded. DIC and Chl-*a* (and associated DO%) presented reverse and synchronous seasonal dynamics. In the nWEC we observed lower values of DIC than in the sWEC, with DIC decreasing at the start of the stratification and increasing back at the stratification breakdown. During the intense summer bloom in 2012 in nWEC, we recorded the lowest DIC value of 1908 µmol kg^{-1}. In sWEC, we observed an important decrease of DIC during spring 2011 with DIC values lower than 2070 µmol kg^{-1}, whereas during the productive periods in 2012 and 2013 DIC values did not fall below 2090 µmol kg^{-1}. The DIC values increased back during fall, firstly in the sWEC then in the nWEC, before reaching their winter maxima. The DIC distribution across the WEC showed marked latitudinal variability between sWEC and nWEC waters.

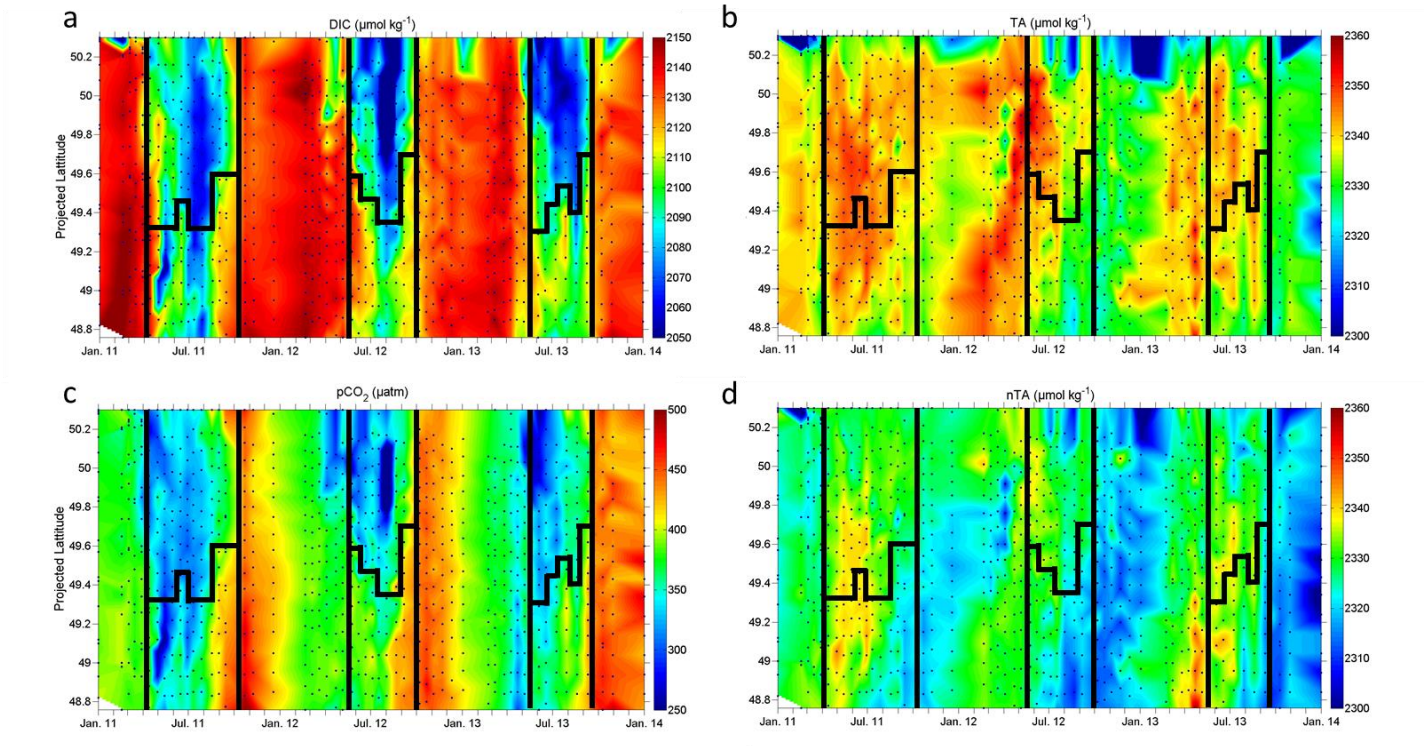


Figure 12: Surface distribution from January 2011 to December 2013 of (A) DIC (in µmol kg^{-1}), (B) TA (in µmol kg^{-1}), (C) pCO_2 (in µatm) and (D) normalized TA after Friis et al. (2003) (in µmol kg^{-1}) in the WEC between Roscoff and Plymouth. Vertical black lines indicate the onset of the breakdown of thermal stratification at fixed station E1 and horizontal black lines represent an estimate of the location of the thermal front (Figure 4).

3.3.3 Partial pressure of CO_2

Figure 12c shows the spatial and temporal distribution of pCO_2, computed from TA and DIC, between Roscoff and Plymouth from 2011 to 2013. Surface water pCO_2 ranged from 168 µatm to 499 µatm (Table 3). During winter, mean pCO_2 values ranged between 370 and 390 µatm across the WEC with lower values in the nWEC compared to sWEC. The same spatio-temporal distribution as DIC was observed for pCO_2 across the WEC during summer. When spring blooms started, the drawdown of pCO_2 showed the same trend as DIC, starting firstly in the nWEC and one to two months later in the sWEC. After the spring blooms, surface water pCO_2 remained substantially below the atmospheric equilibrium until the breakdown of the stratification in nWEC. The lowest pCO_2 value in the nWEC (168 µatm) was observed during the intense summer 2012 bloom. In sWEC we recorded the lowest value of pCO_2 (240 µatm) during the 2011 spring bloom, thus the pCO_2 values observed during the productive period in 2011 were lower than in 2012 and 2013. pCO_2 started to increase generally one month earlier in sWEC than in nWEC before reaching their fall maximum values. After the fall maximum, surface water pCO_2 decreased back to a value close to atmospheric equilibrium in the entire WEC during winter.

3.3.4 pH, calcite and aragonite saturation state of surface seawater

Figure 13 shows the spatial and temporal distribution of pH on the total scale, the calcite (Ω_{Ca}) and aragonite (Ω_{Ar}) saturation state of surface seawater between Roscoff and Plymouth from 2011 to 2013. These parameters were computed from TA, DIC, temperature, salinity and nutrients concentrations with the CO2SYS program (Pierrot et al., 2006) using the equilibrium constants proposed by Mehrbach et al. (1973), refitted by Dickson and Millero (1987) on the total pH scale, as recommended by Dickson et al. (2007). The computed values of pH from DIC and TA have uncertainty of ± 0.006 µatm (Zeebe and Wolf-Galdrow, 2001). Surface water pH ranged from 7.966 to 8.354 (Table 3), with an average value of 8.075. The surface waters of the WEC were always supersaturated ($\Omega > 1$) with respect to calcite and aragonite, with Ω values ranged from 2.63 to 7.08 and from 1.66 to 4.57 for calcite and aragonite, respectively. We observed the highest pH, Ω_{Ca} and Ω_{Ar} values during the most intense phytoplankton blooms, particularly during summer 2012 in nWEC,

and the lowest values during fall when DIC and pCO_2 were the highest. The distribution of these carbonate system parameters was closely related to the distribution of the DIC and pCO_2, described in Sections 3.3.2. and 3.3.3, with high pH, Ω_{Ca} and Ω_{Ar} values when low DIC and pCO_2 values were recorded.

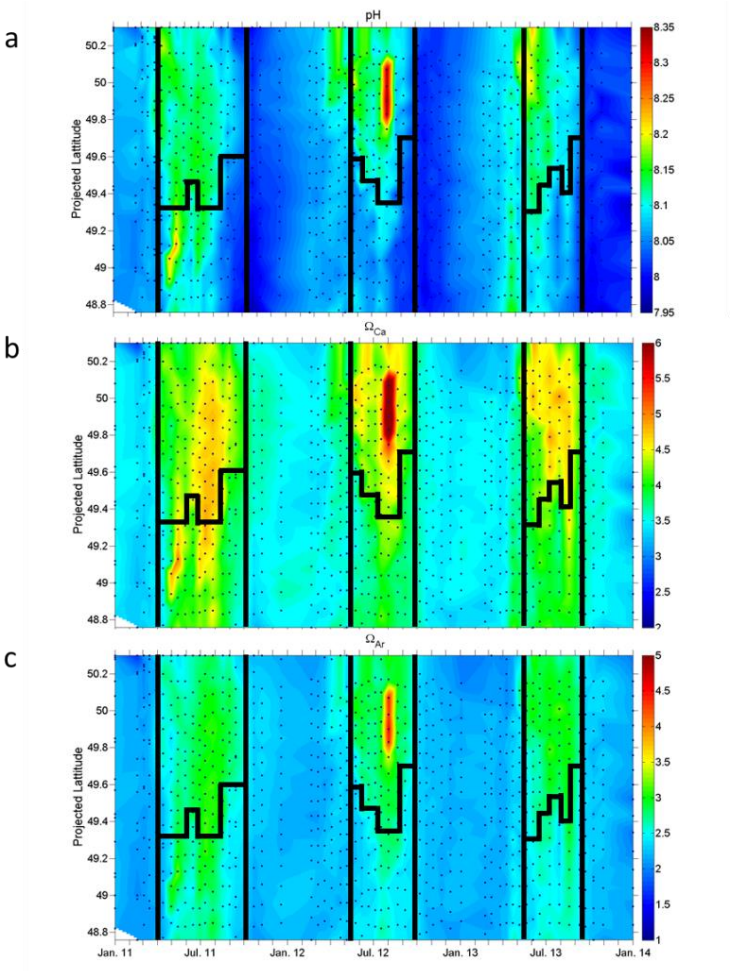


Figure 13: Surface distribution from January 2011 to December 2013 of (A) pH on the total scale, (B) the calcite Ω_{Ca} and (C) aragonite Ω_{Ar} saturation state in the WEC between Roscoff and Plymouth. Vertical black lines indicate the onset of the breakdown of thermal stratification at fixed station E1 and horizontal black lines represent an estimate of the location of the thermal front (Figure 4).

4. Discussion

4.1 Latitudinal dynamics of the carbonate system in the WEC

Previous studies of the carbonate system dynamics in the English Channel were either based on longitudinal transects by Borges and Frankignoulle (2003), Padin et al. (2007) and Dumousseaud et al. (2010), or on fixed stations at E1 and L4 by Kitidis et al. (2012). A similar range of values for DIC/TA (Dumousseaud et al., 2010; Kitidis et al., 2012) and pCO_2 (Table 3 and 5) was recorded in our dataset as those reported in these studies. However, compared to previous studies, our high latitudinal coverage allowed a new separation of the WEC with respect to the distributions of carbonate system parameters and ancillary data. The relatively high temporal frequency employed in this study allowed distinction of temporal differences in carbonate system variability between the two provinces. As mentioned in section 3, DIC and pCO_2 variability were closely related to DO% and Chl-*a* distributions. After the spring bloom in nWEC, Chl-*a* remained low during summer, except during the intense summer bloom in 2012, but DO% was above atmospheric equilibrium and DIC and pCO_2 remained relatively low (under 2090 µmol kg^{-1} and 350 µatm, respectively). These observations suggest the presence of a sub-surface phytoplankton bloom above the thermocline after nutrient depletion in the surface layer, as reported previously by Southward et al. (2005) and by Smyth et al. (2010). The onset and the breakdown of stratification were the main factors controlling the biological activity in nWEC and strongly controlled the DIC/pCO_2 variability. The water column was always mixed during the same period in sWEC. Subsurface Chl-*a* maximum cannot occur in this region and phytoplankton were present until total or near nutrients depletion, throughout the water column and were associated with lower values of pCO_2/DIC. Additional differences between nWEC and sWEC were the late phytoplankton bloom that occurred in nWEC in late summer 2011 and 2013 and the intense summer bloom that occurred in 2012. Late summer blooms delayed the fall increase of DIC and pCO_2 due to organic matter remineralization and the intense 2012 summer bloom decreased surface waters DIC and pCO_2 down to the lowest values observed over the 3 years. The breakdown of stratification in nWEC brought to the surface the deeper waters enriched

CO_2 during fall. These observations suggested a strong control of biological processes on DIC/pCO_2 variability with temporal decoupling between the two provinces.

	Winter	Spring	Summer	Fall
pCO_2 nWEC	350-400	300-360	270-390	410-440
pCO_2 sWEC	370-400	300-390	330-450	420-470
pCO_2 from B & F	360-390	300-340	200-350	400
pCO_2 from P et al.	370	290-350	-	375-425
pCO_2 from D et al.	400-430	310-340	340-350	390-440
pCO_2 from K et al.	350-400	290-310	300-330	400

Table 5: Seasonal range of pCO_2 values (µatm) observed in this study across the WEC from 2011 to 2013 and reported by Borges and Frankignoulle (2003) (B & F), Padin et al. (2007) (P et al.) and Dumousseaud et al. (2010) (D et al.) in thre EC and Kitidis et al. (2012) (K et al.) at stations E1 and L4. These pCO_2 values were extracted from graphs of these studies and they represent the approximate range of pCO_2 values measured during each season.

For TA, as shown in section 3.3, coastal freshwater inputs were significant drivers of latitudinal variability. In addition, TA can be controlled by production (decrease of TA) and dissolution (increase of TA) of calcium carbonate (Wolf-Gadrow et al., 2007). As mentioned in section 2.4, coccolithophore blooms occurred in 2011 in the nWEC as revealed by MODIS-Aqua satellite images (data not shown) and data of flow cytometry at fixed station L4 (Western Channel Observatory) and we discuss here the impact of these blooms of calcifying versus non-calcifying species. On these satellite images, we observed a coccolithophore bloom between 49.9°N and 50.2°N, in early June and a second one at the end of July between 49.6°N and 49.9°N. During the same period, we recorded lower nTA values in these areas, which might be linked to the production of calcium carbonate by the coccolithophores. nTA decreased by nearly 5 to 10 µmol kg^{-1} during this event (Figure 12d). Instead, an increased in nTA can be linked to the uptake of nitrate by phytoplankton (Brewer and Goldman, 1976): an increase of nTA of 1 mole corresponds to 1 mole of nitrate assimilated by phytoplankton. In the middle of the Channel, the winter stock of nitrate ranged from 6 to 10 µmol L^{-1} (Figure 11a) and was entirely depleted just after the spring phytoplankton bloom. At the same time we observed an increase of nTA of 5 to 10 µmol kg^{-1} (Figure 12d), which corresponds to the equi-molar ratio mentioned above. Hence, nitrate depletion seemed to be the main driver of the increase of TA during the productive period in 2011. Only when short coccolithophore blooms occurred, calcium carbonate production decreased TA and counteracted the nitrate

depletion. For the rest of the 3 years, near the coastline TA decreases were essentially driven by freshwater inputs.

Figure 13 showed that pH in WEC varied temporally and spatially reversely to DIC and pCO_2. The variability of *in-situ* pH in the WEC over the seasons (7.97-8.35) exceeded the projection of end-of-century change in oceanic pH (from 8.05 to 7.80 depending of the scenario (IPCC, 2013)). Waldbusser and Salisbury (2013) showed that the pH of coastal surface waters present high variability as a result of many physical and biogeochemical processes. Thus, coastal waters are subject to strong diel to seasonal fluctuations in pH, with characteristic ranges of 0.3 pH units (Duarte et al., 2013). Similar observations can be made for the surface waters of the WEC with inter-seasonal amplitude of pH reaching 0.4 units during our 3 years of study. This implies that the concept of ocean acidification due to anthropogenic CO_2 emissions is difficult to be transposed to coastal ecosystems directly and that ocean acidification experiments on coastal species of the WEC should take into account this natural variability.

4.2 Processes controlling the seasonal pCO_2 variability

The high spatio-temporal coverage of our dataset allowed us to assess and compare the processes controlling the seasonal pCO_2 variability in the provinces of the WEC. In western European shelf zone like the English Channel, the main drivers of pCO_2 variability are the thermodynamic and biological production/respiration of organic matter (Padin et al., 2007; Dumousseaud et al., 2010). The pCO_2 values were computed at the annual mean temperature (T_{mean} = 13.1°C) using CO2SYS (Pierrot et al., 2006) in order to remove the thermal effect on pCO_2 ($pCO_{2,nontherm}$) and assess the biological processes controlling the pCO_2 variability. To evaluate the impact of the temperature on the pCO_2 variability, we computed $pCO_{2,therm}$ according to Equation 18. Equation 18 perturbs the annual mean pCO_2 calculated each year with the observed SST. The $pCO_{2,therm}$ represents realistically the seasonal thermal forced pCO_2 variability during the year (Takahashi et al., 2002).

$$pCO_{2,therm} = pCO_{2,mean} \times e^{0.0423 \times (Tobs - Tmean)} \qquad (18)$$

In Equations 18, "mean" and "obs" stand for annual mean and observed temperatures and pCO_2, respectively. This simple approach to estimate the impact of biological and

thermodynamic effects on pCO_2 variations can provide a reasonable assessment of the relative importance of these processes in coastal ecosystems according to Thomas et al. (2005) and Schiettecatte et al. (2006). Besides thermodynamic and production/respiration of organic matter, additional processes like dissolution/formation of $CaCO_3$, lateral advection and horizontal mixing can have an impact on pCO_2 variability. As discussed above, pelagic dissolution and formation of $CaCO_3$ occurred in the north part of nWEC in early June and at the end of July. These processes are included in the $pCO_{2,nontherm}$. The short time-steps of our computation (two weeks) was much lower than the flushing time in the nWEC (E1 area) and sWEC (ASTAN area) (30 to 90 days according to Dehlez et al, 2004), which makes lateral advection negligible in these areas. The impact of mesoscale eddies (section 2.4) on pCO_2 are very difficult to quantify and therefore it is included in the $pCO_{2,nontherm}$. However, lateral advection near the English coast (L4 area) could not be ignored because sudden freshwater inputs can influence the carbonate system properties on time scales lower than 2 weeks. We therefore chose to apply the normalization of pCO_2 at the annual mean temperature and the Takahashi method only in the two main provinces of the WEC, which are the focus of this study, and exclude the coastal area near L4.

On Figure 14 we quantify the effect of each process on the pCO_2 variability in both provinces. For this we calculated the mean pCO_2, $pCO_{2,nontherm}$ and $pCO_{2,therm}$ every two weeks using the data collected in the sWEC (48.80°N-49.40°N) and the nWEC (49.40°N-50.20°N). Variability of $pCO_{2,therm}$ followed SST variations over the year. Maximum $pCO_{2,therm}$ values (over 450 µatm) occurred in August 2012 and 2013 in the nWEC when the SST was highest. The $pCO_{2,therm}$ in the nWEC during summer was higher than in the sWEC. The thermal stratification occurring in the nWEC, which maintained the surface waters warmer, explained these higher values. In the sWEC and the nWEC the mean seasonal SST amplitudes of 6.6 °C and 8.1 °C, respectively, were equivalent to the $pCO_{2,therm}$ ranges of 106 µatm and 132 µatm, respectively. During winter 2011, mean SST in nWEC was 9.9 °C and was cooler than in sWEC (10.1 °C). A difference of 0.2°C would result in a difference of approximately 3 µatm according to Takahashi et al. (1993) and Figure 14 confirms that during winter the cooling of surface waters in nWEC decreased the $pCO_{2,therm}$ values by approximately 4 µatm compared to sWEC. During this period, the total mean pCO_2 difference between sWEC and nWEC was 17 µatm. The additional 13 µatm difference between sWEC and nWEC resulted from higher $pCO_{2,nontherm}$ values in sWEC (437 µatm) than in nWEC (423 µatm). The CO_2 undersaturation in the northern WEC during winter 2011 was therefore partly

driven by cooler surface water, which accounted for roughly 20%, and mainly by lower respiration process in nWEC than in sWEC.

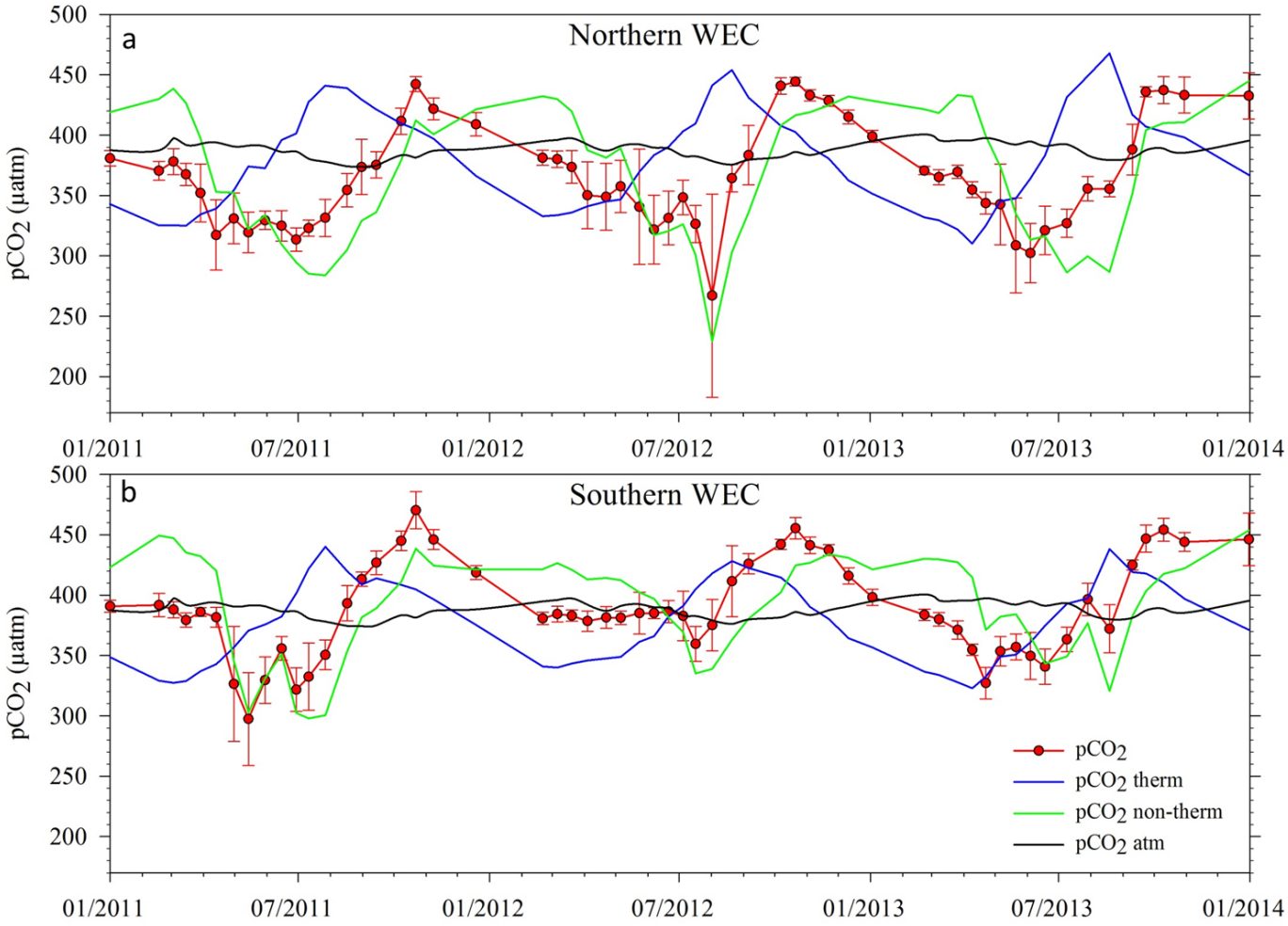


Figure 14: Variations of pCO_2 (filled red circles and red lines), $pCO_{2,nontherm}$ (green lines) and $pCO_{2,therm}$ (blue lines) in nWEC (A, 49.40°N-50.20°N) and sWEC (B, 48.80°N-49.40°N) computed after normalization of pCO_2 to the annual mean temperature ($pCO_{2,non\text{-}therm}$) and after Takahashi et al. (1993) ($pCO_{2,therm}$) from January 2011 to December 2013 (in µatm). The black lines represent the atmospheric pCO_2 ($pCO_{2\ atm}$). The red error bars represent the standard error of mean surface water pCO_2 over each province.

In response to spring phytoplankton blooms the pCO_2 signal was mainly driven by $pCO_{2,nontherm}$ but pCO_2 was compensated by the counteractive thermodynamic influence due to SST increase. The $pCO_{2,nontherm}$ decrease recorded from spring showed that the biological uptake was responsible for the CO_2 undersaturations observed during the productive period in the sWEC and nWEC. The increase of $pCO_{2,nontherm}$ due to organic matter remineralization started at the same time in sWEC and in nWEC but $pCO_{2,nontherm}$ overpassed the atmospheric equilibrium one month earlier in sWEC than in nWEC. The increases of pCO_2 in sWEC and

nWEC were ascribed to biological releases of CO_2, which induced CO_2 oversaturations, of approximately 60 µatm and 40 µatm in sWEC and nWEC, respectively. These estimations of the biological respiration of pCO_2 in nWEC represent an upper limit since mixing of the water column might have brought bottom water with higher pCO_2 into the surface waters. Organic matter remineralization processes exceeded biological production processes at the end of the productive period with pCO_2 above atmospheric equilibrium. Surface waters stayed oversaturated in CO_2 until winter, with higher pCO_2 values in the homogenous system (> 450 µatm) due to the higher remineralization of organic matter compared to the stratified system. The cooling of surface water in winter controlled the decrease of winter pCO_2 until spring. As mentioned above in section 4.1., coccolithophore blooms occurred in nWEC in early June (between 49.9°N and 50.2°N) and at the end of July (between 49.6°N and 49.9°N). During these events nTA depletions of 10 µmol kg^{-1} were observed (Figure 6d). The theoretical computation of the change of seawater carbonate chemistry speciation related to a TA drawdown of -10 µmol kg^{-1} due to calcification lead to an increase in pCO_2 at a constant temperature of 6 µatm. In early June in nWEC, we observed a $pCO_{2,nontherm}$ increase of about 10 µatm (Figure 14), which might suggest that calcification processes contributed to half of this increase. In late July, the CO_2 release by calcification processes might be compensated by organic carbon production because $pCO_{2,nontherm}$ kept constant between the post coccolithophore bloom and the bloom.

Figure 14 confirmed that the biological consumption of pCO_2 started earlier and lasted longer in nWEC compared to sWEC. Similarly, from the end of summer to the beginning of fall, respiration processes were stronger in sWEC than in nWEC. The $pCO_{2,nontherm}$ and $pCO_{2,therm}$ variability in each province clearly shows that the thermodynamic effect counteracted consecutively biological production in spring/summer and organic matter remineralization in fall/winter. Comparing these two representative systems (homogenous vs. stratified) of the WEC, our results show that the differences observed between nWEC and sWEC were clearly related to the structure of the water column. The control of pCO_2 variability in these provinces might be representative of larger provinces of the NW European shelf. For example, the processes driving pCO_2 dynamics in the two provinces of the WEC are likely to exert the same control on pCO_2 dynamics in adjacent Irish (mostly homogeneous) and Celtic (stratified) Seas. This assumption will be discussed in Chapter 4.

4.3 Air-Sea CO_2 exchange

Figure 10c shows the spatial and temporal variability of air-sea CO_2 fluxes between Roscoff and Plymouth in relation with the temperature anomalies at fixed station E1 (Figure 10a) and between Roscoff and Plymouth (Figure 10b). The differences observed between sWEC and nWEC and between homogenous and seasonally stratified water column structures (mentioned in section 3) explained the spatial variability of fluxes of CO_2 across the air-sea interface during the 3 years of study. Thus, air-sea CO_2 fluxes in sWEC and in nWEC exhibited clear different patterns.

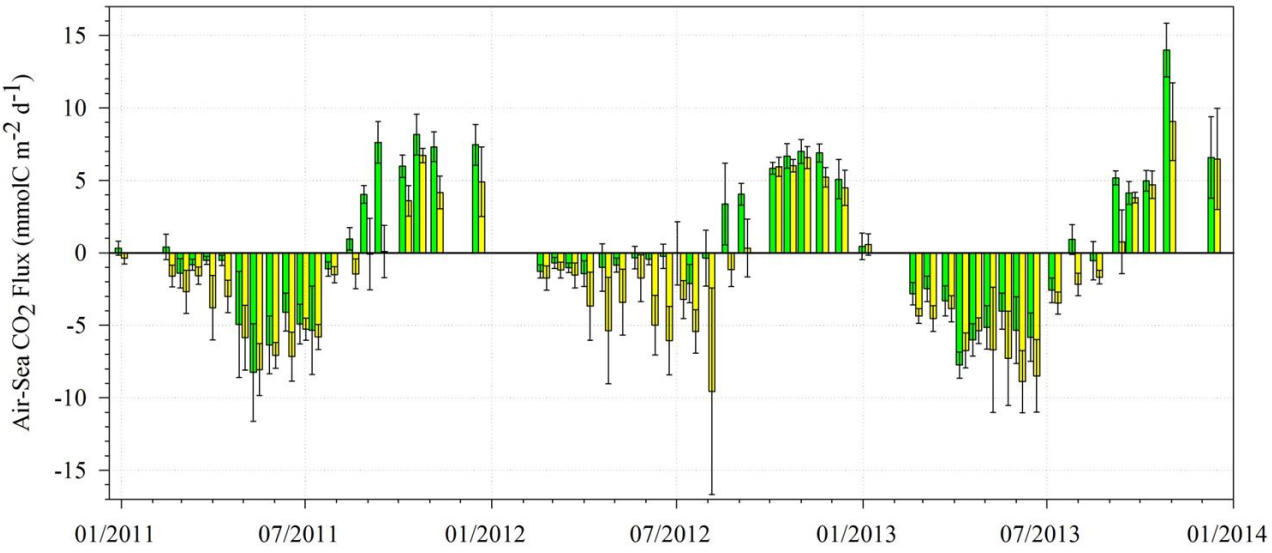


Figure 15 : Calculated air-sea CO_2 fluxes (in mmol C m^{-2} d^{-1}) from January 2011 to December 2013, using the algorithm given by Nightingale et al. (2000), in nWEC (yellow bars, 49.40°N-50.20°N) and in sWEC (green bars,48.80°N-49.40°N). Error bars represent the standard deviation of mean fluxes obtained over each province.

During spring, we found an enhanced oceanic CO_2 sink in nWEC and at E1 (from 5.2 and 9.9 mmol m^{-2} d^{-1}) compared to sWEC and ASTAN (from 0.5 to 6.0 mmol m^{-2} d^{-1}, respectively) (Table 6). Enhanced CO_2 sink was observed during all the productive period in nWEC and surface waters acted as source of CO_2 to the atmosphere firstly in sWEC and one month later in nWEC (Figure 10c and 15). The comparison between SST anomalies (Figure 10b) and air-sea CO_2 fluxes (Figure 10c) clearly shows that nWEC waters started to release CO_2 to the atmosphere when the seasonal stratification broke. The summer air-sea CO_2 fluxes

were positive (CO_2 release) in sWEC and negative (CO_2 sink) in nWEC (Table 6). The CO_2 emissions to the atmosphere during fall (Table 6) were higher in sWEC (from 6.7 and 10.2 mmol m^{-2} d^{-1}) than in the nWEC (from 5.5 to 7.5 mmol m^{-2} d^{-1}). This was due to the important remineralization of organic matter in the well-mixed water column, which induced the strong CO_2 oversaturation observed in this region. During winter, the WEC acted as a sink of CO_2 to the atmosphere with uptake values in nWEC significantly higher than in sWEC. The CO_2 sink observed in winter is in disagreement with previous studies from Borges & Frankignoulle (2003) and Dumousseaud et al. (2010), which found CO_2 emissions from January to March. As seen above in section 4.2., the main driver of this CO_2 sink was the cooling of the surface waters in nWEC, which was not captured in these previous studies. However these ecosystems present an important inter-annual variability (Figures 10c and 15), that has to be considered when comparing with previous studies. The seasonal variability in nWEC (Table 6) was in better agreement with the other studies carried out in the English Channel (Borges & Frankignoulle, 2003; Padin et al., 2007; Dumousseaud et al., 2010; Kitidis et al., 2012) than the flux estimates in sWEC, suggesting that these previous studies were mainly performed in seasonally stratified waters.

	Winter			Spring			Summer			Fall			Annual		
	2011	2012	2013	2011	2012	2013	2011	2012	2013	2011	2012	2013	2011	2012	2013
$FCO_{2\ nWEC}$	-2.3	-0.7	-2.7	-6.9	-5.2	-8.1	-1.6	-2.4	-0.8	5.5	5.8	7.5	**-0.5**	**-0.2**	**-0.4**
$FCO_{2\ sWEC}$	-0.2	-0.1	-1.6	-4.9	-0.6	-6.0	1.2	2.2	1.2	8.0	6.7	10.2	**0.4**	**0.8**	**0.4**
$FCO_{2\ Astan}$	0.2	-0.1	-1.2	-3.6	-0.5	-5.7	2.3	3.0	1.5	8.7	7.5	10.5	**0.7**	**0.9**	**0.5**
$FCO_{2\ E1}$	-2.6	-1.6	-2.9	-7.3	-8.1	-9.9	-2.0	-4.8	-1.5	4.3	6.0	6.7	**-0.7**	**-0.8**	**-0.7**
$FCO_{2\ L4}$	-2.4	-2.1	-2.3	-5.7	-8.8	-9.8	2.1	-3.2	1.2	6.1	5.5	9.9	**0,0**	**-0.8**	**-0.1**
FCO_2 from B & F		-			-1			-			2			**0,5**	
FCO_2 from P et al.		-			-7			-			1			**-0,5**	
FCO_2 from D et al.		-3			-3,5			-2			3			**-0,5**	
FCO_2 from K et al. E1		-2,5			-3			-2			1			**-0,62**	
FCO_2 from K et al. L4		-2,5			-4			-2			1			**-0,55**	

Table 4: Seasonal means of air-sea CO_2 fluxes (F in mmol C m^{-2} d^{-1}) calculated in this study according to Eq.1 for the nWEC [49.40°N-50.20°N] and the sWEC [48.80°N-49.40°N] provinces and at the fixed stations ASTAN, E1 and L4. These fluxes were computed using the gas transfer velocity formulated by Nightingale et al. (2000). Annual means are in mol C m^{-2} y^{-1}. Atmospheric pCO_2 were measured at Mace Head (Ireland) station from the RAMCES network and wind speeds were obtained from the NCEP/NCAR re-analysis project. Also indicated are the air-sea CO_2 fluxes from Borges and Frankignoulle (2003) (B & F), Padin et al. (2007) (P et al.), Dumousseaud et al. (2010) (D et al.) and Kitidis et al. (2012) (K et al.). F values from D et al. are the range of F values for each season in the WEC and the annual mean is the average ranges over the years.

On an annual scale, ASTAN and sWEC acted as sources of CO_2 to the atmosphere with air-sea CO_2 fluxes values ranging from 0.5 to 0.9 mol m^{-2} y^{-1} and from 0.4 to 0.8 mol m^{-2} y^{-1} (Table 6), respectively. E1 and the nWEC were significant sinks of CO_2 with values ranging from -0.7 to -0.8 mol m^{-2} y^{-1} and from -0.2 to -0.5 mol m^{-2} y^{-1}, respectively. The fact that the permanently well-mixed province of the WEC acted as a source of CO_2 to the atmosphere and that the seasonally stratified province of the WEC acted as a sink of CO_2 confirms the hypothesis of Borges (2005). This hypothesis stipulates that permanently well mixed systems are less efficient in exporting organic matter and in absorbing atmospheric CO_2, than seasonally or permanently stratified systems. Annual air-sea CO_2 fluxes estimates for nWEC presented in this study were in the same range as those reported by Padin et al. (2007), -0.5 ± 1.2 mol m^{-2} y^{-1} and those estimated from Dumousseaud et al. (2010) of -0.5 mol m^{-2} y^{-1} (Table 6). Results obtained by Borges and Frankignoulle (2003) described the WEC as a source of CO_2 to the atmosphere of 0.5 ± 0.6 mol m^{-2} y^{-1}. These results were in agreement with our estimations obtained in sWEC, and in contradiction with those obtained in nWEC. Borges and Frankignoule (2003) pointed out that their data were obtained mostly through the middle of the Channel and did not take into account the latitudinal variability of the WEC. The same applies to the studies of Padin et al. (2007) and Dumousseaud et al. (2010) based on transects through the middle of the Channel. Compared to those studies, our dataset gives a new spatio-temporal resolution across the WEC and highlights significant intra and inter-annual differences between homogenous and seasonally stratified systems. For stations E1 and L4, Kitidis et al. (2012) computed air-sea CO_2 fluxes over four years (2007-2010) of -0.62 ± 0.49 and -0.55 ± 0.66 mol m^{-2} y^{-1}, respectively. We computed air-sea CO_2 fluxes at L4 for comparison with the study of Kitidis et al. (2012). Our flux estimates for E1 and L4 ranged between -0.7 and -0.8 mol m^{-2} y^{-1} and between 0.0 and -0.8 mol m^{-2} y^{-1}, respectively (Table 6). These results were in relatively good agreement with the study of Kitidis et al. (2012), who used the same k parameterizations (Nightingale et al., 2000). The contribution of the WEC with annual air-sea CO_2 fluxes ranging from 0.8 to -0.5 mol m^{-2} y^{-1} in its different provinces appears small compared to the average flux of -1.85 mol m^{-2} y^{-1} computed by Borges et al. (2006) for European continental shelves as a whole.

In these ecosystems, the intensity and the chronology of air-sea CO_2 fluxes were highly variable throughout the seasons (Table 6, Figure 10c and 15), but the direction of annual fluxes remained the same and annual estimates relatively close. In Chapter 3 and 4 the sources of this inter-annual variability will be investigated in more details. The good

agreements between the fluxes computed at ASTAN and in the sWEC and between E1 and nWEC fluxes showed that these fixed stations can be considered as representative of entire provinces in these dynamic coastal ecosystems. With the VOS line measurements we covered a larger area of the WEC and we observed that massive spring phytoplankton blooms, which were the main driver of the CO_2 sink in the area, were scattered and usually lasted less than 2 weeks. Thus, a major benefit of the VOS line approach, compared to fixed stations, was to capture most of the CO_2 variability caused by phytoplankton blooms including the patchiness of these events. In the context of a global inorganic carbon observatory for coastal ecosystems (Borges et al., 2010), the frequency of sampling at time series is essential for a robust estimate of air-sea CO_2 fluxes. This type of combined approach with VOS line and fixed stations and adequate sampling frequency can provide a robust assessment of the CO_2 dynamics in continental shelf provinces. The adjacent Irish (mainly homogenous) and Celtic (stratified) Seas, for which data on the carbonate system are sparse, are likely to show similar patterns for CO_2 dynamics as observed in the two provinces of the WEC defined in this study.

4.4 Estimation of Net Ecosystem Production at the fixed stations

NEP estimates based on the DIC budgets (Equation 17) and air-sea CO_2 fluxes were plotted over the three years at the vicinity of ASTAN and E1 stations (Figure 16). At ASTAN, we observed the strongest NEP value (270 mmol C m^{-2} d^{-1}) during the 2011 spring bloom, immediately followed by a heterotrophic period (NEP < 0) with the lowest NEP value (-149 mmol C m^{-2} d^{-1}) recorded over our three years study. NEP increased back after this heterotrophic phase, and this increase was related to a net autotrophic event (NEP > 0) in early summer. After the autotrophic productive period, from mid-summer to the end of fall the ecosystem was heterotrophic with values ranging from -70 to -10 mmol C m^{-2} d^{-1}. During this time ASTAN acted as strong source of CO_2 to the atmosphere due to the remineralization of organic matter. On an annual scale, ASTAN was slightly autotrophic at a rate of 0.7 ± 0.5 mol C m^{-2} y^{-1}.

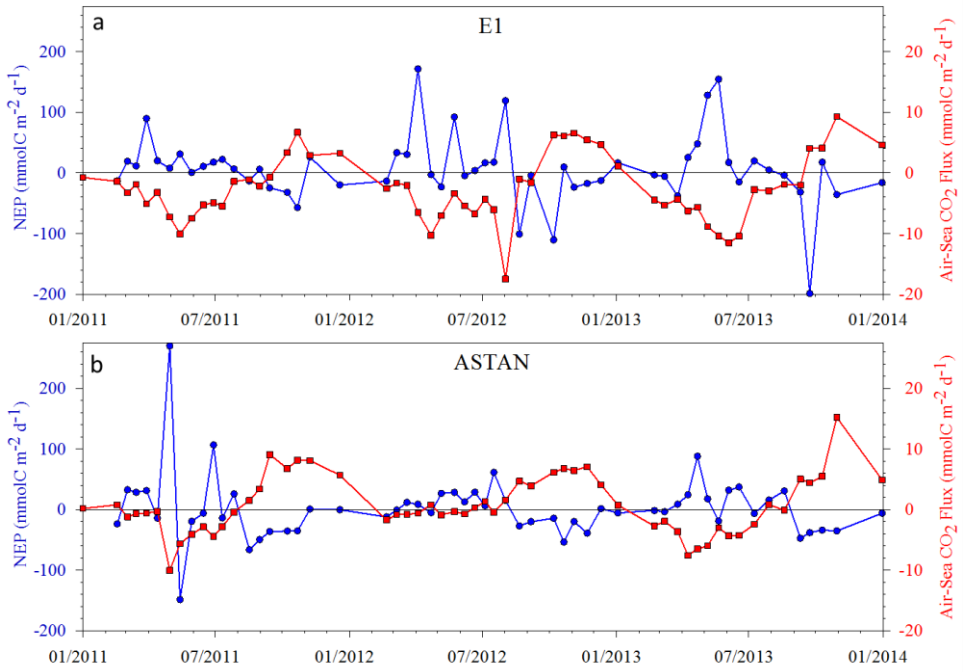


Figure 16: Estimated net ecosystem production (NEP in mmol C m^{-2} d^{-1}, blue circles) and air-sea CO_2 fluxes (in mmol C m^{-2} d^{-1}, red squares) computed using the gas transfer velocity parameterization given by Nightingale et al. (2000) in the vicinity of ASTAN (48.90°N-49.10°N) and E1 (49.80°N-50.00°N) from January 2011 to December 2013.

At E1, during spring and summer, when the ecosystem acted as a sink of atmospheric CO_2 due to biological uptake of CO_2, the surface waters were mostly autotrophic. The autotrophic phase lasted longer than in ASTAN, with higher mean NEP values. Maximum NEP values during the autotrophic period were regularly higher than 100 mmol C m^{-2} d^{-1} and were associated to high Chl-*a* values. From September to winter the surface waters were mostly heterotrophic with few low autotrophic phases. During this time E1 acted as a source of CO_2 to the atmosphere. On an annual scale, the surface waters at E1 were autotrophic with an annual mean NEP value of 2.4 ± 1.0 mol C m^{-2} y^{-1}, more than 3 times higher than in the surface waters at ASTAN (0.7 mol C m^{-2} y^{-1}). For most of the year, the direction of air-sea CO_2 fluxes was clearly related to the trophic status of the mixed layer at both stations ASTAN and E1 (Figure 16).

	Characteristic	2011	2012	2013	Mean
NEP_{nWEC}	SS	2.1	3.5	1.6	2.4
NEP_{sWEC}	WM	0.9	0.2	1.2	0.7
NPP B & F	WM				0.4
NEP_{SBNS}	WM				6.3
NEP_{IS}	WM				0.7
NPP W	-				3.3

Table 5: Annual estimates of net ecosystem production (NEP in mol C m^{-2} y^{-1}) calculated according to Eq. (X) in the vicinity of E1 [49.8°N-50.0°N] and ASTAN [48.9°N-49.1°N] from FerryBox DIC measurements and air-sea CO_2 flux estimates. New primary production (NPP) estimate from Borges and Frankignoulle (2003) in the WEC (NPP B & F, in mol C m^{-2} y^{-1}) was computed from annual N-assimilation rates given by Le Corre et al. (1996) and L'Helguen et al. (1996) using Redfield C:N ratio in the well mixed waters of the WEC. NEP_{SBNS} referred to NEP estimates in the Southern Bight of the North Sea (SBNS) computed by Schiettecatte et al. (2007) and NEP_{IS} referred to NEP estimate from Gazeau et al. (2004) in the Irish Sea (IS). Also indicated is the NEP estimate from Wollast (1998) for worldwilde continental shelves. WM correspond to all-year well-mixed systems and SS to seasonally stratified systems.

As mentioned above in section 2.4., pelagic and benthic calcification can have a significant impact on NEP assessments based on DIC budget. During the two coccolithophore blooms observed in the WEC in 2011, nTA depletions of 10 µmol kg^{-1} due to calcification lead to a theoretical pCO_2 release of 6 µatm and to a theoretical DIC consumption of 5 µmol kg^{-1}. As explained in section 3.4., the CO_2 release was insufficient to overcome the CO_2 under-saturation with respect to atmospheric equilibrium and the impact on air-sea CO_2 fluxes remained rather low. Regarding the DIC budget, with a delta DIC of 5 µmol kg^{-1} due to calcification, the impact of the coccolithophores blooms of June and July on our NEP computation would be less than 10% on the annual mean. Harlay et al. (2010) reported calcification rates during a coccolithophore bloom in the northern Bay of Biscay ranging between 1.4 to 14 mmol $CaCO_3$ m^{-2} d^{-1}. These authors showed that the increase in pCO_2 due to calcification was also insufficient to overcome the under-saturation of CO_2. Benthic calcification is also present in the English Channel, Migné et al. (1998) and Davoult et al. (2009) estimated calcification rates of brittle stars (Ophiothrix fragilis and Acrocnida brachita, respectively) in the eastern English Channel to 18.6 mmol $CaCO_3$ m^{-2} d^{-1} and to 1.9-2.8 mmol $CaCO_3$ m^{-2} d^{-1} respectively. Such calcification rates lead to the release of CO_2 into the surrounding water and potentially further transfer to the atmosphere from 1.3-1.9 mmol C m^{-2} d^{-1} (Davoult et al. (2009)) to 13.2 mmol C m^{-2} d^{-1} (Migné et al. (1998)). Further Golléty et al. (2008) estimated the calcification rate of barnacles in the south part of the WEC (off Roscoff) with values ranging from 13.2 to 49.3 mmol $CaCO_3$ m^{-2} d^{-1}. Several benthic species are present in temperate coastal ecosystems but carbonate system dynamics between benthic

fauna and surrounding waters are difficult to quantify considering the diversity of species. Benthic calcification may influence the CO_2 system of the water-column all year in the well mixed area of the WEC and from fall to early spring in the stratified northern WEC. Our NEP assessments might be impacted by pelagic and benthic calcification but, as we observed from pCO_2 variability (Figure 11), during the spring and summer productive period surface waters remained under-saturated in CO_2, thus mainly controlled by GPP, and a significant sink of CO_2.

To the best of our knowledge, no previous study has assessed NEP in the WEC. Borges & Frankignoulle (2003) referred to the work of Thomas et al. (1999) (and references therein) to assume that NEP can be approximated to new primary production. In well-mixed waters of the WEC, new primary production was estimated at 0.4 mol C m^{-2} y^{-1} (Table 7) according to annual N-assimilation rates using the Redfield C:N ratio reported by Le Corre et al. (1996) and L'Helguen et al. (1996). This new primary production value was of a similar magnitude as our annual mean NEP estimate of 0.7 mol C m^{-2} y^{-1} at ASTAN, but can only serve as a first order comparison. NEP values for the adjacent Southern Bight of the North Sea (SBNS) were computed by Schiettecatte et al. (2007) based on a comprehensive DIC budget in this all-year well mixed system. These authors found an annual mean NEP of 6.3 mol C m^{-2} y^{-1} (Table 7) associated to an annual mean air-sea CO_2 fluxes of -0.7 mol C m^{-2} y^{-1}. These NEP values were much higher than the NEP values found for the WEC in this study. The SBNS differs from WEC in that it receives strong inputs of nutrients and organic and inorganic carbon from several large estuaries (e.g. Scheldt, Rhine/Meuse, Thames) surrounding the North Sea and this might explain the large differences between these NEP estimates. For the adjacent Irish Sea, Gazeau et al. (2004) reported annual NEP values derived by the Land-Ocean Interactions in the Coastal Zone (LOICZ) method for European sites (from non-conservative fluxes of DIC and dissolved inorganic phosphorus). The Irish Sea is mainly characterized by a permanently mixed water column similar to ASTAN and receives much less estuarine inputs than the SBNS. The NEP value of 0.7 mol C m^{-2} y^{-1} found by these authors for the Irish Sea was in agreement with the NEP computation at ASTAN indicating a trend of weak autotrophy for this kind of permanently mixed system despite they acted as sources of CO_2 to the atmosphere.

5. Concluding remarks

In this study, we investigated the biogeochemical processes controlling CO_2 system dynamics using surface VOS line data during three contrasted years. We combined these VOS line data with vertical profiles at fixed stations to assess the hydrographical structure of the water column. This approach proved to be an excellent tool to identify and describe the different processes controlling the dynamics of the CO_2 system parameters. We separated the WEC into two contrasting provinces with regard to the CO_2 dynamics. The seasonally stratified nWEC showed enhanced biological activities characterized by an extensive autotrophic phase, which maintained the pCO_2 below the atmospheric equilibrium until early fall and acted as sink for atmospheric CO_2 at a rate of 0.4 ± 0.1 mol C m^{-2} y^{-1}. The permanently well mixed sWEC was characterized by a shorter autotrophic phase due to a delayed spring phytoplankton growth and an early start of the fall heterotrophic phase, resulting in an annual CO_2 release to the atmosphere of 0.5 ± 0.2 mol C m^{-2} y^{-1}. The contrasted behavior of sWEC and nWEC waters as source and sink of CO_2, with respect to the atmosphere, was supported by our three years of study. Our latitudinal approach resolved the discrepancy between the directions of the fluxes in the WEC observed in previous studies by differentiating between the hydrological regions.

Our study showed that for such systems, a combined approach, based on VOS line and fixed stations can provide a robust assessment of air-sea CO_2 fluxes in these regions. Indeed, VOS lines surface data alone hamper complete assessment of the processes driving air-sea CO_2 fluxes since they do not provide any information on the hydrological properties of the ecosystems explored. Nowadays, many coastal scientific institutes support coastal observatory networks in their adjacent coastal seas where common biogeochemical parameters (temperature, salinity, DIC, TA, O_2) are measured and available at fixed stations. VOS routes should be established in these marginal seas and, as demonstrated in our study, would allow comprehensive assessments of the processes driving air-sea CO_2 fluxes. This combined approach could be applied in similar contrasting continental shelf systems, and notably in the adjacent stratified/homogenous Celtic and Irish Seas, for which such data on the CO_2 system are sparse.

References

Boalch, G.T., Harbour, D.S., Butler, E.I., 1978. Seasonal phytoplankton production in the Western English Channel 1964–1974. Journal of the Marine Biological Association of the UK, 58:943–953.

Borges, A.V., Delille, B. and Frankignoulle, M., 2005. Budgeting sinks and sources of CO_2 in the coastal ocean: Diversity of ecosystems counts. Geophysical Research Letters, 32(14). doi:10.1029/2005GL023053.

Borges, A.V. and Frankignoulle, M., 2003. Distribution of surface carbon dioxide and air-sea exchange in the English Channel and adjacent areas. Journal of Geophysical Research-Oceans, 108(C5). doi:10.1029/2000JC000571.

Borges, A.V., Ruddick, K., Schiettecatte, L.-S. and Delille, B., 2008. Net ecosystem production and carbon dioxide fluxes in the Scheldt estuarine plume. BMC ecology, 8: 15. doi:10.1186/1472-6785-8-15

Borges, A.V., Schiettecatte, L.S., Abril, G., Delille, B. and Gazeau, E., 2006. Carbon dioxide in European coastal waters. Estuarine Coastal and Shelf Science, 70(3): 375-387.

Borges, A. & Co-Authors, 2010. "A Global Sea Surface Carbon Observing System: Inorganic and Organic Carbon Dynamics in Coastal Oceans" in Proceedings of OceanObs'09: Sustained Ocean Observations and Information for Society (Vol. 2), Venice, Italy, 21-25 September 2009, Hall, J., Harrison, D.E. & Stammer, D., Eds., ESA Publication WPP-306.

Bozec, Y., Thomas, H., Schiettecatte, L.S., Borges, A.V., Elkalay, K., and de Baar, H.J.W., 2006. Assessment of the processes controlling seasonal variations of dissolved inorganic carbon in the North Sea. Limnology and Oceanography, 51(6): 2746-2762.

Brewer, P.G. and Goldman, J.C., 1976. Alkalinity changes generated by phytoplankton growth. Limnology and Oceanography, 21(1): 108-117.

Chen, C.T.A. and Borges, A.V., 2009. Reconciling opposing views on carbon cycling in the coastal ocean: Continental shelves as sinks and near-shore ecosystems as sources of atmospheric CO_2. Deep-Sea Research Part II-Topical Studies in Oceanography, 56(8-10): 578-590.

Davoult, D., Harlay, J. and Gentil, F., 2009. Contribution of a dense population of the brittle star

Acrocnida brachiata (Montagu) to the biogeochemical fluxes of CO_2 in a temperate coastal

ecosystem. Estuaries and Coasts, 32:1103–1110.

Delhez, E.J.M., Heemink, A.W. and Deleersnijder, E., 2004. Residence time in a semi-enclosed domain from the solution of an adjoint problem. Estuarine Coastal and Shelf Science, 61(4): 691-702.

Dickson, A.G. and Millero, F.J., 1987. A comparison of the equilibrium constants for the dissociation of carbonic acid in seawater media. Deep-Sea Research Part a - Oceanographic Research Papers, 34(10): 1733-1743.

Doney, S.C., Fabry, V.J., Feely, R.A., and Kleypas, J.A., 2009. Ocean acidification: The other CO_2 problem. Annual Review of Marine Sciences, 1:169-192.

Duarte, C.M., Hendriks, I.E., Moore, T.S., Olsen, Y.S., Steckbauer, A., Ramajo, L., Carstensen, J., Trotter, J.A., and McCulloch, M., 2013. Is ocean acidification an open-ocean syndrome? Understanding anthropogenic impacts on seawater pH. Estuaries and Coasts, 36: 221-236.

Dumousseaud, C., Achterberg, E. P., Tyrrell, T., Charalampopoulou1, A., Schuster, U., Hartman, M. and Hydes, D.J., 2010. Contrasting effects of temperature and winter mixing on the seasonal and inter-annual variability of the carbonate system in the Northeast Atlantic Ocean. Biogeosciences, 7(5): 1481-1492.

EPA, 1997a. In vitro determination of chlorophyll a and pheophytin a in marine and freshwater algae by fluorescence (Arar E.J. & Collins G.B.). Method 445.0, revision 1.2. US-Environmental Protection Agency, Cincinnati, 26p.

Friis, K., Körtzinger, A. and Wallace, D.W.R., 2003. The salinity normalization of marine inorganic carbon chemistry data. Geophysical Research Letters, 30(2). doi:10.1029/2002GL015898.

Garcia-Soto, C., Fernandez, E., Pingree, R.D. and Harbour, D.S, 1995. Evolution and structure of a shelf coccolithophore bloom in the Western English Channel. Journal of Plankton Research, 17(11): 2011-2036.

Gattuso, J.P., Frankignoulle, M. and Wollast, R., 1998. Carbon and carbonate metabolism in coastal aquatic ecosystems. Annual Review of Ecology and Systematic, 29: 405-434.

Gazeau, F., Smith, S.V., Gentili, B., Frankignoulle, M., Gattuso, J.P., 2004. The European coastal zone: characterization and first assessment of ecosystem metabolism. Estuarine, Coastal and Shelf Science, 60(4): 673-694.

Gazeau, F., Borges, A.V., Barrón, C., Duarte, C.M., Iversen, N., Middelburg, J.J, Delille, J.J, Pizay, M.D., Frankignoulle, M., Gattuso, J.P., 2005. Net ecosystem metabolism in a micro-tidal estuary (Randers Fjord, Denmark): evaluation of methods. Marine Ecology-

Progress Series, 301: 23-41.

Golléty, C., Gentil, F. and Davoult, D., 2008. Secondary production, calcification and CO_2 fluxes in the cirripedes Chthamalus montagui and Elminius modestus. Oecologia, 155(1): 133-142.

Harlay, J., Borges, A.V., Van Der Zee, C., Delille, B., Godoi, R.H.M., Schiettecatte, L.-S., Roevros, N., Aerts, K., Lapernat, P.-E., Rebreanu, L., Groom, S., Daro, M.-H., Van Grieken, R. and Chou, L., 2010. Biogeochemical study of a coccolithophore bloom in the northern Bay of Biscay (NE Atlantic Ocean) in June 2004. Progress in Oceanography, 86: 317–336.

Hill, A.E., Brown, J., Fernand, L., Holt, J., Horsburgh, K.J., Proctor, R., Raine, R. and Turrell, W.R., 2008. Thermohaline circulation of shallow tidal seas. Geophysical Research Letters, 35(11), L11605. doi:10.1029/2008GL033459

Kalnay, E., Kanamitsu, M., Kistler, R., Collins, W., Deaven, D., Gandin, L., Iredell, M., Saha, S., White, G., Woollen, J., Zhu, Y., Chelliah, M., Ebisuzaki, W., Higgins, W., Janowlak, J., Mo, K.C., Ropelewski, C., Wang, J., Leetmaa, A., Reynolds, R., Jenne, R., Joseph, D., 1996. The NCEP/NCAR reanalysis project. Bulletin of the American Meteorological Society 77, 437-471.

Kelly Gerreyn, B.A., Hydes, D.J., Fernand, L.J., Jegou, A.M., Lazure, P., Puillat, I., García-Soto, C., 2006. Low salinity intrusions in the western English Channel. Continental Shelf Research 26 (11), 1241–1257.

Kitidis, V., Hardman-Mountford, N.J., Litt, E., Brown, I., Cummings, D., Hartman, S., Hydes, D., Fishwick, J.R., Harris, C., Martinez-Vicente, V., Malcolm, E., Woodward, S., Smyth, T.J., 2012. Seasonal dynamics of the carbonate system in the Western English Channel. Continental Shelf Research 42: 30-40.

Le Corre, P., Wafar, M., L'Helguen, S. and Maguer, J.F., 1996. Ammonium assimilation and regeneration by size-fractionated plankton in permanently well-mixed temperate waters. Journal of Plankton Research, 18(3): 355-370.

L'Helguen, S., Madec, C. and Le Corre, P., 1996. Nitrogen uptake in permanently well-mixed temperate coastal waters. Estuarine, Coastal and Shelf Science, 42(6): 803-818.

Mehrbach, C., Culberso, Ch., Hawley, J.E. and Pytkowic, R.M., 1973. Measurement of apparent dissociation constants of carbonic acid in seawater at atmospheric pressure. Limnology and Oceanography, 18(6): 897-907.

Migné, A., Davoult, D., Gattuso, J.-P., 1998. Calcium carbonate production of a dense population of the brittle star Ophiothrix fragilis (Echinodermata: Ophiuroidea): role in

the carbon cycle of a temperate coastal ecosystem. Marine Ecology Progress Series, 173: 305-308.

Monterey, G. and Levitus, S., 1997. Seasonal variability of mixed layer depth for the world ocean. NOAA Atlas, NESDIS 14,Washington D.C., 96 pp.

Odum, H.T., 1956. Primary production in flowing waters. Limnology and Oceanography, 1(2): 102-117.

Padin, X.A., Vazquez-Rodriquez, M., Rios, A.F. and Perez, F.F., 2007. Surface CO_2 measurements in the English channel and southern bight of north sea using voluntary observing ships. Journal of Marine Systems, 66(1-4): 297-308.

Pierrot, D., Lewis, E., and Wallace, D. W. R., 2006. MS Excel Program Developed for CO_2 System Calculations., ORNL/CDIAC-105. Carbon Dioxide Information Analysis Center, Oak Ridge National Laboratory, U.S. Department of Energy, Oak Ridge, Tennessee.

Pingree, R.D. and Griffiths, D.K., 1978. Tidal fronts on shelf seas around British isles. Journal of Geophysical Research-Oceans and Atmospheres, 83(NC9): 4615-4622.

Reid, P. C., Auger, C., Chaussepied, M., and Burn, M. (Eds.), The channel, report on sub-region 9, quality status report of the North Sea 1993, 153 pp., UK Dep. of the Environ., Républ. Fr. Minist. de l'Environ., Inst. Fr. de Rech. Pour l'Exploit. de la Mer, Brest, 1993.

Schiettecatte, L.S., Gazeau, F., van der Zee, C., Brion, N., Borges, A.V., 2006. Time-series of the partial pressure of carbon dioxide (2001-2004) and preliminary inorganic carbon budget in the Scheldt plume (Belgian coastal waters). Geochemistry Geophysics Geosystems 7: doi:10.1029/2005GC001161.

Schiettecatte, L.S., Thomas, H., Bozec, Y. and Borges, A.V., 2007. High temporal coverage of carbon dioxide measurements in the Southern Bight of the North Sea. Marine Chemistry, 106(1-2): 161-173.

Smyth, T.J., Fishwick, J.R., Al-Moosawi, L., Cummings, D.G., Harris, C., Kitidis, V., Rees, A., Martinez-Vicente, V., and Woodward, E.M.S., 2010. A broad spatio-temporal view of the Western English Channel observatory. Journal of Plankton Research, 32(5): 585-601.

Southward, A.J. & Co-Authors, 2005. Long-term oceanographic and ecological research in the western English Channel. Advances in Marine Biology, 47: 1-105.

Takahashi, T., Olafsson, J., Goddard, J.G., Chipman, D.W. and Sutherland, S.C., 1993. Seasonal variation of CO_2 and nutrients in the high-latitude surface ocean – A

comparative study. Global Biogeochemical Cycles, 7(4): 843-878.

Takahashi, T. et al., 2002. Global sea-air CO_2 flux based on climatological surface ocean pCO_2, and seasonal biological and temperature effects. Deep-Sea Research Part II - Topical Studies in Oceanography, 49(9-10): 1601-1622.

Thomas, H., Bozec, Y., Elkalay, K. and de Baar, H.J.W., 2004. Enhanced open ocean storage of CO_2 from shelf sea pumping. Science, 304(5673): 1005-1008.

Thomas, H., Bozec, Y., Elkalay, K., De Baar, H., Borges, A., Schiettecatte, L.-S., De Baar, H.J.W., 2005. Controls of the surface water partial pressure of the CO_2 in the North Sea. Biogeosciences 2, 323-334.

Thomas, H., Ittekkot, V., Osterroht, C. and Schneider, B., 1999. Preferential recycling of nutrients - the ocean's way to increase new production and to pass nutrient limitation? Limnology and Oceanography, 44(8): 1999-2004.

Wafar, M.V.M., Le Corre, P., Birrien, J.L.,1983. Nutrients and primary production in permanently well-mixed temperate coastal waters. Estuarine, Coastal and Shelf Science, 17(4): 431:446.

Waldbusser, G.G. and Salisbury, J.E., 2014. Ocean Acidification in the Coastal Zone from an Organism's Perspective: Multiple System Parameters, Frequency Domains, and Habitats. Annual Review of Marine Sciences, 6: 221-247.

Walsh, J.J., 1991. Importance of continental margins in the marine biogeochemical cycling of carbon and nitrogen. Nature, 350(6313): 53-55.

Walsh, J.J., Rowe, G.T., Iverson, R.L. and McRoy, C.P., 1981. Biological export of shelf carbon is a sink of the global CO_2 cycle. Nature, 291(5812): 196-201.

Wanninkhof, R. and McGillis, W.R., 1999. A cubic relationship between air-sea CO_2 exchange and wind speed. Geophysical Research Letters, 26(13): 1889-1892.

Weiss, R.F., 1970. Solubility of nitrogen, oxygen and argon in water and seawater. Deep-Sea Research, 17(4): 721-735.

Weiss, R.F., and Price, B.A., 1980. Nitrous oxide solubility in water and seawater. Marine Chemistry, 8: 347-359.

Widdicombe, C.E., Eloire, D., Harbour, D., Harris, R.P. and Somerfield, P.J., 2010. Long-term phytoplankton community dynamics in the Western English Channel. Journal of Plankton Research, 35(5): 643-655.

Wolf-Gladrow, D.A., Zeebe, R.E., Klaas, C., Koertzinger, A. and Dickson, A.G., 2007. Total alkalinity: The explicit conservative expression and its application to biogeochemical processes. Marine Chemistry, 106(1-2): 287-300.

Zeebe R. E. and Wolf-Gladrow, D. A., 2001. CO_2 in seawater: equilibrium, kinetics, isotopes, Elsevier Oceanography Series 65, Amsterdam, 346 pp.

Chapter 3: Spatio-temporal dynamics of biogeochemical processes and air-sea CO_2 fluxes in the Western English Channel based on two years of FerryBox deployment.

This chapter is based on an article published in 2014 in Journal of Marine Systems in a FerryBox special issue: "Spatio-temporal dynamics of biogeochemical processes and air-sea CO_2 fluxes in the Western English Channel based on two years of FerryBox deployment."

P. Marrec, T. Cariou, M. Latimier, E. Macé, P. Morin, M. Vernet and Y. Bozec.

Abstract

From January 2011 to January 2013, a FerryBox system was installed on a Voluntary Observing Ship (VOS), which crossed the Western English Channel (WEC) between Roscoff (France) and Plymouth (UK) up to 3 times a day. The FerryBox continuously measured sea surface temperature (SST), sea surface salinity (SSS), dissolved oxygen (DO), fluorescence and partial pressure of CO_2 (from April 2012) along the ferry track. Sensors were calibrated based on 714 bimonthly surface samplings with precisions of 0.016 for SSS, 3.3 µM for DO, 0.40 µg L^{-1} for Chlorophyll-*a* (Chl-*a*) (based on fluorescence measurements) and 5.2 µatm for pCO_2. Over the 2 years of deployment (900 crossings), we reported 9% of data lost due to technical issues and quality checked data was obtained to allow investigation of the dynamics of biogeochemical processes related to air-sea CO_2 fluxes in the WEC. Based on this unprecedented high-frequency dataset, the physical structure of the WEC was assessed using SST anomalies and the presence of a thermal front was observed around the latitude 49.5°N, which divided the WEC in two main provinces: the seasonally stratified northern WEC (nWEC) and the all-year well-mixed southern WEC (sWEC). These hydrographical properties strongly influenced the spatial and inter-annual distributions of phytoplankton blooms, which were mainly limited by nutrients and light availability in the nWEC and the sWEC, respectively. Air-sea CO_2 fluxes were also highly related to hydrographical properties of the WEC between late April and early September 2012, with the sWEC a weak source of CO_2 to the atmosphere of 0.9 mmol m^{-2} d^{-1}, whereas the nWEC acted as a sink for atmospheric CO_2 of 6.9 mmol m^{-2} d^{-1}. The study of short time-scale dynamics of air-sea CO_2 fluxes revealed that an intense and short (less than 10 days) summer bloom in the nWEC contributed to 29% of the CO_2 sink during the productive period, highlighting the necessity for high frequency observations in coastal ecosystems. During the same period in the sWEC, the tidal cycle was the main driver of air-sea CO_2 fluxes with a mean difference in pCO_2 values between spring and neap tides of +50 µatm. An extraction of day/night data at 49.90°N showed that the mean day-night differences accounted for 16% of the mean CO_2 sink during the 5 months of the study period implying that the diel biological cycle was also significant for air-sea CO_2 flux computations. The 2 years of deployment of our FerryBox allowed an excellent survey of the variability of biogeochemical parameters from inter-annual to diurnal time scales and provided new insights into the dynamics of air-sea CO_2 fluxes in the contrasted ecosystems of the WEC.

1. Introduction

Traditional surveys of the marine environment using research ships or fixed stations have many limitations in terms of cost and spatio-temporal coverage. Autonomous ocean observing systems mounted on commercial shipping lines, here called FerryBox (www.ferrybox.org), have been developed since the 1990s to overcome these problems. The EU FB5 project "FerryBox" (2002-2005) promoted the development of this tool for operational oceanography and encouraged European marine institutes to equip Voluntary Observing Ships (VOS) with FerryBox systems. The progress made on FerryBoxes in the last ten years (Hydes et al., 2010; Petersen et al., 2011) proved the efficiency of these cost-effective systems to deliver high frequency physical, chemical and biological data over a wide range of temporal and spatial scales. The installation of a FerryBox on VOS provides the assurance of a continuous energy supply and sheltered conditions inside the ship with easy maintenance during frequent and regular harbour stops. Moreover, the automated cleaning cycles operated by these systems prevent biofouling. The most regular VOS lines are located in marginal seas, which allow monitoring on the same track with frequent time steps in order to follow the variability of the marine environment over short time scales.

Continental shelf ecosystems are highly dynamic regarding physical, chemical and biological parameters and play a significant role in biogeochemical cycles (Walsh et al., 1991) despite their relatively moderate size compared to the global oceans (7%). In the context of climate change, with increasing water temperature and rising CO_2 levels in the atmosphere and oceans (IPCC, 2007), long-term high-frequency monitoring of marine ecosystem dynamics is essential, particularly in coastal ecosystems (Goberville et al., 2010). The use of VOS equipped with a FerryBox system with sensors for measurement of partial pressure of CO_2 (pCO_2) is highly recommended to better understand present day carbon cycle dynamics, quantify air-sea CO_2 fluxes and determine future long-term trends in CO_2 in response to climate change forcing (Borges et al., 2010). A limited number of studies have investigated pCO_2 dynamics in coastal ecosystem using VOS automated measurement systems (Schneider et al., 2006; Padin et al., 2007; Omar et al., 2010) and very rarely with high-frequency and long-term pCO_2 and ancillary data records. Access to data on additional physic-chemical and biological parameters such as sea surface temperature (SST), sea surface salinity (SSS), dissolved O_2 (DO), chlorophyll-*a* (Chl-*a*) and nutrient concentrations is essential for studying

biogeochemical processes, which control pCO_2 variability at different time scales in coastal ecosystems.

The Western English Channel (WEC) is part of one of the world's largest margins, the North-West European continental shelf. This area is characterized by relatively shallow depths and by intense tidal streams with maximum speeds ranging from 0.5 to 2.0 m s^{-1} (maxima for the entire English Channel (EC)) (Reid et al., 1993). The WEC hosts three different hydrographical structures: all year well-mixed, seasonally stratified and thermal front structures. Such water column characteristics are also observed in adjacent seas of the North-West European continental shelf, i.e. in the Irish Sea and in the North Sea (Hill et al., 2008). Along the French coast (southern WEC (sWEC)), where the tidal currents are the strongest, the water column remains vertically mixed (Wafar et al., 1983), whereas near the English coast (northern WEC (nWEC)), where tidal streams are less intense, seasonal stratification occurs (Smyth et al., 2010). Between these two distinct structures, a frontal zone oscillates, separating well-mixed and stratified waters (Pingree & Griffiths, 1978). In this complex hydrographical context, high-frequency measurements could precisely locate this thermal front and accurately identify the real extent of each hydrographical province. Moreover, previous studies have shown an important spatial and temporal variability of the CO_2 system in the area (Borges and Frankignoulle, 2003; Padin et al., 2007; Dumousseaud et al., 2010; Kitidis et al., 2012). However, these studies were either based on monthly/seasonal measurements on longitudinal transects, or on a fixed station approach (Kitidis et al., 2012), that did not cover both of the hydrographical structures of the WEC.

In the present study, as part of the European cross-border INTERREG IV project MARINEXUS (Our shared seas: Mechanisms of ecosystem change in the Western Channel), we exploited a VOS route between the French and English coasts (Figure 17) from January 2011 to January 2013, which crosses the different hydrographical structures of the WEC described above. Our FerryBox measurements provided a comprehensive new dataset of SST, SSS, DO, Chl-*a* and pCO_2 in the WEC. In this paper, we first discuss the reliability of the FerryBox data over the two years of deployment. We then describe the physical structure of the WEC based on high-frequency spatio-temporal SST and SSS distributions and assess the environmental conditions driving the dynamics of inter-annual phytoplankton blooms in the different provinces of the WEC. Finally, we present the first high-frequency pCO_2 data acquired across the WEC and discuss the processes driving air-sea CO_2 fluxes from late April 2012 to January 2013 at seasonal to diurnal time scales.

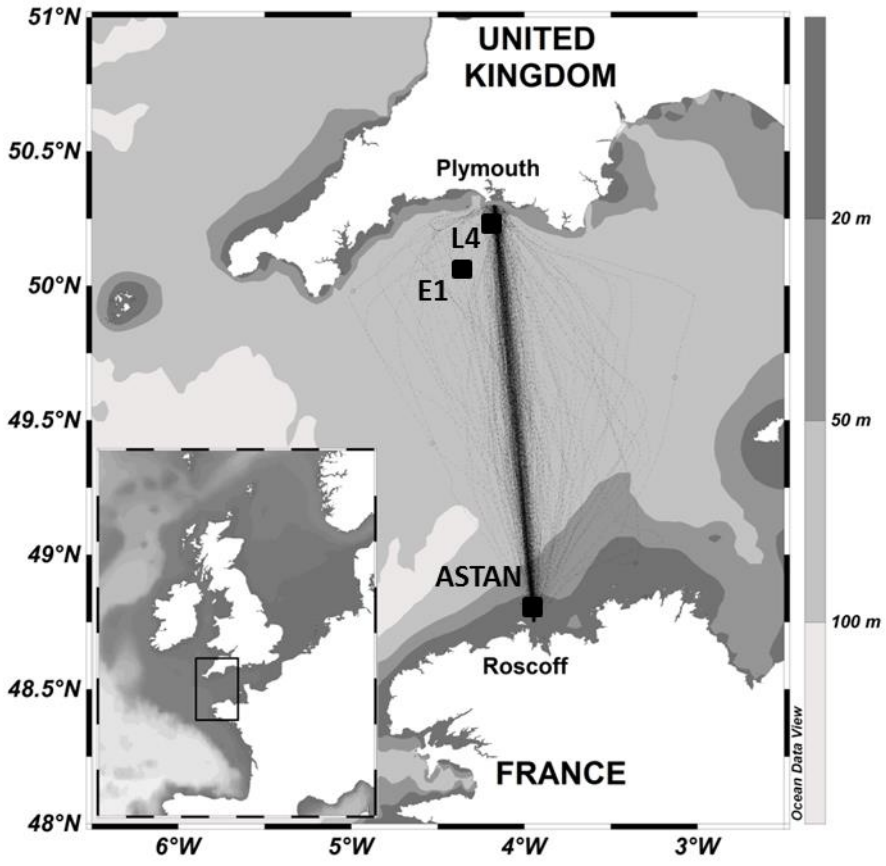


Figure 17: Map and bathymetry of the study area with the tracks of all crossings made in 2012 (2013 are not shown for the clarity of the figure) between Roscoff (France) and Plymouth (UK). The locations of fixed stations E1 and L4 (Western Channel Observatory), and ASTAN (coastal observatory SOMLIT) are also indicated.

2. Material and Methods

2.1 The VOS line and the FerryBox system

In December 2010 we installed a FerryBox system on the Voluntary Observing Ship (VOS) *Armorique* (Brittany Ferries). This vessel crossed the English Channel between Roscoff (France, 48°43'38N 3°59'03E) and Plymouth (United Kingdom, 50°22'12N 4°08'31E) (Figure 17) up to 3 times a day from February to November. The ferry, which does not have a

fixed departure/arrival time during the year, crosses the WEC (100 nautical miles) in 6 hours during the day and 14 hours during the night. A FerryBox is an automated ocean observing system equipped with several sensors. Our FerryBox was built by -4H- JENA and was installed at the engine room level on the *Armorique*. The FerryBox pumped seawater at 4 meters depth with a high flow rate to avoid warming of seawater in the water column circuit. The pump was operational only when the ferry was sufficiently far from the harbours to avoid introducing particle-rich waters into the system. The data acquisition of the sensors was performed every minute under a LabView environment and data were automatically sent and stored in our database in Roscoff at the end of each crossing. From January 2011 to January 2013 the ferry performed more than 900 crossings with data acquisition.

A Sea Bird SBE 38 temperature sensor recorded the *in-situ* seawater temperature with a precision of 0.001°C and a Sea Bird SBE 45 thermosalinograph recorded the temperature and salinity inside the seawater circuit of the Ferry Box with precisions of 0.002°C and 0.005, respectively. Dissolved oxygen concentrations were measured using an Aanderaa Optode 3835 and a Turner Designs C3 fluorometer measured chlorophyll-*a* fluorescence. From April 2012 a Contros HydroC/CO_2 FT sensor was used for measurements of the partial pressure of CO_2 (pCO_2) in seawater. This sensor measured the pCO_2 continuously in a headspace behind a membrane equilibrator with a non-dispersive infrared detector (Fietzek and Körtzinger, 2010). Sensors were calibrated and/or adjusted based on bimonthly discrete measurements made on the ferry (see section 3.1.).

2.2 Bimonthly discrete sampling

Between January 2011 and January 2013, discrete sampling was performed on 40 return crossings between Roscoff and Plymouth with a total of 714 sampling locations in the WEC. During each cruise, 18 water samples were taken from the FerryBox seawater circuit for the determination of dissolved oxygen (DO), dissolved inorganic carbon (DIC), total alkalinity (TA), nutrients (NO_3^-, NO_2^-, PO_4^{3-} and SiO_4^-), chlorophyll-*a* (Chl-*a*) and salinity. Discrete salinity samples were measured on a portasal salinometer at the SHOM (Service Hydrographique et Oceanographique de la Marine) with a precision of 0.002. DO concentrations were determined within a week of sampling by the Winkler method using a potentiometric end-point determination with an estimated accuracy of 0.5 µmol L^{-1}. The

oxygen saturation level (DO%) was then calculated according to Weiss (1970) from the observed DO and the DO at saturation using the *in-situ* temperature and salinity data. In 2011, DIC and TA were collected in 100 mL and 250 mL borosilicate glass bottles, respectively, poisoned with 100 µL of saturated $HgCl_2$, and analyzed within a week of sampling. DIC was determined with an AIRICA system (Marianda Inc.) after acidification of a 2.3 mL aliquot with phosphoric acid, extraction by a carrier gas (N_2) and detection with a LICOR-7000 IR detector. TA was measured with a TA-ALK 2 system (Appolo SciTech.) by the Gran electro-titration method on 25 mL aliquots. The accuracies of DIC and TA measurements were determined with Certified Reference Materials (CRM) provided by A. G. Dickson, Scripps Institution of Oceanography (Batch 92). CRM standards were measured at the start and at the end of each day of analysis and every 10 samples during the runs. Accuracies of the DIC and TA measurements were 1.5 µmol kg^{-1} and 3 µmol kg^{-1}, respectively, based on bi-annual measurements of different batches. In 2012, because of the large amount of samples collected, we chose to analyse DIC and TA at the national facility for analysis of carbonate system parameters (SNAPO-CO_2, LOCEAN, Paris), which allows simultaneous measurements of DIC/TA by potentiometric titration. DIC and TA were collected in 500 mL borosilicate glass bottles, poisoned with 300 µL of $HgCl_2$, stored at 4°C and analyzed simultaneously by potentiometric titration derived from the method developed by Edmond (1970) using a closed cell. The calculation of equivalence points was done using a non-linear regression (D.O.E. 1994). These simultaneous DIC and TA analyse were performed at the SNAPO-CO_2 with an accuracy of ±2 µmol kg^{-1} for DIC and TA. Inter-calibration between the two DIC methods and two TA methods confirmed the accuracies of TA and DIC of ±2 µmol kg^{-1} and ±3 µmol kg^{-1}, respectively. To determine chlorophyll-*a* concentrations (Chl-*a*), 0.5 L of seawater were filtered through glass-fibre filters (Whatman GF/F) and immediately frozen. Samples were extracted in 5 mL of acetone. Correction for phaeopigments was carried out using the acidification method with an HCl solution, after primary fluorescence measurements using a fluorometer (Turner Designs model 10 AU digital fluorometer) to calculate Chl-*a* concentrations according to EPA (1997). The estimated accuracy was 0.05 µg L^{-1}. Nutrient concentrations (NO_3^-, NO_2^-, PO_4^{3-} and SiO_4^-) were determined using an AA3 auto-analyser (AXFLOW) following the method of Aminot and Kérouel (2007) with accuracies of 0.02 µg L^{-1}, 1 ng L^{-1}, 1ng L^{-1} and 0.01 µg L^{-1} for NO_3^-, NO_2^-, PO_4^{3-} and SiO_4^-, respectively.

2.3 CO_2 system and air-sea CO_2 fluxes calculation

Seawater pCO_2 values were calculated from TA, DIC, temperature, salinity and nutrient concentrations with the CO2SYS program (Pierrot et al., 2006) using the equilibrium constants of CO_2 proposed by Mehrbach et al. (1973), refitted by Dickson and Millero (1987) on the seawater pH scale, as recommended by Dickson et al. (2007). The computed values of pCO_2 from DIC and TA have an uncertainty of ± 5.8 µatm (Zeebe and Wolf-Gladrow, 2001), which does not include uncertainties in the dissociation constants and ignores the contribution of organic compounds to alkalinity (Koeve et al., 2011, Hope et al., 2012). The WEC waters are open continental shelf waters, which are weakly influenced by estuarine plumes. Organic matter levels are thus low, except in the vicinity of Plymouth. Organic compounds therefore do not significantly influence alkalinity in most of the WEC. The calculated pCO_2 values allowed us to adjust the Contros HydroC/CO_2 FT data (see Section 3.1.). Atmospheric pCO_2 ($pCO_{2\ air}$) was calculated from the CO_2 molar fraction (xCO_2) at the Mace Head site (53°33'N 9°00'W, southern Ireland) of the RAMCES network (Observatory Network for Greenhouse gases) and from the water vapor pressure (pH_2O) using the Weiss and Price (1980) equation. Atmospheric pressure (Patm) in the middle of the WEC (49°50'N, 4°00'W) was obtained from the NCEP/NCAR re-analysis project (Kalnay et al., 1996).

The fluxes of CO_2 across the air-sea interface (F) were computed from the pCO_2 air-sea gradient ($\Delta pCO_2 = pCO_{2\ water} - pCO_{2\ air}$, µatm) according to:

$$F = k * \alpha * \Delta pCO_2 \quad (19),$$

where k is the gas transfer velocity (m s^{-1}) and α is the solubility coefficient of CO_2 (mol atm^{-1} m^{-3}) calculated after Weiss (1970). The exchange coefficient k was computed as a function of wind speed with the algorithm given by Nightingale et al. (2000) established in the Southern Bight of the North Sea (SBNS):

$$k = (0.222 * u_{10}^2 + 0.333 * u_{10}) * (Sc/660)^{-0.5} \quad (20)$$

where u_{10} is the wind speed data at 10 m height (m s^{-1}) and *Sc* the Schmidt number at *in-situ* SST. The SBNS and the WEC present similar environmental characteristics: these two shallow continental shelves are both close to land with high tidal currents controlling the physical structure of the water column. Wind speeds along the ferry track were extracted from daily wind speed data corrected at 10 m height from the NCEP/NCAR re-analysis project

provided by the NOAA-ESRL Physical Sciences Division, (Boulder, CO, USA, http://wwww.esrl.noaa.gov/psd/).

3. Results and discussion

3.1 Reliability of the FerryBox system

From January 2011 to January 2013, the correlation between 530 discrete SSS samples and sensor data was very robust (Figure 18a). Two SBE45 sensors calibrated using the SHOM (Service Hydrographique et Océanographique de la Marine) calibration facility were rotated in order to prevent sensor drift during the two-year deployment. During the deployment of the second SBE45 sensor from April 2011 to January 2013, we observed a temporal drift (-0.00013 PSU day^{-1}, n=472, r^2=0.78) and corrected the raw data. With regular maintenance and calibration by discrete measurements, high precision (0.016) and long-term stability in SSS measurements was attained on our FerryBox (Figure 18a).

Over the two-year sampling period, two Optodes were used. We applied salinity and temperature corrections to the raw Optode data using the Aanderaa correction methods. Figure 18b shows the correlation between sensor data corrected to *in-situ* SST and SSS and from inherent sensor offsets during each deployment, versus the discrete measurements (n=653, r^2=0.97, Figure 18b). We obtained a precision of 3.3 µM based on the standard deviation of residuals of similar range as reported by Hydes et al. (2009) also on a FerryBox system (3 to 5 µM), this being lower than the accuracy stated by the manufacturer (8 µM or 5%). We observed abnormally high positive residual differences during two crossings (February 2011 and December 2011) (Figure 18b). During these crossings the sea was particularly rough and many bubbles were observed inside the seawater circuit, which might be due to our water inlet being too shallow for very rough seas. During several crossings, we observed a few highly negative residuals. There was no clear explanation for these values, which might be related to sampling operations or quality of the Winkler reagents during given transects. Our results indicate that Aanderaa Optodes are suitable sensors for long-term deployment on a FerryBox when the Optode sensor is regularly rotated to avoid major sensor drift.

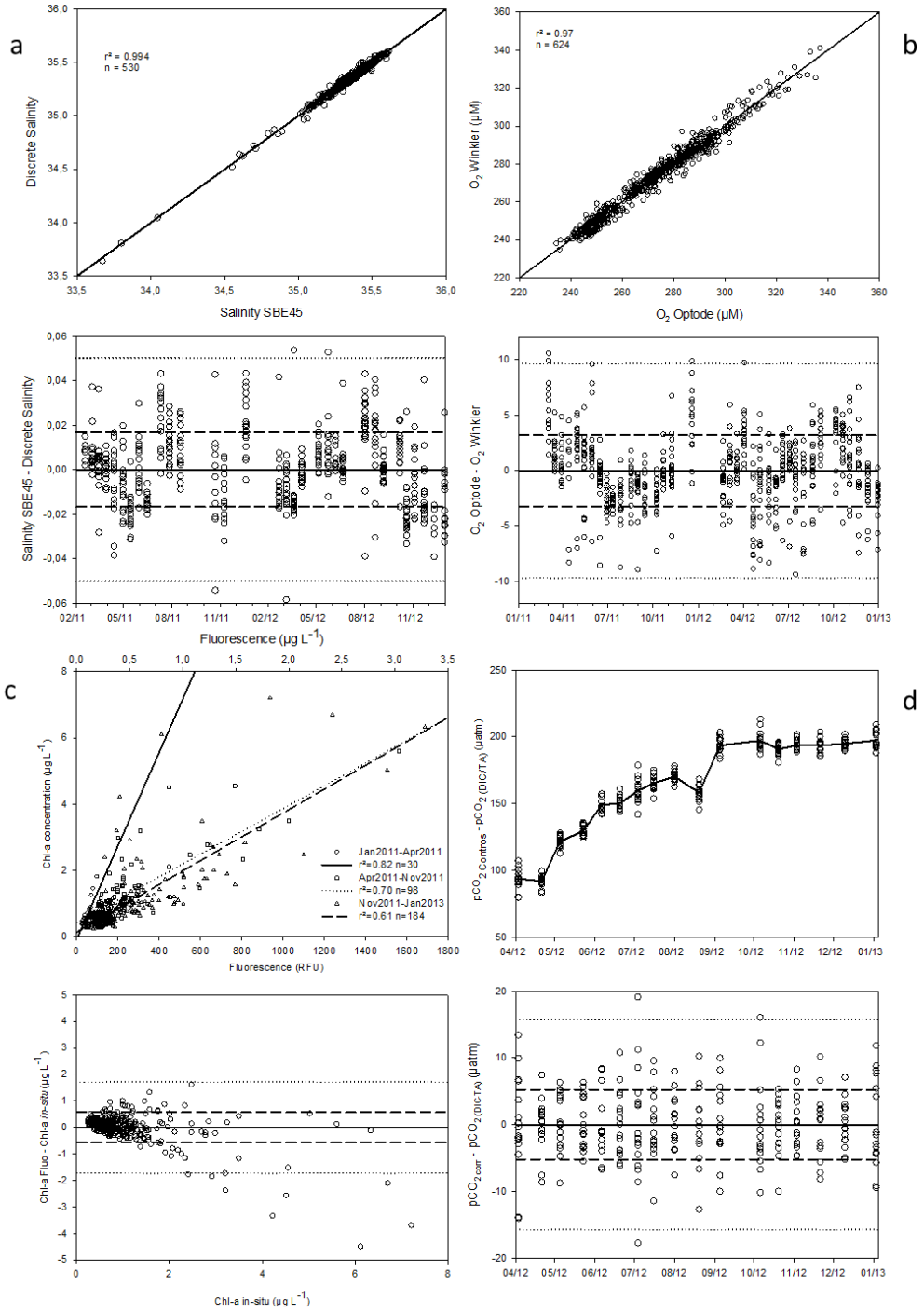


Figure 18: Adjustment of high frequency data of (A) SSS, (B) DO, (C) Chl-*a* and (D) pCO_2 based on bimonthly discrete measurements. For SSS and DO, top plots show the discrete measurements versus corrected sensor values. For Chl-*a*, the top plot shows the discrete measurements versus fluorescence in relative fluorescence units (RFU) and, during the third deployment, versus fluorescence data converted into Chl-*a* concentration by the C3 software. For pCO_2, top plot shows the differences between pCO_2 data from the HydroC/CO_2 FT sensor before correction and pCO_2 calculated from DIC/TA discrete measurements (µatm) during the deployment of the sensor. Bottom plots show differences between sensor values and discrete measurements over time. Dashed lines represent standard deviation of the differences between sensor values and discrete measurements whereas dotted lines represent three times the standard deviation.

Figure 18c shows the correlation between sensor data and discrete Chl-*a* measurements for the three deployments of C3 instruments. Two C3 sensors were used from January 2011 to January 2013 with two rotations during this period. During the two firsts deployments we recorded fluorescence in relative fluorescence units (RFU) and during the third deployment fluorescence data were converted into Chl-*a* concentration by the C3 software. The most significant correlation between FerryBox data and discrete measurements was observed from January 2011 to April 2011, with an r^2 of 0.82 from 30 measurements. Between April 2011 and November 2011 and between November 2011 and January 2013 correlations were weaker, but still significant with an r^2 of 0.70 and 0.61, respectively. The use of fluorescence data converted into Chl-*a* concentration was based on laboratory calibration of the C3 sensor using a phytoplankton culture. This single specy calibration is probably not representative of the phytoplankton diversity of the natural system, potentially inducing errors in the estimated Chl-*a*. After correction of raw fluorescence data (in RFU and in µg L^{-1}) by the respective linear regression coefficients, we plotted the differences of corrected estimates of Chl-*a* and Chl-*a* concentrations measured in the laboratory versus the Chl-*a* laboratory measurements (Figure 18c). Between 0 and 3 µg L^{-1}, the Chl-*a* difference is homogeneously distributed around 0 with a standard deviation of 0.36 µg L^{-1}. Beyond 3 µg L^{-1} important deviations from 0 were observed. The potential sources of error might be due to the different phytoplankton species composition in WEC surface water in different seasons (Southward et al., 2005; Guilloux et al., 2013) and/or the effect of fluorescence quenching (Xing et al., 2012) since most of the crossings were performed during daytime. Despite the high standard deviation, high-frequency fluorescence data do permit the use of Chl-*a* variations as an indicator of the presence of phytoplankton in surface waters of the WEC.

The HydroC/CO_2 FT pCO_2 sensor was installed on the FerryBox in April 2012. We applied the algorithm of Takahashi et al. (1993) to the sensor data to correct for the warming of seawater inside the seawater circuit using the differences between *in-situ* and seawater-circuit temperature. Between April 2012 and January 2013, we analysed 264 DIC and TA samples to calculate pCO_2 values. The difference between sensor pCO_2 data and discrete measurements of pCO_2 through time allowed us to estimate the drift of the sensor (Figure 18d). This drift was not always linear; we corrected the high-frequency data using step-by-step interpolations between each crossing from the bimonthly offsets observed. Regular zeroing can also be performed to follow any potential drift of the instrument with time, but software issues during our deployment prevented access to this procedure. The origin of the

high offset (90 µatm) observed at the beginning of the deployment is not well defined. One month before the deployment, immediately after the manufacturer calibrated the HydroC/CO_2 FT, we tested this sensor in the laboratory against a classical equilibration system with IR detection (LICOR 7000) (Bozec et al., 2012). These tests did not show any significant offset between the two types of measurements. The HydroC/CO_2 FT was then stored for one month prior to its installation on the FerryBox. The one-month storage period and new environmental conditions might explain the high offset observed at the beginning of the deployment (Figure 18d). The pCO_2 values during the deployment ranged between 160 µatm and 460 µatm. The difference between corrected sensor data and discrete measurements through time (Figure 18d) had a standard deviation of 5.2 µatm which was better than the level of deviation announced by the manufacturer, which is ± 1% of upper range value (200 to 1000 µatm, thus 10 µatm). To the best of our knowledge this was the first time that the Contros HydroC/CO_2 FT sensor has been deployed on a FerryBox system and it was a relatively long deployment compared to other studies using this sensor (Fielder et al., 2012; Saderne et al., 2013). This sensor proved to have sufficient reliability to study pCO_2 variability in dynamic coastal ecosystems, which exhibit a wide range of pCO_2 values (150-500 µatm). However the precision obtained with this sensor was low compared to state-of-the-art pCO_2 analyzers. The maintenance and calibration of the Contros HydroC/CO_2 FT sensors are relatively simple and low cost, and we believe the data quality obtained with this sensor will be improved by setting up routine zeroing values with the manufacturer to more accurately estimate the drift of the sensor.

Automated ocean observing systems such as the FerryBox are subject to technical issues inherent to high-technology equipment deployed in challenging environments over long periods. During the two years of deployment, we limited the data loss due to technical issues to 9%. The proximity of the ferry terminal to our laboratory and the high frequency of crossings facilitated rapid intervention on technical issues and were major benefits to avoid extended periods of instrument downtime. We thus obtained a very comprehensive dataset, with sufficient precision to allow assessment of the dynamics of biogeochemical processes and air-sea CO_2 fluxes in the WEC.

3.2 Observation of the physical structure of the WEC

Previous studies (e.g. Pingree and Griffiths, 1978) have shown that the WEC is characterized by the presence of a thermal front from late spring to early fall, which periodically separates the two main provinces, the northern WEC (nWEC) and the southern WEC (sWEC). Measurements undertaken by coastal observatories on either side of the WEC (Figure 17) have been used to describe the physical structure of the water column at fixed stations representative of each province. Station E1 (50.03°N 4.37°W; depth 75m; Western Channel Observatory) is representative of seasonally stratified open shelf seas of the nWEC (Smyth et al., 2010). The Astan station (48°46'40N 3°56'15W; depth 60m; Roscoff Coastal Observatory (SOMLIT)) is representative of an all-year well-mixed water column system of the sWEC as described by Wafar et al. (1983).

Figure 19a shows SST distribution in the WEC from high-frequency FerryBox measurements from the 14th of February 2011 to the 31st of December 2012. SST followed classical dynamics with warmer surface waters from spring to summer and cooling from autumn to winter. The coolest SST was recorded in February 2011 (8.2°C) close to the English coast and the warmest SST was recorded in late July 2011 (19.4°C). In both years the coolest STTs were observed in the nWEC close to the English coast and the warmest SSTs in the nWEC stratified waters. Winter and early spring 2011 were colder than in 2012. The mean annual temperature amplitudes were approximately 10°C.

Figure 19c shows SST anomalies (dT) obtained from the difference between SST and mean SST from running averages performed on 500 consecutive SST measurement steps (a crossing corresponded to approximately 300-400 minutes or steps). dT allowed us to distinguish the two main hydrographical provinces in the WEC. For each SST step a mean SST was calculated from the 500 next SST records. The mean SST was thus always different but represented the mean SST of each transect. From mid-spring to early autumn, negative dT values were related to the coolest waters of the well-mixed sWEC and positive dT values were related to the seasonally stratified nWEC waters. FerryBox high-frequency measurements clearly reveal the presence and the oscillations of a thermal front separating the two provinces. The mean position of the thermal front (horizontal black line on Figure 19c) was located between 49.4°N and 49.6°N. The highest positive and negative dT values were observed during summer when the differences in SST between nWEC and sWEC were the

most marked. In 2011, differentiation between the two provinces was first observed in early May and one month later in 2012. Figure 19a shows that warming of surface waters started earlier in 2011 than in 2012 and this explains the one-month delay in 2012 in the separation of the WEC to northern and southern provinces. The end of separation between the two provinces occurred in mid-September for both years. In the following sections, all references to nWEC and sWEC will be based on the SST anomaly distinguished on Figure 3c.

In addition to SST distribution across the WEC, high-frequency SSS measurements provided details on the physical structure of the WEC. Figure 19b shows the distribution of SSS across the WEC over the years 2011 and 2012. Maximum SSS values (>35.50) were recorded from autumn 2011 to spring 2012 in the entire WEC except near the English coast. During almost all the year low salinities (<35.3) were observed near the coast at a latitude north of 50°N due to freshwater inputs from the Plymouth rivers. In July 2012, freshwater inputs from these rivers decreased SSS even further south of 49.9°N. In the southern part of the WEC, from February to June 2011, low salinity (<35.30) surface waters were also observed and salinity dropped below 35.10 (Figure 19b). According to Kelly-Gerreyn et al. (2006), low saline waters from the Loire plume can reach the southern part of the WEC and these coastal waters are also influenced by freshwater discharges from Britanny rivers. In 2012, such low saline surface waters were not recorded, but some minor freshwater inputs lowered SSS off the French coast during spring. Negative dT anomalies were recorded up to 50°N and were related to these freshwater inputs (Figure 19c), which have lower SST than seasonally stratified open shelf waters of the nWEC. Therefore, from SSS observations, a third zone could be distinguished along the English coast in addition to the two mentioned above.

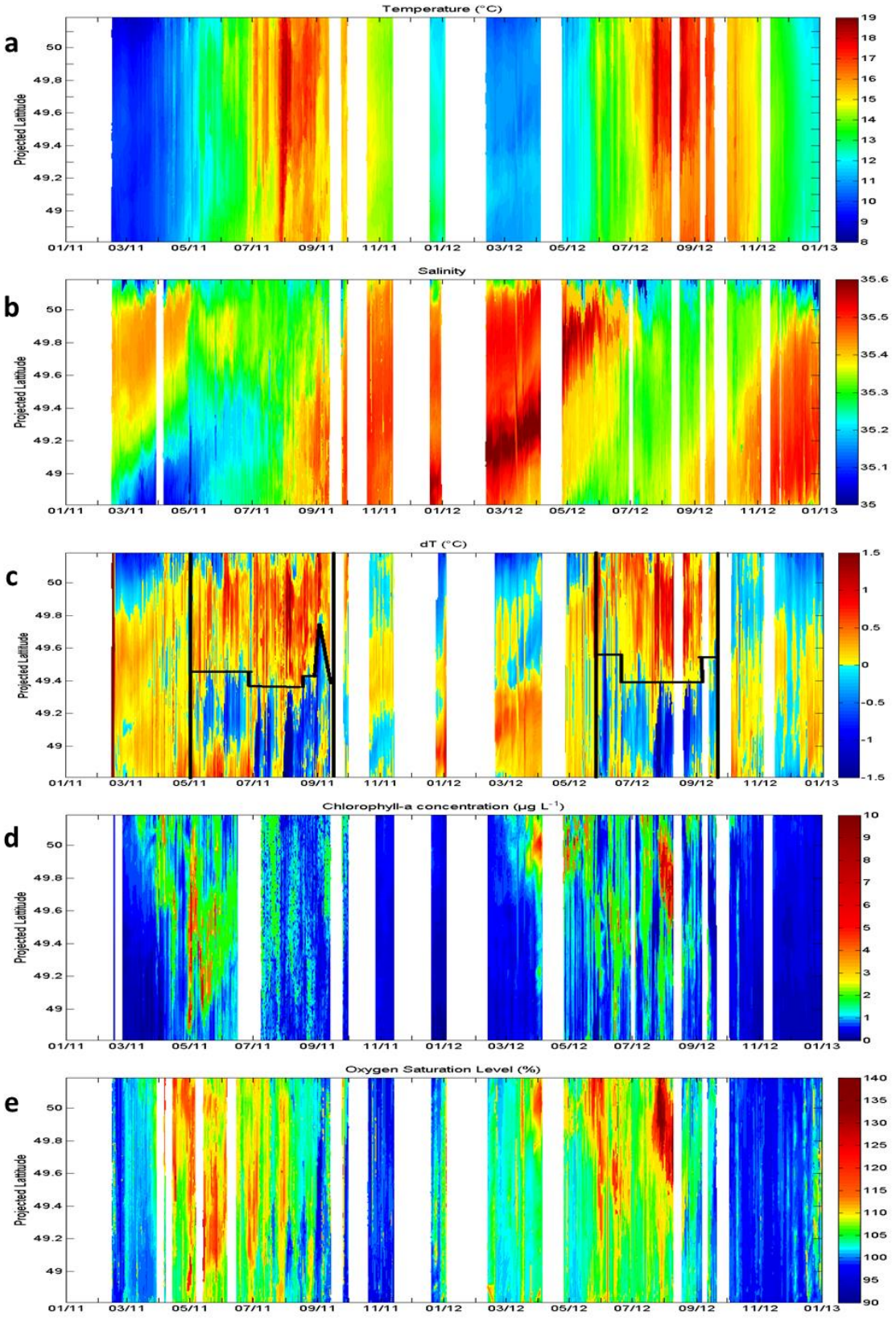


Figure 19: Surface distributions of (a) SST (°C), (b) SSS, (c) SST anomaly (°C), (d) Chl-*a* (µg L^{-1}) and (e) DO% in the WEC between Roscoff and Plymouth for the years 2011 and 2012. On Figure 3c, the horizontal black lines represent an estimate of the location of the thermal front; the vertical black lines approximately delimit the period when stratification occurred in the northern WEC.

3.3 Inter-annual dynamics of phytoplankton blooms

DO%, which can be used as an indicator of biological processes, and Chl-*a* distribution patterns showed clear similarities during 2011 and 2012 in the WEC (Figure 19d and 19e). During winter, Chl-*a* concentrations were lower than 0.5 µg L^{-1} and DO% values were close to equilibrium (100%). During both years, the productive period, marked by Chl-*a* increase, started more than one month earlier in the nWEC than in the sWEC and DO% oversaturations followed these Chl-*a* increases. This delay was mainly due to the fact that in the nWEC the tidal streams were lower than in the south (Pingree and Griffiths, 1978) and the stratification of the water column occurred when surface seawater heated up, as seen above, with the installation of the thermal front (Figure 19c). These two factors allowed phytoplankton to benefit from better light conditions in the nWEC than in the sWEC with the installation of a euphotic zone. Surface waters of the WEC remained oversaturated in DO compared to the atmospheric equilibrium for the duration of the productive period. After the productive period, the remineralization phase started as seen from DO% undersaturation, high NO_2^- concentrations and low Chl-*a* values (Figure 19e, 20d and 19d). In 2011 and 2012, dominant heterotrophic processes were first observed in the sWEC and more than one month later in the nWEC. The remineralization processes, occurring mainly in deeper waters and at the sediment interface, affected the entire water column in the sWEC. In the nWEC, these processes took place under the mixed layer depth and only affected the surface waters after the breakdown of the thermocline. This might explain why dominant heterotrophy was observed first in the sWEC. From the distribution of DO% and Chl-*a* in these two contrasted provinces (Figure 19c) it clearly appeared that hydrographical properties of the water column strongly influenced the seasonal phytoplankton bloom distributions and production/remineralization processes.

The two years of FerryBox records allowed us to observe important inter-annual variations and significant differences between the seasonally stratified nWEC and the all-year well-mixed sWEC.

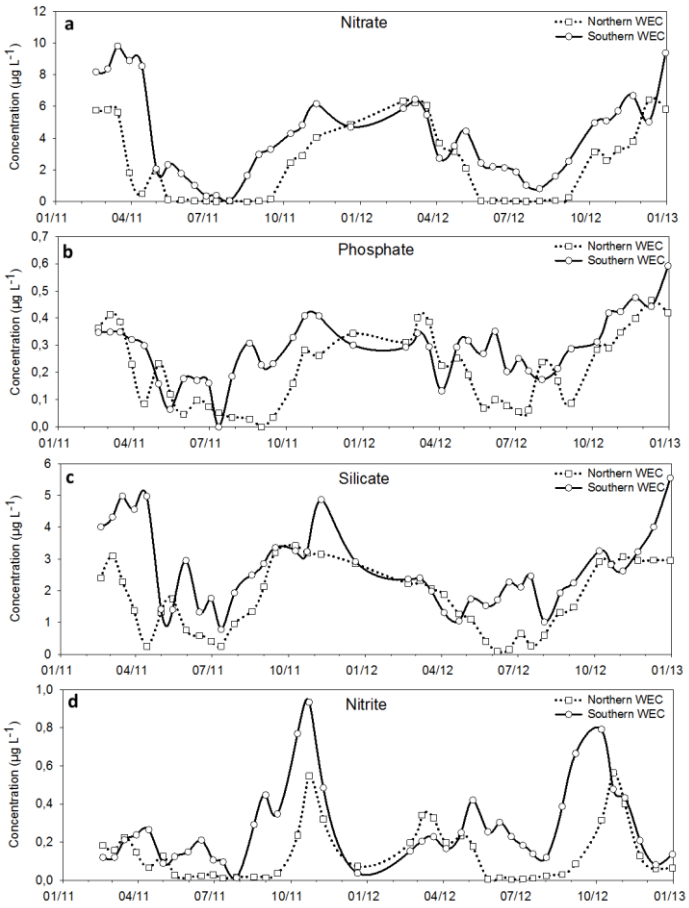


Figure 20: NO_3^- (a), PO_4^{3-} (b), SiO_4^- (c) and NO_2^- (d) concentrations (µg L^{-1}) in 2011 and 2012 at 48.9°N (representative of the southern WEC, black line, empty circles) and at 49.9°N (representative of the northern WEC, dashed lines, empty squares) from bimonthly discrete measurements.

The most significant inter-annual variation was observed in the sWEC. In 2011 an important spring bloom occurred from May to June (Figure 19d and 19e), whereas in 2012 no such intense phytoplankton bloom was observed at this time. Figure 20 shows that in 2011 the winter pool of nutrients decreased abruptly once the bloom started with significant consumption of SiO_4^- in May and total NO_3^- depletion in July. In 2012 the decrease was less important: NO_3^- was not totally depleted during the summer period and SiO_4^- did not significantly decrease. In 2012, nutrient availability was not the limiting factor for phytoplankton blooms and phytoplankton blooms did not deplete nutrient concentrations like in 2011. As reported by previous studies, the main factor controlling the phytoplankton production in the well-mixed waters of the WEC is the light availability (Boalch et al., 1978; Wafar et al., 1983; L'Helguen et al., 1996). During our study period, we observed variable meteorological conditions throughout the years. These variable meteorological conditions

controlled directly the light availability, which was likely the main factor responsible for the strong inter-annual variability of phytoplankton blooms in the sWEC.

In the nWEC, inter-annual variations were also observed, especially in the intensity and chronology of blooms. From April to June 2011, a succession of blooms occurred and DO% remained strongly oversaturated (>110%) even when surface Chl-*a* concentrations were low. Following the first spring phytoplankton blooms, surface NO_3^- was totally depleted until the end of the productive period (Figure 20a). The second spring phytoplankton bloom in 2011 might be linked to a freshwater input (Figure 19b), which brought nutrients in early May (Figure 20) when they were almost depleted. DO% remained relatively high even when surface Chl-*a* concentrations were low during the productive period. These observations suggest the presence of a sub-surface phytoplankton bloom above the thermocline after nutrient depletion in the surface layer, as reported previously by Southward et al. (2005) and by Smyth et al. (2010). After the spring blooms, we observed extremely low NO_3^- and SiO_4^- concentrations in the surface waters. However, as observed by Smyth et al. (2010), these nutrients might still be available at the thermocline and allow sub-surface phytoplankton blooms at the interface between deep and surface waters. This might explain the relatively high DO% observed even when surface Chl-*a* concentrations were low. Moreover Chl-*a* values are representative of phytoplankton stocks but not always of their biological activity, which can be indicated by DO%. In 2012, the early spring bloom was more intense than in 2011 (Figure 19d), but less extended in time and space over the following weeks. After the initial 2012 spring bloom, NO_3^- and SiO_4^- were also totally depleted and PO_4^{3-} decreased significantly (Figures 20). However, from the end of July to mid-August 2012 a third massive phytoplankton bloom (Chl-*a* >10 µg L^{-1}) was recorded, followed by the highest DO% (>135%) values observed. During this period, NO_3^- was totally depleted but we observed an increase in PO_4^{3-} (Figure 20a and 20b). Figure 19b clearly shows freshwater inputs from the English coast in July 2012, which might have provided an input of nutrients to the nutrient-depleted nWEC surface waters. In the nWEC, the main limiting factor for phytoplankton growth was nutrient availability. The lower tidal streams compare to the sWEC and the stratification of the water column allowed phytoplankton to benefit from better light availability in contrast to the all-year well-mixed sWEC. The short time-scale dynamics of these blooms and their impact on air-sea CO_2 fluxes are discussed in section 3.4.

3.4 Short time-scale dynamics of pCO_2 and air-sea CO_2 fluxes

Figure 21 shows the spatio-temporal distribution of the SST anomaly (Section 3.2.), of partial pressure of CO_2 (pCO_2, in µatm), of pCO_2 normalized to the mean temperature of 13 °C (pCO_2@Tmean) according to Takahashi et al. (1993) and of air-sea CO_2 fluxes (in mmol m^{-2} d^{-1}) in the WEC between the end of April 2012 and January 2013. The pCO_2 values were adjusted from bimonthly discrete measurements (see section 3.1.). During the first half of the sample period, the contrast between the seasonally stratified nWEC and the all-year well-mixed sWEC was clear.

In the nWEC, from April to September 2012, surface seawater was strongly undersaturated in CO_2 compared to the atmospheric equilibrium and during this period the nWEC acted as a net sink of atmospheric CO_2 with maximum values higher than 50 mmol m^{-2} d^{-1} during the intense summer bloom and with a mean CO_2 sink of 6.9 mmol m^{-2} d^{-1} from late April to September 2012 (at 49.90°N). This extreme CO_2 sink was brief and lasted less than a few days. Only a VOS regularly crossing the WEC would be able to catch the spatial and temporal expansion of this event. At the same time, in the sWEC, surface seawater pCO_2 remained close to, but over, the atmospheric equilibrium and this province acted mainly as a source of CO_2 to the atmosphere with a mean air-sea CO_2 flux value of 0.9 mmol m^{-2} d^{-1} from late April to September (at 48.90°N). By removing the thermal effect on pCO_2 (pCO_2@Tmean, Figure 21c), we observed that biological processes mainly controlled pCO_2 variability from April to September 2012 in the nWEC. In the sWEC the control of biological processes was less clear and during summer thermodynamic processes mostly controlled pCO_2 variability. These results were in agreement with the observations made in section 3.3, which indicated that in spring-summer 2012 intense and successive phytoplankton blooms were recorded in the nWEC, whereas biological activity was weak in the sWEC. Remineralization processes started earlier in the sWEC (Figure 20d) than in the nWEC resulting in increasing surface water pCO_2 (Figure 21b) and decreasing DO% below 100% (Figure 19e). In October and November 2012 when organic matter remineralization was at its highest level, pCO_2 and air-sea CO_2 fluxes were homogeneous across the WEC. From the hydrographical properties of the water column (Figure 21a) it clearly appears that the division of the WEC into two main provinces strongly influenced the spatio-temporal distribution of pCO_2 and air-sea CO_2 fluxes.

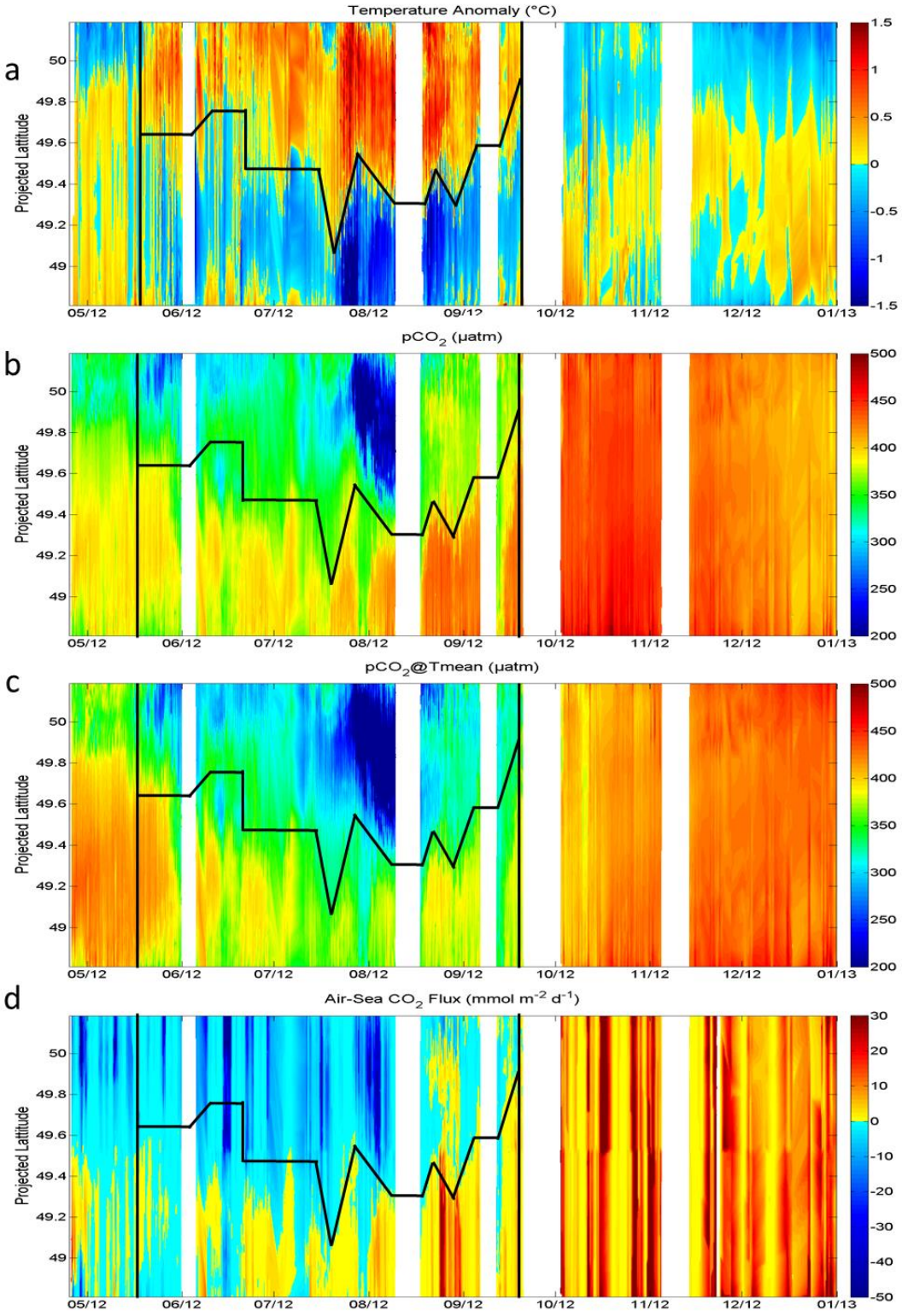


Figure 21: From the 25th April 2012 to the 1st January 2013, surface distributions of (a) temperature anomaly (°C), (b) pCO_2 (µatm), (c) pCO_2 normalized at the mean temperature of 13°C (pCO_2@13°C) from Takahashi et al. (1993) (µatm) and (d) air-sea CO_2 fluxes (mmol m^{-2} d^{-1}) from the algorithm of Nightingale et al. (2000) between Roscoff and Plymouth in the WEC. Negative fluxes indicate a transfer from the atmosphere into the ocean. The black lines represent an estimate of the location of the thermal front; the vertical black lines approximately delimit the period when stratification occurred in the northern WEC.

To better understand how tidal cycles and phytoplankton blooms impacted air-sea CO_2 fluxes, we extracted high-frequency FerryBox and ancillary data at 48.90°N (well-mixed, sWEC) and at 49.90°N (seasonally stratified, nWEC) from the 3rd of July to the 10th of August (Figure 22).

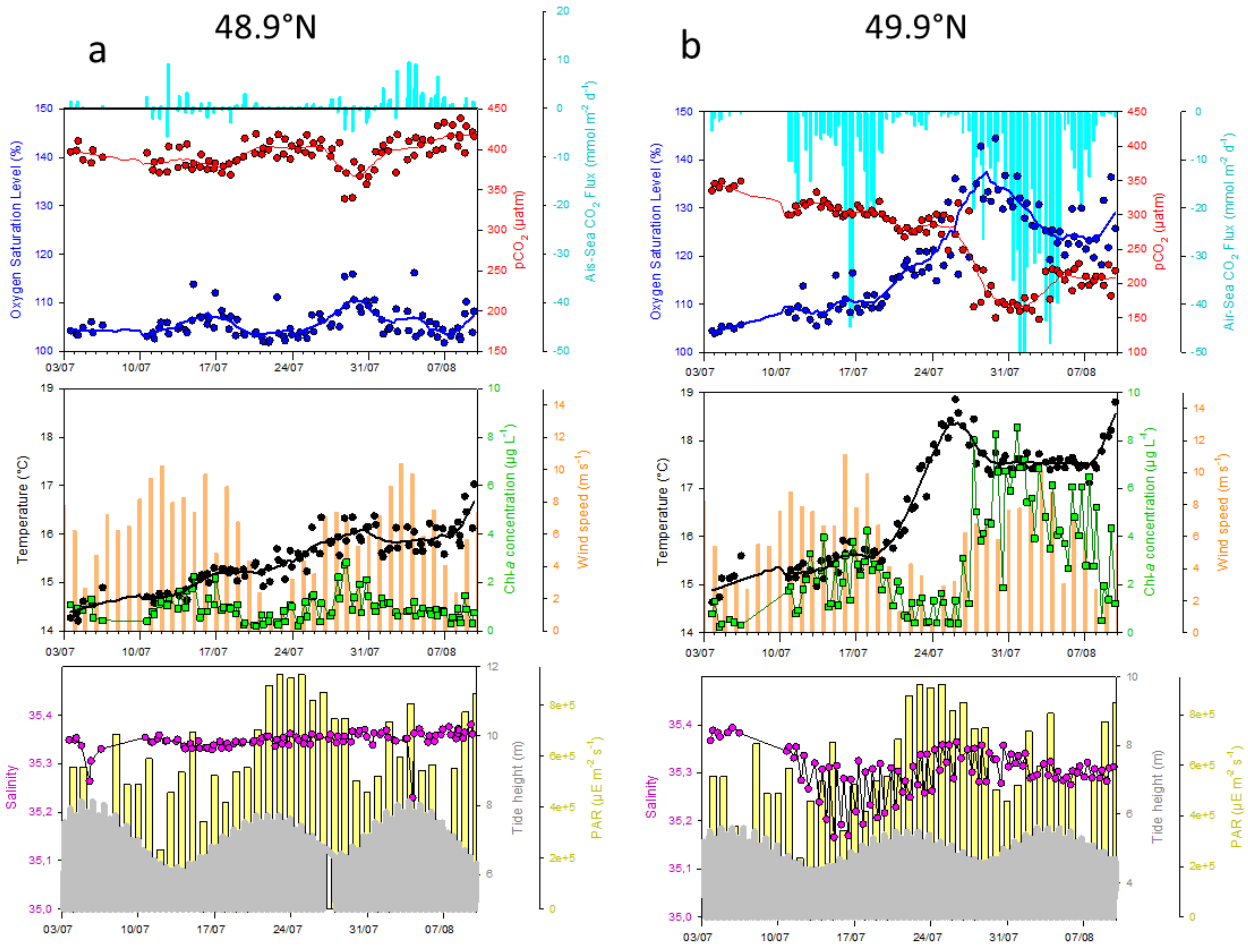


Figure 22: Extraction of high-frequency FerryBox and ancillary data from the 3rd July to the 10th August at 48.90°N (southern WEC, a) and 49.90°N (northern WEC, b). From the top to the bottom: variations of DO% (blue), pCO_2 (µatm, red) and air-sea CO_2 fluxes (mmol m^{-2} d^{-1}, cyan); variations of SST (°C, black), Chl-*a* concentrations (µg L^{-1}, green) and wind speeds (m s^{-1}, orange); variations of salinity (purple), tide height (m, grey) and daily-integrated photosynthetically active radiation (PAR, µE m^{-2} s^{-1}, yellow).

At 48.9°N (Figure 22a), the temperature increased continuously, starting around 14.5°C and reaching 17°C in August. During this month DO% remained around 105% and pCO_2 values ranged between 350 µatm and 450 µatm. Chl-*a* concentration remained low (around 1 µg L^{-1}) except during the two neap tides when we observed values higher than 2 µg L^{-1}. During the neap tides the tidal streams were weaker and thus favored phytoplankton development in the more stable euphotic zone. At the same time the highest values of DO%

(around 115%) and lowest values of pCO_2 (around 350 µatm) were recorded. The difference between the highest pCO_2 values during spring tide and the lowest pCO_2 values during neap tide was approximately 50 µatm. In July, CO_2 emission was therefore generally higher at spring tide with values ranging from 2 to 10 mmol m^{-2} d^{-1} depending on wind speed whereas a drawdown of CO_2 of -5 mmol m^{-2} d^{-1} was observed at neap tide when surface waters were undersaturated in CO_2 compared to the atmosphere. In the sWEC the tidal cycle (neap tide/spring tide) was therefore the main factor controlling phytoplankton abundance, DO% and pCO_2 variability. sWEC waters remained a source of CO_2 to the atmosphere during this period because pCO_2 was mostly driven by higher temperature in summer in the absence of significant biological activity.

At 49.9°N (Figure 22b), in the seasonally stratified nWEC, the variability of biogeochemical parameters was more contrasted. From the 3rd of July to the 10th of August surface seawater pCO_2 remained under the atmospheric equilibrium and ranged between 350 µtm and 150 µatm with DO% ranging between 105% and 140%. During this month pCO_2 and DO% signals showed opposite dynamics. From early July to mid-July, a first phytoplankton bloom was observed with Chl-*a* concentration higher than 3 µg L^{-1} and SST around 15.5°C. During this period DO% increased progressively to reach values of 110% and pCO_2 simultaneously decreased to 300 µatm. At the same time nutrients concentrations were low or totally depleted (Figure 20) in the nWEC. Salinity decreased in mid-July in the upper nWEC (Figure 19b and Figure 22b) and might have been linked to nutrient inputs into the system from freshwater discharge. SST then increased abruptly due to intense incident solar radiation and low wind speed, which rapidly warmed the surface layer (Figure 22b). From Chl-*a* concentration, no surface phytoplankton bloom was observed during the heating of surface water when photosynthetically active radiation (PAR) values were the highest. However, DO% started to increase significantly during surface water warming, suggesting the biological activity. After this abrupt SST increase, an intense phytoplankton bloom was recorded during 10 days with maximum Chl-*a* concentrations higher than 8 µg L^{-1}. The lowest pCO_2 and highest DO% values were observed during this bloom in late-July and early-August and the maximum CO_2 sink occurred with values higher than 40 mmol m^{-2} d^{-1}. In the nWEC, tidal cycles did not seem to have any impact on phytoplankton blooms, in contrast to the sWEC. The contrast between nWEC and sWEC air-sea CO_2 fluxes was highly apparent during this month and during the productive period with mean values of -6.9 mmol m^{-2} d^{-1} and 0.9 mmol m^{-2} d^{-1}, respectively. The CO_2 sink recorded from the 27th July to the 7th August had a major

impact on the air-sea CO_2 fluxes in the nWEC and accounted for 29% of the CO_2 sink during the productive period (at 49.90°N). Without high-frequency crossing of the VOS, such an event would not have been captured, which would lead to an important underestimation of the CO_2 sink during the productive period in the nWEC.

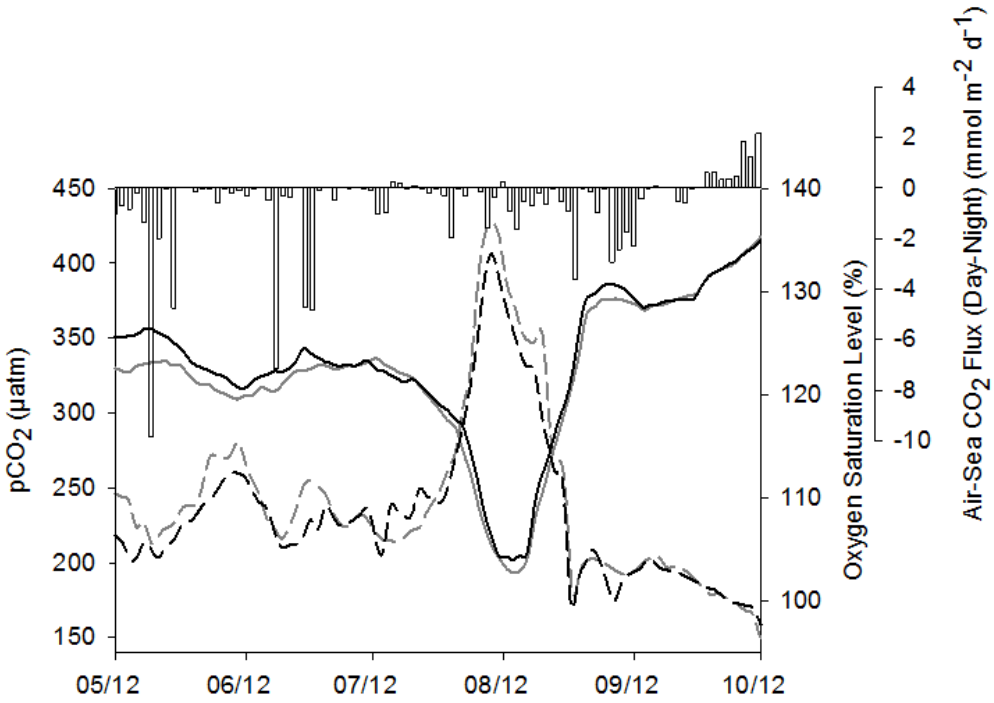


Figure 23: Variations of mean daily (grey) and nightly (black) DO% values (dashed lines) and pCO_2 (µatm) (solid lines) from the 25th April 2012 to the 1st October 2012 at 49.90°N. The bars represent the difference between daily and nightly computed air-sea CO_2 fluxes (mmol m^{-2} d^{-1}) averaged every 3 days.

Figure 23 shows the variation of mean daily and nightly DO% and pCO_2 over five months at 49.90°N and the difference between daily and nightly air-sea CO_2 flux during this period. We plotted pCO_2 to relate its variability directly to diurnal air-sea CO_2 fluxes. It should be noted that pCO_2@Tmean, which is usually plotted versus DO% to evaluate the impact of the diel biological cycle, showed similar variations as pCO_2. Mean DO% during daytime was usually higher than nightly DO% with a maximum difference higher than 6%. An opposite trend was observed for pCO_2 (and pCO_2@Tmean, not shown) with daily values lower than nighttime values with a maximum difference around -30 µatm. Mean DO% and pCO_2 differences between day and night were 2% and -10 µatm from the 25th of April to the 1st of September, respectively. DO% accuracy was 1.2% (at 14°C and at a salinity of 35.3) considering the 3.3 µmol L^{-1} standard deviation of the Optode (section 3.1.), meaning the observed DO% mean difference of 2% was significant. pCO_2 data from the HydroC/CO_2 FT

sensor had a standard deviation of 5.2 µatm between discrete and sensor values, therefore the mean day-night difference of -10 µatm was significant. Differences were significant during the productive season (with a range of -1% to 6% for DO% and of -30 to 5 µatm for pCO_2) and allowed us to estimate the impact of the diel biological cycle. During daytime, biological production in surface waters released DO and consumed CO_2, whereas during nighttime respiration was dominant and was responsible for the lower DO% and higher pCO_2 (and pCO_2@Tmean) values recorded. In order to assess the impact of diurnal cycles on air-sea CO_2 exchanges we computed the difference between daytime and nighttime air-sea CO_2 fluxes. From late April to September the mean day-night air-sea CO_2 flux difference was -0.9 mmol m^{-2} d^{-1} with a minimum value of -10.5 mmol m^{-2} d^{-1}. This mean day-night difference accounted for 16% of the mean CO_2 sink during this period and thus was significant for air-sea CO_2 flux computation. These day-night means were calculated from data extracted at 49.90°N and the time of extraction was not always concomitant to the daytime minimum and nighttime maximum pCO_2 values during the diel cycle. These values represent a first estimate of the potential impact of diurnal cycle on air-sea CO_2 fluxes but might be underestimated. Previous studies that specifically investigated the diurnal variability of pCO_2 in a coastal ecosystem based on continuous mooring pCO_2 data reported similar diurnal dynamics. Bozec et al. (2011) reported that monthly air-sea CO_2 flux estimates in the Bay of Brest (France) would be 8 to 36% lower if pCO_2 measurements were made only during the daytime and would be 8 to 37% higher if pCO_2 measurements were made only at nighttime during the productive season. In the nWEC, at Station L4 (50°15.00N; 4°13.02W, Figure 1), Litt et al. (2010) reported pCO_2 variation of 40 µatm between daytime minimum and nighttime maximum over 20h at a fixed station. Although our high-frequency pCO_2 FerryBox measurements did not cover an entire diel cycle, diurnal biological cycles were observed and our results confirm the necessity to take into account this variability for air-sea CO_2 flux estimates. The high frequency of crossing between Roscoff and Plymouth was an important advantage of this VOS line and allowed us to estimate the potential impact of the biological diel cycle on the air-sea CO_2 fluxes in the WEC.

4. Concluding remarks and perspectives

During the two years of deployment of our FerryBox, we obtained high-frequency data with sufficient precision to investigate the dynamics of biogeochemical processes related to air-sea CO_2 fluxes in the WEC. The SST anomaly was a suitable proxy for precise location of the position of the thermal front, which divided the WEC into two contrasted hydrographical provinces: the seasonally stratified northern WEC and the all-year well-mixed southern WEC. Based on a high-frequency dataset we assessed for the first time the dynamics of phytoplankton blooms and associated biogeochemical processes, which allowed us to develop a better understanding of the spatial and the temporal variability of these events in two contrasted provinces and over two contrasted years. In the sWEC, light availability seemed to be the main factor controlling phytoplankton blooms before total nutrient depletion, whereas tidal cycles (neap/spring tides) appeared to have an influence on phytoplankton abundance. In the nWEC, nutrients (mainly NO_3^-) were totally depleted in both years and were the main limiting factor for phytoplankton blooms. Air-sea CO_2 fluxes were also highly related to the hydrographical properties of the WEC between late April and early September 2012: the sWEC was a weak source of CO_2 to the atmosphere of 0.9 mmol m^{-2} d^{-1}, whereas the seasonally stratified nWEC acted as a sink for atmospheric CO_2 of 6.9 mmol m^{-2} d^{-1}. The necessity to obtain high-frequency observations in coastal ecosystems (as recommended by Borges et al. (2010)) was highlighted in our study by the intense and short (less than 10 days) summer bloom in the nWEC, which contributed to 29% of the CO_2 sink during the productive period. Furthermore, an extraction of day/night data at 49.90°N showed that the mean day/night pCO_2 difference, linked to the diel biological cycle, accounted for 16% of the mean CO_2 sink during the 5 month study period.

Petersen et al. (2011) showed that since FerryBoxes only provide sea surface measurements, a coupling with fixed station profiles can add a new dimension to the VOS routes. Many coastal fixed stations are operated by research institutes to measure common biogeochemical parameters, which could be coupled with FerryBox data to further investigate the pCO_2 dynamics in coastal ecosystems. The two years of deployment of our FerryBox showed that these new instruments are essential tools for future studies of the variability of biogeochemical parameters from diurnal to inter-annual time-scales in dynamic coastal ecosystems such as the WEC. Long-term deployments of FerryBoxes are challenging in terms

of maintenance and long term funding, but critical to assess anthropogenic forcings (e.g. ocean acidification, eutrophication) on coastal ecosystems in the context of climate change.

References

Boalch, G.T., Harbour, D.S., Butler, E.I., 1978. Seasonal phytoplankton production in the Western English Channel 1964–1974. J. Mar. Biol. Assoc. UK. 58, 943–953.

Borges, A.V., Alin, S.R., Chavez, F.P., Vlahos, P., Johnson, K.S., Holt, J.T., Balch, W.M., Bates, N., Brainard, R., Cai, W.J., 2010. A global sea surface carbon observing system: inorganic and organic carbon dynamics in coastal oceans. Proceedings of OceanObs'09: Sustained Ocean Observations and Information for Society (Vol. 2), Venice, Italy, 21-25 September 2009, Hall, J., Harrison, D.E. & Stammer, D., Eds., ESA Publication WPP-306.

Borges, A.V., Frankignoulle, M., 2003. Distribution of surface carbon dioxide and air-sea exchange in the English Channel and adjacent areas. J. Geophys Res. 108.

Bozec, Y., Merlivat, L., Baudoux, A.-C., Beaumont, L., Blain, S., Bucciarelli, E., Danguy, T., Grossteffan, E., Guillot, A., Guillou, J., 2011. Diurnal to inter-annual dynamics of pCO_2 recorded by a CARIOCA sensor in a temperate coastal ecosystem (2003–2009). Mar. Chem. 126, 13–26.

Bozec, Y., Cariou, T., Macé, E., Morin, P., Thuillier, D., Vernet, M., 2012. Seasonal dynamics of air-sea CO_2 fluxes in the inner and outer Loire estuary (NW Europe). Estuarine Coastal Shelf Sci. 100, 58-71.

DOE, 1994. Handbook of methods for the analysis of the various parameters of the carbon dioxide system in sea water, version 2.

Dickson, A.G. and Millero, F.J., 1987. A comparison of the equilibrium constants for the dissociation of carbonic acid in seawater media. Deep Sea Res. A - Oceanographic Research Papers 34, 1733-1743.

Dickson, A.G., Sabine, C.L. and Christian, J.R. (Eds.), 2007. Guide to best practices for ocean CO_2 measurements. PICES Special Publication 3, 191 pp.

Dumousseaud, C., Achterberg, E.P., Tyrrell, T., Charalampopoulou, A., Schuster, U., Hartman, M., Hydes, D.J., 2010. Contrasting effects of temperature and winter mixing on the seasonal and inter-annual variability of the carbonate system in the Northeast Atlantic Ocean. Biogeosciences 7, 1481–1492.

Edmond, J., 1970. High Precision Determination of Titration Alkalinity and Total Carbon Dioxide Content of Sea Water by Potentiometric Titration. Deep Sea Res. and Oceanographic Abstracts 17, 737–750.

EPA, 1997a. In vitro determination of chlorophyll a and pheophytin a in marine and freshwater algae by fluorescence (Arar E.J. & Collins G.B.). Method 445.0, revision 1.2. US-Environmental Protection Agency, Cincinnati, 26p.

Fiedler, B., Fietzek, P., Vieira, N., Silva, P., Bittig, H.C., Körtzinger, A., 2013. In Situ CO_2 and O_2 Measurements on a Profiling Float. J. of Atmos. Oceanic Technol. 30, 112–126.

Fietzek, P., Körtzinger, A., 2010. Optimization of a membrane-based NDIR sensor for dissolved carbon dioxide. Proceedings of OceanObs'09: Sustained Ocean Observations and Information for Society (Vol. 2), Venice, Italy, 21-25 September 2009, Hall, J., Harrison, D.E. & Stammer, D., Eds., ESA Publication WPP-306.

Goberville, E., Beaugrand, G., Sautour, B., Tréguer, P., Team, S., 2010. Climate-driven changes in coastal marine systems of western Europe. Mar. Ecol. Prog. Ser. 408, 129–148.

Guilloux, L., Rigault-Jalabert, F., Jouenne, F., Ristori, S., Viprey, M., Not, F., Vaulot, D., Simon, N., 2013. An annotated checklist of marine phytoplankton taxa at the SOMLIT-Astan time series off Roscoff (western Channel, France): data collected from 2000 to 2010. Cah. Biol. Mar. 54, 247-256.

Hill, A.E., Brown, J., Fernand, L., Holt, J., Horsburgh, K.J., Proctor, R., Raine, R., Turrell, W.R., 2008. Thermohaline circulation of shallow tidal seas. Geophys. Res. Lett. 35.

Hydes, D.J., Colijn, F., Petersen, W., Mills, F.S.D., Durand, D., NIVA, B.N., 2010. The way forward in developing and integrating FerryBox technologies. Proceedings of OceanObs 9.

Hydes, D.J., Hartman, M.C., Kaiser, J., Campbell, J.M., 2009. Measurement of dissolved oxygen using optodes in a FerryBox system. Estuarine Coastal Shelf Sci. 83, 485–490.

Kalnay, E., Kanamitsu, M., Kistler, R., Collins, W., Deaven, D., Gandin, L., Iredell, M., Saha, S., White, G., Woollen, J., Zhu, Y., Chelliah, M., Ebisuzaki, W., Higgins, W., Janowlak, J., Mo, K.C., Ropelewski, C., Wang, J., Leetmaa, A., Reynolds, R., Jenne, R., Joseph, D., 1996. The NCEP/NCAR reanalysis project. Bull. Amer. Meteor. Soc. 77, 437-471.

Kelly-Gerreyn, B.A., Hydes, D.J., Jégou, A.M., Lazure, P., Fernand, L.J., Puillat, I., Garcia-Soto, C., 2006. Low salinity intrusions in the western English Channel. Cont. Shelf Res. 26, 1241–1257.

Kitidis, V., Hardman-Mountford, N.J., Litt, E., Brown, I., Cummings, D., Hartman, S., Hydes, D., Fishwick, J.R., Harris, C., Martinez-Vicente, V., Woodward, E.M.S., Smyth, T.J., 2012. Seasonal dynamics of the carbonate system in the Western English Channel. Cont. Shelf Res. 42, 30–40.

L'Helguen, S., Madec, C., LeCorre, P., 1996. Nitrogen in permanently well-mixed temperate coastal waters. Estuarine Coastal Shelf Sci. 42, 803–818.

Litt, E.J., Hardman-Mountford, N.J., Blackford, J.C., Mitchelson-Jacob, G., Goodman, A., Moore, G.F., Cummings, D.G., Butenschon, M., 2010. Biological control of pCO_2 at station L4 in the Western English Channel over 3 years. J. Plankton Res. 32, 621–629.

Mehrbach, C., Culberso, Ch., Hawley, J.E. and Pytkowic, R.M., 1973. Measurement of apparent dissociation constants of carbonic acid in seawater at atmospheric pressure. Limnol. Oceanogr. 18, 897-907.

Nightingale, P.D., Malin, G., Law, C.S., Watson, A.J., Liss, P.S., Liddicoat, M.I., Boutin, J., Upstill-Goddard, R.C., 2000. In situ evaluation of air-sea gas exchange parameterizations using novel conservative and volatile tracers. Global Biogeochem. Cycles 14, 373–387.

Omar, A.M., Olsen, A., Johannessen, T., Hoppema, M., Thomas, H., Borges, A.V., 2010. Spatiotemporal variations of fCO_2 in the North Sea. Ocean Sci. 6, 77–89.

Padin, X.A., Vázquez-Rodríquez, M., Ríos, A.F., Pérez, F.F., 2007. Surface CO_2 measurements in the English Channel and Southern Bight of North Sea using voluntary observing ships. J. Mar. Syst. 66, 297–308.

Petersen, W., Schroeder, F., Bockelmann, F.-D., 2011. FerryBox - Application of continuous water quality observations along transects in the North Sea. Ocean Dynamics 61, 1541–1554.

Pierrot, D., Lewis, E., and Wallace, D. W. R., 2006. MS Excel Program Developed for CO_2 System Calculations., ORNL/CDIAC-105. Carbon Dioxide Information Analysis Center, Oak Ridge National Laboratory, U.S. Department of Energy, Oak Ridge, Tennessee.

Pingree, R., Griffiths, D., 1978. Tidal Fronts on Shelf Seas Around British-Isles. J. Geophys. Res., C: Oceans and Atmos. 83, 4615–4622.

Reid, P. C., Auger, C., Chaussepied, M., and Burn, M. (Eds.), The channel, report on sub-region 9, quality status report of the North Sea 1993, 153 pp., UK Dep. of the Environ., Républ. Fr. Minist. de l'Environ., Inst. Fr. de Rech. Pour l'Exploit. de la Mer, Brest, 1993.

Saderne, V., Fietzek, P., Herman, P.M.J., 2013. Extreme Variations of pCO_2 and pH in a Macrophyte Meadow of the Baltic Sea in Summer: Evidence of the Effect of Photosynthesis and Local Upwelling. PLoS One 8, e62689.

Schneider, B., Kaitala, S., Maunula, P., 2006. Identification and quantification of plankton

bloom events in the Baltic Sea by continuous pCO_2 and chlorophyll a measurements on a cargo ship. J. Mar. Syst. 59, 238–248.

Smyth, T.J., Fishwick, J.R., AL-Moosawi, L., Cummings, D.G., Harris, C., Kitidis, V., Rees, A., Martinez-Vicente, V., Woodward, E.M.S., 2009. A broad spatio-temporal view of the Western English Channel observatory. J. Plankton Res. 32, 585–601.

Southward, A.J., Langmead, O., Hardman-Mountford, N.J., Aiken, J., Boalch, G.T., Dando, P.R., Genner, M.J., Joint, I., Kendall, M.A., Halliday, N.C., Harris, R.P., Leaper, R., Mieszkowska, N., Pingree, R.D., Richardson, A.J., Sims, D.W., Smith, T., Walne, A.W., Hawkins, S.J., 2005. Long-term oceanographic and ecological research in the western English Channel, in: Southward, A.J., Tyler, P.A., Young, C.M., Fuiman, L.A. (Eds.), Adv. Mar. Biol. 47, 1–105.

Takahashi, T., Olafsson, J., Goddard, J.G., Chipman, D.W. and Sutherland, S.C., 1993. Seasonal variation of CO_2 and nutrients in the high-latitude surface ocean – A comparative study. Global Biogeochem. Cycles 7, 843-878.

Wafar, M.V.M., Le Corre, P., Birrien, J.L.,1983. Nutrients and primary production in permanently well-mixed temperate coastal waters. Estuarine Coastal Shelf Sci. 17, 431:446.

Walsh, J.J., 1991. Importance of continental margins in the marine biogeochemical cycling of carbon and nitrogen. Nature 350, 53-55.

Weiss, R.F., 1970. Solubility of nitrogen, oxygen and argon in water and seawater. Deep Sea Res. 17, 721-735.

Weiss, R.F., and Price, B.A., 1980. Nitrous oxide solubility in water and seawater. Mar. Chem. 8, 347-359.

Xing, X., Claustre, H., Blain, S., D'Ortenzio, F., Antoine, D., Ras, J., Guinet, C., 2012. Quenching correction for in vivo chlorophyll fluorescence acquired by autonomous platforms: A case study with instrumented elephant seals in the Kerguelen region (Southern Ocean). Limnol. Oceanogr.: Methods 10, 483–495.

Zeebe R. E. and Wolf-Gladrow, D. A., 2001. CO_2 in seawater: equilibrium, kinetics, isotopes, Elsevier Oceanography Series 65, Amsterdam, 346 pp.

Chapter 4: Dynamics of air-sea CO_2 fluxes in the north-west European shelf based on Voluntary Observing Ship (VOS) and satellite observations.

This chapter is based on an article to be submitted to Biogeoscience Discussion in November 2014: "Dynamics of air-sea CO_2 fluxes in the north-west European shelf based on Voluntary Observing Ship (VOS) and satellite observations."

P. Marrec, T. Cariou, E. Macé, P. Morin, K. Paxman, L. A. Salt, M. Vernet and Y. Bozec.

Abstract

From January 2011 to December 2013, we constructed a comprehensive pCO_2 dataset based on voluntary observing ship (VOS) measurements in the Western English Channel (WEC). We subsequently estimated surface pCO_2 and air-sea CO_2 fluxes in north-west European continental shelf waters using multiple linear regressions (MLRs) from remotely sensed sea surface temperature (SST), chlorophyll-*a* concentration (Chl-*a*), the gas transfer velocity coefficient (K), photosynthetically active radiation (PAR) and modeled mixed layer depth (MLD). We developed specific MLRs for the seasonally stratified northern WEC (nWEC) and the permanently well-mixed southern WEC (sWEC) and calculated surface pCO_2 with relative uncertainties of 17 µatm and 16 µatm, respectively. We extrapolated the relationships obtained for the WEC based on the 2011-2013 dataset 1) temporally over a decade and 2) spatially in the adjacent Celtic and Irish Seas (CS and IS), two regions which exhibit hydrographical and biogeochemical characteristics similar to those of WEC waters. We validated these extrapolations with pCO_2 data from the SOCAT database and obtained relatively robust results with an average precision of 4 ± 22 µatm in the seasonally stratified nWEC and the southern and northern CS (sCS and nCS), but less promising results in the permanently well-mixed sWEC, IS and Cap Lizard (CL) waters. On an annual scale, seasonally stratified systems acted as a sink of CO_2 from the atmosphere of -0.4, -0.9 and -0.4 mol C m^{-2} $year^{-1}$ in the nCS, sCS and nWEC, respectively, whereas, permanently well-mixed systems acted as source of CO_2 to the atmosphere of 0.2, 0.4 and 0.4 mol C m^{-2} $year^{-1}$ in the sWEC, CL and IS, respectively. We scaled these mean annual fluxes over six provinces and obtained an annual average uptake of -1.0 Tg C $year^{-1}$ over the decade. Air-sea CO_2 fluxes showed important inter-annual variability resulting in significant differences in the intensity and/or direction of annual fluxes, with biological activity, SST and wind speed as the main drivers. From 2003 to 2013, we observed a pCO_2 increase of 2.6 ± 0.5 µatm $year^{-1}$ in our study area, higher than the atmospheric increase of 1.9 µatm yr^{-1}, concomitant with a SST cooling of -0.07°C $year^{-1}$. We hypothesize that changes in seawater carbonate chemistry might be responsible for this observed pCO_2 increase. For the first time, we estimated the seasonal and long-term dynamics of pCO_2 and associated air-sea CO_2 fluxes over this part of the north-western European continental shelf.

1. Introduction

Continental shelf seas, as an interface between land, ocean and atmosphere, host a multitude of biogeochemical processes (Walsh 1991; Liu et al., 2010) and play a key role in the global carbon cycle (Walsh et al. 1981; Muller-Karger et al., 2005; Bauer et al., 2013). Even though marginal seas occupy only 7% of global oceanic area, they host enhanced biological activity, which accounts for 15% to 30% of global oceanic primary production (Gattuso et al., 1998). These productive regions are characterized by enhanced air-sea CO_2 fluxes compared to open oceans (Tsunogai et al., 1999; Thomas et al., 2004) and are particularly vulnerable to anthropogenic forcings such as eutrophication and ocean acidification (Borges and Gypsen, 2010; Borges et al., 2010a; Wallace et al., 2014). In a context of climate change, with rising anthropogenic CO_2 levels in the atmosphere and the oceans (IPCC, 2013), it is essential to better constrain carbon cycle dynamics and particularly air-sea CO_2 fluxes. Given the large diversity and heterogeneity of coastal ecosystems, this goal remains challenging. Rapid expansion of partial pressure of CO_2 (pCO_2) observations over the past decade have allowed the first assessments of the contribution of coastal ecosystems in terms of global air-sea CO_2 fluxes (Borges et al., 2005; Cai et al., 2006; Chen and Borges, 2009; Cai, 2011). However, extrapolation from local to global estimates still involves large uncertainties and many continental shelf seas remain under-sampled.

Accurate estimates of air-sea CO_2 fluxes in continental shelf seas still suffer from lack of sufficient spatial and temporal coverage. Surveys based on seasonal sampling during oceanographic campaigns and time-series at fixed locations are limited due to the large temporal and spatial variability of these systems. The use of voluntary observing ships (VOS) can improve the coverage of coastal areas at a lesser cost. The recent advances made in this field (Schneider et al., 2006, 2014; Padin et al., 2007; Omar et al., 2010; Marrec et al., 2014) can be combined with other new approaches. Since the 2000s, pCO_2 predictions based on remote sensing techniques have been successfully developed for open ocean areas (Lefèvre et al., 2002; Ono et al., 2004; Olsen et al., 2004; Rangama et al. 2005; Gleidhill et al., 2008; Padin et al., 2009; Chierici et al., 2009, 2012). These estimates were based on the use of multiple linear regressions (MLRs) to relate surface ocean pCO_2 to sea surface temperature (SST), chlorophyll-*a* concentration (Chl-*a*) and occasionally also mixed layer depth (MLD), sea surface salinity (SSS) or geographical position (latitude and longitude). More complex

neural networks and self-organizing map techniques have also given promising results (Lefèvre et al., 2005; Telszewski et al. 2009; Friedrich and Oschlies, 2009). In continental shelf seas the development of remotely-sensed approaches is more challenging because of higher temporal and spatial variability of biogeochemical processes. The complex optical properties of these systems can also impede computations based on satellite ocean-color data. These techniques have nevertheless been used to conduct successful assessments of pCO_2 variability in coastal areas (Lohrenz and Cai, 2006; Sallisbury et al., 2008; Borges et al., 2010b; Shadwick et al., 2010; Hales et al., 2012; Jo et al., 2012; Signorini et al., 2013).

To efficiently constrain surface pCO_2 in dynamic shelf seas from remotely sensed data, a comprehensive pCO_2 dataset with sufficient spatial and temporal resolution is essential. In addition to a robust intra-annual temporal resolution, acquisition of pCO_2 measurements over several years is necessary in order to take into consideration the important inter-annual variability of biogeochemical processes in coastal seas. From 2011 to 2013, we collected an extensive pCO_2 dataset based on VOS observations in the Western English Channel (WEC), which is part of the north-west European continental shelf. We used MLR to develop algorithms to predict surface pCO_2 and air-sea CO_2 fluxes from remotely sensed SST, chlorophyll-*a* concentrations (Chl-*a*), wind speeds (to calculate the gas transfer velocity coefficient K), photosynthetically active radiation (PAR) and from modeled mixed layer depth (MLD). We extrapolated the relationships obtained in the WEC based on the 2011-2013 dataset 1) temporally over a decade; and 2) spatially in the adjacent Celtic and Irish Seas (CS and IS), two regions where pCO_2 data are very sparse. Based on the reconstructed decadal dataset, we investigated the inter and multi-annual variability of pCO_2 and air-sea CO_2 fluxes over the shelf.

2. Study area

The WEC is part of one of the world's largest margins, the North-West European continental shelf. We studied this area from January 2011 with a VOS (Fig. 23) equipped with an autonomous ocean observing system, called FerryBox, featuring several sensors (Sect. 3.1., Marrec et al., 2013; Marrec et al., 2014). This area is characterized by relatively shallow depths and by intense tidal streams with maximum speeds ranging from 0.5 to 2.5 m s^{-1}

(Pingree, 1980; Reid et al., 1993). Along the French coast (southern WEC (sWEC)), where the tidal currents are the strongest, the water column remains vertically mixed (Wafar et al., 1983; L'Helguen et al., 1996), whereas near the English coast (northern WEC (nWEC)), where tidal streams are less intense, seasonal stratification occurs (Smyth et al., 2010). Between these two distinct structures, a frontal zone oscillates, separating well-mixed and stratified waters (Pingree et al., 1975). In this complex hydrographical context, high-frequency measurements from FerryBox data allowed us to precisely locate this thermal front and to accurately identify the real extent of each hydrographical province (Marrec et al, 2014).

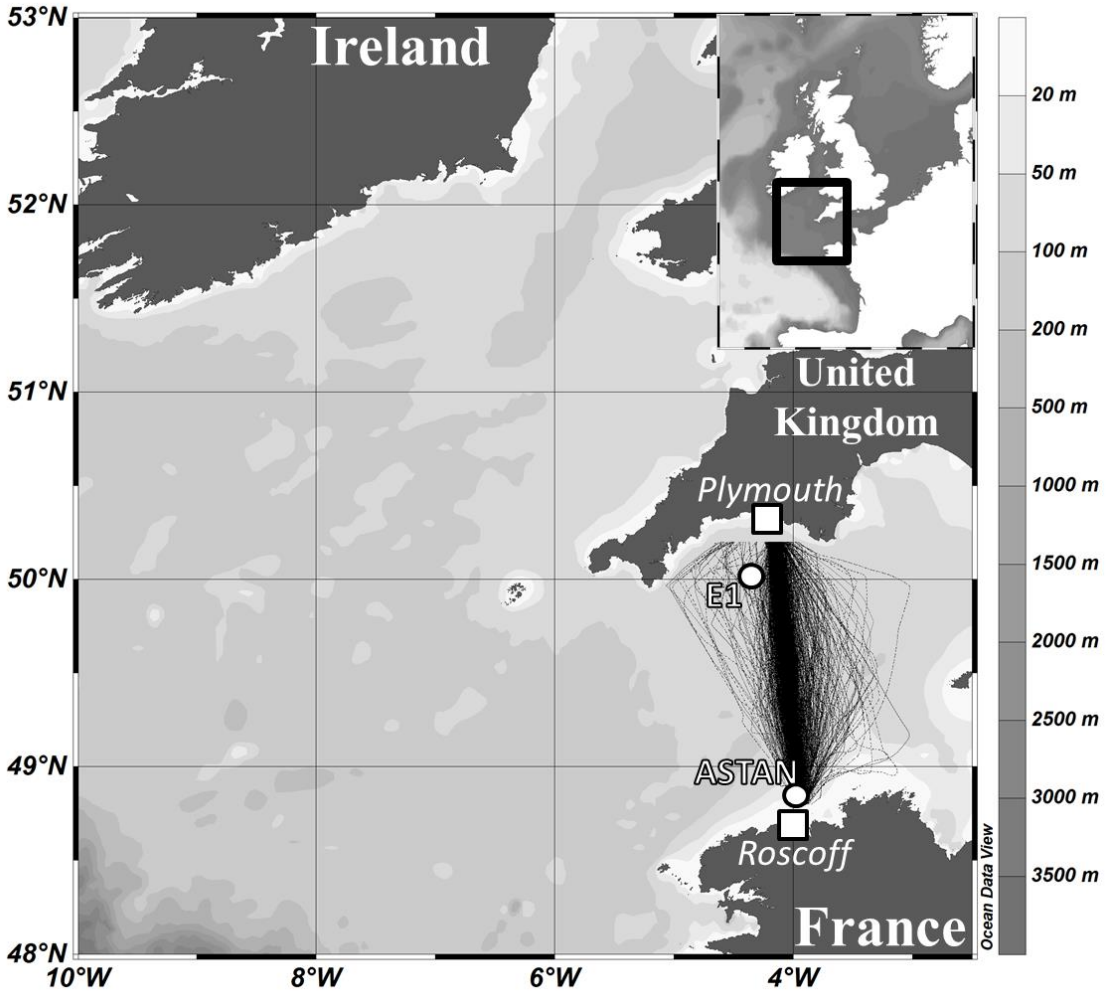


Figure 24: Map and bathymetry of the study area with the tracks of all crossings made from 2011 to 2013 by the ferry *Armorique* between Roscoff (France and Plymouth (UK). The location of fixed stations E1 (Western Channel Observatory) and ASTAN (coastal observatory SOMLIT) are also indicated.

Satellite SST data (Fig. 25, Sect. 3.2.) combined with Ferrybox measurements allowed us to further define the different hydrographical provinces of the north-west European continental shelf. Water column characteristics similar to those in the WEC are also observed in adjacent seas, i.e. the Irish Sea (IS) and the Celtic Sea (CS) (Pingree et Griffiths, 1978; Pingree, 1980; Holligan, 1981; Simpson, 1981; Hill et al., 2008). Figure 25 shows averaged July and August SST from 2003 to 2013 between 48°N and 53°N and 3.5°W and 10°W. The coolest surface waters indicate areas where the water column is well-mixed and the warmest SST, areas with seasonal stratification. The Ushant front (Pingree et al., 1975; Morin, 1984, Sournia et al., 1990) separates the seasonally stratified southern Celtic Sea (sCS) and nWEC from the permanently well-mixed sWEC. Such a frontal structure is also observed off the Penwith Peninsula (in the west of Cornwall, UK), around the Cap Lizard (CL) and thereafter we refer to these well-mixed waters as CL. The St. Georges Channel front separates permanently well-mixed southern IS (sIS) waters from the seasonally stratified northern CS (nCS) waters. In addition to the similar hydrographical properties, the WEC, CS and IS also exhibited similar seasonal dynamics and biogeochemical processes (Pingree et al., 1978; Pemberton et al., 2004; Smyth et al., 2010). Based on these observations, we defined five key hydrographical provinces (Fig. 25).

We then developed algorithms for both seasonally stratified and permanently well-mixed systems in the WEC (Sect. 3.3.) to estimate surface pCO_2 from environmental variables, and we applied these algorithms in adjacent CS and IS based on satellite and modeled data (Sect. 4.2. and 4.3.). We did not include coastal areas strongly influenced by riverine inputs (Fig. 25) such as the Bristol Channel, coastal Irish waters, surface waters in vicinity of Plymouth and the eastern part of the sIS (which is also seasonally stratified). We chose to study only the southern part of the IS because of the complexity of the northern IS, which has successive stratified, frontal and mixed systems (Simpson and Hunter, 1974) and is influenced by freshwater inputs (Gowen et al., 1995). The study of this permanently well-mixed system allowed us to apply our algorithm developed for the sWEC to estimate for the first time air-sea CO_2 fluxes in the IS. In the south-west corner of our study area, at the shelf break, internal tides and turbulence favor vertical mixing which sustains biological activity by supplying nutrients to the photic zone (Pingree et al., 1981; Joint et al., 2001; Sharples et al., 2007). Because the internal tides at the shelf break induce specific biogeochemical properties and our algorithms are not intended to predict surface pCO_2 in this province, we excluded the shelf break region (Fig. 24) from our study area.

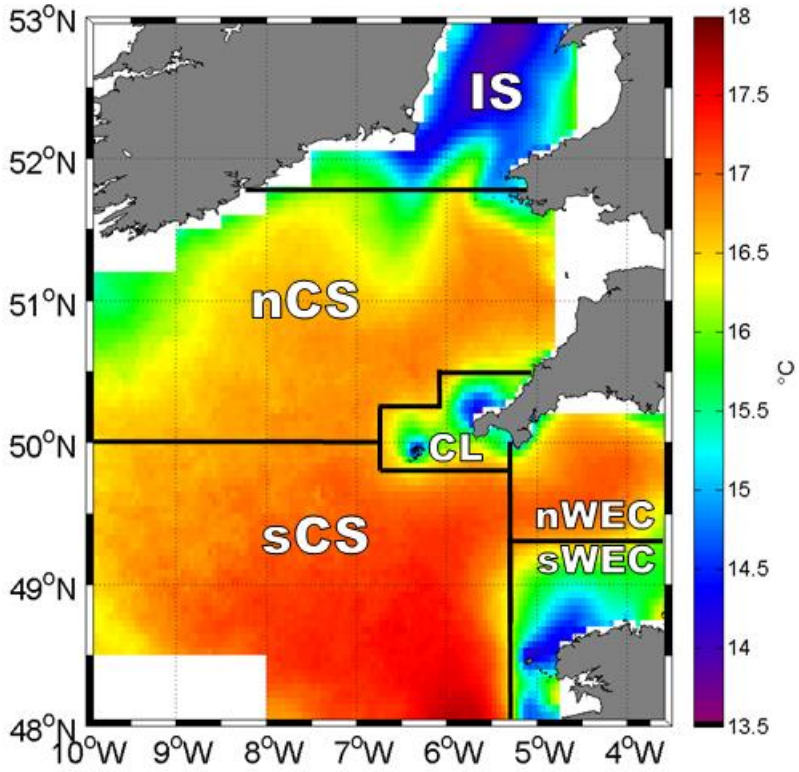


Figure 25: Mean July and August satellite SST (°C) between 2003 and 2013 with delimitation of defined hydrographical provinces: Irish Sea (IS), northern Celtic Sea (nCS), southern CS (sCS), Cap Lizard province (CL), northern Western English Channel (nWEC) and southern WEC (sWEC). The warmest SST are characteristic of seasonally stratified areas and the coldest of permanently well-mixed systems.

3. Material and Methods

3.1 FerryBox datasets

From January 2011 to January 2014, a FerryBox system was installed on the Voluntary Observing Ship (VOS) *Armorique* (Brittany Ferries). This vessel crossed the English Channel between Roscoff (France, 48°43'38N 3°59'03E) and Plymouth (United Kingdom, 50°22'12N 4°08'31E) (Fig. 24) up to three times a day. The FerryBox continuously measured sea surface temperature (SST), salinity and partial pressure of CO_2 (pCO_2, from April 2012) along the ferry track with more than 600 crossings with pCO_2 acquisition. Between January 2011 and January 2014, discrete sampling was performed on 57 return crossings between Roscoff and Plymouth with a total of 1026 sampling locations in the WEC.

During each cruise, 18 water samples were taken from the FerryBox seawater circuit for the determination of dissolved inorganic carbon (DIC), total alkalinity (TA) and associated salinity and nutrient concentrations (Marrec et al, 2013). Seawater pCO_2 values were calculated from TA, DIC, temperature, salinity and nutrient concentrations with the CO2SYS program (Pierrot et al., 2006) using the equilibrium constants of CO_2 proposed by Mehrbach et al. (1973), refitted by Dickson and Millero (1987) on the seawater pH scale, as recommended by Dickson et al. (2007). The computed values of pCO_2 from DIC and TA have uncertainties of ±5.8 µatm (Zeebe and Wolf-Galdrow, 2001). Sensors were calibrated and/or adjusted based on these bimonthly discrete measurements (Marrec et al, 2014). Based on the comparison between high-frequency pCO_2 data obtained with a Contros HydroC/CO_2 FT sensor and bimonthly pCO_2 data calculated from DIC/TA, we estimated uncertainties relative to high-frequency pCO_2 measurements of ±5.2 µatm (Marrec et al., 2014). We built a composite monthly dataset of *in-situ* SST and pCO_2 data over 3 years based on both high-frequency and bimonthly measurements. We used bimonthly discrete pCO_2 data between January 2011 and April 2012 and high-frequency pCO_2 data from April 2012 to January 2014. SST monthly means were calculated from FerryBox high-frequency data.

3.2 Satellite and other environmental data

Satellite-derived Chl-*a* concentrations (µg L^{-1}) were acquired from the Moderate Resolution Imaging Spectroradiometer (MODIS) aboard the Aqua satellite. Daily images were provided by the Natural Environment Research Council (NERC) Earth Observation Data Acquisition and Analysis Service (NEODAAS) at a spatial resolution of 1.1 km. Monthly mean Chl-*a* estimates were computed from January 2003 to December 2013 from these individual images over our study area (Fig. 24). WEC, CS and IS waters are optically complex shelf waters (Joint and Groom, 2000; Darecki et al., 2003; McKee et al., 2007). These shelf seas present both Case 1 and Case 2 optical water types (Morel et Prieur, 1977; Morel et al., 2006) depending on their hydrographical properties (seasonally stratified or homogeneous), the proximity to the coast, and the period of the year. In Case 1 waters, the optical properties are dominated by chlorophyll and associated degradation products as in open ocean waters. In coastal waters, classified as Case 2, suspended particulate sediments and yellow substances of terrestrial origin induce important biases on chlorophyll-a

concentration estimates and special algorithms have been developed for these waters (Gohin et al., 2002). As shown by Groom et al. (2009), who explain how a coastal station in the nWEC (L4) can be considered as Case 1 or Case 2 depending on various parameters, it is difficult to label our studied provinces as Case 1 or Case 2 waters. However sWEC, CL and IS present more similarities with Case 2 waters, especially during winter, whereas nWEC and CS are closer to Case 1 waters. The NEODAAS provided satellite Chl-*a* estimates based on the OC3 algorithm, more specific to Case 1 waters, and on the OC5 algorithm (Gohin et al., 2002), developed in the riverine input affected coastal waters of the Eastern English Channel and the Bay of Biscay (Seine, Loire, Gironde). Chl-*a* estimates based on the OC3 algorithm show enhanced Chl-*a* concentrations during winter, particularly in near-coast and in well-mixed provinces, whereas Chl-*a* estimates from the OC5 algorithm tend to underestimate the Chl-*a* concentrations especially during spring and summer (data not shown). We chose to use the OC3 algorithm in this study, which seemed more suitable and more representative of the biological activity dynamics, and we binned monthly 1.1km satellite data into 0.05° x 0.05° grid cells over our study area. We extracted monthly mean Chl-*a* values along the ship track from January 2011 to December 2013 (Fig. 26b) to predict pCO_2 based on MLRs (see below).

Satellite-based SST (°C) data were acquired from the Advanced Very High Resolution Radiometer (AVHRR) instrument. Monthly mean SST estimates were computed from January 2003 to January 2014 from individual images with a spatial resolution of 1.1km by the NEODAAS. A validation between monthly *in-situ* SST and associated satellite SST showed a robust correlation (R^2=0.97, N=448, $p<0.001$ and RMSE=0.43). We gridded 1.1 km resolution satellite SST into 0.05° x 0.05° cells as with all other remotely sensed and modeled parameters.

Photosynthetically active radiation (PAR, in E m^{-2} d^{-1}) data were retrieved from the Ocean Biology Processing Group (McClain, 2009; http://oceancolor.gsfc.nasa.gov). We used the Level 3 monthly merged PAR product from MODIS Aqua. PAR were used as a variable in the MLRs as an indicator of the amount of light available for phytoplankton, which presented inter-annual variation over our study period (Fig. 26c). Based on the observations of L'Helguen et al. (1996), Marrec et al. (2014) suggested that light availability might be an important factor responsible for the strong inter-annual variability of phytoplankton blooms in the sWEC.

Mixed layer depth (MLD), which was one of the variables used in algorithm development for the seasonally stratified nWEC and in the spatial extrapolation of this algorithm in the adjacent CS, was computed from the MARS3D model (Lazure and Dumas, 2008; Berger et al., 2014) developed in the PREVIMER project (Charria et al., 2014). MLD was defined as the shallowest depth corresponding to a temperature or density difference with the surface water higher than $\delta T = 0.5$ °C or $\delta Dens = 0.125$ (Monterey and Levitus, 1997). We compared the model outputs with MLD calculated from the temperature and salinity profile at the fixed station E1 off Plymouth (50.03°N, 4.37°W, depth 75m) from January 2006 to January 2014. Measurements were undertaken fortnightly by the Western Channel Observatory (NERC National Capability of the Plymouth Marine Laboratory and Marine Biological Association, www.westernchannelobservatory.org.uk). Profiles were obtained by a Seabird SBE 19+ with precision for temperature and computed salinity of 0.005°C and 0.002, respectively. In-situ and modeled MLD at the E1 station showed a good correlation (R^2=0.82, N=89), validating use of modeled MLD in our computations. Modeled MLD were binned in the 0.05° x 0.05° grid in seasonally stratified provinces and were extracted along the ship track in the nWEC to be included in the pCO_2 algorithms. We chose to use the MLD over depth ratio (MLDr) in the MLR computation instead of MLD. During winter in seasonally stratified areas, the whole water column is mixed. However, depths are not homogeneous (ranging from -20 to -200 m), thus the use of MLD winter values, which corresponded approximately to the bathymetry, would lead to bias in MLR computation. MLD, in our algorithms, was only an indicator of the presence or absence of stratification of the water column, particularly concerning the start and the end of stratification. Figure 3e shows the monthly MLDr ratio in the nWEC between Roscoff and Plymouth.

Monthly wind speed data (m s^{-1}) corrected to 10 m height were obtained from the NCEP/NCAR re-analysis project (Kalnay et al., 1996) provided by the NOAA-ESRL Physical Sciences Division (Boulder, CO, USA, http://www.esrl.noaa.gov/psd/). We extracted the 2.5° latitude by 2.5° longitude global grid wind speed values over the study area and we binned these data into our 0.05°*0.05° grid. Wind speed data was used in the computation of the gas transfer velocity of CO_2 (K) used for the calculation of air-sea CO_2 fluxes (Sect. 3.5.) and in algorithm development (Sect. 3.3.) as an indicator of wind stress. Figure 3d shows the monthly computed K values used in the algorithm development along the Ferry route from 2011 to 2013.

3.3 Development of pCO_2 algorithms

We developed two specific algorithms to estimate surface seawater pCO_2 in each of the hydrographical provinces of the WEC (seasonally stratified nWEC and permanently well-mixed sWEC) in order to apply them on a larger spatial and temporal scale in the adjacent Celtic and Irish Seas. We used MLRs to predict pCO_2 in each province based on monthly mean values of Chl-*a*, SST, K, the gas transfer velocity (Sect. 3.5.), PAR, MLD (for the nWEC) and from a time variable TI (Eq. (21) and (22)) representative of the seasonality (Friedrich and Oschlies, 2009; Lefèvre et al., 2005; Signorini et al., 2013) according to:

$$pCO_{2,MLR} = a_0 + \sum_{i=1}^{n} a_i * p_i \qquad (21)$$

$$TI = \sin\left(\frac{2*\pi*(Day-\alpha)}{365}\right) \qquad (22)$$

where $pCO_{2,MLR}$ is the predicted pCO_2, a_0 is the intercept of the MLR and a_i is the coefficient related to each variable p_i. In Eq. (22), Day is the 15th day of each month (Julian day) and α a value between 0 and 365 chosen by iteration to optimize the seasonal phasing until the minimum standard deviation on residuals and the best correlation coefficient R^2 are obtained by the MLR. All of these parameters were binned in 0.05° latitude intervals (Fig. 26 and 28) between 48.80°N (off Roscoff) and 50.20°N (off Plymouth). The northern latitude limit of 50.20°N is relatively far from Plymouth in order to exclude effects of freshwater inputs from the Tamar and Plym rivers, which influence the biogeochemical properties of the area (Smyth et al., 2010) and are not representative of nWEC waters. The WEC is divided into sWEC and nWEC at 49.40°N from the average position of the thermal front separating the two hydrographical provinces during the period of study (Fig. 25, and Marrec et al. 2014). MLRs were applied on these binned monthly values in each province using the "*regress"* Matlab® function. The performance of regional algorithms was evaluated by the correlation coefficient R^2, the adjusted R^2, the root-mean-square error (RMSE) and the p-values (for each of the parameters and for the regression). The R^2, the adjusted R^2 and RMSE between observed and predicted data represent the capacity (the R^2 and the adjusted-R^2) and uncertainty (RMSE) of the algorithms to predict pCO_2. The coefficient of determination R^2 indicates the amount of

total variability explained by the regression mode. The adjusted-R^2 is the coefficient of determination of the MLR adjusted to the degree of freedom, which depends on the number of variables used. In each MLR presented in the study, the adjusted R^2 and R^2 were similar, thus only R^2 is presented.

MLR coefficients were calculated based on our three year dataset and the goal of the study is to apply the algorithms over a decade (2003-2013) over the study area (Fig. 24). The anthropogenic increase in atmospheric CO_2 increases surface ocean pCO_2 by approximately 1.7 µatm yr^{-1} (Thomas et al., 2008; Le Quéré et al., 2010), equivalent to 17 µatm over 10 years. When we computed the algorithms, we considered this factor in the computations by adding a correction term ΔX (Eq. (23)) on the right term of Eq. (21) (Shadwick et al., 2010; Signorini et al., 2013) with:

$$\Delta X = \frac{1.7}{12} * \Delta m \qquad (23)$$

where Δm (month) is equal to the number of months since July 2012, the middle of our study period (2011-2013). For example, in January 2013, ΔX would be equal to (1.7/12)*(+6) and in January 2012 ΔX would be (1.7/12)*(-6). The same reference month (i.e. July 2012) was used to extrapolate the algorithms from January 2003.

We normalized each of the variables p_i (Eq. (24)) using the mean ($p_{i,m}$) and the standard deviation ($p_{i,StdDev}$) of p_i over study period. The normalized coefficients, which are directly comparable and dimensionless, allowed us to evaluate the relative contribution, or weight, of each of the independent variables (i.e. SST, Chl-*a*, TI, K, PAR and MLD) in the prediction of the dependent variable (i.e. $pCO_{2,MLR}$).

$$p_{i,s} = \frac{(p_i - p_{i,m})}{p_{i,StdDev}} \qquad (24)$$

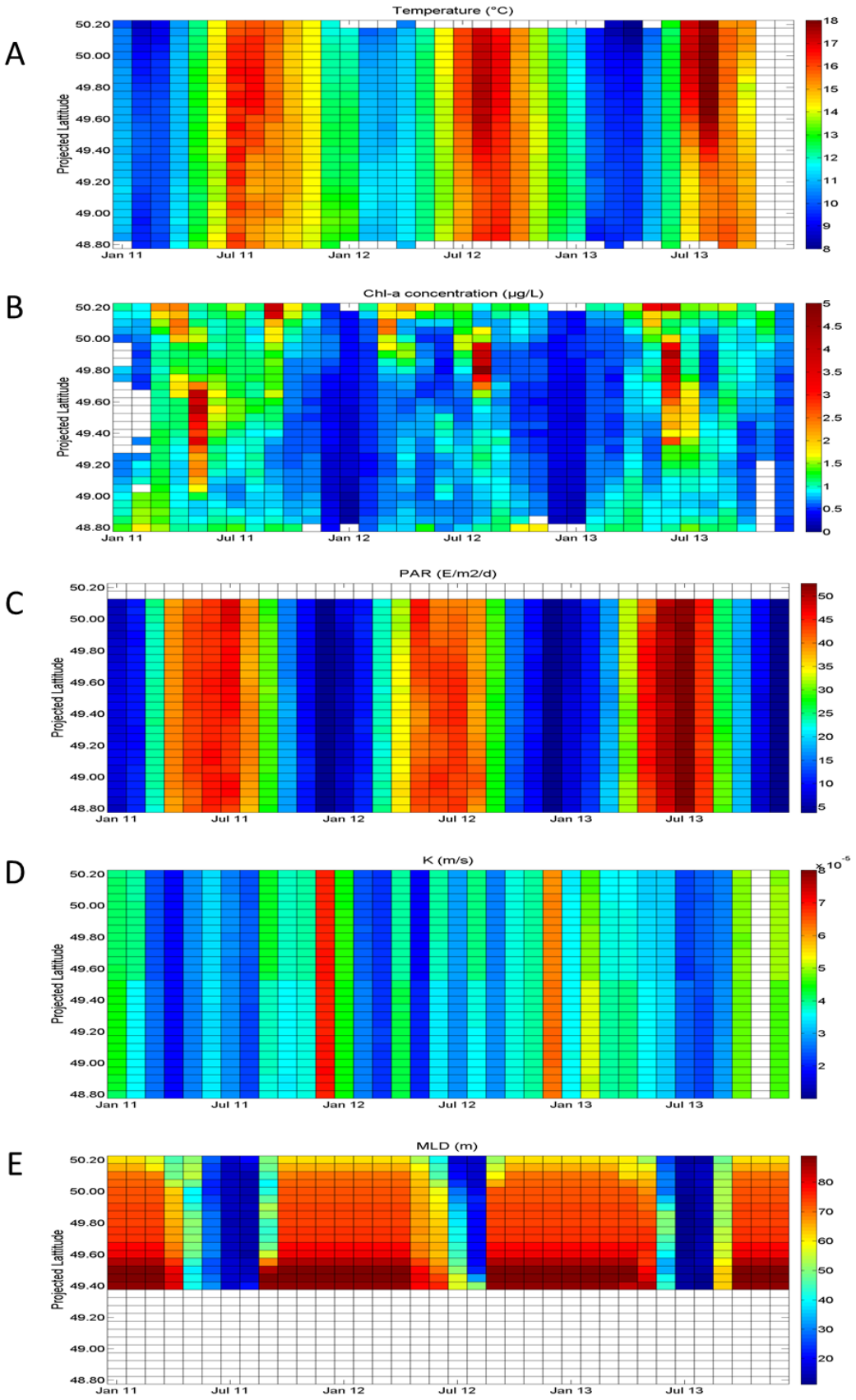


Figure 26: Distribution of monthly gridded (A) SST (°C), (B) Chl-*a* (µg L^{-1}), (C) PAR (E m^{-2} d^{-1}), (D) K (m s^{-1}) and (E) MLD over depth ratio MLDr in the WEC between Roscoff and Plymouth from January 2011 to December 2013.

3.4 SOCAT data

The Surface Ocean CO_2 ATlas (SOCAT) database (http://www.socat.info/, Bakker et al., 2014) is an international collection of underway ocean CO_2 measurements. This compilation currently includes approximately 6.3 million measurements from more than 1850 cruises from 1968 to 2011. From January 2003 to January 2011, more than 46,000 pCO_2 and associated SST and salinity values were available over the study area (Fig. 27, Table 8). From 2003 to 2011, in sWEC, nWEC and sCS, pCO_2 values from SOCAT were available for 64% to 79% of the months (Table 8), mainly from along the same south-west/north-east route (Fig. 27) operated principally by three voluntary observing ships (details available on the SOCAT website) which crossed these provinces up to twice per month, almost every month from 2003 to 2011. In nCS and IS, the data coverage was sparser and in CL no data were available. We binned all of these data into the study grid on a monthly basis. The binned data were then averaged over each defined province (Fig. 25, Sect. 2) to compare them to the pCO_2 estimates computed using the algorithms from remotely-sensed data.

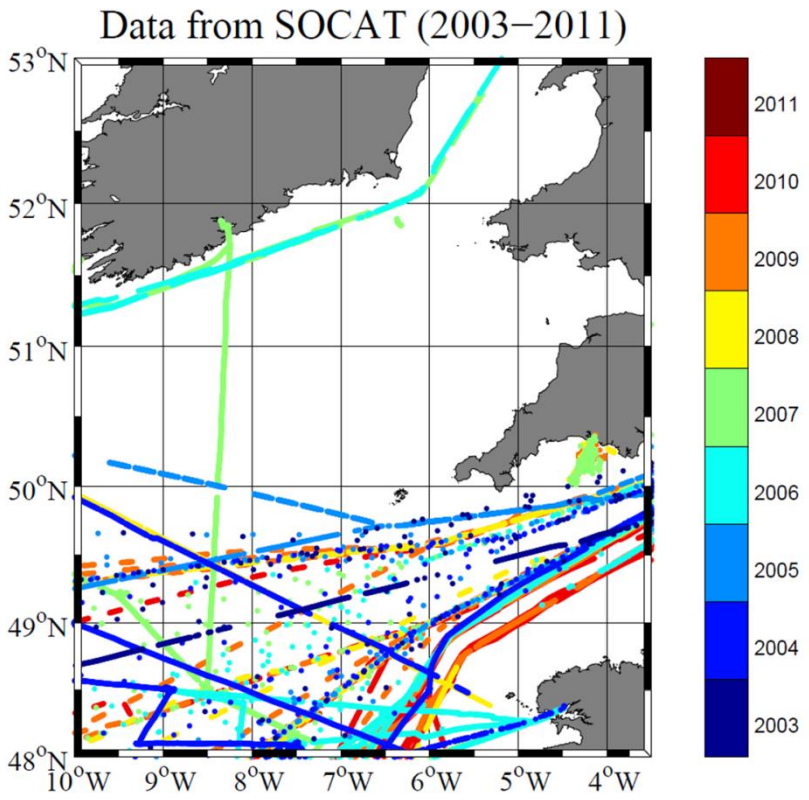


Figure 27: Map of available SOCAT surface pCO_2 data with color-coded respective year of acquisition between 2003 and 2011.

Region	Area (km²)	Nb of Obs.	% Time Coverage
IS	18115	635	5%
nCS	58035	3979	7%
sCS	65943	31079	79%
nWEC	11912	9855	77%
sWEC	12167	3147	64%
CL	5412	0	0%

Table 6: Area (in km²) of each defined province (Fig. (2)), number of available SOCAT pCO_2 data and the percentage of available monthly SOCAT pCO_2 data between 2003 and 2011.

3.5 Calculation of air-sea CO_2 fluxes

The fluxes of CO_2 across the air-sea interface (F) were computed from the pCO_2 air-sea gradient ($\Delta pCO_2 = pCO_{2\ water} - pCO_{2\ air}$, µatm) according to:

$$F = K * \alpha * \Delta pCO_2 \quad (25)$$

where K is the gas transfer velocity (m s^{-1}) and α is the solubility coefficient of CO_2 (mol atm^{-1} m^{-3}) calculated after Weiss (1970). The exchange coefficient K was computed as a function of wind speed with the algorithm given by Nightingale et al. (2000) established in the Southern Bight of the North Sea (SBNS):

$$K = (0.222 * u_{10}^2 + 0.333 * u_{10}) * \left(\frac{Sc}{660}\right)^{-0.5} \quad (26)$$

where u_{10} is the wind speed data at 10 m height (m s^{-1}) and *Sc* the Schmidt number at *in-situ* SST. The SBNS and the WEC present similar environmental characteristics: these two shallow continental shelves are both close to land with high tidal currents controlling the physical structure of the water column. We also computed gas transfer velocity with the Wanninkhof et al. (1992) and with the Wanninkhof and McGillis (1999) parameterizations for long-term winds to give a range of computed air-sea CO_2 fluxes. Wind speeds along the ferry track and over the study area were extracted from monthly wind speed data corrected at 10 m height from the NCEP/NCAR re-analysis project (Sect. 3.2.). Atmospheric pCO_2 ($pCO_{2\ air}$) was calculated from the CO_2 molar fraction (xCO_2) at the Mace Head site (53°33'N 9°00'W, southern Ireland) of the RAMCES network (Observatory Network for Greenhouse gases) and from the water vapor pressure (pH_2O) using the Weiss and Price (1980) equation. Atmospheric pressure (P_{atm}) over the study area was obtained from the NCEP/NCAR re-analysis project (Kalnay et al., 1996).

sWEC *48.80°N-49.40°N*

Variables	MLR Coeff	1	2	3	% of variability	Coeff. Values	Std.Err.
	a0	397.23	397.88	397.89	-	648.20	17.69
SST	a1	-43.75	-26.14	-28.73	**22.2%**	-14.03	1.25
CHLA	a2	-15.88	-7.74	-8.38	**6.5%**	-22.58	2.62
TI	a3	-83.11	-63.56	-67.42	**52.2%**	-67.42	3.48
PAR	a5	-	-16.44	-19.35	**15.0%**	-1.23	0.08
K	a6	-	-	-5.38	**4.2%**	-5.14×10^5	1.11×10^5
	R^2	**0.65**	**0.79**	**0.80**		**N=398**	
	RMSE (µatm)	**21.1**	**16.3**	**15.8**		**α = 336**	**p<0.001**

nWEC *49.40°N-50.20°N*

Variables	MLR Coeff	1	2	3	4	% of variability	Coeff. Values	Std.Err.
	a0	377.42	377.43	377.48	377.38	-	450.47	14.03
SST	a1	-12.15	-26.28	-27.2	-19.74	**15.2%**	-7.99	1.00
CHLA	a2	-7.93	-9.93	-9.6	-8.32	**6.4%**	-12.75	1.39
TI	a3	-47.31	-74.73	-77.2	-69.88	**53.9%**	-69.88	4.21
PAR	a5	-	21.66	20.48	19.87	**15.3%**	1.26	0.19
K	a6	-	-	-3.95	-3.45	**2.7%**	-3.37×10^5	0.96×10^5
MLD	a7	-	-		-8.48	**6.5%**	-27.19	4.58
	R^2	**0.79**	**0.81**	**0.82**	**0.83**		**N=510**	
	RMSE (µatm)	**18.5**	**17.7**	**17.3**	**16.9**		**α = 26**	**p<0.001**

Table 7: MLR normalized coefficients for each variable in sWEC and nWEC with corresponding R^2 and RMSE values. Percentages of variability explained by each variable were computed only when all the variables were included in the MLR. Non-normalized coefficient values are given for the last step of the MLR with their standard error (Std.Err.). N values are the number of values used in the MLR and α is the value between 0 and 365 chosen by iteration to optimize the seasonal phasing.

4. Results and discussion

4.1 Performance of MLR

We performed MLRs to estimate surface pCO_2 in the nWEC based on SST, Chl-*a*, the time variable TI, K and PAR in the sWEC and by including MLDr (MLD/depth ratio). Table 9 shows the MLR normalized coefficients used in the algorithms and their evolutions when we added new variables in the computations. The corresponding R^2 and RMSE are the indicators of the performance of the MLR at each addition of a new variable. Based on SST, Chl-*a*, TI, and 398 and 510 monthly gridded observations, we obtained R^2 of 0.65 and 0.79 with RMSE of 21.1 µatm and 18.5 µatm, in the sWEC and nWEC respectively (Table 9). The inclusion of PAR, K and MLDr (only in nWEC) increased R^2 values up to 0.80 and 0.83 in sWEC and nWEC with respective RMSE of 15.8 µatm and 16.9 µatm (Fig. 29a and 29b). The RMSE accounted for less than 10% of the amplitude of the pCO_2 signal (approximately 200 µatm). For each variable and each MLR, we calculated the p-values which were all inferior to 0.001 (not shown in Table 9), meaning that all of the variables were statistically significant in the MLR.

From the normalized coefficients, we calculated the percentages of variability explained by each variable. Normalized coefficients showed that in both provinces, TI contributed to half of the predicted pCO_2 (Table 9). The seasonal pCO_2 signal, which was strongly controlled by biological processes (Marrec et al., 2013), followed an average dynamic closed to a sinusoidal signal. Therefore, the time variable TI contributed to more than half of the variability of the pCO_2 signal, highlighting the strong seasonality observed on this signal (Fig. 28a). Beside TI, the most significant variables in terms of relative contribution were SST and PAR, with 22% and 15% in sWEC and both with 15% in nWEC, respectively. Chl-*a* contributed for 7% and 6% in the sWEC and nWEC, respectively, a relatively low value considering that, as reported by Marrec et al. (2013), biological processes are the main driver of seasonal pCO_2 variability in the WEC. The contribution of K in the MLR was small but by adding K in the computation, R^2 increased by 0.02 and 0.01 with a decrease of the RMSE of 0.4 µatm in the sWEC and the nWEC. Similarly, MLDr addition improved the performance of the MLR despite its relatively small contribution compared to the other normalized coefficients. Due to the complexity of the algorithms, a quantitative

interpretation of non-normalized coefficients is difficult. For example, according to our model, pCO_2 decreases by 14.3 µatm when SST increases by 1°C (Table 9). This value is in contradiction with the expected thermodynamic relationship between SST and pCO_2 from Takahashi et al. (1993). The goal of this study was to develop suitable algorithms to predict pCO_2 variability in continental shelf seas by maximizing the performance of the MLR and not to define empirical relationships between the variables and pCO_2.

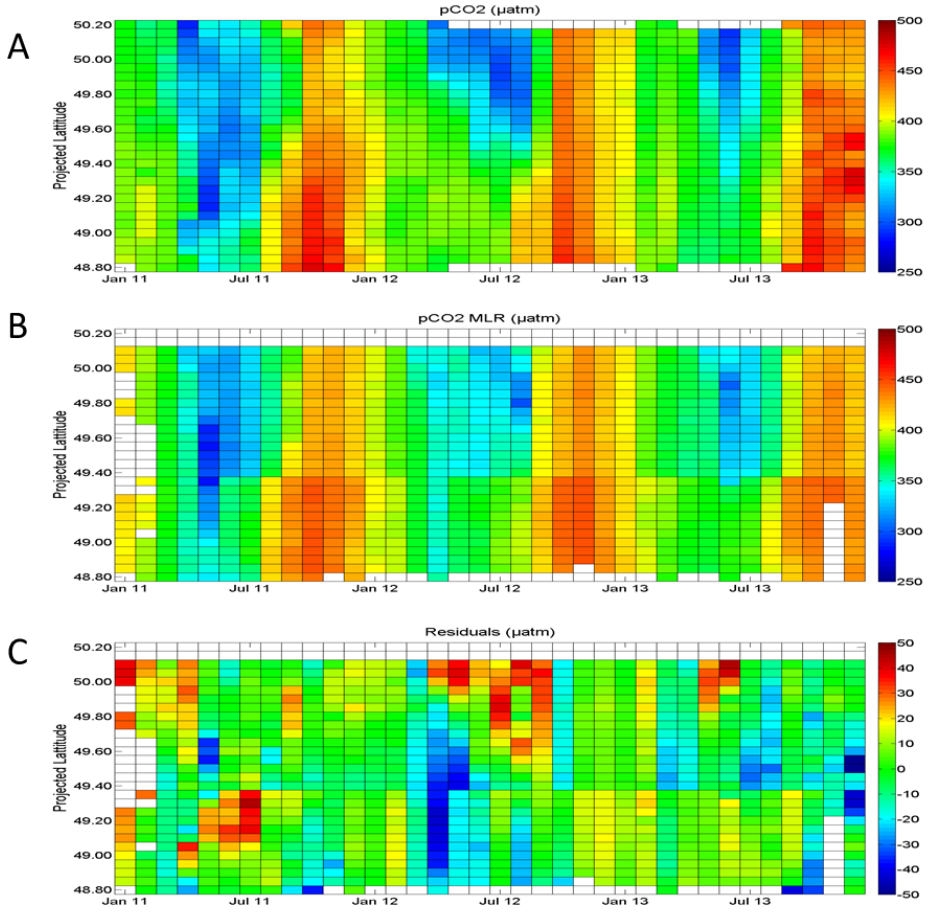


Figure 28: Distribution of monthly gridded (A) pCO_2 (µatm) based on bimonthly DIC/TA measurements (January 2011 to March 2012) and on high-frequency pCO_2 measurements (April 2012 to December 2013) in WEC, (B) $pCO_{2,MLR}$ (µatm) computed from nWEC and sWEC algorithms and (C) residuals (pCO_2-$pCO_{2,MLR}$ in µatm) between Roscoff and Plymouth from January 2011 to December 2013.

Figures 28a, 28b and 28c show the monthly binned (0.05° of latitude) pCO_2, pCO_2 predicted from MLR coefficients ($pCO_{2,MLR}$) and associated residuals ($pCO_{2,obs} - pCO_{2,MLR}$) from January 2011 to January 2014 between Roscoff and Plymouth. As mentioned above, the observed pCO_2 signal was characterized by a strong seasonality with values higher than 450

µatm in autumn and values lower than 300 µatm during spring and summer. As explained by Marrec et al. (2013), in the sWEC the productive period in spring/summer (characterized by pCO_2 decrease due to biological activity) is shorter and less intense than in the nWEC. Furthermore, the sWEC shows enhanced and longer remineralization processes in fall, leading to higher pCO_2 values in homogeneous systems than in stratified systems. Thus, the dynamics of pCO_2 in both provinces presents important inter-annual variability. In the sWEC, pCO_2 values lower than 350 µatm were observed during spring 2011, whereas at the same period of 2012 and 2013, pCO_2 remained close to the atmospheric equilibrium, between 350 and 400 µatm. As the pCO_2 simulation by the MLR is mainly driven by a seasonal cycle (TI), which is the same every year, these inter-annual discrepancies can yield bias in the MLR simulation. For the sWEC the MLR model overestimated pCO_2 during spring and summer 2011 (residuals up to 30 µatm, Fig. 28b and 28c) and underestimated pCO_2 in spring 2012 (residuals down to -50 µatm, Fig. 28b and 28c) by simulating an average decrease of pCO_2 both years. On Fig. 29c and 29d, residuals are plotted vs. observed pCO_2 in the sWEC and nWEC, and on Fig. 29e and 29f monthly mean residuals over each province are plotted vs. months from January 2011 to December 2013. In the sWEC, when observed pCO_2 ($pCO_{2,Obs}$) values were below 350 µatm, as in spring 2011, $pCO_{2,MLR}$ values were much higher than $pCO_{2,Obs}$ and residuals were highly negative. In the sWEC, residuals as a function of the observed pCO_2 were not homogeneously distributed, with high negative residuals when pCO_2 was below 350 µatm and high positive residuals when pCO_2 was over 450 µatm. In the nWEC, the main inter-annual variations were linked to the duration of the productive period (Marrec et al., 2014), when the lowest pCO_2 values were recorded. The distribution of residuals was more homogeneous, the less pronounced inter-annual variability, explaining the better performance of the algorithms (R^2) in this part of the WEC.

Shadwick et al. (2010) and Signorini et al. (2013) undertook similar studies on the Scotian Shelf and the north-east American continental shelf, respectively. They estimated pCO_2 as a function of SST, Chl-*a* and K, and from SST, salinity, Chl-*a* and a time variable (TI), respectively, using MLR. Based on 14 monthly mean values from a high-frequency dataset at a moored buoy, the algorithm developed by Shadwick et al. (2010) attained a R^2 of 0.81 with an associated standard error of 13 µatm. They extrapolated this algorithm over the entire Scotian Shelf region to investigate pCO_2 and air-sea CO_2 fluxes from remotely-sensed data from 1999 to 2008. Signorini et al. (2013) reported R^2 and associated RMSE ranging from 0.42 to 0.87 and from 22.4 µatm to 36.9 µatm, respectively. They divided the north-east

American continental shelf into 5 distinct regions according to their physical and biogeochemical attributes. Their study was based on SOCAT surface ocean pCO_2 and the environmental variables used to predict pCO_2 came from remotely-sensed and modeled data. The performances of our MLRs are within the same range as those in these previous studies. We developed our algorithms based on a 3 year dataset obtained during highly contrasting years, which contributed to the robustness of our model to predict a representative seasonal cycle of pCO_2 as seen in the nWEC. However, the WEC is a highly dynamic continental shelf ecosystem characterized by strong inter-annual variations. Very exceptional events, inherent to continental shelf areas, remain difficult to simulate with our method, which explain the lower performances of our MLR for the sWEC.

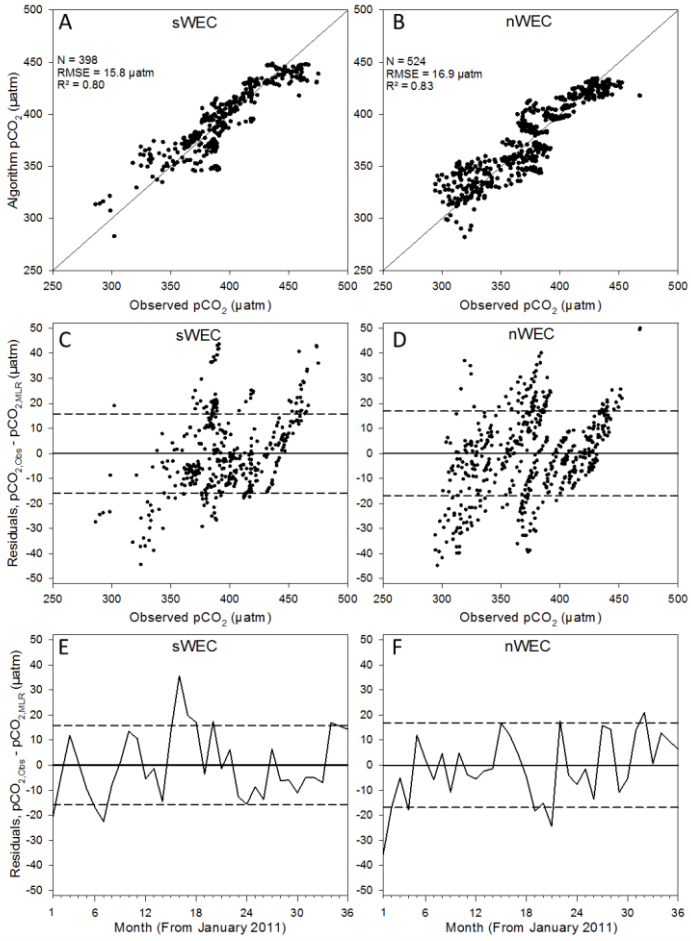


Figure 29: Observed monthly gridded pCO_2 (µatm) versus $pCO_{2,MLR}$ computed from the algorithms developed in sWEC (A) and in nWEC (B) with respective number of values (N), R^2 and RMSE. Residuals between observed pCO_2 and predicted pCO_2 in function of observed pCO_2 values (µatm) in sWEC (C) and nWEC (D). Mean monthly residuals (µatm) over sWEC (E) and nWEC (F) in function of the months from January 2011. On plots C, D, E and F the dashed lines represents the RMSE of MLR developed in sWEC (±15.8 µatm) and nWEC (±16.9 µatm).

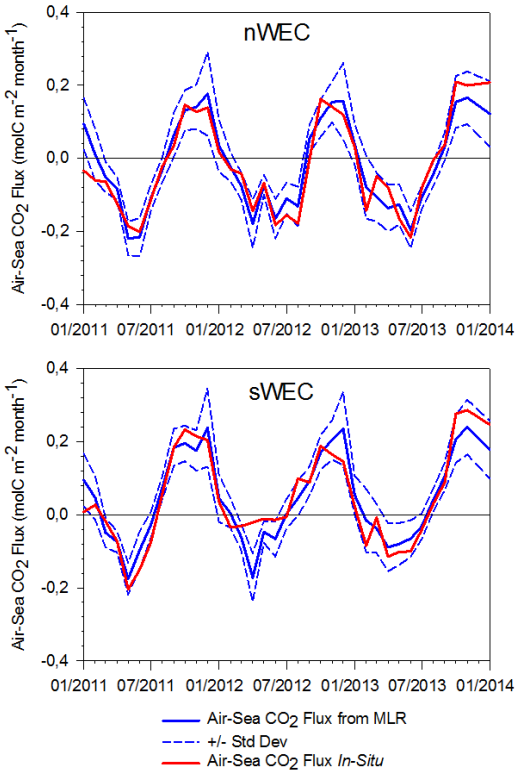


Figure 30: Monthly air-sea CO_2 fluxes (mol C m^{-2} $month^{-1}$) computed from observed pCO_2 (in red) and $pCO_{2,MLR}$ (in blue) data in nWEC and sWEC from 2011 to 2013 using Nightingale et al. (2000) gas transfer velocity K. Dashed lines represent fluxes computed from $pCO_{2,MLR}$ plus and minus respective RMSE.

We compared air-sea CO_2 fluxes (Eq. (25)) calculated from observed pCO_2 and from pCO_2 simulation (Fig. 30 and Table 10). Figure 30 shows the air-sea CO_2 flux variation in the sWEC and the nWEC based on $pCO_{2,obs}$ and $pCO_{2,MLR}$ from January 2011 to January 2014. Fluxes were computed from the mean monthly pCO_2 of each province and the standard deviation on MLR fluxes corresponds to MLR fluxes computed plus and minus the RMSE obtained in the respective provinces (Table 9). Seasonal air-sea CO_2 flux cycles were well described by the algorithm-defined pCO_2, particularly for the nWEC, with both provinces acting as a sink of atmospheric CO_2 during spring and summer and as source of CO_2 to the atmosphere during autumn and winter. The inter-annual variability of pCO_2 observed in the sWEC during spring and summer was also reflected in the flux computations, the fluxes based on MLR overestimating the CO_2 sink in spring 2012. Table 10 reports the annual flux estimates in both provinces based on *in-situ* pCO_2 observations and $pCO_{2,MLR}$. On an annual scale, the seasonally stratified nWEC waters acted as a sink of atmospheric CO_2 at a rate of

0.1 to 0.4 mol C m^{-2} $year^{-1}$ based on *in-situ* pCO_2 measurements. Fluxes computed from $pCO_{2,MLR}$ also indicated that the nWEC acts as a sink of atmospheric CO_2, but we observed some discrepancies between the magnitude of *in-situ* and MLR based fluxes in 2011 and 2013. The permanently well-mixed sWEC waters acted as a source of CO_2 to the atmosphere from 2011 to 2013 ranging between 0.4 and 0.6 mol C m^{-2} $year^{-1}$, and annual CO_2 fluxes computed from observed and modeled pCO_2 were in good agreement. The performances of our algorithms to estimate monthly surface pCO_2 allowed us to compute suitable air-sea CO_2 fluxes in WEC provinces during three contrasted years.

Year	Northern WEC		Southern WEC	
	Obs.	MLR	Obs.	MLR
2011	-0.4 (-0.8 / -0.2)	-0.1 (-0.2 / 0.2)	0.4 (0.9 / 0.9)	0.6 (1.2 / 1.2)
2012	-0.3 (-0.7 / -0.3)	-0.2 (-0.4 / -0.1)	0.6 (1.2 / 1.0)	0.5 (0.9 / 0.9)
2013	-0.1 (-0.3 / 0.1)	-0.3 (-0.8 / -0.3)	0.5 (0.9 / 0.9)	0.5 (0.9 / 0.9)

Table 8: Air-sea CO_2 fluxes (in mol C m^{-2} $year^{-1}$) calculated from observed pCO_2 and from pCO_2 obtained by MLR along the ferry track in nWEC and sWEC using Nightingale et al. (2000) k parametrization. Values in brackets were computed using Wanninkhof et al. (1992) and Wanninkhof and McGillis (1999) k parameterizations for long-term winds to give a range of computed air-sea CO_2 fluxes.

4.2 Spatial and temporal extrapolation of the algorithms

We applied the previous algorithms (Sect. 4.1.) over our study area (Fig. 25) from monthly mean remotely-sensed SST, Chl-*a*, PAR, and K (based on wind speeds) in the permanently well-mixed sWEC, IS and CL and by adding modeled MLD in the seasonally stratified nWEC, sCS and nCS. The pCO_2 values computed from these variables were averaged by province from January 2003 to December 2013 (Fig. 8). The available SOCAT pCO_2 data (Fig. 27 and Table 8) were binned into 0.05° * 0.05° grid cells and averaged over the provinces. SOCAT pCO_2 monthly mean data were superimposed on the algorithm pCO_2 time series (Fig. 31, red dots).

For the nWEC (Fig. 31d), the comparison between predicted and SOCAT pCO_2 values showed that SOCAT data fitted well with computed pCO_2. The SOCAT data followed the main features of the seasonal cycle described by the model and are in relatively good quantitative agreement. Spring pCO_2 minima were in the same range, despite the discrepancy of time-scales. During autumn and winter, maximum values were not always reached, suggesting a relatively small overestimation of modeled pCO_2 values. In the sCS (Fig. 31c),

where SOCAT data covered most months from 2003 to 2011, observed data fitted reasonably well the predicted pCO_2 during spring and summer. During autumn and winter, the model predicted surface water pCO_2 oversaturations compared to atmospheric equilibrium, but only few SOCAT pCO_2 data were above equilibrium values. The limited amount of SOCAT data available for the nCS and IS did not show any major discrepancy with the predicted pCO_2. For the sWEC (Fig. 31e), the predicted pCO_2 values were higher than the data from SOCAT, our algorithm thus mainly overestimating the pCO_2. During spring, the minimal SOCAT pCO_2 values were rarely reached by the model. Figure 27 shows that the SOCAT data available for the sWEC were acquired along the Ushant front (Pingree et al., 1975; Morin, 1984; Sournia et al., 1990) at the border of the province (sWEC, nWEC and sCS) delimited based on summer SST (Fig. 25). This border is a frontal zone between well-mixed and stratified systems with enhanced biological activity due to the constant supply of nutrients from the deep layer of stratified systems, especially in summer when the winter nutrient stock is totally depleted (Holligan, 1981; Morin, 1984, Le Fèvre, 1986, Le Boyer et al., 2009). This enhanced productivity might induce biological consumption of CO_2 which would explain the overestimation of modeled pCO_2 in the frontal zone. The SOCAT data were not representative of a homogeneous system, hindering a direct comparison.

Directly comparing monthly mean pCO_2 values obtained from algorithms and the SOCAT pCO_2 data could generate an important bias because of the timescale difference between these datasets. Monthly gridded SOCAT data were mainly based on measurements performed at daily scales. Computed pCO_2 values were representative of the average monthly pCO_2 variability, which tends to smooth extreme values obtained at shorter timescales and prevent any observation of short-term processes. Despite this time-scale discrepancy the mean differences between predicted and observed pCO_2 were 1 ± 25 µatm in the sCS, 4 ± 24 µatm in the nWEC and 7 ± 17 µatm in the nCS, on an annual scale. Considering the uncertainties relative to the MLR of 17 µatm (Sect. 4.1.), these results are very promising and allowed us to validate the extrapolation of our method over our study area. The results obtained in the sWEC were less promising as explained above and in Sect. 4.1. The comparison with SOCAT data provided indications on the MLR performance on a wider spatial scale. For the first time, we thus computed the seasonal and long-term dynamics of pCO_2 and associated air-sea CO_2 fluxes over a decade for this part of the north-western European continental shelf (Sect. 4.3.) despite the relative uncertainties inherent to the method.

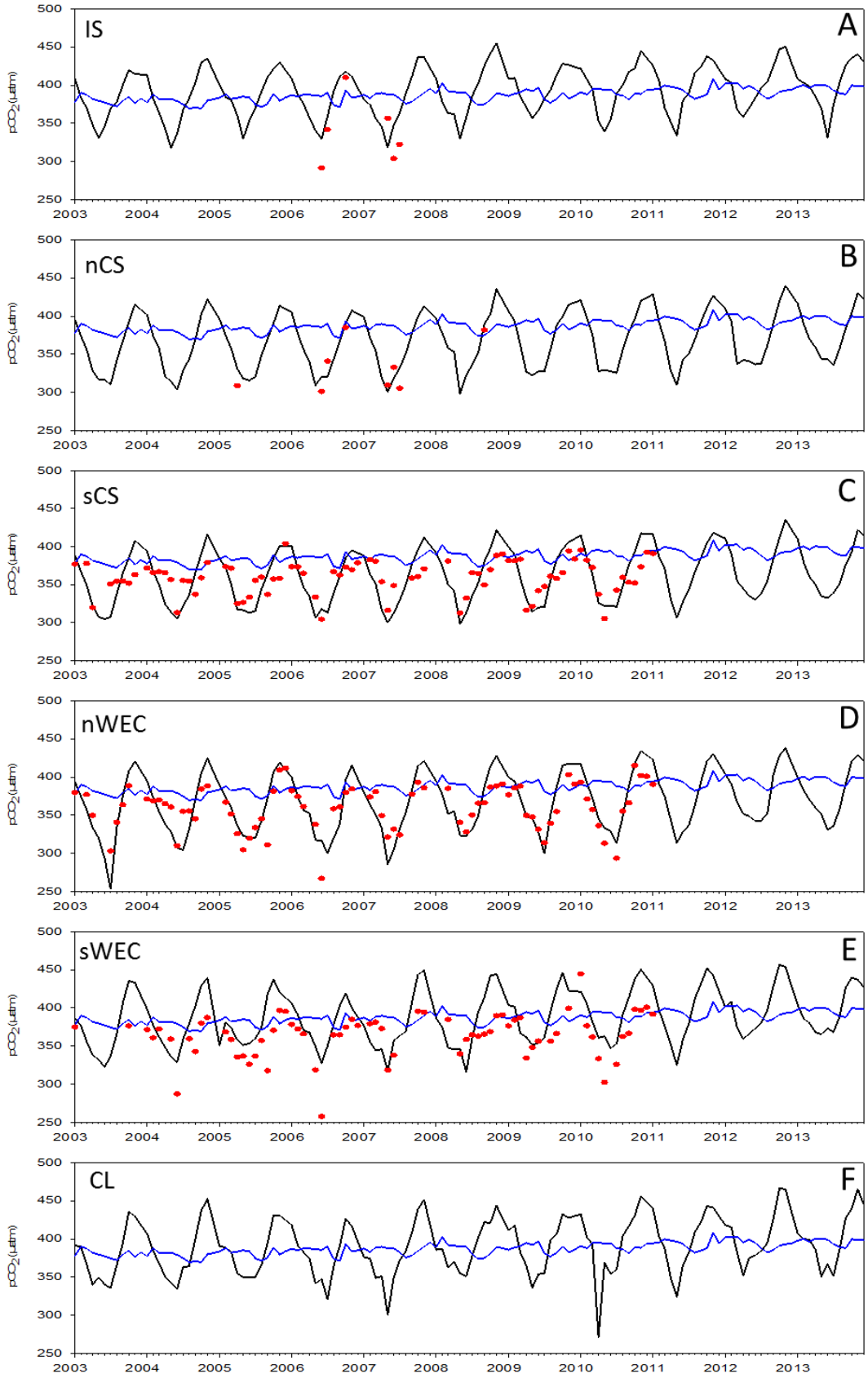


Figure 31: Time series of monthly $pCO_{2,MLR}$ (µatm, in black) averaged over IS (A), nCS (B), sCS (C), nWEC (D), sWEC (E) and CL (F) provinces from 2003 to 2013. Monthly mean corresponding SOCAT data (red dots) are shown for comparison. The blue lines represent the atmospheric pCO_2.

4.3 Seasonal variability of biogeochemical properties in stratified vs. permanently well-mixed systems

Figures 32 to 35 show the monthly values of SST, Chl-*a*, computed pCO_2 and associated air-sea CO_2 fluxes in the stratified and homogeneous regions of our study area defined on Fig. 25. Based on *in-situ* MLD data at fixed station E1 (Western Channel Observatory of Plymouth, Fig. 24) and on modeled MLD (Sect. 3.2., data not shown), we generally observed an onset of stratification in the nWEC and CS from April to October. Modeled MLD data indicated that water column stratification generally started one month earlier and ended one month later in the CS than in the nWEC. The formation of shallow surface layers (≈ 30 m in the CS and 15 m in the nWEC) triggers the initiation of spring phytoplankton blooms in the CS and nWEC (Pingree, 1980). The earlier onset of stratification in the CS than in the nWEC, due to less intense tidal streams (Pingree, 1980), is consistent with the preliminary signs of the spring bloom observed firstly in the CS (Fig. 33). In the CS, the April and May spring bloom, characterized by Chl-*a* values between 1 and 5 µg L^{-1}, was followed by low surface Chl-*a* concentrations (<1 µg L^{-1}) for the rest of the year because of total nutrient depletion in the surface layer after the spring bloom. In the nWEC, spring phytoplankton blooms occurred from May and Chl-*a* values remained between 1 and 2 µg L^{-1} until September with particularly elevated Chl-*a* in July, as previously reported by Smyth et al. (2010). pCO_2 values below 350 µatm were first observed in the CS from April and one month after in the nWEC (Fig. 34). Surface waters were undersaturated in CO_2 with respect to the atmosphere (Fig. 31 and 34) in seasonally stratified systems from February to October. This pCO_2 undersaturation is mainly driven by thermodynamical processes in February and March and by biological processes until October (Marrec et al., 2013). After the spring phytoplankton blooms, pCO_2 values remained low until September despite the apparent lack of biological activity in surface waters. However, subsurface phytoplankton blooms can occur within the thermocline at the interface with the deep cold water pool, which is not depleted in nutrients (Pemberton et al., 2004; Southward et al., 2005; Smyth et al., 2010). The nWEC and CS waters acted as a sink of atmospheric CO_2 during this period with monthly mean air-sea CO_2 flux values between 0 and -0.4 mol C m^{-2} $month^{-1}$ (Fig. 35 and 36). The lowest pCO_2 values were recorded in May in the CS and in July in the nWEC, consistent with previous Chl-*a* observations. From September to November, organic matter remineralization processes and the breakdown of stratification increased surface pCO_2 and resulted in pCO_2

oversaturation of surface waters with respect to the atmosphere. During this period, the nWEC and the CS acted as a source of CO_2 to the atmosphere at a rate of 0 to 0.3 mol C m^{-2} $month^{-1}$.

The study of the seasonal dynamics of Chl-*a* from satellite observations in the all-year well-mixed sWEC, CL and IS is more complex than in adjacent seasonally stratified systems. In the IS, we obtain abnormally high Chl-*a* satellite estimates based on the OC3 algorithm (Sect. 3.2.) most of the year caused by elevated suspended particles and colored dissolved organic matter concentrations (McKee and Cunningham, 2006). However, Chl-*a* has a minor contribution (7%, Table 9) in the computation of pCO_2 in homogeneous systems and does not have a large effect on pCO_2 prediction. The areas defined as sWEC and CL are not only representative of homogeneous systems, they also include tidal mixing frontal zones. These frontal regions host higher biological production than well-mixed systems (Pingree et al., 1975). The CL area is almost entirely influenced by these thermal fronts due to its small size, whereas they only impact the sWEC area at its borders (Ushant Front). On monthly mean satellite data, it clearly appeared that enhanced biological activity occurred at the border of the sWEC (Fig. 33). In the central part of the sWEC, Chl-*a* values remained low (<1 µg L^{-1}) for most of the year, except in June where a spring phytoplankton bloom was observed. As reported by previous studies (Boalch et al., 1978; L'Helguen et al., 1986; Wafar et al., 1983), the main factor controlling phytoplankton production was light availability. In June, day length is the longest and meteorological conditions are generally favorable, which explains the peak in Chl-*a* values. In all-year well-mixed provinces, the lowest pCO_2 values were observed in June (Fig. 31 and 34) with minima around 320 µatm. During autumn, pCO_2 values reached maximum values around 450 µatm caused by organic matter remineralization processes. Biological processes are the main driver of pCO_2 variability in the WEC (Marrec et al., 2013) and this biological control is representative of temperate coastal ecosystems in Europe (Borges et al., 2006; Bozec et al., 2005; Bozec et al., 2006). The productive period is shorter in all-year well-mixed systems than in seasonally stratified areas (Marrec et al., 2013; Marrec et al., 2014). Surface pCO_2 values were below the atmospheric equilibrium from March to July in the sWEC, CL and IS, whereas these patterns are observed from February to September in the CS and the nWEC (Fig. 31, 35, 36).

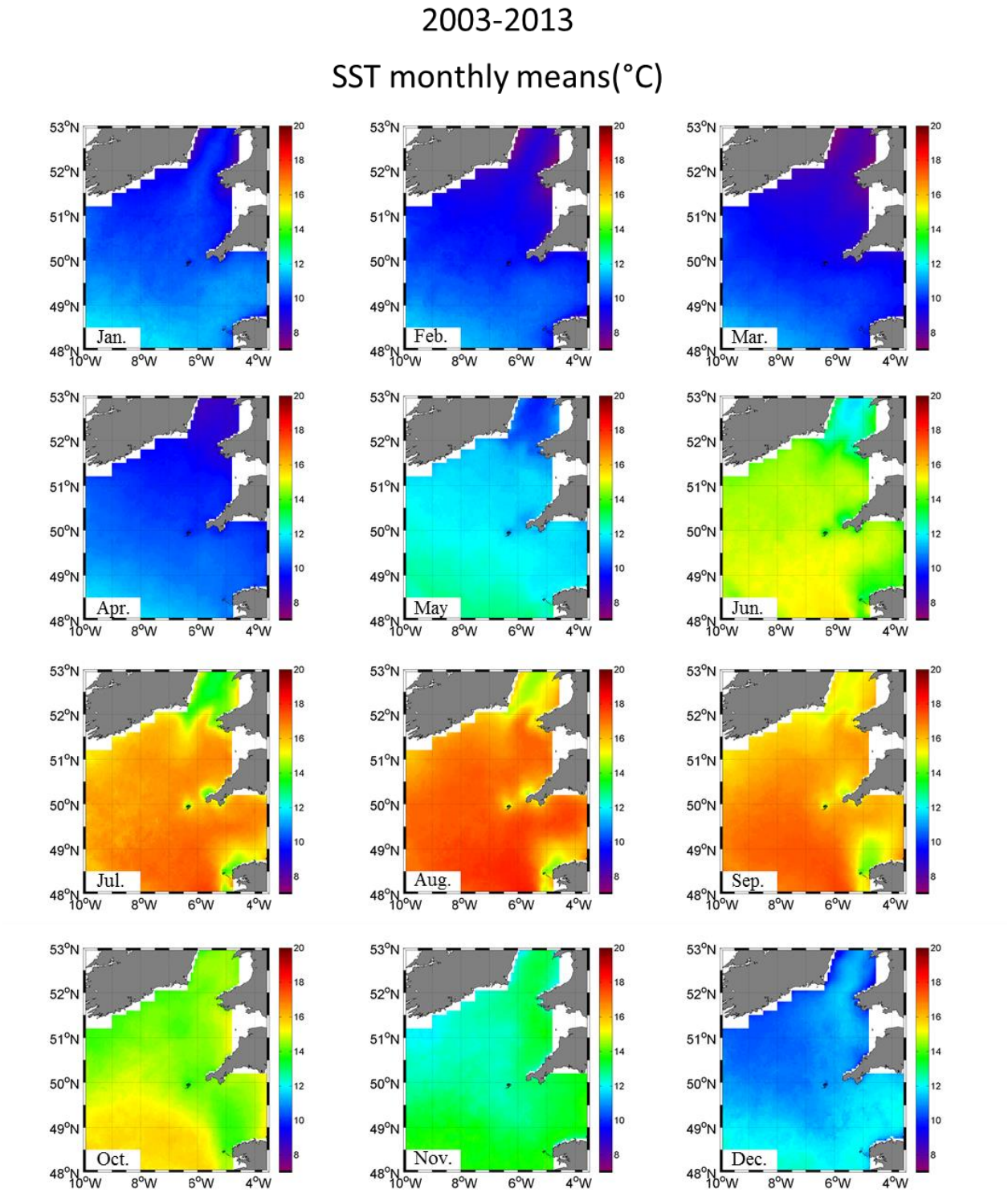


Figure 32: Monthly satellite SST (°C) averaged from 2003 to 2013 from January (top left corner) to December (bottom right corner).

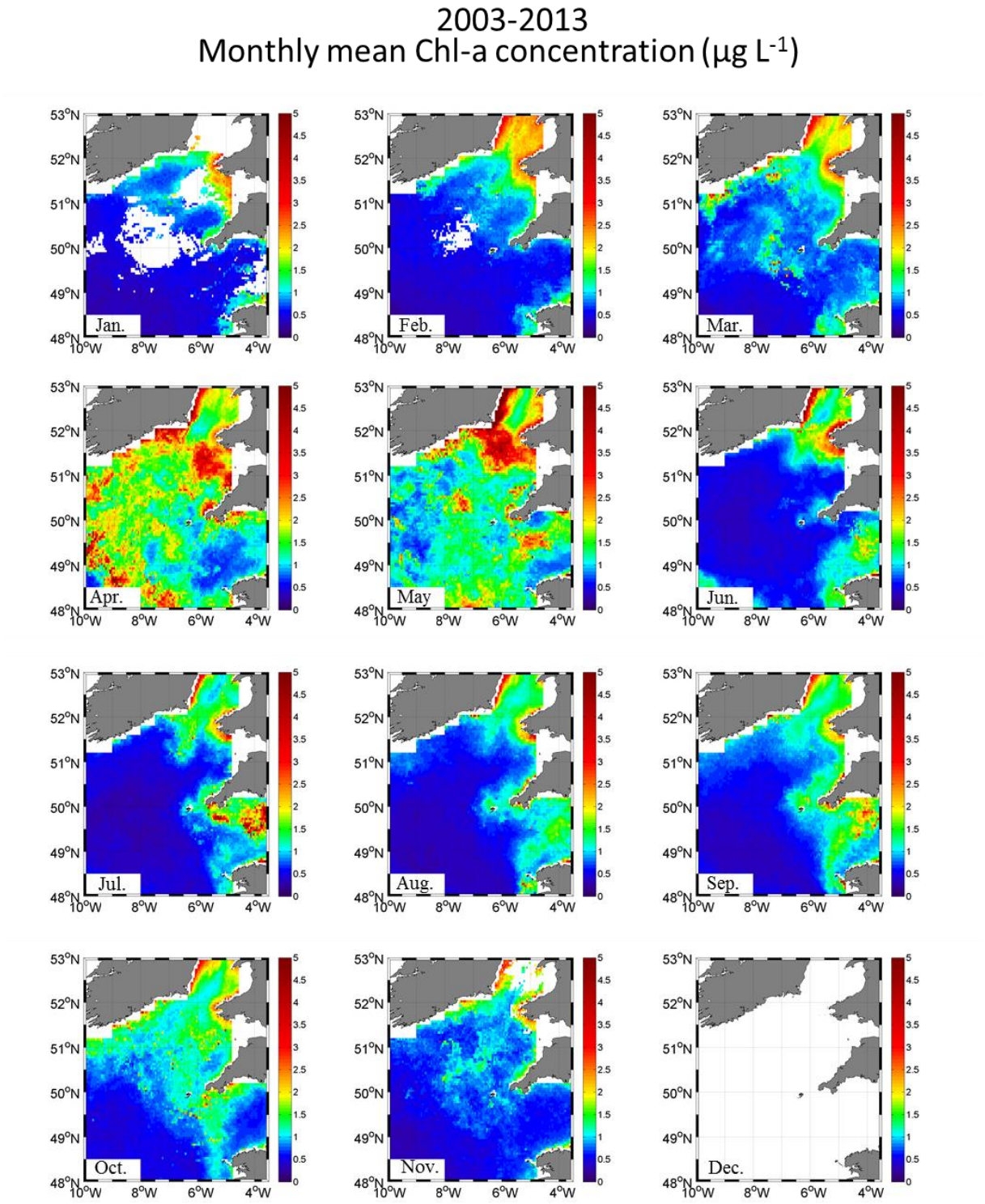


Figure 33: Monthly satellite Chl-*a* (µg L^{-1}) averaged from 2003 to 2013 from January (top left corner) to December (bottom right corner).

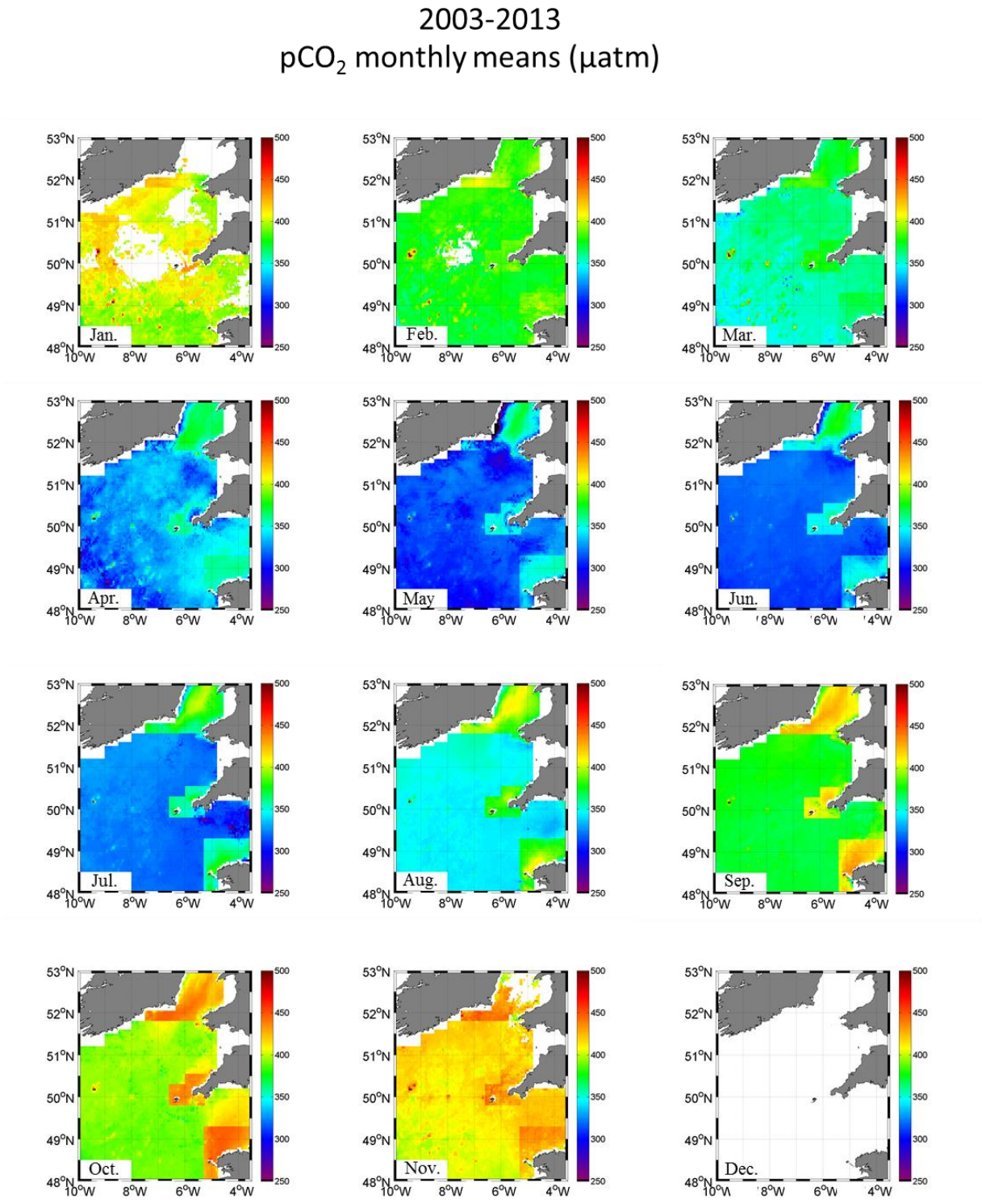


Figure 34: Monthly $pCO_{2,MLR}$ (µatm) computed from the algorithms developed in seasonally stratified and in permanently well-mixed systems averaged from 2003 to 2013 from January (top left corner) to December (bottom right corner).

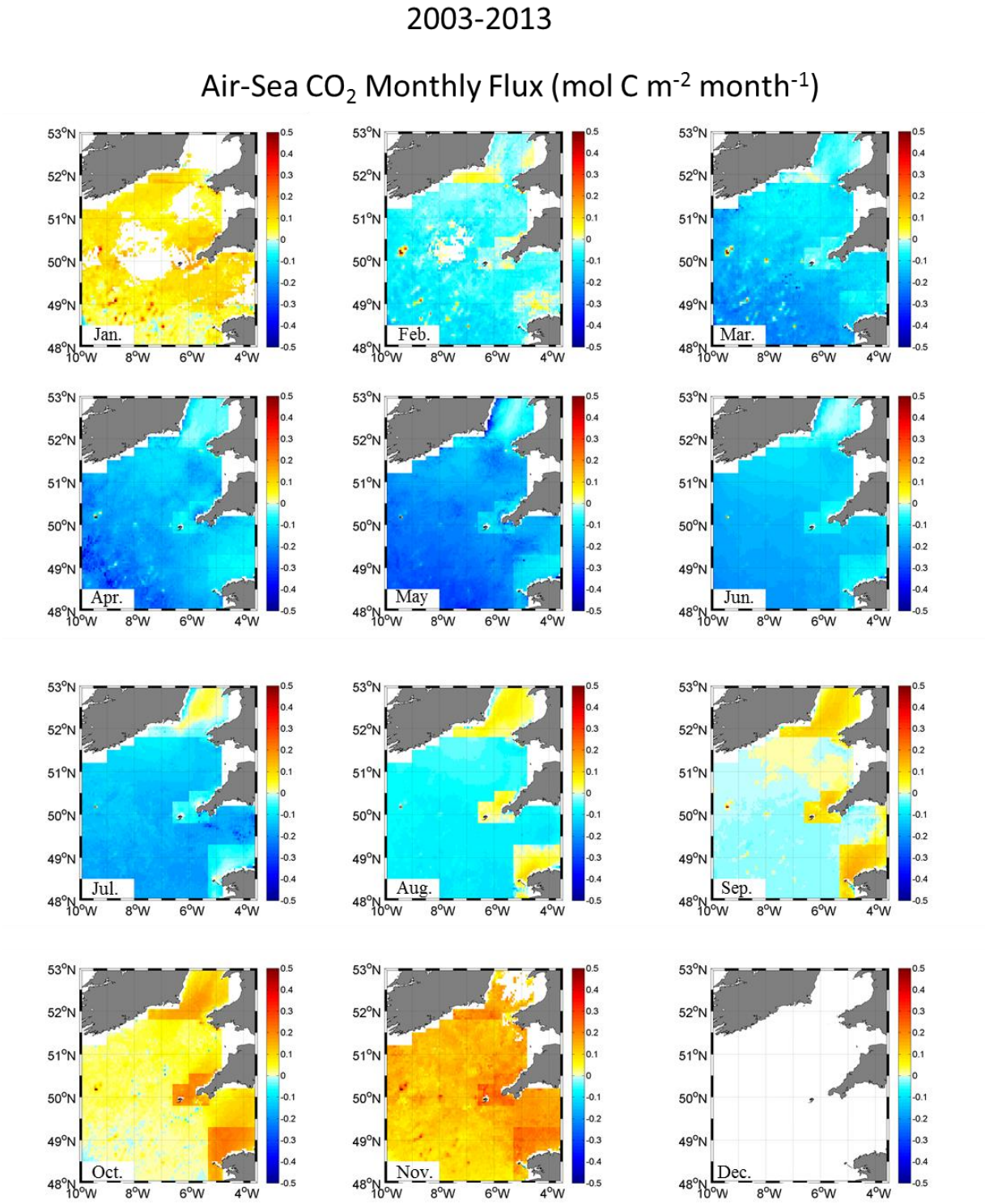


Figure 35: Monthly air-sea CO_2 fluxes (mol C m^{-2} $month^{-1}$) computed from $pCO_{2,MLR}$ and using Nightingale et al. (2000) K-wind relationship averaged from 2003 to 2013 from January (top left corner) to December (bottom right corner). Negative values indicate CO_2 sink.

On an annual scale, the permanently well-mixed sWEC, IS and CL acted as source of CO_2 to the atmosphere at a mean rate (from 2003 to 2013) of 0.2, 0.4 and 0.4 mol C m^{-2} $year^{-1}$, respectively, (Table 11) whereas the seasonally stratified systems acted as sinks of atmospheric CO_2, with mean values over 11 years of -0.4, -0.9 and -0.4 mol C m^{-2} $year^{-1}$ for the nCS, sCS and nWEC, respectively (Table 11). Air-sea CO_2 fluxes computed from predicted pCO_2 corroborate the hypothesis of Borges et al. (2005), with permanently well mixed systems acting as sources of CO_2 to the atmosphere and seasonally stratified systems acting as a sink of atmospheric CO_2. The only available flux estimate for the CS is based on a study by Frankignoulle and Borges (2001), reported in Borges et al. (2006), which indicated that the CS acts as sink of CO_2 of -0.8 mol C m^{-2} $year^{-1}$. In the sCS we obtained an averaged flux value of -0.9 mol C m^{-2} $year^{-1}$, which is in agreement with this previous study, underlying the robustness of our MLR. Further, we report what is, to the best of our knowledge, the first estimate of air-sea CO_2 flux in the IS of 0.4 mol C m^{-2} $year^{-1}$. Borges et al. (2006) reported a mean annual air-sea CO_2 flux value of -1.9 mol C m^{-2} $year^{-1}$ in European coastal waters based on a compilation of annually integrated fluxes computed from field measurements.

	Seasonnaly Stratified			Permanently Mixed		
Year	**nCS**	**sCS**	**nWEC**	**sWEC**	**CL**	**IS**
2003	-0.4 (-0.9/-0.4)	-0.9 (-1.9/-1.1)	-0.4 (-0.8/-0.2)	0.0 (0.0/0.3)	0.3 (0.6/0.7)	0.2 (0.4/0.4)
2004	-0.4 (-0.7/-0.3)	-0.8 (-1.6/-1.1)	-0.2 (-0.4/0.0)	0.3 (0.4/0.6)	0.6 (1.4/1.2)	0.4 (0.9/0.7)
2005	-0.4 (-0.8/-0.2)	-0.9 (-1.9/-1.1)	-0.3 (-0.6/-0.1)	0.1 (0.0/0.1)	0.4 (0.9/0.9)	0.4 (0.8/0.7)
2006	-0.6 (-1.2/-0.6)	-1.2 (-2.4/-1.7)	-0.7 (-1.4/-0.8)	-0.1 (-0.2/0.0)	0.2 (0.4/0.5)	0.2 (0.3/0.3)
2007	-0.7 (-1.4/-0.8)	*-1.2 (-2.6/-1.9)*	*-0.9 (-1.9/-1.3)*	-0.5 (-1.2/-0.9)	-0.3 (-0.8/-0.5)	0.0 (-0.2/0.0)
2008	-0.4 (-0.7/-0.3)	-0.8 (-1.8/-1.2)	-0.3 (-0.6/-0.2)	0.1 (0.1/0.3)	0.5 (1.0/0.9)	0.5 (0.9/0.7)
2009	*-0.3 (-0.5/0.0)*	*-0.7 (-1.3/-0.4)*	*0.0 (0.1/0.6)*	0.6 (1.4/1.8)	0.7 (1.6/1.8)	0.6 (1.3/0.9)
2010	*-0.3 (-0.5/-0.2)*	-0.8 (-1.5/-0.9)	-0.1 (-0.1/0.1)	0.5 (1.2/1.0)	0.6 (1.3/1.1)	0.5 (1.2/0.7)
2011	-0.4 (-0.9/-0.5)	-0.8 (-1.7/-1.1)	-0.3 (-0.7/-0.3)	0.3 (0.6/0.5)	0.4 (0.9/0.8)	0.3 (0.7/0.5)
2012	-0.4 (-0.9/-0.5)	-0.8 (-1.6/-1.1)	-0.2 (-0.5/-0.2)	0.3 (0.6/0.5)	0.7 (1.4/1.1)	0.5 (0.9/0.6)
2013	-0.6 (-1.3/-0.7)	-1.2 (-2.7/-1.9)	-0.5 (-1.1/-0.6)	0.0 (-0.1/0.0)	0.4 (0.8/0.7)	0.3 (0.6/0.5)
Mean (mol C m^{-2} yr^{-1})	-0.4 (-0.9/-0.4)	-0.9 (-1.9/-1.2)	-0.4 (-0.7/-0.3)	0.2 (0.3/0.4)	0.4 (0.9/0.8)	0.4 (0.7/0.5)
Mean (Tg C yr^{-1})	-0.30 (-0.62/-0.28)	-0.72 (-1.52/-0.97)	-0.05 (-0.10/-0.04)	0.02 (0.04/0.05)	0.03 (0.06/0.05)	0.08 (0.15/0.12)

Table 9: Annual air-sea CO_2 fluxes (in mol C m^{-2} $year^{-1}$) in the seasonally stratified (nCS, sCS and nWEC) and permanently provinces (sWEC, CL and IS) of our study area between 2003 and 2013 and the mean annual fluxes over the decade using Nightingale et al. (2000) k parametrization. Scaled annual fluxes over province areas (Table 2) in Tg C $year^{-1}$ were calculated from the mean annual fluxes over the decade. Fluxes in brackets were calculated using Wanninkhof et al. (1992) and Wanninkhof and McGillis (1999) k parameterizations for long-term winds.

We scaled these mean annual fluxes over province areas (Table 8 and 11) and obtained air-sea CO_2 fluxes of -0.30, -0.72 and -0.05 Tg C $year^{-1}$ in the nCS, sCS and nWEC, and of 0.02, 0.03 and 0.08 Tg C $year^{-1}$ in the sWEC, CL and IS, respectively. These fluxes correspond to an absorption of -0.95 Tg C $year^{-1}$ over our study area. Compared to the Borges et al. (2006) estimates over European continental shelves of -68.1 Tg C $year^{-1}$, the contribution of our study area appears small. Scaled to the surface covered by our study area (172000 km², Table 8), which represents 5% of the European continental shelf area reported by Borges et al. (2006), this value corresponds to -3.4 Tg C $year^{-1}$. Chen and Borges (2009) reported air-sea CO_2 flux of -16.1 Tg C $year^{-1}$ in the north-east Atlantic continental shelf region from a mean flux value of -0.8 mol C m^{-2} $year^{-1}$. Regarding the lack of such estimates for the CS, IS and to a lesser extent WEC before our study, the results presented here allow for the first time to estimate air-sea CO_2 fluxes in these provinces of the north-west European shelf. Moreover this study provides relevant information concerning the seasonality of pCO_2 and air-sea CO_2 fluxes over 11 years, and more particularly on inter-annual and multi-annual variability (Sect. 4.4.).

4.4 Inter and multi-annual variability of pCO_2 and air-sea CO_2 fluxes

Monthly surface ocean pCO_2 derived from algorithms (Fig. 31) showed important inter-annual variability regarding the seasonal cycle of CO_2 in each province. Monthly air-sea CO_2 fluxes (Fig. 36) followed the same trend as pCO_2, resulting in significant inter-annual differences in the intensity and/or direction of annual fluxes (Table 11 and Fig. 36).

The IS and CL remained overall annual sources of CO_2 to the atmosphere from 2003 to 2013, except in 2007 when they acted as sinks of atmospheric CO_2. In the sWEC, the annual 11-year average flux value of 0.2 mol C m^{-2} $year^{-1}$ corresponds to annual values ranging from -0.5 to 0.6 mol C m^{-2} $year^{-1}$. The sWEC acted as a sink of atmospheric CO_2 in 2006 and 2007, and as a source of CO_2 to the atmosphere or neutral for the other years. In 2007, in permanently well-mixed systems, a particularly intense spring phytoplankton bloom (data not shown) occurred, which resulted in important CO_2 undersaturation and a CO_2 sink. The CO_2 outgassing during autumn 2007 was one of the lowest observed over the decade

(Fig. 36), due to relatively weak wind speeds at this time (data not shown) and resulting low K values. The association of these two features explained the annual CO_2 sink obtained in 2007. Seasonally stratified systems showed variability in the intensity of annual air-sea CO_2 fluxes but remained sinks of atmospheric pCO_2 over the decade. In addition to the changes of ocean-atmosphere pCO_2 gradient, the wind-dependent gas transfer velocity has a strong influence on air-sea CO_2 fluxes. For example, during autumn 2009, monthly pCO_2 values were in the same range as the other years (Fig. 31) but we observed peaks of CO_2 outgassing in response to more intense monthly wind speeds (> 10 m s^{-1}).

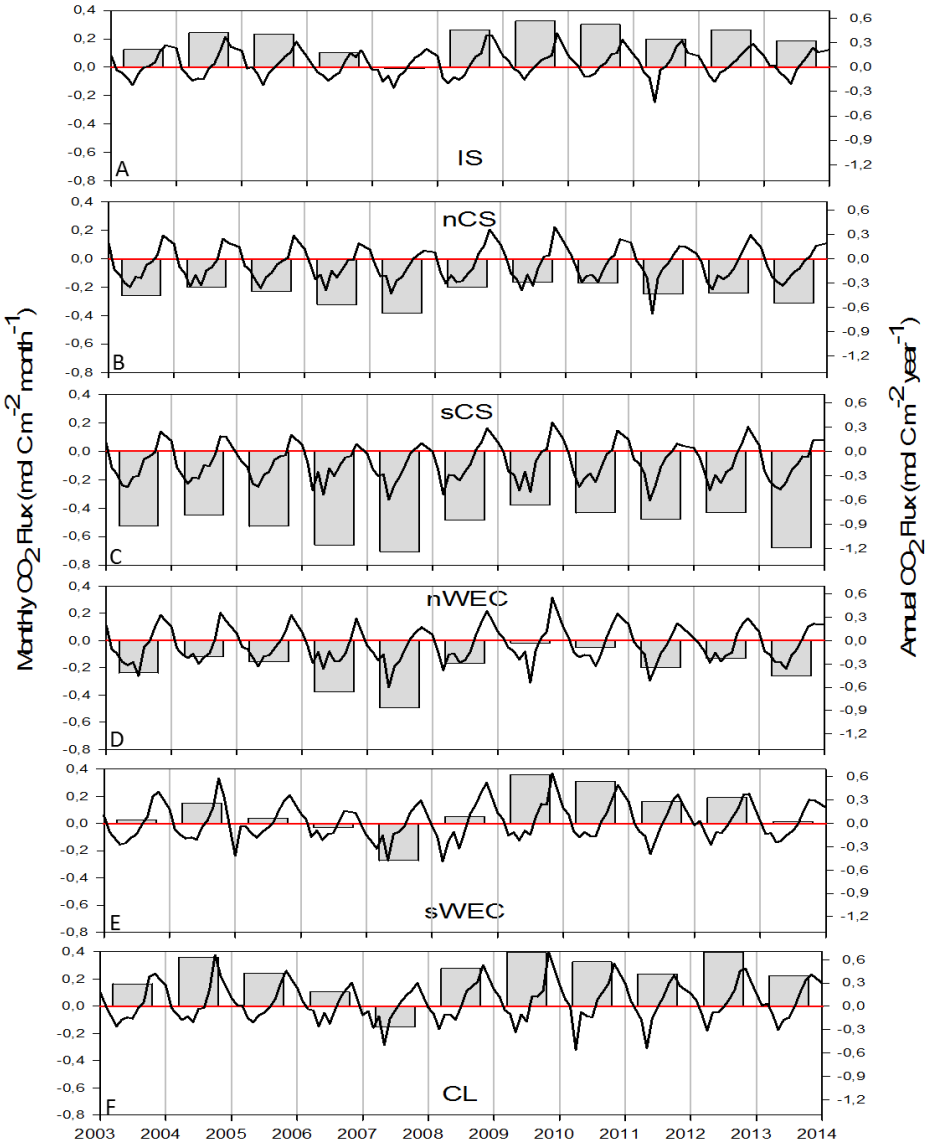


Figure 36: Monthly air-sea CO_2 fluxes (black lines, left hand side Y-axis, mol C m^{-2} $month^{-1}$) computed from $pCO_{2,MLR}$ and using Nightingale et al. (2000) K-wind relationship in IS (A), nCS (B), sCS (C), nWEC (D), sWEC (E) and CL (F) provinces from 2003 to 2013. Negative values indicate CO_2 sink. Integrated annual CO_2 fluxes (vertical grey bars, right hand side y-axis, mol C m^{-2} $year^{-1}$).

As mentioned above in Sect. 4.1., our method precluded establishment of empirical relationships between the variables and pCO_2, and it is therefore difficult to quantitatively and directly interpret the influence of each variable in the pCO_2 simulation. Instead, we computed SST, Chl-*a*, $pCO_{2,MLR}$ and $pCO_{2,atm}$ anomalies from monthly data minus mean values over the decade in the nWEC (Fig. 37). In 2003, 2006 and 2007 we observed strong positive Chl-*a* and SST anomalies during spring (2003 and 2007) and summer (2006). These anomalies suggest a connection between abnormally high SST and biological activity. Strong negative $pCO_{2,MLR}$ anomalies followed positive SST and Chl-*a* anomalies (Fig. 37) and annual fluxes reported for these years reached the lowest values (Fig. 37, Table 11). It confirms that biological activity is one of the main drivers of inter-annual pCO_2 variability and reveals that SST and Chl-*a* are linked in seasonally stratified areas.

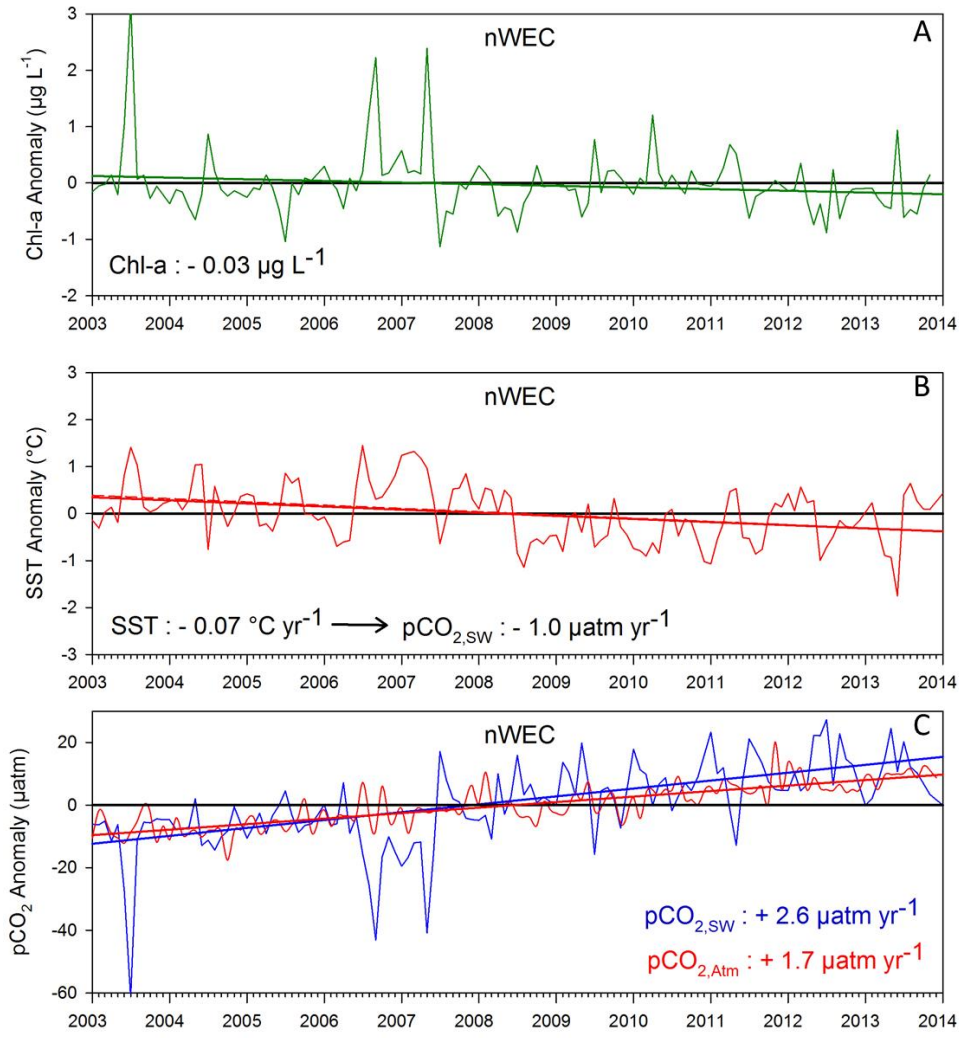


Figure 37: Chl-*a* (A, µg L^{-1}), SST (B, °C), $pCO_{2,MLR}$ and atmospheric pCO_2 (C, in blue and red respectively) anomalies in nWEC from 2003 to 2013. Solid straight lines represent the 10-years trends of each anomalies obtained by linear regression, with corresponding slope values.

Computations of Chl-*a*, SST and pCO_2 anomalies allowed trend analysis of these parameters (Fig. 37). The negative decadal trend for Chl-*a* was biased by the strong positive anomalies observed in 2003, 2006 and 2007 and cannot be considered as relevant. The SST anomaly showed a decrease of 0.07°C per year and 0.73°C from 2003 to 2013. The same trend was also observed in adjacent seas (data not shown). Treguer et al. (2014) reported a SST decrease from 1998 to 2013 in two sites in Western Brittany of -0.01 and -0.02°C $year^{-1}$ while the ARIVO (Analyse, Reconstruction et Indicateur de la Variabilité Océanique) dataset from von Schuckmann et al. (2009), updated by Treguer et al. (2014), reveals a cooling trend for the period 2002-2012, calculating from monthly SST anomalies, in our study area of -0.05 to -0.15 °C $decade^{-1}$. The SST trend we observed from 2003 to 2013 might be biased by the occurrence of a heat wave during summer 2003 and explain the stronger decrease reported in our study compared to those of Treguer et al. (2014) and Von Schuckmann et al. (2009). As mentioned by Treguer et al. (2013), based on Kosaka and Xie (2013), this cooling has recently been corroborated at a planetary scale, including Western Europe. Simultaneously, surface seawater pCO_2 increased by 2.6 ± 0.5 µatm yr^{-1}, while atmospheric pCO_2 rose by 1.7 µatm yr^{-1} (Fig. 37), a similar value to those reported by Thomas et al. (2008) and Le Quéré et al. (2010). The uncertainty of the seawater pCO_2 increase (± 0.5 µatm yr^{-1}) was obtained by addition of random values from the normal distribution with mean 0 and standard deviation of 17 µatm to monthly seawater pCO_2 values. We performed this procedure 10 times on the monthly seawater pCO_2 dataset for the nWEC, which confirmed that the observed increase was significant. The increase of $pCO_{2,MLR}$ was 0.9 µatm yr^{-1} higher than the atmospheric rise. According to Takahashi et al. (1993), a SST decrease of 0.07°C yr^{-1} would lead to a surface seawater pCO_2 decrease of 1.0 µatm yr^{-1}, which is in contradiction with our observations. These results indicate that the increase of seawater pCO_2 from 2003 to 2013 cannot be explained by thermodynamic processes. Metzl et al. (2010) reported similar SST and pCO_2 trends over the North Atlantic Sub-Polar Gyre (NASPG) from 2001 to 2008. They suggested, based on a DIC/TA dataset that these trends were primarily explained by changes in seawater carbonate chemistry and that recent increase of convective processes/vertical mixing in the NASPG may explain these changes. Wind speed is a driver of the vertical mixing of the ocean surface mixed layer. An increase of wind speed would result in stronger vertical mixing. We did not observe any relevant trend concerning wind speed over the decade (data not shown). The north-west European continental shelf is, at a large scale, connected to the eastern boundary current (Arhan et al., 1994) fed by the North Atlantic drift. The observations made by Metzl et al. (2010) in the NASPG might explain the results we obtained in the CS, WEC

and IS, even if biogeochemical processes occurring in such continental shelf ecosystems are not directly comparable to those occurring in the open ocean.

5. Concluding remarks and perspectives

Based on a three-year dataset of pCO_2 measurements acquired on a VOS in the WEC we estimated surface ocean pCO_2 and air-sea CO_2 fluxes in the north-west European continental shelf waters using MLRs from remotely sensed SST, Chl-*a*, PAR and wind speed and from modeled MLD (in the nWEC). We computed surface pCO_2 in the seasonally stratified nWEC and the permanently well-mixed sWEC based on specific MLRs with relative uncertainties of 17 µatm and 16 µatm, respectively. These continental shelf ecosystems are characterized by strong inter-annual variability, thus developing algorithms over three contrasted years was a major benefit for the application of these relationships on a wider temporal scale. In adjacent Celtic and Irish seas, which have similar hydrographical and biogeochemical characteristics as WEC waters, previous pCO_2 observations and air-sea CO_2 flux estimates were very sparse. We thus extrapolated our algorithms spatially to the IS and CS and temporally from 2003 to 2013. We validated these extrapolations with pCO_2 data from the SOCAT database. On an annual scale, seasonally stratified systems acted as a sink of atmospheric of -0.4, -0.9 and -0.4 mol C m^{-2} $year^{-1}$ in the nCS, sCS and nWEC, respectively, whereas, permanently well-mixed systems acted as source of CO_2 to the atmosphere of 0.2, 0.4 and 0.4 mol C m^{-2} $year^{-1}$ in the sWEC, CL and IS, respectively. For the first time, seasonal and long-term dynamics of pCO_2 and associated air-sea CO_2 fluxes over this part of the north-western European continental shelf were evaluated over a decade, despite the relatively high uncertainties inherent to the method. The reconstructed decadal datasets highlighted the importance of multi-annual study of air-sea CO_2 fluxes in continental shelf seas. As mentioned by Keller et al. (2014), it can be difficult to detect relevant trends in the seawater pCO_2 signal, particularly in coastal areas with high inter and intra-annual variability. However, from 2003 to 2013, we observed a significant pCO_2 increase over our study area which was not driven by thermodynamic processes, as a SST cooling was recorded. This pCO_2 increase could not be explained by the concomitant atmospheric increase and we hypothesize that changes in seawater carbonate chemistry might be responsible.

Beaugrand et al. (2000) and Treguer et al. (2013) demonstrated that coastal marine systems of Western Europe are connected to large scale North-Atlantic atmospheric circulation, the North Atlantic Oscillation (NAO), and there is a consensus that these coastal systems are highly sensitive to natural and anthropogenic climate change (Goberville et al. 2010, 2013). Thomas et al. (2008) investigated the influence of the NAO on air-sea CO_2 fluxes in the North Atlantic and suggested that multi-annual variability of the ocean CO_2 system was linked to the NAO phasing. Salt et al. (2013) demonstrated the connection between NAO forcings and pH and CO_2 variability in the North Sea, another shelf sea of the north-western European continental shelf. A similar approach could be applied on our dataset in the future to investigate the possible links between large-scale climatic indices and the multi-annual variability of pCO_2 and air-sea CO_2 on this part of the north-western European continental shelf, which is closely connected to North Atlantic open ocean waters.

References

Arhan, M., Colin de Verdière, A., Mémery, L.: The eastern boundary of the subtropical North Atlantic, J. Phys. Oceanogr., 24, 1295-1316, 1994.

Bakker, D. C. E., Pfeil, B., Smith, K., Hankin, S., Olsen, A., Alin, S. R., Cosca, C., Harasawa, S., Kozyr, A., Nojiri, Y., O'Brien, K. M., Schuster, U., Telszewski, M., Tilbrook, B., Wada, C., Akl, J., Barbero, L., Bates, N. R., Boutin, J., Bozec, Y., Cai, W.-J., Castle, R. D., Chavez, F. P., Chen, L., Chierici, M., Currie, K., de Baar, H. J. W., Evans, W., Feely, R. A., Fransson, A., Gao, Z., Hales, B., Hardman-Mountford, N. J., Hoppema, M., Huang, W.-J., Hunt, C. W., Huss, B., Ichikawa, T., Johannessen, T., Jones, E. M., Jones, S. D., Jutterström, S., Kitidis, V., Körtzinger, A., Landschützer, P., Lauvset, S. K., Lefèvre, N., Manke, A. B., Mathis, J. T., Merlivat, L., Metzl, N., Murata, A., Newberger, T., Omar, A. M., Ono, T., Park, G.-H., Paterson, K., Pierrot, D., Ríos, A. F., Sabine, C. L., Saito, S., Salisbury, J., Sarma, V. V. S. S., Schlitzer, R., Sieger, R., Skjelvan, I., Steinhoff, T., Sullivan, K. F., Sun, H., Sutton, A. J., Suzuki, T., Sweeney, C., Takahashi, T., Tjiputra, J., Tsurushima, N., van Heuven, S. M. A. C., Vandemark, D., Vlahos, P., Wallace, D. W. R., Wanninkhof, R., Watson, A. J.: An update to the Surface Ocean CO_2 Atlas (SOCAT version 2), Earth Sys. Sci. Data, 6, 69-90, doi:10.5194/essd-6-69-2014, 2014.

Bates, N. R., Best, M. H. P., Neely, K., Garley, R., Dickson, A. G., Johnson, R. J.: Detecting anthropogenic carbon dioxide uptake and ocean acidification in the North Atlantic Ocean, Biogeosciences, 9, 2509-2522, doi:10.5194/bg-9-2509-2012, 2012.

Bauer, J. E., Cai, W.-J., Raymond, P. A., Bianchi, T. S., Hopkinson, C. S., Regnier, P. A. G.: The changing carbon cycle of the coastal ocean, Nature, 504, 61-70, doi:10.1038/nature12857, 2013.

Beaugrand, G., Ibanez, F., Reid, P. C.: Spatial, seasonal and long-term fluctuations of plankton in relation to hydroclimatic features in the English Channel, Celtic Sea and Bay of Biscay, Mar. Ecol.-Prog. Ser., 200, 93-102, 2000.

Berger, B. H., Dumas, F., Petton, S., Lazure, P.: Evaluation of the hydrology and dynamics of the operational Mars3d configuration of the bay of Biscay, Mercator Ocean-Quaterly Newsletter, 49, 60-68, 2014.

Boalch, G. T., Harbour, D. S. and Butler, A. I.: Seasonal phytoplankton production in the western English Channel 1964-1974, J. Mar. Biol. Assoc. UK., 58, 943-953, 1978.

Borges, A. V., Delille, B., Frankignoulle, M.: Budgeting sinks and sources of CO_2 in the coastal ocean: Diversity of ecosystems counts, Geophys. Res. Lett., 32, L14601, doi:10.1029/2005GL023053, 2005.

Borges, A. V., Schiettecatte, L.-S., Abril, G., Delille, B., Gazeau, F.: Carbon dioxide in European coastal waters, Estuar. Coast. Shelf S., 70, 375-387. doi:10.1016/j.ecss.2006.05.046, 2006.

Borges, A. V., Gypens, N.: Carbonate chemistry in the coastal zone responds more strongly to eutrophication than to ocean acidification, Limnol. Oceanogr., 55, 1-8, 2010.

Borges, A. V. and Frankignoulle, M.: Distribution of surface carbon dioxide and air-sea exchange in the English Channel and adjacent areas, J. Geophys. Res., 108, 1-14. doi:10.1029/2000JC000571, 2003.

Borges, A. V., Alin, S. R., Chavez, F. P., Vlahos, P., Johnson, K. S., Holt, J. T., Balch, W. M., Bates, N., Brainard, R., Cai, W. J., Chen, C. T. A., Currie, K., Dai, M., Degrandpre, M., Delille, B., Dickson, A., Evans, W., Feely, R. A., Friederich, G. E., Gong, G.-C., Hales, B., Hardman-Mountford, N., Hendee, J., Hernandez-Ayon, J. M., Hood, M., Huertas, E., Hydes, D., Ianson, D., Krasakopoulou, E., Litt, E., Luchetta, A., Mathis, J., McGillis, W. R., Murata, A., Newton, J., Ólafsson, J., Omar, A., Perez, F. F., Sabine, C., Salisbury, J. E., Salm, R., Sarma, V. V. S. S., Schneider, B., Sigler, M., Thomas, H., Turk, D., Vandemark, D., Wanninkhof, R., Ward, B.: A global sea surface carbon observing system: inorganic and organic carbon dynamics in coastal oceans, Proceedings of OceanObs'09: Sustained Ocean Observations and Information for Society (Vol. 2), Venice, Italy, 21-25 September 2009, Hall, J., Harrison, D.E. & Stammer, D., Eds., ESA Publication WPP-306, 2010a.

Borges, A. V., Ruddick, K., Lacroix, G., Nechad, B., Asteroca, R., Rousseau, V., Harlay, J.: Estimating pCO_2 from remote sensing in the Belgian coastal zone, ESA Special Publications, 686, 2-7, 2010b.

Bozec, Y., Thomas, H., Elkalay, K., de Baar, H. J. W.: The continental shelf pump for CO_2 in the North Sea - evidence from summer observation, Mar. Chem., 93, 131-147. doi:10.1016/j.marchem.2004.07.006, 2005.

Bozec, Y., Thomas, H., Schiettecatte, L.-S.: Assessment of the processes controlling seasonal variations of dissolved inorganic carbon in the North Sea, Limnol. Oceanogr., 51, 2746-2762, 2006.

Cai, W.-J.: Estuarine and coastal ocean carbon paradox: CO_2 sinks or sites of terrestrial carbon incineration?, Annu. Rev. Mar. Sci., 3, 123-145, doi:10.1146/annurev-marine-120709-

142723, 2011.

Cai, W.-J., Dai, M., Wang, Y.: Air-sea exchange of carbon dioxide in ocean margins: A province-based synthesis, Geophys. Res. Lett., 33, 1-4, doi:10.1029/2006GL026219, 2006.

Charria, G., Repecaud, M.: PREVIMER: A contribution to in situ coastal observing systems. Mercator Ocean - Quaterly Newsletter, 49, 9-20, 2014.

Chen, C. A., Borges, A. V.: Reconciling opposing views on carbon cycling in the coastal ocean : Continental shelves as sinks and near-shore ecosystems as sources of atmospheric CO_2, Deep-Sea Res. Pt. II, 56, 578-590, doi:10.1016/j.dsr2.2008.12.009, 2009.

Chierici, M., Olsen, A., Johannessen, T., Trinañes, J., Wanninkhof, R.: Algorithms to estimate the carbon dioxide uptake in the northern North Atlantic using shipboard observations, satellite and ocean analysis data, Deep-Sea Res. Pt. II, 56, 630-639, doi:10.1016/j.dsr2.2008.12.014, 2009.

Chierici, M., Signorini, S. R., Mattsdotter-Björk, M., Fransson, A., Olsen, A.: Surface water fCO_2 algorithms for the high-latitude Pacific sector of the Southern Ocean, Remote Sens. Environ., 119, 184-196, doi:10.1016/j.rse.2011.12.020, 2012.

Darecki, M., Weeks, A., Sagan, S., Kowalczuk, P., Kaczmarek, S.: Optical characteristics of two contrasting Case 2 waters and their influence on remote sensing algorithms, Cont. Shelf Res., 23, 237-250, doi:10.1016/S0278-4343(02)00222-4, 2003.

Dickson, A. G. and Millero, F. J.: A comparison of the equilibrium constants for the dissociation of carbonic acid in seawater media, Deep-Sea Res., 34, 1733-1743, 1987.

Dickson, A. G., Sabine, C. L., and Christian, J. R.: Guide to best practices for ocean CO_2 measurements, PICES Special Publication 3, IOCCP report No. 8, 191 pp., 2007.

Dumousseaud, C., Achterberg, E. P., Tyrrell, T., Charalampopoulou, A., Schuster, U., Hartman, M., Hydes, D. J.: Contrasting effects of temperature and winter mixing on the seasonal and inter-annual variability of the carbonate system in the Northeast Atlantic Ocean, Biogeosciences, 7, 1481-1492, doi:10.5194/bg-7-1481-2010, 2010.

Friedrich, T., Oschlies, A.: Neural network-based estimates of North Atlantic surface pCO_2 from satellite data: A methodological study, J. Geophys. Res., 114, 1-12. doi:10.1029/2007JC004646, 2009.

Gattuso, J. P., Frankignoulle, M., Wollast, R.: Carbon and carbonate metabolism in coastal aquatic ecosystems, Annu. Rev. Ecol. Sys., 29, 405-434, 1998.

Gledhill, D. K., Wanninkhof, R., Millero, F. J., Eakin, M.: Ocean acidification of the Greater

Caribbean Region 1996-2006, J. Geophys. Res., 113, 1-11, doi:10.1029/2007JC004629, 2008.

Goberville, E., Beaugrand, G., Edwards, M.: Synchronous response of marine plankton ecosystems to climate in the Northeast Atlantic and the North Sea, J. Marine Syst., 129, 189-202. doi:10.1016/j.jmarsys.2013.05.008, 2014.

Goberville, E., Beaugrand, G., Sautour, B., Tréguer, P., Somlit, T.: Climate-driven changes in coastal marine systems of western Europe, Mar. Ecol.-Prog. Ser., 408, 129-147. doi:10.3354/meps08564, 2010.

Gohin, F., Druon, J. N., Lampert, L.: A five channel chlorophyll concentration algorithm applied to SeaWiFS data processed by SeaDAS in coastal waters, Int. J. Remote Sens., 23, 1639-1661, 2002.

Gowen, R. J., Stewart, B. M.: Regional differences in stratification and its effect on phytoplankton production and biomass in the northwestern Irish Sea, J. Plankton Res., 17, 753-769, 1995.

Groom, S., Martinez-Vicente, V., Fishwick, J., Tilstone, G., Moore, G., Smyth, T., Harbour, D.: The Western English Channel observatory: Optical characteristics of station L4, J. Marine Syst., 77, 278-295, doi:10.1016/j.jmarsys.2007.12.015, 2009.

Hales, B., Strutton, P.G., Saraceno, M., Letelier, R., Takahashi, T., Feely, R., Sabine, C., Chavez, F.: Satellite-based prediction of pCO_2 in coastal waters of the eastern North Pacific, Prog. Oceanogr., 103, 1-15, doi:10.1016/j.pocean.2012.03.001, 2012.

Hickman, A., Moore, C., Sharples, J., Lucas, M., Tilstone, G., Krivtsov, V., Holligan, P.: Primary production and nitrate uptake within the seasonal thermocline of a stratified shelf sea, Mar. Ecol.-Prog. Ser., 463, 39-57, doi:10.3354/meps09836, 2012.

Hill, E., Brown, J., Fernand, L., Holt, J., Horsburgh, K. J., Proctor, R., Raine, R., Turrell, W. R.: Thermohaline circulation of shallow tidal seas, Geophys. Res. Lett., 35, L11605, doi:10.1029/2008GL033459, 2008.

Holligan, P. M.: Biological implications of fronts on the northwest European continental shelf, Philos. T. R. Soc. S-A, 302, 547-562, 1981.

IPCC: Climate Change 2013: The Physical Science Basis. Contribution of Working Group I to the Fifth Assessment Report of the Intergovernmental Panel on Climate Change [Stocker, T.F., D. Qin, G.-K. Plattner, M. Tignor, S.K. Allen, J. Boschung, A. Nauels, Y. Xia, V. Bex and P.M. Midgley (eds.)]. Cambridge University Press, Cambridge, United Kingdom and New York, NY, USA, 1535 pp, 2013.

Jo, Y.-H., Dai, M., Zhai, W., Yan, X.-H., Shang, S.: On the variations of sea surface pCO_2 in

the northern South China Sea: A remote sensing based neural network approach, J. Geophys. Res., 117, 1-13, doi:10.1029/2011JC007745, 2012.

Joint, I. and Groom, S.: Estimation of phytoplankton production from space: current status and future potential of satellite remote sensing, J. Exp. Mar. Biol. Ecol., 250, 233–255, 2000.

Joint, I., Wollast, R., Chou, L., Batten, S., Elskens, M., Edwards, E., Hirst, A., Burkill, P., Groom, S., Gibb, S., Miller, A., Hydes, D., Dehairs, F., Antia, A., Barlow, R., Rees, A., Pomroy, A., Brockmann, U., Cummings, D., Lampitt, R., Loijens, M., Mantoura, F., Miller, P., Raabe, T., Alvarez-Salgado, X., Stelfox, C., Woolfenden, J.: Pelagic production at the Celtic Sea shelf break, Deep-Sea Res. Pt. II, 48, 3049-3081, doi:10.1016/S0967-0645(01)00032-7, 2001.

Kalnay, E., Kanamitsu, M., Kistler, R., Collins, W., Deaven, D., Gandin, L., Iredell, M., Saha, S., White, G., Woollen, J., Zhu, Y., Chelliah, M., Ebisuzaki, W., Higgins, W., Janowlak, J., Mo, K. C., Ropelewski, C., Wang, J., Leetmaa, A., Reynolds, R., Jenne, R., Joseph, D.: The NCEP/NCAR reanalysis project, Bull. Amer. Meteor. Soc., 77, 437-471, 1996.

Keller, K. M., Joos, F., and Raible, C. C.: Time of emergence of trends in ocean biogeochemistry, Biogeosciences, 11, 3647-3659, 2014.

Kitidis, V., Hardman-Mountford, N. J., Litt, E., Brown, I., Cummings, D., Hartman, S., Hydes, D., Fishwick, J. R., Harris, C., Martinez-Vicente, V., Woodward, E. M. S., Smyth, T. J.: Seasonal dynamics of the carbonate system in the Western English Channel, Cont. Shelf Res., 42, 30-40, doi:10.1016/j.csr.2012.04.012, 2012.

Kosaka, Y., Xie, S.-P.: Recent global-warming hiatus tied to equatorial Pacific surface cooling, Nature, 501, 403-407, doi:10.1038/nature12534, 2013.

L'Helguen, S., Madec, C., Le Corre, P.: Nitrogen uptake in permanently well-mixed temperate coastal waters., Estuar. Coast. Shelf S., 42, 803-818, doi:10.1006/ecss.1996.0051, 1996.

Lazure, P. and Dumas, F.: An external–internal mode coupling for a 3D hydrodynamical model for applications at regional scale (MARS), Adv. Water Resour., 31, 233-250, doi:10.1016/j.advwatres.2007.06.010, 2008.

Le Boyer, A., Cambon, G., Daniault, N., Herbette, S., Le Cann, B., Marié, L., Morin, P.: Observations of the Ushant tidal front in September 2007, Cont. Shelf Res., 29, 1026-1037, doi:10.1016/j.csr.2008.12.020, 2009.

Le Quéré, C., Takahashi, T., Buitenhuis, E. T., Rödenbeck, C., Sutherland, S. C.: Impact of climate change and variability on the global oceanic sink of CO_2, Global Biogeochem. Cy., 24, GB4007, doi:10.1029/2009GB003599, 2010.

Le Fèvre, J.: Aspects of the biology of frontal systems, Adv. Mar. Biol., 23, 163-299, 1986.

Lefèvre, N., Aiken, J., Rutllant, J., Daneri, G., Lavender, S., Smyth, T.: Observations of pCO_2 in the coastal upwelling off Chile: Spatial and temporal extrapolation using satellite data, J. Geophys. Res., 107, 8-1, 2002.

Lefèvre, N., Watson, A. J., Watson, A. R.: A comparison of multiple regression and neural network techniques for mapping in situ pCO_2 data, Tellus B, 57, 375-384, 2005.

Liu, K.-K., Atkinson, L., Quinones, R., and Talaue-McManus, L. (eds.): Carbon and Nutrient Fluxes in Continental Margins A Global Synthesis. IGBP Book Series, Springer, Heidelberg, Germany, 744 pp., 2010.

Lohrenz, S. E., Cai, W.-J.: Satellite ocean color assessment of air-sea fluxes of CO_2 in a river-dominated coastal margin, Geophys. Res. Lett., 33, 2-5. doi:10.1029/2005GL023942, 2006.

Marrec, P., Cariou, T., Collin, E., Durand, A., Latimier, M., Macé, E., Morin, P., Raimund, S., Vernet, M., Bozec, Y.: Seasonal and latitudinal variability of the CO_2 system in the western English Channel based on Voluntary Observing Ship (VOS) measurements, Mar. Chem., 155, 29-41, 2013.

Marrec, P., Cariou, T., Latimier, M., Macé, E., Morin, P., Vernet, M., Bozec, Y.: Spatio-temporal dynamics of biogeochemical processes and air–sea CO_2 fluxes in the Western English Channel based on two years of FerryBox deployment, J. Marine Syst., doi:10.1016/j.jmarsys.2014.05.010, 2014.

McClain, C. R.: A decade of satellite ocean color observations, Annu. Rev. Mar. Sci., 1, 19-42, doi:10.1146/annurev.marine.010908.163650, 2009.

McKee, D., Cunningham, A.: Identification and characterisation of two optical water types in the Irish Sea from in situ inherent optical properties and seawater constituents, Estuar. Coast. Shelf S., 68, 305-316, doi:10.1016/j.ecss.2006.02.010, 2006.

McKee, D., Cunningham, A., Dudek, A.: Optical water type discrimination and tuning remote sensing band-ratio algorithms: Application to retrieval of chlorophyll and Kd(490) in the Irish and Celtic Seas, Estuar. Coast. Shelf S., 73, 827-834, doi:10.1016/j.ecss.2007.03.028, 2007.

Mehrbach, C., Culberso, C., Hawley, J. E. and Pytkowic, R. M.: Measurement of apparent dissociation constants of carbonic acid in seawater at atmospheric pressure. Limnol. Oceanogr., 18, 897-907, 1973.

Metzl, N., Corbière, A., Reverdin, G., Lenton, A., Takahashi, T., Olsen, A., Johannessen, T., Pierrot, D., Wanninkhof, R., Ólafsdóttir, S. R., Olafsson, J., Ramonet, M.: Recent

acceleration of the sea surface fCO_2 growth rate in the North Atlantic subpolar gyre (1993-2008) revealed by winter observations, Global Biogeochem. Cy., 24, GB4004, doi:10.1029/2009GB003658, 2010.

Monterey, G. and Levitus, S.: Seasonal variability of mixed layer depth for the world ocean, NOAA Atlas, NESDIS 14, Washington D.C., 96 pp, 1997.

Morel, A., Gentili, B., Chami, M., Ras, J.: Bio-optical properties of high chlorophyll Case 1 waters and of yellow-substance-dominated Case 2 waters, Deep-Sea Res. Pt. I, 53, 1439-1459, doi:10.1016/j.dsr.2006.07.007, 2006.

Morel, A., Prieur, L.: Analysis of variations in ocean color, Limnol. Oceanogr., 22, 709-722, doi:10.4319/lo.1977.22.4.0709, 1977.

Morin, P.: Evolution des éléments nutritifs dans les systems frontaux de l'Iroise: assimilation et regeneration; relation avec les structures hydrologiques et les cycles de développemnt du phytoplankton, PhD thesis in the Univ. Bretagne Occid., 320pp, 1984.

Muller-Karger, F. E., Varela, R., Thunell, R., Luerssen, R., Hu, C., and Walsh J. J.: The importance of continental margins in the global carbon cycle, Geophys. Res. Lett., 32, L01602, doi:10.1029/2004GL021346, 2005.

Nightingale, P. D., Malin, G., Law, C. S., Watson, A. J., Liss, P. S., Liddicoat, M. I., Boutin, J., Upstill-Goddard, R. C.: In situ evaluation of air-sea gas exchange parameterizations using novel conservative and volatile tracers, Global Biogeochem. Cy., 14, 373-387, 2000.

Olsen, A., Triñanes, J., Wanninkhof, R.: Sea–air flux of CO_2 in the Caribbean Sea estimated using in situ and remote sensing data, Remote Sens. Environ., 89, 309-325, doi:10.1016/j.rse.2003.10.011, 2004.

Omar, A. M., Olsen, A., Johannessen, T.: Spatiotemporal variations of fCO_2 in the North Sea, Ocean Sci., 6, 77-89, 2010.

Ono, T., Saino, T., Kurita, N., Sasaki, K.: Basin-scale extrapolation of shipboard pCO_2 data by using satellite SST and Chl a, Int. J. Remote Sens., 25, 3803-3815, 2004.

Padin, X. A., Navarro, G., Gilcoto, M., Rios, A. F., Pérez, F. F.: Estimation of air–sea CO_2 fluxes in the Bay of Biscay based on empirical relationships and remotely sensed observations, J. Marine Syst., 75, 280-289, doi:10.1016/j.jmarsys.2008.10.008, 2009.

Padin, X. A., Vazquezrodriquez, M., Rios, A. F., Perez, F. F.: Surface CO_2 measurements in the English Channel and Southern Bight of North Sea using voluntary observing ships, J. Marine Syst., 66, 297-308, doi:10.1016/j.jmarsys.2006.05.011, 207.

Pemberton, K., Rees, A. P., Miller, P. I., Raine, R., Joint, I.: The influence of water body

characteristics on phytoplankton diversity and production in the Celtic Sea, Cont. Shelf Res., 24, 2011-2028, doi:10.1016/j.csr.2004.07.003, 2004.

Pierrot, D., Lewis, E., and Wallace, D. W. R.: MS Excel Program Developed for CO_2 System Calculations, ORNL/CDIAC-105, Carbon Dioxide Information Analysis Center, Oak Ridge National Laboratory, U.S. Department of Energy, Oak Ridge, Tennessee, 2006.

Pingree, R. D., Pugh, P. R., Holligan, P. M., Forster, G. R., Summer phytoplankton blooms and red tides along tidal fronts in the approaches to the English Channel, Nature, 258, 672-677, 1975.

Pingree, R. D. and Griffiths, D. K.: Tidal fronts on the shelf seas around the British Isles, J. Geophys. Res., 83, 4615-4622, 1978.

Pingree, R. D., Holligan, P. M., Mardell, G. T.: The effects of vertical stability on phytoplankton distributions in the summer on the northwest European Shelf, Deep-Sea Res., 25, 1011-1028, 1978.

Pingree, R. D.: Physical oceanography of the Celtic Sea and the English Channel, In Banner, F. T., Collins, B. and Massie, K. S. (Eds), The Northwest European Shelf Seas: The Sea-bed and the Sea in Motion. Elsevier, Amsterdam, 638 pp, 1980.

Pingree, R. D., Mardell G. T. and Cartwright, D. E.: Slope Turbulence, internal waves and phytoplankton growth at the Celtic Seas shelf-break, Philos. T. R. Soc. S-A, 302, 663-682, 1981.

Rangama, Y., Boutin, J., Etcheto, J., Merlivat, L., Takahashi, T., Delille, B., Frankignoulle, M. and Bakker D. C. E.: Variability of the net air-sea CO_2 flux inferred from shipboard and satellite measurements in the Southern Ocean south of Tasmania and New Zealand, J. Geophys. Res., 110, 1-17, doi:10.1029/2004JC002619, 2005.

Reid, P. C., Auger, C., Chaussepied, M., and Burn, M.: The channel, report on sub-region 9, quality status report of the North Sea 1993 (Eds.), UK Dep. of the Environ., Républ. Fr. Minist. de l'Environ., Inst. Fr. de Rech. Pour l'Exploit. de la Mer, Brest. 153 pp, 1993.

Salisbury, J., Vandemark, D., Hunt, C., Campbell, J., McGillis, W., Mcdowell, W.: Seasonal observations of surface waters in two Gulf of Maine estuary-plume systems: Relationships between watershed attributes, optical measurements and surface pCO_2, Estuar. Coast. Shelf S., 77, 245-252, doi:10.1016/j.ecss.2007.09.033, 2008.

Salt, L. A., Thomas, H., Prowe, A. E. F., Borges, A. V., Bozec, Y., de Baar, H. J. W.: Variability of North Sea pH and CO_2 in response to North Atlantic Oscillation forcing, J. Geophys. Res., 118, 1584-1592, doi:10.1002/2013JG002306, 2013.

Schneider, B., Gustafsson, E., Sadkowiak, B.: Control of the mid-summer net community

production and nitrogen fixation in the central Baltic Sea: An approach based on pCO_2 measurements on a cargo ship, J. Marine Syst., 136, 1-9, doi:10.1016/j.jmarsys.2014.03.007, 2014.

Schneider, B., Kaitala, S., Maunula, P.: Identification and quantification of plankton bloom events in the Baltic Sea by continuous pCO_2 and chlorophyll a measurements on a cargo ship, J. Marine Syst., 59, 238-248, doi:10.1016/j.jmarsys.2005.11.003, 2006.

Shadwick, E. H., Thomas, H., Comeau, A., Craig, S. E., Hunt, C. W., Salisbury, J. E.: Air-Sea CO_2 fluxes on the Scotian Shelf: seasonal to multi-annual variability, Biogeosciences, 7, 3851-3867, doi:10.5194/bg-7-3851-2010, 2010.

Sharples, J., Tweddle, J.F.: Spring-neap modulation of internal tide mixing and vertical nitrate fluxes at a shelf edge in summer, Limnol. Oceanogr., 52, 1735-1747, 2007.

Signorini, S. R., Mannino, A., Najjar, R. G., Friedrichs, M. A. M., Cai, W.-J., Salisbury, J., Wang, Z. A., Thomas, H., Shadwick, E. H.: Surface ocean pCO_2 seasonality and sea-air CO_2 flux estimates for the North American east coast, J. Geophys. Res., 118, 5439-5460. doi:10.1002/jgrc.20369, 2013.

Simpson, J.H., Hunter, J.R.: Fronts in the Irish Sea, Nature, 250, 404-406, 1974.

Simpson, J. H., Crisp, D. J., Hearn, C.: The shelf-sea fronts: Implications of their existence and behavior, Philos. T. R. Soc. S-A, 302, 531-546, 1981.

Smyth, T. J., Fishwick, J. R., AL-Moosawi, L., Cummings, D. G., Harris, C., Kitidis, V., Rees, A., Martinez-Vicente, V., Woodward, E. M. S.: A broad spatio-temporal view of the Western English Channel observatory, J Plankton Res., 32, 585-601. doi:10.1093/plankt/fbp128, 2009.

Sournia, A., Brylinski, J. M., Dallot, S.: Fronts hydrologiques au large des côtes françaises: Les sites-ateliers de programme Frontal, Oceanol. Acta, 13, 413-438, 1990.

Southward, A. J., Langmead, O., Hardman-Mountford, N. J., Aiken, J., Boalch, G. T., Dando, P. R., Genner, M. J., Joint, I., Kendall, M. A., Halliday, N. C., Harris, R. P., Leaper, R., Mieszkowska, N., Pingree, R. D., Richardson, A. J., Sims, D. W., Smith, T., Walne, A. W., Hawkins, S. J.: Long-term oceanographic and ecological research in the Western English Channel, Adv. Mar. Biol., 47, 1-105, 2005.

Takahashi, T., Olafsson, J., Goddard, J. G., Chipman, D. W. and Sutherland, S. C.: Seasonal variation of CO_2 and nutrients in the high-latitude surface ocean - A comparative study, Global Biogeochem. Cy., 7, 843-878, 1993.

Telszewski, M., Chazottes, A., Schuster, U., Watson, A.J., Moulin, C., Bakker, D. C. E., González-Dávila, M., Johannessen, T., Körtzinger, A., Lüger, H., Olsen, A., Omar, A.,

Padin, X. A., Rios, A. F., Steinhoff, T., Santana-Casiano, M., Wallace, D. W. R. and Wanninkhof, R.: Estimating the monthly pCO_2 distribution in the North Atlantic using a self-organizing neural network, Biogeosciences, 6, 1405-1421, 2009.

Thomas, H., Bozec, Y., Elkalay, K., de Baar, H. J. W., 2004. Enhanced open ocean storage of CO_2 from shelf sea pumping, Science, 304, 1005-8, doi:10.1126/science.1095491, 2004.

Thomas, H., Bozec, Y., Elkalay, K., de Baar, H. J. W., Borges, A. V., Schiettecatte, L.-S.: Controls of the surface water partial pressure of CO_2 in the North Sea, Biogeosciences, 2, 323-334, doi:10.5194/bg-2-323-2005, 2005.

Thomas, H., Prowe, F., van Heuven, S., Bozec, Y., de Baar, H. J. W., Schiettecatte, L.-S., Suykens, K., Kone´, M., Borges, A. V., Lima, I. D., Doney, S. C.: Rapid decline of the CO_2 buffering capacity in the North Sea and implications for the North Atlantic Ocean, Global Biogeochem. Cy., 21, GB4001, 2007.

Thomas, H., Prowe, F. E., Lima, I. D., Doney, S. C., Wanninkhof, R., Greatbatch, R. J., Schuster, U., Corbière, A.: Changes in the North Atlantic Oscillation influence CO_2 uptake in the North Atlantic over the past 2 decades, Global Biogeochem. Cy., 22, GB4027, doi:10.1029/2007GB003167, 2008.

Tréguer, P., Goberville, E., Barrier, N., L'Helguen, S., Morin, P., Bozec, Y., Rimmelin-Maury, P., Czamanski, M., Grossteffan, E., Cariou, T., Répécaud, M., Quéméner, L.: Large and local-scale influences on physical and chemical characteristics of coastal waters of Western Europe during winter, J. Marine Syst., 139, 79-90, doi:10.1016/j.jmarsys.2014.05.019, 2014.

Tsunogai, S., Watanabe, S., Sato, T.: Is there a "continental shelf pump" for the absorption of atmospheric CO_2?, Tellus B, 51, 701-712, 1999.

Wafar, M. V. M., Corre, P. L., Birrien, J. L.: Nutrients and primary production in permanently well-mixed temperate coastal waters, Estuar. Coast. Shelf S., 17, 431-446, 1983.

Wallace, R. B., Baumann, H., Grear, J. S., Aller, R. C., Gobler, C. J.: Coastal ocean acidification: The other eutrophication problem, Estuar. Coast. Shelf S., 148, 1-13, doi:10.1016/j.ecss.2014.05.027, 2014.

Walsh, J. J., Rowe, G. T., Iverson, R. L., McRoy, C. P.: Biological export of shelf carbon is a sink of the global CO_2 cycle, Nature, 291, 196-201, 1981.

Walsh, J. J.: Importance of continental margins in the marine biogeochemical cycling of carbon and nitrogen, Nature, 350, 53-55, 1991.

Wanninkhof, R.: Relationship between wind speed and gas exchange over the ocean, J. Geophys. Res., 97, 7373-7382, doi:10.1029/92JC00188, 1992.

Wanninkhof, R., Mcgillis, W. R.: A cubic relationship between air-sea CO_2 exchange and wind speed, Geophys. Res. Lett., 26, 1889–1892, 1999.

Weiss, R.F.: Solubility of nitrogen, oxygen and argon in water and seawater, Deep-Sea Res. 17, 721-735, 1970.

Weiss, R.F., and Price, B.A.: Nitrous oxide solubility in water and seawater, Mar. Chem., 8, 347-359, 1980.

Zeebe R. E. and Wolf-Gladrow, D. A.: CO_2 in seawater: equilibrium, kinetics, isotopes, Elsevier Oceanography Series, 65, Amsterdam, 346 pp., 2001.

Chapter 5: Summary, concluding remarks and perspectives

1. Summary

During my PhD and in this manuscript, I investigated three distinct aspects of the CO_2 system dynamics over the North-West European continental shelf. Firstly, based on three years of bimonthly discrete samplings from a Voluntary Observing Ship, I described and discussed the seasonal and inter-annual biogeochemical variability of the surface waters of the Western English Channel, with a main focus on the CO_2 system and air-sea CO_2 exchanges. Secondly, I presented and assessed the short time-scale dynamics of biogeochemical processes and air-sea CO_2 fluxes in the Western English Channel based on two years of high-frequency measurements from a FerryBox. Finally, I developed algorithms to estimate surface pCO_2 and air-sea CO_2 fluxes from remote sensing and modeled data in the surface waters of the WEC and Adjacent Celtic and Irish Seas over a decade.

1.1 Three years of bimonthly measurements

Based on 1019 surface samples of surface waters between Roscoff and Plymouth, from December 2010 to December 2013, we assessed for the first time the seasonal and latitudinal biogeochemical dynamics and CO_2 system variability in the WEC. We developed an innovative method to precisely delimit the spatial and temporal expanse of the seasonally stratified nWEC and the permanently well-mixed sWEC by combining surface water VOS measurements and hydrographical profiles at fixed stations. The seasonal stratification exerted a strong control on the biogeochemical processes and generally defined the biologically productive period in nWEC waters with a strong control on the CO_2 system dynamics. We revealed that biological production/respiration processes were the main driver of pCO_2 variability from spring to fall and that thermodynamical processes controlled the pCO_2 variability during winter. The most explicit feature of this study was the opposite behavior of seasonally stratified and permanently well-mixed systems regarding air-sea CO_2 fluxes directions. On the one hand, from 2011 to 2013, the nWEC waters acted as sink for atmospheric CO_2 at a rate of -0.4 ± 0.1 mol C m^{-2} y^{-1} and were characterized by enhanced biological activities. On the other hand, the sWEC waters acted as source of CO_2 to the atmosphere at a rate of $+0.5 \pm 0.2$ mol C m^{-2} y^{-1} and were characterized by a shorter and lower

biological productivity period. Both provinces of the WEC were characterized by important inter-annual variability regarding the chronology and/or the intensity of the CO_2 system dynamics during the seasons. However, on an annual scale, air-sea CO_2 fluxes in both provinces preserved their specific directions and remained relatively constant. We performed NEP estimates from DIC budgets and these calculations revealed that surface waters at fixed stations E1 (nWEC) and ASTAN (sWEC) were both autotrophic at rates of 2.4 ± 1.0 mol C m^{-2} y^{-1} and 0.7 ± 0.5 mol C m^{-2} y^{-1}, respectively.

The combined approach comprising bimonthly discrete samples from VOS lines and coastal fixed station observations provided new insights into the control of air-sea CO_2 fluxes in the different provinces of the WEC. I recommend applying this combined approach in other continental shelf systems to study the CO_2 system dynamics. The principal advantage of our approach was to perform regular (bimonthly) measurements of nutrients, TA and DIC, parameters for which automated sensors need to be developed or optimized. Indeed, emerging nutrients sensors still suffer from long-term instabilities and require important maintenance tasks (Petersen et al., 2014) while TA and DIC sensors are still at early stage of development (Aßmann et al. 2011; Aßmann, 2012; Wang et al., 2013).

We still have to unravel some aspects of the CO_2 system dynamic of the WEC such as the processes controlling the variability of surface water alkalinity and the processes leading to the decreases of sea surface salinity in sWEC waters. We could also investigate the CO_2 system dynamics through a Redfieldian approach based on our nutrients dataset and the trophic status of WEC ecosystems using NEP estimates from nitrate and phosphate concentrations (Gazeau et al., 2005; Bozec et al., 2006). In addition to our bimonthly surface dataset between Roscoff and Plymouth, water column measurements of biogeochemical parameters including DIC and TA measurements are performed either side of the WEC since 2007. Water column measurements of DIC/TA and 16 other biogeochemical parameters are performed bi-monthly at ASTAN in the sWEC, as part of the SOMLIT national observation network. The Western Channel Observatory has performed a similar survey at fixed stations E1 and L4 (Kitidis et al., 2012). Besides maintaining on the long-term these coastal carbon observatories in the context of climate change, an integrative study of the biogeochemical dynamics of the WEC on the long term should be possible by coupling VOS surface and water column fixed station datasets. Such an approach could improve considerably the biogeochemical models developed in WEC and adjacent CS and IS waters.

1.2 High frequency measurements

In the second part of this manuscript we combined two years of FerryBox high-frequency measurements between Roscoff and Plymouth, with 9 months of high-frequency pCO_2 data. We described and analyzed the performance of our FerryBox system and its sensors. It was the first deployment of a CONTROS HydroC/CO_2 FT sensor on a FerryBox system reported in the literature. The sensor showed an important drift during the 9 months of deployment, which was evaluated based on our bimonthly pCO_2 data computed from DIC/TA. In 2012, due to technical issues we could not have access to the automated electronic zero values, which normally allows to follow any potential drift of the sensor. Thus, we considered a linear drift between each bimonthly transect based on our computed pCO_2. In 2013, we had access to the automated zero values during the second deployment of the CONTROS HydroC CO_2/FT sensor, which allowed us to follow the "electronic" drift of the sensor. However, when comparing these zero values to the drift observed using the pCO_2 calculated from bimonthly DIC/TA measurements, we found that these drifts were not similar. Thus, the potential advantage of the regular "zeroing" of the sensor to obtain a better estimate of the inherent drift was not useful. We still have to understand the reasons of these discrepancies in collaboration with the manufacturer in order to optimize such deployment. However, with a bimonthly survey of the drift of the sensor from pCO_2 (DIC/TA) measurements, the calibration of the sensor was still feasible, considering a linear drift between two consecutive crossings. This approach might induce additional uncertainties on the pCO_2 signal.

Our high-frequency data allowed us to investigate the dynamics of biogeochemical processes related to air-sea CO_2 fluxes in the WEC on a shorter time-scale than in the bimonthly survey. We used the same method as in Chapter 2, based on SST anomalies to divide the WEC into seasonally stratified nWEC and all-year well-mixed sWEC. We also observed that these hydrographical properties strongly influenced the spatial and inter-annual distributions of phytoplankton blooms. Based on our dataset, we demonstrated that the biological productivity was mainly limited by nutrients and light availability in the nWEC and the sWEC, respectively. We described with an unprecedented definition the short time-scale biogeochemical dynamics of WEC surface waters, particularly in July and early August 2012

by extracting FerryBox and ancillary data in the vicinity of ASTAN and E1 fixed stations. In sWEC waters, the short time-scale approach showed the influence of tidal cycles (neap tide/spring tide) on Chl-*a*, DO% and pCO_2. During the neap tides the tidal current were weaker and thus favoured phytoplankton development in the more stable water column, with a mean difference in pCO_2 values between spring and neap tides of +50 µatm. In nWEC waters, we observed the start and the development of an intense summer bloom in 2012. We recorded extreme DO% increase and pCO_2 drawdown and we quantified that this 10 days event accounted for 29% of the CO_2 sink during the productive period (from May to mid-September). In our bimonthly approach we also captured this brief event, thus our seasonal and annual flux estimates based on bimonthly data were not impacted by an unfortunate omission of the intense CO_2 sink. However, such event highlights the necessity of high frequency observations in coastal ecosystems.

In addition to the key features provided by the short time-scale processes occurring in WEC waters, an extraction of day/night data at 49.90°N (nWEC) allowed a first estimate of the impact of diel production/respiration processes on DO% and pCO_2 variability. The mean day-night differences accounted for 16% of the mean CO_2 sink during the 5 months of the study period, implying that the diel biological cycle was also significant for air-sea CO_2 flux computations. The impact of biological diel cycle on air-sea CO_2 fluxes from FerryBox measurements is only a first estimate. Since April 2014, we have installed a new pCO_2 sensor (SAMI-pCO_2) on an autonomous mooring at the ASTAN fixed station. The high-frequency pCO_2 records from this mooring will reveal the influence of the tidal cycles on pCO_2 variability and potentially provide us a more accurate estimate of the diurnal cycle of the CO_2 system in sWEC waters. The combination of moored buoy and FerryBox measurements will allow an even more detailed survey of the short time-scale variability of pCO_2 and air-sea CO_2 exchanges in the highly dynamic WEC. It will help us to better apprehend the processes controlling the CO_2 signal from diurnal to inter-annual time-scale and thus give us the essential background to attempt modeling the future response of coastal seas under climate change.

1.3 Development of pCO_2 algorithms and air-sea CO_2 flux in WEC, CS and IS over a decade

Finally, we intended to extend in time and space surface pCO_2 observations and evaluate air-sea CO_2 fluxes by predicting pCO_2 from remote-sensing and modeled data. We developed algorithms linking our surface pCO_2 to remotely sensed sea surface temperature (SST), chlorophyll-a concentrations (Chl-*a*), the gas transfer velocity coefficient (K), photosynthetically active radiation (PAR) and modeled mixed layer depth (MLD). We established specific relationships between our three years pCO_2 dataset and these environmental variables, using multiple linear regressions, for the seasonally stratified nWEC and the permanently well-mixed sWEC waters. We obtained relative uncertainties of 17 µatm and 16 µatm for monthly surface pCO_2 estimates in nWEC and sWEC, respectively. We extrapolated the relations obtained in WEC based on the 2011-2013 dataset 1) temporally over a decade (2003-2013) and 2) spatially in the adjacent Celtic and Irish Seas (CS and IS), two regions which present similar hydrographical and biogeochemical properties to WEC waters. Since a decade, considerable efforts have been made to compile open ocean and coastal pCO_2 data by the Surface Ocean CO_2 ATlas (SOCAT). We used available SOCAT pCO_2 data in our study area to validate these extrapolations and obtained relatively robust results considering time scale discrepancies between SOCAT and monthly predicted pCO_2 data.

Based on these promising results, we retrieved monthly surface pCO_2 estimates for this part of the North-West European continental shelf over a decade. According to our computations, seasonally stratified systems acted as a sink of atmospheric of -0.4, -0.9 and -0.4 mol C m^{-2} $year^{-1}$ in nCS, sCS and nWEC, respectively, whereas, permanently well-mixed systems acted as source of CO_2 to the atmosphere of +0.2, +0.4 and +0.4 mol C m^{-2} $year^{-1}$ in sWEC, CL and IS, respectively. Regarding the lack of such estimates before our study in CS, IS and to a lesser extend WEC, the results can considerably improve estimates of spatial and temporal variability of air-sea CO_2 exchanges in these coastal seas. Air-sea CO_2 fluxes showed important inter-annual variability resulting in significant differences in the intensity and/or direction of annual fluxes with biological activity, SST and wind speed as main drivers. From 2003 to 2013, we observed a pCO_2 increase of +2.6 ± 0.5 µatm yr^{-1}, higher than the atmospheric increase of +1.9 µatm yr^{-1}, concomitant with a SST cooling of -0.07°C yr^{-1}

recorded over our study area. We hypothesize that changes in seawater carbonate chemistry might be responsible for this observed pCO_2 increase. However, as mentioned by Keller et al. (2014), the study of long-term trend over a decade can be difficult to detect relevant climatologic trends on the seawater pCO_2 signal, particularly in coastal areas with high inter and intra-annual variability.

The relative uncertainty of pCO_2 computed from remote sensing and modeled data is rather high but the results obtained are promising. This approach is cost effective (in money and time) and offers an excellent coverage. The amount of surface *in-situ* pCO_2 data grows exponentially and these data are now easily available on data portals as SOCAT to develop and validate algorithms. In the future, we could apply our method to the entire North-West European continental shelf, with an adequate division of the shelf area in representative biogeochemical provinces and by developing specific algorithms in each province. For example, the western part of the continental shelf off Ireland and Scotland (Outer Hebrides) are poorly documented in terms of air-sea CO_2 fluxes. We could extend our method to these areas by relying on the *in-situ* data of the CO_2 system currently acquired during seasonal cruises within the CANDYFLOSS project (NERC, collaboration SBR/NOCS).

We tested a specific ocean color algorithm (OC5, Gohin et al., 2002) to estimate surface Chl-*a* over our study area, but this algorithm was too specific to surface waters influenced by river plumes and inadequate to open shelf waters. We chose to use the OC3 algorithms developed in open ocean waters, which gave satisfactory results for most seasons but overestimated Chl-*a* concentrations in winter, particularly in well-mixed sWEC and IS waters. The use of remotely sensed techniques in coastal system is more complex that in the open ocean due to the optically complex coastal waters (suspended matter and color dissolved organic matter). The improvement of ocean color products will certainly reduce uncertainties of this method in coastal waters.

1.4 Conclusion

From tidal to multi-annual variability, from a fixed station off Roscoff to the North-West European continental shelf and from seawater samples to satellite data, this PhD thesis provides an integrative overview of the complexity of the CO_2 system dynamics in coastal seas and the ongoing challenges to achieve. A multi-scale approach is essential to constrain past, present and future exchanges and fates of the inorganic carbon in coastal systems. The combination of autonomous platforms, discrete samplings and remotely-sensed data is a relevant illustration of the upcoming progress that will be made in coastal biogeochemistry thanks to the innovations in observational capabilities.

2. Concluding Remarks and Perspectives

2.1 Time-scale discrepancies and other uncertainties of the CO_2 system in coastal seas

Recent global synthesis of air-sea CO_2 fluxes in the coastal ocean compiled worldwide measurements of pCO_2 and annual flux estimates (Cai et al., 2006; Chen and Borges, 2008; Cai, 2011; Laruelle et al., 2010). These surveys provided essential CO_2 exchange rates for global carbon budget analysis. Most of the annual estimates reported were based on seasonal oceanographic surveys, which provided snapshots of the ocean at a given time. However, coastal ecosystems are characterized by intense biogeochemical and air-sea CO_2 exchange variability from tidal to inter-annual time scales. Thus, the inadequate representation of the full range of temporal variability can impact the overall net annual air-sea CO_2 fluxes. In our study, we investigated the variability of the CO_2 system from daily to inter-annual time scales. Figures 38 and 39 illustrate the different time-scales we used in this study. From the 5th of June to the 10th of August 2012, we represented the distribution of surface pCO_2 and air-sea CO_2 fluxes based on high-frequency FerryBox measurements, bimonthly samplings and monthly mean pCO_2 used for the algorithms development. Figure 40 shows the same datasets extracted at the vicinity of fixed station E1 and ASTAN and Table 12 reports the monthly air-sea CO_2 flux estimates in July 2012 obtained from the different approaches. At E1 and ASTAN, we obtained mean monthly air-sea CO_2 flux estimates of -6.8 ± 1.2 mmol C m^{-2} d^{-1} and -0.1 ± 0.5 mmol C m^{-2} d^{-1}, respectively, with the different time-scale approaches. For E1 we report an uncertainty of 18% of the monthly estimate whereas at ASTAN we find opposite flux directions depending on the method used. These examples illustrate the potential impact of the temporal resolution on air-sea CO_2 flux computations. Moreover, our study of high-frequency pCO_2 variability (Chapter 3), which quantified that a brief (10 days) and intense summer phytoplankton bloom accounted for 29% of the CO_2 sink recorded during the productive period, highlighted the importance of a multi-temporal scale approach.

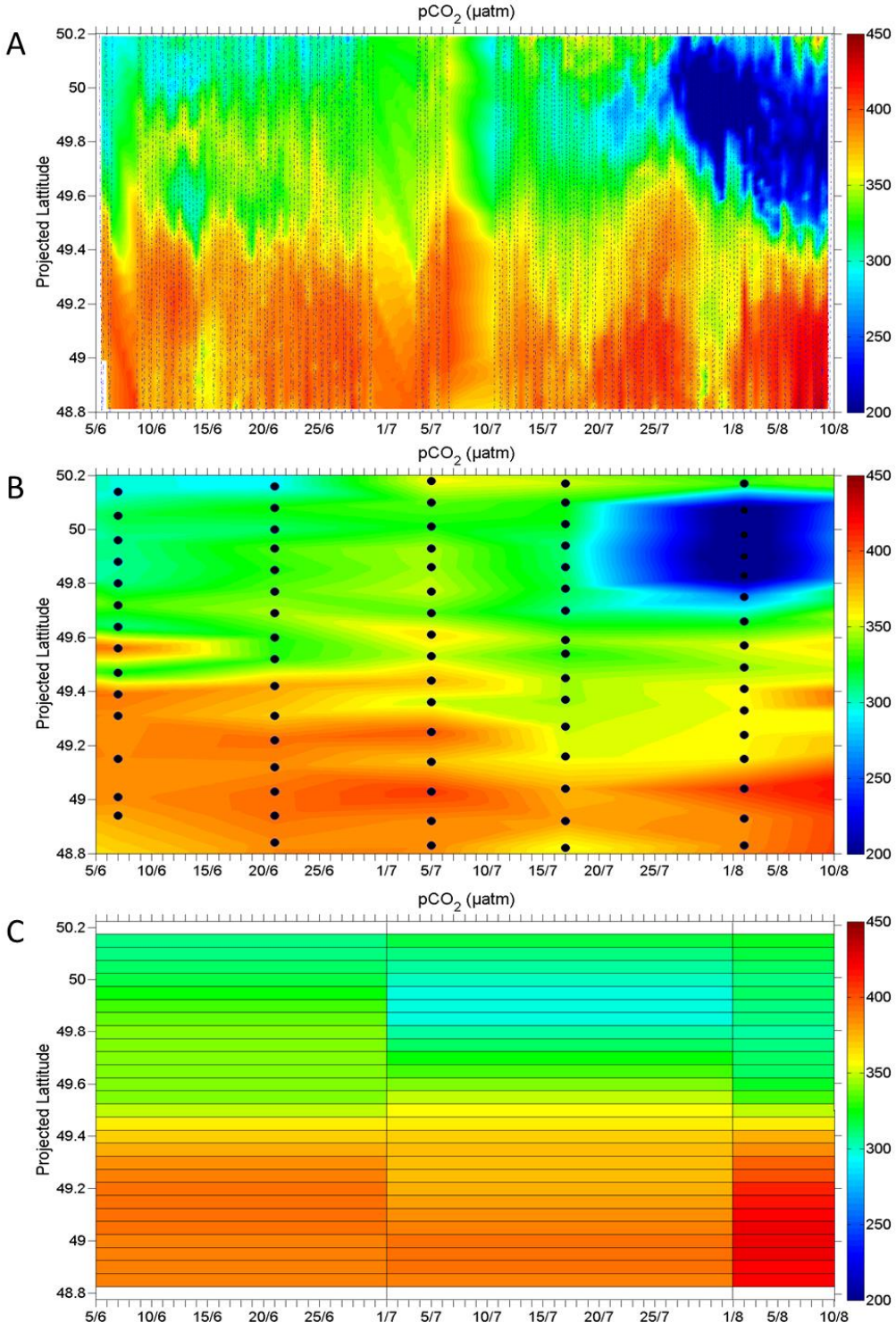


Figure 38: Distribution of surface pCO_2 (µatm) from the 5th of June 2012 to the 10th of August 2012 between Roscoff and Plymouth based on (A) high-frequency FerryBox pCO_2 measurements, (B) bimonthly DIC/TA discrete samplings and (C) monthly mean of high-frequency FerryBox measurements (data used in Chapter 4).

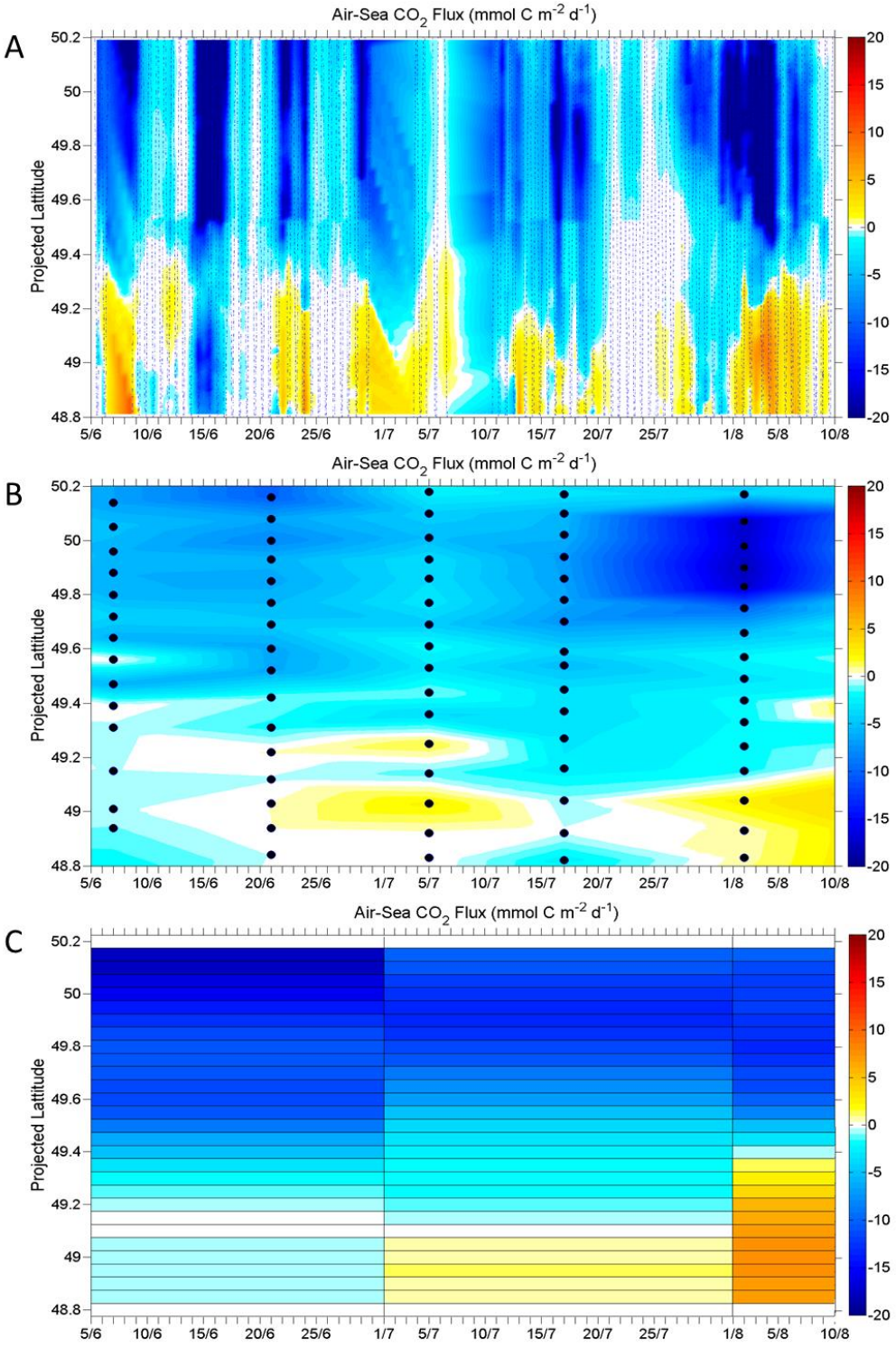


Figure 39: Distribution of surface air-sea CO_2 fluxes (mmol C m^{-2} d^{-1}) from the 5th of June 2012 to the 10th of August 2012 between Roscoff and Plymouth based on (A) high-frequency FerryBox pCO_2 measurements, (B) bimonthly pCO_2 and (C) monthly mean of high-frequency FerryBox pCO_2 measurements. The fluxes were computed using the algorithm given by Nightingale et al. (2000) with NCEP daily (A), two-weeks (centered on the date of each crossing) daily average (B) and monthly (C) wind speeds.

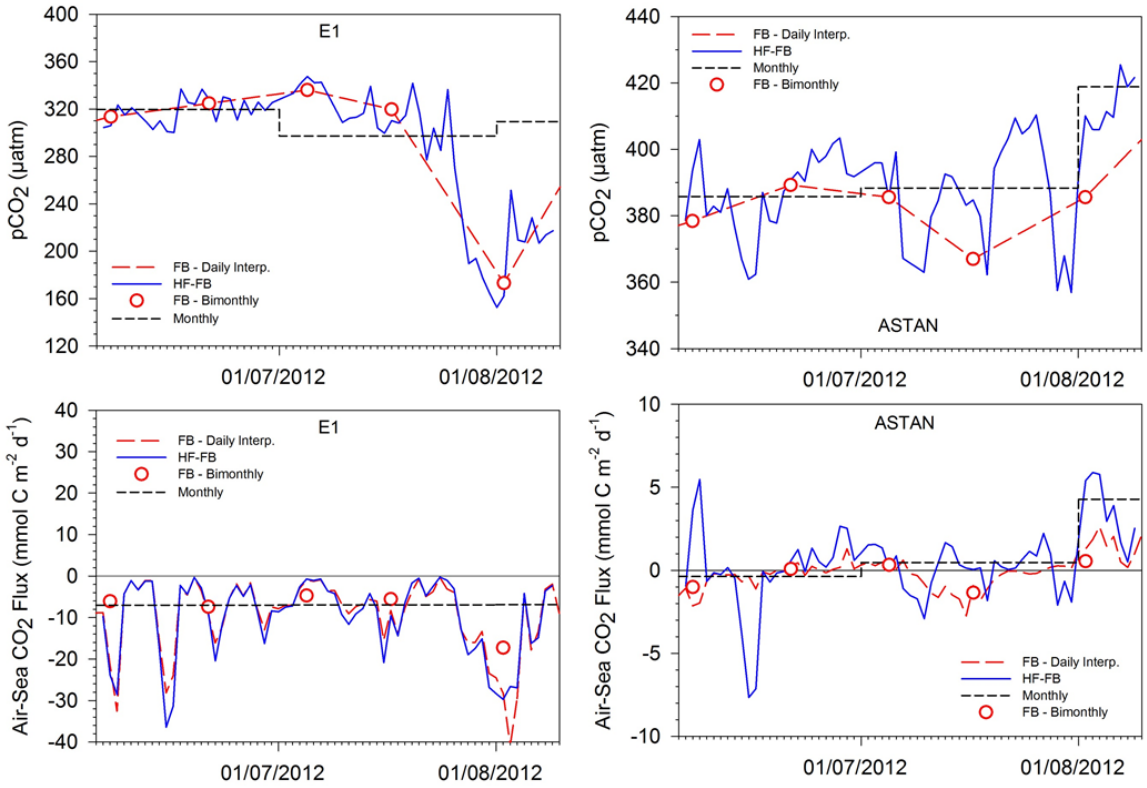


Figure 40: pCO_2 (in µatm) and calculated air-sea CO_2 fluxes (in mmol C m^{-2} d^{-1}) in the vicinity of E1 (49.90°N-50.10°N) and ASTAN (48.80°N-49.00°N) fixed station at different time-scales. Blue lines represent high-frequency FerryBox (HF-FB) pCO_2 measurements and air-sea CO_2 fluxes computed from daily wind speeds. Red circles represent pCO_2 calculated from bimonthly DIC/TA discrete samplings and air-sea CO_2 fluxes calculated from two-weeks (centered on the date of each crossing) daily average wind speeds (FB-Bimonthly). Long-dashed red lines represent the daily-interpolated pCO_2 from bimonthly samplings and the associated fluxes computed from these daily pCO_2 values and from daily wind speeds. Dashed black lines are the monthly average pCO_2 values and associated fluxes computed from monthly wind speeds (as in Chapter 4).

	HF	FB -Daily interp	FB Bimonthly	Monthly
E1	-7,8	-7,2	-5,1	-6,9
ASTAN	0,1	-0,4	-0,5	0,5

Table 10: Air-sea CO_2 fluxes (in mmol C m^{-2} d^{-1}) in the vicinity of E1 and ASTAN at different time-scales in July 2012. HF are the fluxes based on high-frequency FerryBox pCO_2 measurements, FB-DailyInterp are fluxes calculated from daily-interpolated bimonthly pCO_2 values and from daily wind speeds, FB-Bimonthly are fluxes computed from bimonthly pCO_2(DIC/TA) measurements and from two-weeks (centered on the date of each crossing) daily average wind speeds, and Monthly correspond to fluxes calculated from monthly mean pCO_2 and monthly wind speed. We used the gas transfer parametrization of Nightingale et al. (2000).

In addition to the uncertainties induced by the temporal resolution on air-sea CO_2 flux computations, a major and well documented source of error of air-sea CO_2 exchange is attributed to the parametrization of the gas transfer velocity (Wanninkhof et al., 2009, for a review). Many algorithms have been developed to determined gas transfer velocity as a function of wind speed. The last revisited algorithm given by Wanninkhof (2014) reported an associated uncertainty of 20% of this parametrization. Figure 41 illustrates a comparative study of the impact of different gas transfer velocity parametrizations on air-sea CO_2 fluxes from June to August 2012 based on high-frequency pCO_2 measurements and Table 13 reports the different monthly mean flux values. Based on all the parametrizations for July 2012, we obtained a mean CO_2 sink of -9.0 ± 1.8 mmol C m^{-2} d^{-1}, corresponding to a mean uncertainty of 20% depending on the choice of the parametrization. Another source of errors to consider for the flux computations is the source of the wind speed data and their space and time distributions (Boutin et al., 2002; Naegler et al., 2006). In this study, we used four-time daily to monthly wind speed data retrieved from the NCEP products. The spatial resolution of these wind speeds was perhaps not the most suitable for our coastal study but we chose to keep a certain consistency along the manuscript. Furthermore, gas transfer cannot be adequately quantified with wind speed alone. Surfactant films, bubble entrainment, breaking waves, rain, boundary layer stability or friction velocity can also affect gas transfer processes. All these sources of air-sea CO_2 flux uncertainties emphasize the need for accurate parameterizations. A rigorous uncertainty analysis of air-sea CO_2 exchanges is challenging because of the multiple sources of uncertainty of these individual components including surface pCO_2 measurements.

K parametrization	Air-Sea CO_2 Flux July 2012 (mmol C m^{-2} d^{-1})
Nightingale et al. (2000)	-7,82
Wanninkhof et al. (1992)	-11,27
Wanninkhof et McGillis (1999)	-6,19
Sweeney et al. (2007)	-9,81
Ho et al. (2006)	-9,67
Wanninkhof (2014)	-9,12

Table 11: Air-sea CO_2 fluxes (in mmol C m^{-2} d^{-1}) comptuted from HF-FB pCO_2 measurements in July 2012 in the vicinity of E1 using different gas transfer parametrizations.

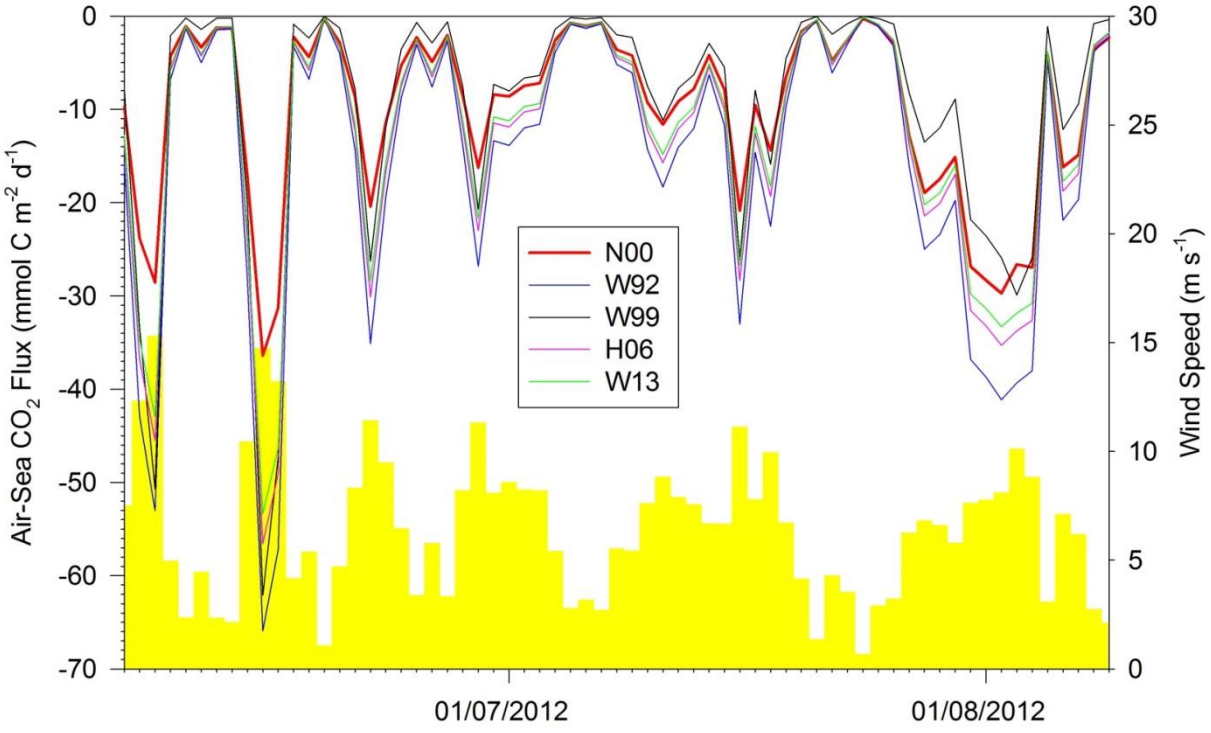


Figure 41: Air-sea CO_2 fluxes (in mmol C m^{-2} d^{-1}, left axis) calculated from high-frequency FerryBox pCO_2 measurements in the vicinity of E1 fixed station from the 5th of June 2012 to the 10th of August 2012 using different gas transfer velocity parametrizations. N00 (in red) refers to Nightingale et al. (2000) parametrization, W92 (in blue) to Wanninkhof et al. (1992), W99 (in black) to Wanninkhof & McGillis (1999), H06 (in pink) to Ho et al. (2006) and W13 to Wanninkhof (2013). The yellow bars represent daily NCEP wind speeds (in m s^{-1}, right axis).

The pCO_2 values presented in this study were all based from DIC and TA measurements, as the high-frequency FerryBox pCO_2 values were calibrated from discrete measurements. The use of the DIC/TA pair for pCO_2 calculation induced an internal consistency of 6 µatm according to Zeebe and Wolf-Gladrow (2001), with analytical accuracies of ± 4 µmol kg^{-1} and ± 2 µmol kg^{-1} for TA and DIC, respectively. However, alkalinity measurements in coastal waters and in waters with high biological activity are subject to discrepancies due to the contribution of organic matter to alkalinity (Cai et al., 1998; Hernandez-Ayon et al., 2007; Muller and Bleie, 2008; Kim and Lee, 2009; Koeve et al., 2012; Hoppe et al., 2012). As organic alkalinity is not considered in the current thermodynamic model for the CO_2 system calculations, this organic contribution would result in errors in the calculated pCO_2. The use of different parametrizations of dissociation constants also yields different results in the CO_2 system calculation (Wanninkhof et al., 1999; Lee et al., 2000), particularly in coastal waters (Hydes et al., 2010; Salt, 2014). I would

recommend to overdetermine the CO_2 system by measuring ideally more than two carbonate variables or preferably pH instead of TA, in order to unravel the CO_2 system dynamics in coastal ecosystems. Furthermore, as recommended by Borges et al. (2010), I suggest adapting standard operating procedures (SOP) and quality control (QC) protocols of CO_2 measurements, which are well established for open ocean, to coastal waters.

2.2 Towards global coastal carbon observatories

In this thesis we argued that there is currently a necessity to better understand the present day spatial and temporal variability of the CO_2 system in coastal ecosystems. Our approach, which studied the multi-faceted dynamics of the CO_2 system in the WEC and by extension in the western part of the North-West European continental shelf, partially fitted the current scientific objectives for a sustained coastal inorganic carbon observational network (Borges et al., 2010; Ciais et al., 2014).

The main challenge would be the construction of an intensive, integrated, international and interdisciplinary global coastal carbon observatory. A particular attention should be given to dramatically under-sampled continental shelves mostly in the southern hemisphere and the Artic regions. The recent technological advances, including new sensors, platforms, computing and modelling capabilities should help to develop such an observatory.

Key features for the development of coastal carbon observatories

Coastal fixed stations

Many coastal fixed stations are operated by research institutes to measure common biogeochemical parameters and more recently CO_2 system parameters. Repeated discrete sampling over the water column (i.e. ASTAN, E1, L4) or autonomous moored buoy equipped with pCO_2 sensors (i.e. MAREL buoy off Brest, ASTAN buoy) provide essential time-series from hourly (MAREL) (Bozec et al., 2011) to monthly (E1) time-scales. As shown in Chapter 2, it is particularly important to carefully select fixed stations representative of wider

biogeochemical provinces in order to, for example, avoid aliasing due to slowing moving fronts. Water column measurements of CO_2 system parameters afford fundamental process details, particularly in stratified ecosystems. However, the maintenance of such repeated survey requires lots of material (Ships, CTD, Niskin bottles) and human resources and therefore consequent and continuous funding. Moorings are the most valuable and cost-effective tools to provide information on the high-frequency variability of pCO_2. Major advances are and will be achieved with emerging sensor technology for DIC and TA, optimization of current pCO_2 sensors, progresses in bio-fouling resistance and improvement of power supply.

Oceanographic surveys

Global estimates of air-sea CO_2 fluxes for continental shelves and most of the historical observational data came from oceanographic surveys performed by research vessels. Research cruises are insofar the only method to investigate the vertical and basin-wide distribution of DIC variables and relevant physical, biological and chemical processes over the full water column in continental shelves. Furthermore, with such cruises, it is also possible to investigate smaller scale processes as those occurring along frontal structures or continental slopes, sites characterized by enhanced and intense biogeochemical processes. Despite a rather poor temporal resolution and higher costs, this kind of surveys must be maintained on multi-annual and decadal time-scales to study the long-term CO_2 system dynamics on full basin scale, and global carbon flows.

Voluntary Observing Ships

The exploitation of voluntary observing ships (VOS) presents numerous advantages in term of costs, energy supply, sheltered conditions and maintenance. In marginal seas, regular VOS lines cruise the same track with frequent time steps, which allow following the variability of the marine environment over short time scales with a wide spatial coverage. I demonstrated in Chapter 3 the promising abilities of our FerryBox system to provide an excellent survey of the pCO_2 and ancillary data variability in the WEC with a temporal resolution lower than one day. Currently, efforts are being made to develop pH, TA and DIC sensors for FerryBox systems (Petersen et al., 2014), and to optimize existing pCO_2 sensors in

order to completely constrain the CO_2 system. Furthermore, platforms of opportunity, as FerryBoxes, are ideal to integrate other innovative sensors (nutrients, flow cytometers, fast repetition rate fluorometers …) due to their protected environment and easy access for maintenance. However, according to our recent experience in FerryBox, long-term deployments are challenging in terms of maintenance and long-term funding, thus I encourage the scientific community to continue their efforts in terms of sustained funding towards VOS expansion.

Remote sensing approaches

The development of algorithms to predict surface pCO_2 from remote sensing data (Chl-*a*, SST, PAR …) is a suitable approach to extend pCO_2 observations and evaluate air-sea CO_2 fluxes. This technique has been successfully applied in the open ocean (Lefèvre et al., 2002; Ono et al., 2004; Olsen et al., 2004; Rangama et al. 2005; Gleidhill et al., 2008; Padin et al., 2009; Chierici et al., 2009, 2012) with uncertainties of the predicted pCO_2 lower than 10 µatm. Such method is more challenging to apply in continental shelf areas because of higher temporal and spatial variability of biogeochemical processes than in open oceans. In Chapter 4 we assessed the monthly pCO_2 variability over a decade in the western part of the North-West European continental shelf. Remotely sensed pCO_2 estimates proved to be relevant method for extrapolating surface carbon observations over wider spatial and temporal scales. Improvements in remote sensing products in coastal waters are an essential requirement to enhance the extrapolation of surface pCO_2 due to the complex optical properties of continental shelf waters. More complex neural networks and self-organizing maps techniques have also been used with promising achievements in the open ocean (Lefèvre et al., 2005; Telszewski et al. 2009; Friedrich and Oschlies, 2009) and have been applied in coastal waters (Hales et al., 2012; Jo et al., 2012). These techniques, which classified coastal areas into biogeochemical provinces, can improve the algorithms to predict surface pCO_2 from remote sensing data. Such methods could be tested over the North-West European continental shelf.

Modelization

Based on the previous recommendations and on the ongoing advances in modelling, coupled physical and biogeochemical models in coastal seas (reviewed in Moisan, 2010)

would certainly gain substantial robustness. However, models for continental shelf systems are particularly difficult to develop because local, regional and global scales come together all at the level of continental shelf systems (Hofmann et al., 2011). The prospective complete CO_2 system dataset resulting from the development of such coastal carbon observatories similar to the one used in this thesis at global scale would allow efficiently forcing and validating models. These models are outstanding tools for extrapolating data to larger time scales and forecasting the response of the coastal ecosystems to future climate change and anthropogenic forcings.

The recent and future technological advances and an adequate strategy in terms of data archiving, management and synthesis will considerably contribute to a better understanding of the coastal carbon cycle and to develop an integrated global coastal observatory. Our recommendations are mainly focused on inorganic carbon. Similar recommendations are applicable to the study of organic carbon dynamics in order to completely constrain the coastal carbon cycle. Global coastal carbon observatories should also further consider the land-to-sea continuum (Regnier et al, 2013), from terrestrial systems watersheds to rivers, to coastal systems and to the open oceans, then overpass the traditional field or disciplinary limitations and eliminate conventionally defined subsystem boundaries. The ongoing progresses arising from such observatories require continuous efforts and funding, estimated around 50 million US dollars per years by Borges et al. (2010).

2.3 Long-term time series and climate change

The coastal oceans are vulnerable to anthropogenic forcings (climate change, eutrophication, ocean acidification, land-use modification …) (Harley et al., 2006) and particularly the carbon cycle due to the intensity of organic and inorganic carbon fluxes. In this context, the development of a global coastal carbon observatory will provide a deeper understanding of present biogeochemical processes impacting the CO_2 system in order to better predict the future changes of the ocean. Impacts of climate oscillations (NAO, SAM, ENSO, …) on air-sea CO_2 fluxes and CO_2 system dynamics are still poorly documented in

coastal ecosystems (Thomas et al., 2008; Salt et al., 2013) due to the lack of long-term time series.

The coastal oceans support a disproportional biological activity compared to their surface, and have a major economic and social interest (fisheries, touristic activity, ecosystem diversity, surrounding population density …), which represent 13 trillion dollars worth of services annually (Constanza et al., 1997). Beyond the CO_2 system, the development of integrated coastal observatories surveying long-term physical, biological and chemical variability must be supported. It would provide critical evidence of the vulnerability of these ecosystems caused by anthropogenic activities, make the policymakers and the population aware of the perturbations threatening coastal seas and allow assessing and mitigating the potential impacts of climate change in coastal marine ecosystems.

References

Aßmann, S., 2012. Entwicklung und Qualifizierung autonomer Messsysteme für den pHWert und die Gesamtalkalinität von Meerwasser. Dissertation Kiel University, Kiel, Germany.

Aßmann, S., Frank, C., Kötzinger, A., 2011. Spectrophotometric high-precision seawater pH determination for use in underway measuring systems. Ocean Science Discussion 8(3), 1339–1367.

Borges, A. V., Alin, S. R., Chavez, F. P., Vlahos, P., Johnson, K. S., Holt, J. T., Balch, W. M., Bates, N., Brainard, R., Cai, W. J., Chen, C. T. A., Currie, K., Dai, M., Degrandpre, M., Delille, B., Dickson, A., Evans, W., Feely, R. A., Friederich, G. E., Gong, G.-C., Hales, B., Hardman-Mountford, N., Hendee, J., Hernandez-Ayon, J. M., Hood, M., Huertas, E., Hydes, D., Ianson, D., Krasakopoulou, E., Litt, E., Luchetta, A., Mathis, J., McGillis, W. R., Murata, A., Newton, J., Ólafsson, J., Omar, A., Perez, F. F., Sabine, C., Salisbury, J. E., Salm, R., Sarma, V. V. S. S., Schneider, B., Sigler, M., Thomas, H., Turk, D., Vandemark, D., Wanninkhof, R., Ward, B., 2010. A global sea surface carbon observing system: inorganic and organic carbon dynamics in coastal oceans. Proceedings of OceanObs'09: Sustained Ocean Observations and Information for Society (Vol. 2), Venice, Italy, 21-25 September 2009, Hall, J., Harrison, D.E. & Stammer, D., Eds., ESA Publication WPP-306.

Boutin, J., Etcheto, J., Merlivat, L., Rangama, Y., 2002. Influence of gas exchange coefficient parameterisation on seasonal and regional variability of CO_2 air-sea fluxes. Geophysical Research Letters 29(8), 1182.

Bozec, Y., Thomas, H., Schiettecatte, L., Borges, A. V., Elkalay, K., de Baar, H. J. W., 2006. Assessment of the processes controlling seasonal variations of dissolved inorganic carbon in the North Sea. Limnology and Oceanography 51(6), 2746–2762.

Bozec, Y., Merlivat, L., Baudoux, A-C., Beaumont, L., Blain, S., Bucciarelli, E., Danguy, T., Grossteffan, E., Guillot, A., Guillou, J., Répécaud, M., Tréguer, P., 2011. Diurnal to inter-annual dynamics of pCO_2 recorded by a CARIOCA sensor in a temperate coastal ecosystem (2003–2009). Marine Chemistry 126, 13–26.

Cai, W. -J., Wang, Y., Hodson, R., 1998. Acid-base properties of dissolved organic matter in the estuarine waters of Georgia, USA. Geochimica et Cosmochimica Acta 62(3), 473–483.

Cai, W.-J., Dai, M., Wang, Y., 2006. Air-sea exchange of carbon dioxide in ocean margins: A

province-based synthesis. Geophysical Research Letters 33, L12603.

Cai, W.-J., 2011. Estuarine and Coastal Ocean Carbon Paradox: CO_2 Sinks or Sites of Terrestrial Carbon Incineration. Annual Review of Marine Science 3, 123–145.

Chen, C.A., Borges, A.V., 2009. Reconciling opposing views on carbon cycling in the coastal ocean : Continental shelves as sinks and near-shore ecosystems as sources of atmospheric CO_2. Deep Sea Research Part II: Topical Studies in Oceanography 56, 578–590.

Chierici, M., Olsen, A., Johannessen, T., Trinanes, J., Wanninkhof, R., 2009. Algorithms to estimate the carbon dioxide uptake in the northern North Atlantic using shipboard observations, satellite and ocean analysis data. Deep Sea Research Part II: Topical Studies in Oceanography 56, 630–639.

Chierici, M., Signorini, S. R., Mattsdotter-Björk, M., Fransson, A., Olsen, A., 2012. Surface water fCO_2 algorithms for the high-latitude Pacific sector of the Southern Ocean. Remote Sensing of Environment 119, 184–196.

Ciais, P., Dolman, A. J., Bombelli, A., Duren, R., Peregon, A., Rayner, P. J., Miller, C., Gobron, N., Kinderman, G., Marland, G., Gruber, N., Chevallier, F., Andres, R. J., Balsamo, G., Bopp, L., Bréon, F.-M., Broquet, G., Dargaville, R., Battin, T. J., Borges, A., Bovensmann, H., Buchwitz, M., Butler, J., Canadell, J. G., Cook, R. B., DeFries, R., Engelen, R., Gurney, K. R., Heinze, C., Heimann, M., Held, A., Henry, M., Law, B., Luyssaert, S., Miller, J., Moriyama, T., Moulin, C., Myneni, R. B., Nussli, C., Obersteiner, M., Ojima, D., Pan, Y., Paris, J.-D., Piao, S. L., Poulter, B., Plummer, S., Quegan, S., Raymond, P., Reichstein, M., Rivier, L., Sabine, C., Schimel, D., Tarasova, O., Valentini, R., Wang, R., van der Werf, G., Wickland, D., Williams, M., Zehner, C., 2014. Current systematic carbon-cycle observations and the need for implementing a policy-relevant carbon observing system. Biogeosciences 11, 3547–3602.

Costanza, R., d'Arge, R., De Groot, R., Farber, S., Grasso, M., Hannon, B., Limburg, K., Naeem, S., O'neill, R. V., Paruelo, J., 1997. The value of the world's ecosystem services and natural capital. Nature 387, 253-260.

Friedrich, T., Oschlies, A., 2009. Neural network-based estimates of North Atlantic surface pCO_2 from satellite data: A methodological study. Journal of Geophysical Research 114, C03020.

Gazeau, F., Borges, A. V., Barrón, C., Duarte, C. M., Iversen, N., Middelburg, J. J., Delille, B., Pizay, M. D., Frankignoulle, M., Gattuso, J. P., 2005. Net ecosystem metabolism in a micro-tidal estuary (Randers Fjord, Denmark): evaluation of methods. Marine Ecology

Progress Series 301, 23–41.

Gledhill, D. K., Wanninkhof, R., Millero, F. J., Eakin, M., 2008. Ocean acidification of the Greater Caribbean Region 1996–2006. Journal of Geophysical Research 113, C10031.

Gohin, F., Druon, J., Lampert, L., 2002. A five channel chlorophyll concentration algorithm applied to SeaWiFS data processed by SeaDAS in coastal waters. International Journal of Remote Sensing 23(8), 1639–1661.

Hales, B., Strutton, P. G., Saraceno, M., Letelier, R., Takahashi, T., Feely, R., Sabine, C., Chavez, F., 2012. Satellite-based prediction of pCO_2 in coastal waters of the eastern North Pacific. Progress in Oceanography 103, 1–15.

Harley, C., Hughes, A. R., Hultgren, K. M., Miner, B. G., Sorte, C. J. B., Thornber, C. S., Rodriguez, L. F., Tomanek, L., Williams, S. L., 2006. The impacts of climate change in coastal marine systems. Ecology Letters 9, 228-241.

Hernández-Ayon, J. M., Zirino, A., Dickson, A. G., Camiro-Vargas, T., Valenzuela, E., 2007. Estimating the contribution of organic bases from microalgae to the titration alkalinity in coastal seawaters. Limnology and Oceanography: Methods 5, 225–232.

Hofmann, E. E., Cahill, B., Fennel, K., Friedrichs, M. A. M., Hyde, K., Lee, C., Mannino, A., Najjar, R. G., O'Reilly, J. E., Wilkin, J., Xue, J., 2011. Modeling the dynamics of continental shelf carbon. Annual review of marine science 3, 93–122.

Hoppe, C. J. M., Langer, G., Rokitta, S. D., Wolf-Gladrow, D. A., Rost, B., 2012. Implications of observed inconsistencies in carbonate chemistry measurements for ocean acidification studies. Biogeosciences 9, 2401–2405.

Hydes, D., Loucaides, S., Tyrrell, T., 2010. Report on a desk study to identify likely sources of error in the measurements of carbonate system parameters and related calculations, particularly with respect to coastal waters and ocean acidification experiments. Supplement to DEFRA contract ME4133 "DEFRApH monitoring project". Southampton, UK, National Oceanography Centre Southampton, 53pp. (National Oceanography Centre Southampton Research and Consultancy Report, 83).

Jo, Y.-H., Dai, M., Zhai, W., Yan, X.-H., Shang, S., 2012. On the variations of sea surface p CO_2 in the northern South China Sea: A remote sensing based neural network approach. Journal of Geophysical Research 117, C08022.

Keller, K. M., Joos, F., and Raible, C. C., 2014. Time of emergence of trends in ocean biogeochemistry. Biogeosciences 11, 3647-3659.

Kim, H.-C., Lee, K., 2009. Significant contribution of dissolved organic matter to seawater alkalinity. Geophysical Research Letters 36, L20603.

Kitidis, V., Hardman-Mountford, N. J., Litt, E., Brown, I., Cummings, D., Hartman, S., Hydes, D., Fishwick, J. R., Harris, C., Martinez-Vicente, V., Woodward, E. M. S., Smyth, T. J., 2012. Seasonal dynamics of the carbonate system in the Western English Channel. Continental Shelf Research 42, 30–40.

Koeve, W., Oschlies, A., 2012. Potential impact of DOM accumulation on fCO_2 and carbonate ion computations in ocean acidification experiments. Biogeosciences 9, 3787–3798.

Laruelle, G. G., Dürr, H. H., Slomp, C. P., Borges, A. V., 2010. Evaluation of sinks and sources of CO_2 in the global coastal ocean using a spatially-explicit typology of estuaries and continental shelves. Geophysical Research Letters 37, L15607.

Lee, K., Millero, F., Byrne, R., 2000. The recommended dissociation constants for carbonic acid in seawater. Geophysical Research Letters 27(2), 229–232.

Lefèvre, N., Aiken, J., Rutllant, J., Daneri, G., Lavender, S., Smyth, T., 2002. Observations of pCO_2 in the coastal upwelling off Chile: Spatial and temporal extrapolation using satellite data. Journal of Geophysical Research 107, C6,3055.

Lefèvre, N., Watson, A. J., Watson, A. R., 2005. A comparison of multiple regression and neural network techniques for mapping in situ pCO_2 data. Tellus B 57, 375–384.

Moisan, J. R., 2010. Coupled circulation/biogeochemical models to estimate carbon flux. See Liu, K. K., Atkinson, L., Quinones, R., Talaue-McManus, L., 2010, pp. 539-58.

Muller, F. L. L., Bleie, B., 2008. Estimating the organic acid contribution to coastal seawater alkalinity by potentiometric titrations in a closed cell. Analytica Chimica Acta 619, 183–91.

Naegler, T., Ciais, P., Rodgers, K., Levin, I., 2006. Excess radiocarbon constraints on air-sea gas exchange and the uptake of CO_2 by the oceans. Geophysical Research Letters 33, L11802.

Olsen, A., Triñanes, J. A., Wanninkhof, R., 2004. Sea–air flux of CO_2 in the Caribbean Sea estimated using in situ and remote sensing data. Remote Sensing of Environment 89, 309–325.

Ono, T., Saino, T., Kurita, N., Sasaki, K., 2004. Basin-scale extrapolation of shipboard pCO_2 data by using satellite SST and Chl-*a*. International Journal of Remote Sensing 25 (19), 3803–3815.

Padin, X. A., Navarro, G., Gilcoto, M., Rios, A. F., Pérez, F. F., 2009. Estimation of air–sea CO_2 fluxes in the Bay of Biscay based on empirical relationships and remotely sensed observations. Journal of Marine Systems 75, 280–289.

Petersen, W., 2014. FerryBox systems: State-of-the-art in Europe and future development.

Journal of Marine Systems, in press.

Rangama, Y., Boutin, J., Etcheto, J., Merlivat, L., Takahashi, T., Delille, B., Frankignoulle, M., Bakker, D. C. E., 2005. Variability of the net air–sea CO_2 flux inferred from shipboard and satellite measurements in the Southern Ocean south of Tasmania and New Zealand. Journal of Geophysical Research 110, C09005.

Regnier, P., Friedlingstein, P., Ciais, P., Mackenzie, F. T., Gruber, N., Janssens, I. A., Laruelle, G. G., Lauerwald, R., Luyssaert, S., Andersson, A. J., Arndt, S., Arnosti, C., Borges, A. V., Dale, A. W., Gallego-Sala, A., Goddéris, Y., Goossens, N., Hartmann, J., Heinze, C., Ilyina, T., Joos, F., LaRowe, D. E., Leifeld, J., Meysman, F. J. R., Munhoven, G., Raymond, P. A., Spahni, R., Suntharalingam, P., Thullner, M., 2013. Anthropogenic perturbation of the carbon fluxes from land to ocean. Nature Geoscience 6, 597–607.

Salt, L. A., Thomas, H., Prowe, A. E. F., Borges, A. V., Bozec, Y., de Baar, H. J. W., 2013. Variability of North Sea pH and CO_2 in response to North Atlantic Oscillation forcing. Journal of Geophysical Research: Biogeosciences 118, 1-9.

Salt, L. A., 2014. Process studies of the carbonate system in coastal and ocean environments of the Atlantic Ocean. PhD Thesis.

Telszewski, M., Chazottes, A., Schuster, U., Watson, A., Moulin, C., Bakker, D., González-Dávila, M., Johannessen, T., Körtzinger, A., Lüger, H., Olsen, A., Omar, A., Padin, X. A., Rios, A. F., Streinhoff, T., Santana-Casiano, M., Wallace, D. W. R., Wanninkhof, R., 2009. Estimating the monthly pCO_2 distribution in the North Atlantic using a self-organizing neural network. Biogeosciences 6, 1405–1421.

Thomas, H., Friederike Prowe, A. E., Lima, I. D., Doney, S. C., Wanninkhof, R., Greatbatch, R. J., Schuster, U., Corbière, A., 2008. Changes in the North Atlantic Oscillation influence CO_2 uptake in the North Atlantic over the past 2 decades. Global Biogeochemical Cycles 22, GB4027.

Wang, Z. A., Chu, S. N., Hoering, K. A., 2013. High-frequency spectrophotometric measurements of total dissolved inorganic carbon in seawater. Environmental Sciences Technology 47, 7840–7847.

Wanninkhof, R., Lewis, E., Feely, R. A., Millero, F. J., 1999. The optimal carbonate dissociation constants for determining surface water pCO_2 from alkalinity and total inorganic carbon. Marine Chemistry 65, 291–301.

Wanninkhof, R., Asher, W.E., Ho, D.T., Sweeney, C., McGillis, W.R., 2009. Advances in quantifying air-sea gas exchange and environmental forcing. Annual review of marine science 1, 213–44.

Wanninkhof, R., 2014. Relationship between wind speed and gas exchange over the ocean revisited. Limnology and Oceanography: Methods 12, 351–362.

Zeebe R. E. and Wolf-Gladrow, D. A., 2001. CO_2 in seawater: equilibrium, kinetics, isotopes, Elsevier Oceanography Series 65, Amsterdam, 346 pp.

Remerciements

CV and bibliography of author



Pierre Marrec

PhD Student in Oceanography
Biological Station of Roscoff, Marine Chemistry Team
4 Place Georges Teissier
29280 Roscoff, France

07/09/1988
French
☎ 0033298292317
pmarrec@sb-roscoff.fr

PhD Details

- *PhD title:* Spatio-temporal dynamics of the carbonate system and air-sea CO_2 fluxes in the English Channel/North Atlantic continental shelf.
- *Host institute:* Biological Station of Roscoff, UMR71144 CNRS/UPMC, Marine Chemistry Team.
- *University:* UPMC, Paris VI, Ecole doctorale des Sciences de l'Environnement d'Ile de France (ED129).
- *PhD advisor:* Dr Pascal Morin — *Co-advisor:* Dr Yann Bozec
- *Start of the PhD:* 1st of October 2011 — *End of the PhD:* 31st of December 2014

Education

- Master's Degree in Chemistry of Marine Environments (2009-2011), European Institute of Marine Studies (IUEM), Plouzané, Brest, France.
- Licence of Chemistry (2006-2009), University of Brest (UBO), France.

Publications

- **P. Marrec**, T. Cariou, E. Collin, A. Durand, M. Latimier, E. Macé, P. Morin, S. Raimund, M. Vernet, Y. Bozec. *Seasonal and latitudinal variability of the CO_2 system in the western English Channel based on Voluntary Observing Ship (VOS) measurements.* 2013, Marine Chemistry, 155, 29-41.
- **P. Marrec**, T. Cariou, M. Latimier, E. Macé, P. Morin, M. Vernet, Y. Bozec. *Spatio-temporal dynamics of biogeochemical processes and air-sea CO_2 fluxes in the Western English Channel based on two years of FerryBox deployment.* Accepted, Journal of Marine System, FerryBox Special Issue.
- **P. Marrec**, T. Cariou, E. Macé, P. Morin, K. Paxman, L. Salt, M. Vernet, Y. Bozec. *Dynamics of pCO2 and air-sea CO2 fluxes in the North-West European Shelf based on Voluntary Observing Ship (VOS) and satellite datasets.*. Submited in Biogeoscience.

Conferences – Oral and Poster Presentations

- *Dynamics of air-sea CO_2 fluxes based on FerryBox measurements and satellite-based prediction of pCO_2 in the Western English Channel.* EGU2014, BG3.1. session, Vienna, Austria, 27 Apr.–02 May 2014. Oral presentation.
- *Spatio-temporal dynamics of air-sea CO_2 fluxes in the Western English Channel (WEC) based on FerryBox measurments.* Ocean Fluxes Greenhouse Gazes Science ESA-EGU-SOLAS International Workshop, Plouzané, France. Sept. 2013. Poster.
- *Spatio-temporal dynamics of air-sea CO_2 fluxes in the Western English Channel (WEC) based on FerryBox measurments.* 6th Internationnal SOLAS Summer School, Xiamen, China. Aug. 23–Sept. 2, 2013. Poster and oral communication (selected for a registration and travel grant).
- *Spatio-temporal dynamics of biogeochemical parameters and air-sea CO_2 fluxes in the Western English Channel (WEC) based on Voluntary Observing Ship (VOS) measurements with a FerryBox system.* 5th FerryBox Workshop, Celebrating 20 Years of Alg@line, Finnish Environment Institute (SYKE), Helsinki, Finland. Apr. 24-25, 2013. Poster.
- *Times-series analysis of the CO_2 dynamics in the Western English Channel using Voluntary Observing Ships (VOS).* Time-series analysis in marine science and application for industry, Logonna-Daoulas, France. Sept. 17-21, 2012. Poster (selected for a registration grant).

Field Experience

- *2011-2014:* More than 50 crossings between Roscoff (France), Plymouth (UK) and Cork (Ireland) on Voluntary Observing Ships to collect biogeochemical samples for my PhD thesis and to calibrate the FerryBox sensors.
- *2011-2014:* Bimonthly samplings for the Roscoff Coastal Observatory (SOMLIT)
- *2011-2012:* 3 CARBORHONE Cruises (10 days each) in the Gulf of Lion (Mediterranean Sea, France) to study the dynamics of air-sea CO_2 fluxes in the Rhone plume.
- *Apr. 2011:* Scientific cruise (10 days) in South Tasmania coastal seas. Bio-optical and Chl-*a* measurements.

Educational Research Experience

- *January-June 2011:* Work placement in the University of Technology, Sydney (UTS) in the Climate Change Cluster (C3) on the synthesis of the bio-optical properties of the Tasman Sea.
- *January-February 2010:* Work placement of 2 months in the European Institute of Marine Studies (IUEM) in Plouzané, on the analysis of trace metal in seawater by mass spectrometry (ICP-MS).

Liste of figures

Figure 1: Compilation of CO_2 records in air trapped in sea ice cores from Antarctica and temperature anomaly over the past 800 kyr adapted from Lüthi et al. (2008). .....- 3 -

Figure 2: Evolution of the atmospheric CO_2 during the last 2000 years in ppm from the Law Dome (Antarctica) ice core and firn air records adapted from MacFarling Meure et al. (2006). .....- 4 -

Figure 3: CO_2 emissions trajectories and atmospheric CO_2 concentrations from historical data (black lines) and four of the RCPs for the 21st century (colored lines), adapted from Doney et al. (2014). .....- 5 -

Figure 4: Simplified schematic of the global carbon cycle (IPCC, 2013). Numbers represent carbon stocks in Pg C and annual carbon exchange fluxes in Pg C yr^{-1}. Black numbers and arrows indicate carbon stocks and exchange fluxes estimated for the time prior to the Industrial Era. Red arrows and numbers indicate annual "anthropogenic" fluxes averaged over the 2000-2009 time period. .....- 6 -

Figure 5: Regulation of natural atmospheric CO_2 changes by the ocean by the solubility pumps, the organic carbon pump and the $CaCO_3$ counter pump (from IPCC, 2007). .....- 8 -

Figure 6: Effect of various processes on the carbonate system parameters (from Zeebe and Wolf-Gladrow, 2001). .....- 14 -

Figure 7: Map and bathymetry of the study area with the locations of the 1019 stations sampled along the 57 Ferry transects from January 2011 to December 2013 and location of the fixed stations ASTAN, E1 and L4. .....- 31 -

Figure 8: Surface distribution from January 2011 to December 2013 of (A) temperature (°C), (B) salinity, (C) DO% and (D) Chl-a (µg L^{-1}) in the WEC between Roscoff and Plymouth. Vertical black lines indicate the onset of the breakdown of thermal stratification at fixed station E1 and horizontal black lines represent an estimate of the location of the thermal front (Figure 4). .....- 38 -

Figure 9: Profiles of temperature (left) and salinity (right) from January 2011 to December 2013 at fixed stations ASTAN, E1 and L4. - 40 -

Figure 10: (A) Difference between the surface temperature and the temperatures recorded along the CTD profiles (dTMP, in °C) at the fixed station E1 from January 2011 to December 2013. (B) SST anomalies (dSST, in °C) from the difference between SST and mean SST for each Roscoff-Plymouth bimonthly transect. (C) Surface distribution from January 2011 to December 2013 of air-sea CO_2 fluxes (in mmol C m^{-2} d^{-1}) computed with the Nightingale et al. (2000) k-wind parametrization. Vertical black lines indicate the onset of the breakdown of thermal stratification at fixed station E1 and horizontal black lines represent an estimate of the location of the thermal front. The horizontal dotted line indicates the latitudinal location of fixed station E1. - 43 -

Figure 11: Surface distribution from January 2011 to December 2013 of (A) NO_3^-, (B) NO_2^-, (C) PO_4^{3-} and (D) SiO_4^- concentration (µmol L^{-1}) in the WEC between Roscoff and Plymouth. Vertical black lines indicate the onset of the breakdown of thermal stratification at fixed station E1 and horizontal black lines represent an estimate of the location of the thermal front (Figure 4). - 45 -

Figure 12: Surface distribution from January 2011 to December 2013 of (A) DIC (in µmol kg^{-1}), (B) TA (in µmol kg^{-1}), (C) pCO_2 (in µatm) and (D) normalized TA after Friis et al. (2003) (in µmol kg^{-1}) in the WEC between Roscoff and Plymouth. Vertical black lines indicate the onset of the breakdown of thermal stratification at fixed station E1 and horizontal black lines represent an estimate of the location of the thermal front (Figure 4). - 48 -

Figure 13: Surface distribution from January 2011 to December 2013 of (A) pH on the total scale, (B) the calcite Ω_{Ca} and (C) aragonite Ω_{Ar} saturation state in the WEC between Roscoff and Plymouth. Vertical black lines indicate the onset of the breakdown of thermal stratification at fixed station E1 and horizontal black lines represent an estimate of the location of the thermal front (Figure 4). - 50 -

Figure 14: Variations of pCO_2 (filled red circles and red lines), $pCO_{2,nontherm}$ (green lines) and $pCO_{2,therm}$ (blue lines) in nWEC (A, 49.40°N-50.20°N) and sWEC (B, 48.80°N-49.40°N) computed after normalization of pCO_2 to the annual mean temperature ($pCO_{2,non\text{-}therm}$) and after Takahashi et al. (1993) ($pCO_{2,therm}$) from January

2011 to December 2013 (in µatm). The black lines represent the atmospheric pCO_2 ($pCO_{2\ atm}$). The red error bars represent the standard error of mean surface water pCO_2 over each province. .....- 55 -

Figure 15: Calculated air-sea CO_2 fluxes (in mmol C m^{-2} d^{-1}) from January 2011 to December 2013, using the algorithm given by Nightingale et al. (2000), in nWEC (yellow bars, 49.40°N-50.20°N) and in sWEC (green bars,48.80°N-49.40°N). Error bars represent the standard deviation of mean fluxes obtained over each province. .....- 57 -

Figure 16: Estimated net ecosystem production (NEP in mmol C m^{-2} d^{-1}, blue circles) and air-sea CO_2 fluxes (in mmol C m^{-2} d^{-1}, red squares) computed using the gas transfer velocity parameterization given by Nightingale et al. (2000) in the vicinity of ASTAN (48.90°N-49.10°N) and E1 (49.80°N-50.00°N) from January 2011 to December 2013. ....- 61 -

Figure 17: Map and bathymetry of the study area with the tracks of all crossings made in 2012 (2013 are not shown for the clarity of the figure) between Roscoff (France) and Plymouth (UK). The locations of fixed stations E1 and L4 (Western Channel Observatory), and ASTAN (coastal observatory SOMLIT) are also indicated.....- 76 -

Figure 18: Adjustment of high frequency data of (A) SSS, (B) DO, (C) Chl-a and (D) pCO_2 based on bimonthly discrete measurements. For SSS and DO, top plots show the discrete measurements versus corrected sensor values. For Chl-a, the top plot shows the discrete measurements versus fluorescence in relative fluorescence units (RFU) and, during the third deployment, versus fluorescence data converted into Chl-a concentration by the C3 software. For pCO_2, top plot shows the differences between pCO_2 data from the HydroC/CO_2 FT sensor before correction and pCO_2 calculated from DIC/TA discrete measurements (µatm) during the deployment of the sensor. Bottom plots show differences between sensor values and discrete measurements over time. Dashed lines represent standard deviation of the differences between sensor values and discrete measurements whereas dotted lines represent three times the standard deviation.....- 81 -

Figure 19: Surface distributions of (a) SST (°C), (b) SSS, (c) SST anomaly (°C), (d) Chl-a (µg L^{-1}) and (e) DO% in the WEC between Roscoff and Plymouth for the years 2011 and 2012. On Figure 3c, the horizontal black lines represent an estimate of the location

of the thermal front; the vertical black lines approximately delimit the period when stratification occurred in the northern WEC. .....- 86 -

Figure 20: NO_3^- (a), PO_4^{3-} (b), SiO_4^- (c) and NO_2^- (d) concentrations (µg L^{-1}) in 2011 and 2012 at 48.9°N (representative of the southern WEC, black line, empty circles) and at 49.9°N (representative of the northern WEC, dashed lines, empty squares) from bimonthly discrete measurements. .....- 88 -

Figure 21: From the 25th April 2012 to the 1st January 2013, surface distributions of (a) temperature anomaly (°C), (b) pCO_2 (µatm), (c) pCO_2 normalized at the mean temperature of 13°C (pCO_2@13°C) from Takahashi et al. (1993) (µatm) and (d) air-sea CO_2 fluxes (mmol m^{-2} d^{-1}) from the algorithm of Nightingale et al. (2000) between Roscoff and Plymouth in the WEC. Negative fluxes indicate a transfer from the atmosphere into the ocean. The black lines represent an estimate of the location of the thermal front; the vertical black lines approximately delimit the period when stratification occurred in the northern WEC. .....- 91 -

Figure 22: Extraction of high-frequency FerryBox and ancillary data from the 3rd July to the 10th August at 48.90°N (southern WEC, a) and 49.90°N (northern WEC, b). From the top to the bottom: variations of DO% (blue), pCO_2 (µatm, red) and air-sea CO_2 fluxes (mmol m^{-2} d^{-1}, cyan); variations of SST (°C, black), Chl-a concentrations (µg L^{-1}, green) and wind speeds (m s^{-1}, orange); variations of salinity (purple), tide height (m, grey) and daily-integrated photosynthetically active radiation (PAR, µE m^{-2} s^{-1}, yellow)..- 92 -

Figure 23: Variations of mean daily (grey) and nightly (black) DO% values (dashed lines) and pCO_2 (µatm) (solid lines) from the 25th April 2012 to the 1st October 2012 at 49.90°N. The bars represent the difference between daily and nightly computed air-sea CO_2 fluxes (mmol m^{-2} d^{-1}) averaged every 3 days. .....- 94 -

Figure 24: Map and bathymetry of the study area with the tracks of all crossings made from 2011 to 2013 by the ferry Armorique between Roscoff (France and Plymouth (UK). The location of fixed stations E1 (Western Channel Observatory) and ASTAN (coastal observatory SOMLIT) are also indicated.....- 108 -

Figure 25: Mean July and August satellite SST (°C) between 2003 and 2013 with delimitation of defined hydrographical provinces: Irish Sea (IS), northern Celtic Sea

(nCS), southern CS (sCS), Cap Lizard province (CL), northern Western English Channel (nWEC) and southern WEC (sWEC). The warmest SST are characteristic of seasonally stratified areas and the coldest of permanently well-mixed systems.....- 110 -

Figure 26: Distribution of monthly gridded (A) SST (°C), (B) Chl-a (µg l^{-1}), (C) PAR (E m^{-2} d^{-1}), (D) K (m s^{-1}) and (E) MLD over depth ratio MLDr in the WEC between Roscoff and Plymouth from January 2011 to December 2013. .....- 116 -

Figure 27: Map of available SOCAT surface pCO_2 data with color-coded respective year of acquisition between 2003 and 2011.....- 117 -

Figure 28: Distribution of monthly gridded (A) pCO_2 (µatm) based on bimonthly DIC/TA measurements (January 2011 to March 2012) and on high-frequency pCO_2 measurements (April 2012 to December 2013) in WEC, (B) $pCO_{2,MLR}$ (µatm) computed from nWEC and sWEC algorithms and (C) residuals (pCO_2-$pCO_{2,MLR}$ in µatm) between Roscoff and Plymouth from January 2011 to December 2013. .....- 121 -

Figure 29: Observed monthly gridded pCO_2 (µatm) versus $pCO_{2,MLR}$ computed from the algorithms developed in sWEC (A) and in nWEC (B) with respective number of values (N), R^2 and RMSE. Residuals between observed pCO_2 and predicted pCO_2 in function of observed pCO_2 values (µatm) in sWEC (C) and nWEC (D). Mean monthly residuals (µatm) over sWEC (E) and nWEC (F) in function of the months from January 2011. On plots C, D, E and F the dashed lines represents the RMSE of MLR developed in sWEC (±15.8 µatm) and nWEC (±16.9 µatm). .....- 123 -

Figure 30: Monthly air-sea CO_2 fluxes (mol C m^{-2} $month^{-1}$) computed from observed pCO_2 (in red) and $pCO_{2,MLR}$ (in blue) data in nWEC and sWEC from 2011 to 2013 using Nightingale et al. (2000) gas transfer velocity K. Dashed lines represent fluxes computed from $pCO_{2,MLR}$ plus and minus respective RMSE. .....- 124 -

Figure 31: Time series of monthly $pCO_{2,MLR}$ (µatm, in black) averaged over IS (A), nCS (B), sCS (C), nWEC (D), sWEC (E) and CL (F) provinces from 2003 to 2013. Monthly mean corresponding SOCAT data (red dots) are shown for comparison. The blue lines represent the atmospheric pCO_2. .....- 127 -

Figure 32: Monthly satellite SST (°C) averaged from 2003 to 2013 from January (top left corner) to December (bottom right corner). .....- 130 -

Figure 33: Monthly satellite Chl-a (µg l^{-1}) averaged from 2003 to 2013 from January (top left corner) to December (bottom right corner).....- 131 -

Figure 34: Monthly $pCO_{2,MLR}$ (µatm) computed from the algorithms developed in seasonally stratified and in permanently well-mixed systems averaged from 2003 to 2013 from January (top left corner) to December (bottom right corner).....- 132 -

Figure 35: Monthly air-sea CO_2 fluxes (mol C m^{-2} $month^{-1}$) computed from $pCO_{2,MLR}$ and using Nightingale et al. (2000) K-wind relationship averaged from 2003 to 2013 from January (top left corner) to December (bottom right corner). Negative values indicate CO_2 sink.....- 133 -

Figure 36: Monthly air-sea CO_2 fluxes (black lines, left hand side Y-axis, mol C m^{-2} $month^{-1}$) computed from $pCO_{2,MLR}$ and using Nightingale et al. (2000) K-wind relationship in IS (A), nCS (B), sCS (C), nWEC (D), sWEC (E) and CL (F) provinces from 2003 to 2013. Negative values indicate CO_2 sink. Integrated annual CO_2 fluxes (vertical grey bars, right hand side y-axis, mol C m^{-2} $year^{-1}$).....- 136 -

Figure 37: Chl-a (A, µg l^{-1}), SST (B, °C), $pCO_{2,MLR}$ and atmospheric pCO_2 (C, in blue and red respectively) anomalies in nWEC from 2003 to 2013. Solid straight lines represent the 10-years trends of each anomalies obtained by linear regression, with corresponding slope values.....- 137 -

Figure 38: Distribution of surface pCO_2 (µatm) from the 5th of June 2012 to the 10th of August 2012 between Roscoff and Plymouth based on (A) high-frequency FerryBox pCO_2 measurements, (B) bimonthly DIC/TA discrete samplings and (C) monthly mean of high-frequency FerryBox measurements (data used in Chapter 4).....- 163 -

Figure 39: Distribution of surface air-sea CO_2 fluxes (mmol C m^{-2} d^{-1}) from the 5th of June 2012 to the 10th of August 2012 between Roscoff and Plymouth based on (A) high-frequency FerryBox pCO_2 measurements, (B) bimonthly pCO_2 and (C) monthly mean of high-frequency FerryBox pCO_2 measurements. The fluxes were computed using the algorithm given by Nightingale et al. (2000) with NCEP daily (A), two-weeks (centered on the date of each crossing) daily average (B) and monthly (C) wind speeds.....- 164 -

Figure 40: pCO_2 (in µatm) and calculated air-sea CO_2 fluxes (in mmol C m^{-2} d^{-1}) in the vicinity of E1 (49.90°N-50.10°N) and ASTAN (48.80°N-49.00°N) fixed station at

different time-scales. Blue lines represent high-frequency FerryBox (HF-FB) pCO_2 measurements and air-sea CO_2 fluxes computed from daily wind speeds. Red circles represent pCO_2 calculated from bimonthly DIC/TA discrete samplings and air-sea CO_2 fluxes calculated from two-weeks (centered on the date of each crossing) daily average wind speeds (FB-Bimonthly). Long-dashed red lines represent the daily-interpolated pCO_2 from bimonthly samplings and the associated fluxes computed from these daily pCO_2 values and from daily wind speeds. Dashed black lines are the monthly average pCO_2 values and associated fluxes computed from monthly wind speeds (as in Chapter 4).....- 165 -

Figure 41: Air-sea CO_2 fluxes (in mmol C m^{-2} d^{-1}, left axis) calculated from high-frequency FerryBox pCO_2 measurements in the vicinity of E1 fixed station from the 5th of June 2012 to the 10th of August 2012 using different gas transfer velocity parametrizations. N00 (in red) refers to Nightingale et al. (2000) parametrization, W92 (in blue) to Wanninkhof et al. (1992), W99 (in black) to Wanninkhof & McGillis (1999), H06 (in pink) to Ho et al. (2006) and W13 to Wanninkhof (2013). The yellow bars represent daily NCEP wind speeds (in m s^{-1}, right axis). .....- 167 -

List of Tables

Table 1: Global anthropogenic CO_2 budget accumulated since the Industrial Revolution (from IPCC, 2013). Negative flux is equivalent to a gain of carbon by the corresponding reservoirs.....- 8 -

Table 2: Dates of transects Roscoff-Plymouth-Roscoff between the 22nd of December 2010 and the 13th December 2013 and number of samples for each month. .....- 34 -

Table 3: Seasonal means of SST (°C), SSS, DO%, Chl-a (µg L^{-1}), NO_3^- (µmol L^{-1}), NO_2^- (µmol L^{-1}), PO_4^{3-} (µmol L^{-1}), SiO_4^- (µmol L^{-1}), DIC (µmol kg^{-1}), TA (µmol kg^{-1}), pH and pCO2 (µatm) in the nWEC and the sWEC from 2011 to 2013 based on the VOS line measurements. The range of values measured each season is given by the numbers in brackets. Each season is defined as follows: winter (from the 1st of January to the 31st of March), spring (from the 1st of April to the 30th of June), summer (from the 1st of July to the 30th of September) and fall (from the 1st of October to the 31st of December).....- 39 -

Table 4: Mixed layer depth (in m) at fixed station E1 (Western Channel Observatory) computed from CTD profiles between 2011 and 2013.....- 41 -

Table 5: Seasonal range of pCO_2 values (µatm) observed in this study across the WEC from 2011 to 2013 and reported by Borges and Frankignoulle (2003) (B & F), Padin et al. (2007) (P et al.) and Dumousseaud et al. (2010) (D et al.) in thre EC and Kitidis et al. (2012) (K et al.) at stations E1 and L4. These pCO_2 values were extracted from graphs of these studies and they represent the approximate range of pCO_2 values measured during each season. .....- 52 -

Table 6: Seasonal means of air-sea CO_2 fluxes (F in mmol C m^{-2} d^{-1}) calculated in this study according to Eq.1 for the nWEC [49.40°N-50.20°N] and the sWEC [48.80°N-49.40°N] provinces and at the fixed stations ASTAN, E1 and L4. These fluxes were computed using the gas transfer velocity formulated by Nightingale et al. (2000). Annual means are in mol C m^{-2} y^{-1}. Atmospheric pCO_2 were measured at Mace Head (Ireland) station from the RAMCES network and wind speeds were obtained from the NCEP/NCAR re-analysis project. Also indicated are the air-sea CO_2 fluxes from Borges and

Frankignoulle (2003) (B & F), Padin et al. (2007) (P et al.), Dumousseaud et al. (2010) (D et al.) and Kitidis et al. (2012) (K et al.). F values from D et al. are the range of F values for each season in the WEC and the annual mean is the average ranges over the years. .....- 58 -

Table 7: Annual estimates of net ecosystem production (NEP in mol C m^{-2} y^{-1}) calculated according to Eq. (X) in the vicinity of E1 [49.8°N-50.0°N] and ASTAN [48.9°N-49.1°N] from FerryBox DIC measurements and air-sea CO_2 flux estimates. New primary production (NPP) estimate from Borges and Frankignoulle (2003) in the WEC (NPP B & F, in mol C m^{-2} y^{-1}) was computed from annual N-assimilation rates given by Le Corre et al. (1996) and L'Helguen et al. (1996) using Redfield C:N ratio in the well mixed waters of the WEC. NEP_{SBNS} referred to NEP estimates in the Southern Bight of the North Sea (SBNS) computed by Schiettecatte et al. (2007) and NEP_{IS} referred to NEP estimate from Gazeau et al. (2004) in the Irish Sea (IS). Also indicated is the NEP estimate from Wollast (1998) for worldwilde continental shelves. WM correspond to all-year well-mixed systems and SS to seasonally stratified systems. .....- 62 -

Table 8: Area (in km²) of each defined province (Fig. (2)), number of available SOCAT pCO_2 data and the percentage of available monthly SOCAT pCO_2 data between 2003 and 2011.....- 118 -

Table 9: MLR normalized coefficients for each variable in sWEC and nWEC with corresponding R^2 and RMSE values. Percentages of variability explained by each variable were computed only when all the variables were included in the MLR. Non-normalized coefficient values are given for the last step of the MLR with their standard error (Std.Err.). N values are the number of values used in the MLR and α is the value between 0 and 365 chosen by iteration to optimize the seasonal phasing.....- 119 -

Table 10: Air-sea CO_2 fluxes (in mol C m^{-2} $year^{-1}$) calculated from observed pCO_2 and from pCO_2 obtained by MLR along the ferry track in nWEC and sWEC using Nightingale et al. (2000) k parametrization. Values in brackets were computed using Wanninkhof et al. (1992) and Wanninkhof and McGillis (1999) k parameterizations for long-term winds to give a range of computed air-sea CO_2 fluxes.....- 125 -

Table 11: Annual air-sea CO_2 fluxes (in mol C m^{-2} $year^{-1}$) in the seasonally stratified (nCS, sCS and nWEC) and permanently provinces (sWEC, CL and IS) of our study area

between 2003 and 2013 and the mean annual fluxes over the decade using Nightingale et al. (2000) k parametrization. Scaled annual fluxes over province areas (Table 2) in Tg C year^{-1} were calculated from the mean annual fluxes over the decade. Fluxes in brackets were calculated using Wanninkhof et al. (1992) and Wanninkhof and McGillis (1999) k parameterizations for long-term winds. ..... - 134 -

Table 12: Air-sea CO_2 fluxes (in mmol C m^{-2} d^{-1}) in the vicinity of E1 and ASTAN at different time-scales in July 2012. HF are the fluxes based on high-frequency FerryBox pCO_2 measurements, FB-DailyInterp are fluxes calculated from daily-interpolated bimonthly pCO_2 values and from daily wind speeds, FB-Bimonthly are fluxes computed from bimonthly pCO_2(DIC/TA) measurements and from two-weeks (centered on the date of each crossing) daily average wind speeds, and Monthly correspond to fluxes calculated from monthly mean pCO_2 and monthly wind speed. We used the gas transfer parametrization of Nightingale et al. (2000). ..... - 165 -

Table 13: Air-sea CO_2 fluxes (in mmol C m^{-2} d^{-1}) comptuted from HF-FB pCO_2 measurements in July 2012 in the vicinity of E1 using different gas transfer parametrizations..... - 166 -

Dynamics of the carbonate system and air-sea CO_2 fluxes in north-western European shelf waters: A multi-scale approach

Pierre Marrec

The raise of atmospheric CO_2 due to anthropogenic activities is a major driver of the climate change. The ocean plays a key role in the uptake of this anthropogenic CO_2. The constraint of air–sea CO_2 fluxes and their variability at various time and spatial levels remain a central task in global carbon cycle and climate studies. The contribution of open ocean to this uptake is presently rather well quantified, whereas the role of the coastal ocean to this process remains ambiguous due to the diversity and the high spatio-temporal variability of the CO_2 system and air-sea CO_2 fluxes in these ecosystems. This PhD thesis investigated the spatial and temporal variability of the CO_2 system and air-sea CO_2 fluxes in contrasted ecosystems of the north-west European continental shelf. These highly dynamic biogeochemical ecosystems host numerous key hydrographical structures (permanently well-mixed, seasonally stratified, frontal structures, estuarine) of temperate zones, in which the dynamic of the CO_2 system were poorly documented. In 2010, we installed an autonomous ocean observing system with high precision oceanographic sensors (FerryBox) on the Voluntary Observing Ship (VOS) Armorique (Brittany Ferries), which crosses the western English Channel (WEC) up to three times a day between Roscoff (France) and Plymouth (UK). Firstly, based on three years of bimonthly discrete samplings on the VOS, we described and discussed the seasonal and inter-annual biogeochemical variability of the surface waters of the WEC, with a main focus on the CO_2 system and air-sea CO_2 exchanges. Secondly, in 2012, we deployed for the first time a next generation partial pressure of CO_2 (pCO_2) sensor (Contros HydroC/CO_2 FT). We evaluated the high-frequency measurements using the bimonthly discrete measurements and assessed the short-time scale processes driving air-sea CO_2 fluxes in the WEC. Finally, based on the three years of comprehensive pCO_2 dataset, we developed algorithms relating our surface pCO_2 to remotely sensed and modeled variables. We extrapolated the relations obtained in the WEC based on the 2011-2013 dataset 1) temporally over a decade; and 2) spatially in the adjacent Celtic and Irish Seas (CS and IS), two regions where pCO_2 data are very sparse.. Based on this reconstructed decadal dataset, we investigated the inter and multi-annual variability of pCO_2 and air-sea CO_2 fluxes over the north-west European shelf.

From tidal to multi-annual variability, from a fixed station off Roscoff to the north-west European continental shelf and from seawater samples to satellite data, this PhD thesis provides an integrative overview of the complexity of the CO_2 system dynamics in coastal seas and the ongoing challenges to achieve.

KEYWORDS: NORTH-WEST EUROPEAN SHELF, CARBON DIOXIDE, AIR-SEA CO_2 EXCHANGES, VOLUNTARY OBSERVING SHIP, HIGH-FREQUENCY, REMOTE SENSING.